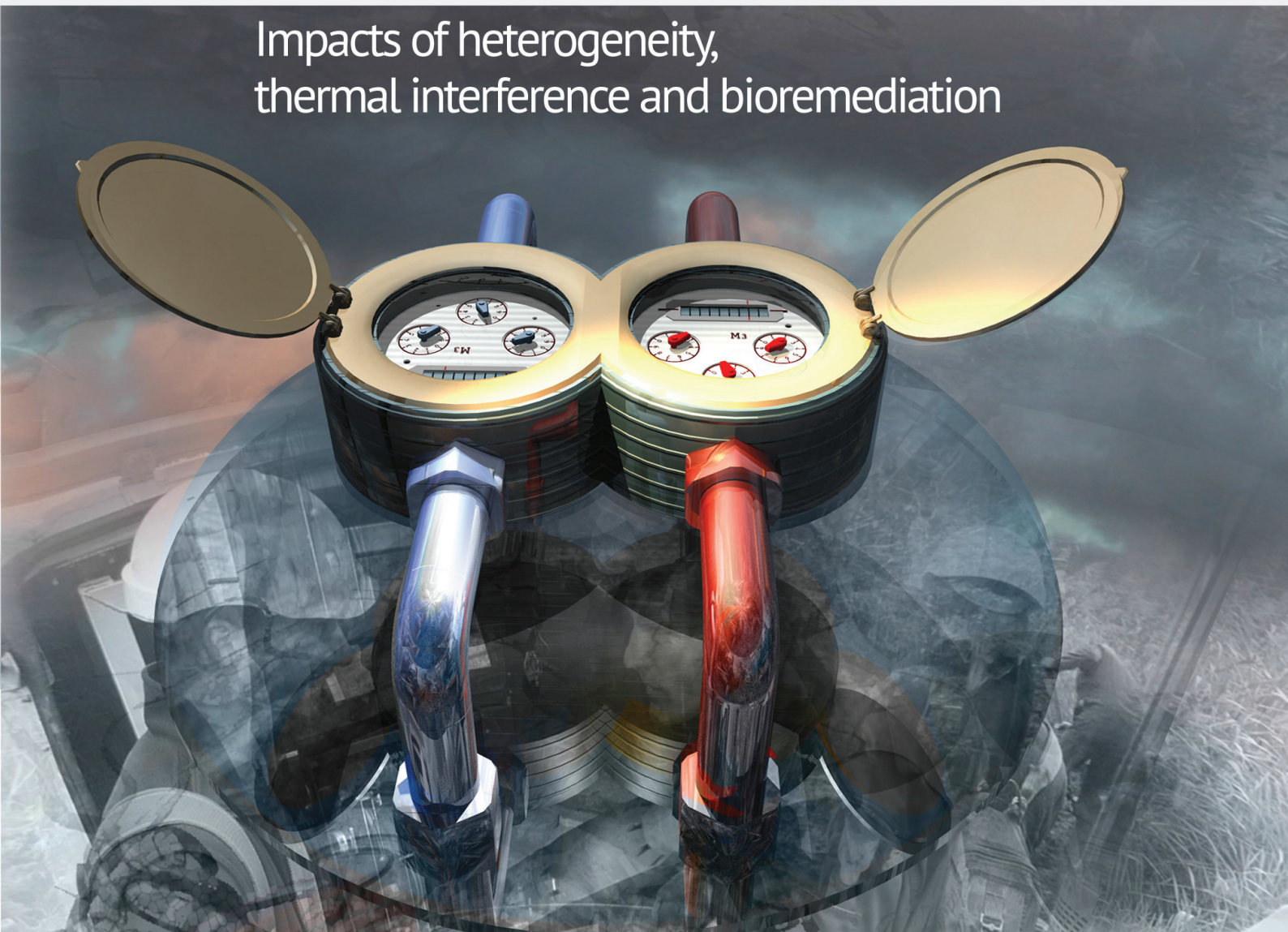


Modelling and monitoring of aquifer thermal energy storage

Impacts of heterogeneity,
thermal interference and bioremediation



Wijbrand Sommer

Modelling and monitoring of Aquifer Thermal Energy Storage

Impacts of heterogeneity, thermal interference and
bioremediation

Wijbrand Sommer

Thesis committee

Promotor

Prof. Dr H.H.M. Rijnaarts
Professor of Environmental Technology
Wageningen University

Co-promotors

Dr J.T.C. Grotenhuis
Assistant professor, sub-department of Environmental Technology
Wageningen University

Dr J. Valstar
Senior geohydrologist at Subsurface and Groundwater Systems
Deltares, Delft

Other members

Prof. Dr T.J. Heimovaara, Delft University of Technology
Prof. Dr P.J. Stuyfzand, VU University Amsterdam
Prof. Dr S.E.A.T.M. van der Zee, Wageningen University
Prof. Dr L.E.M. Vet, Wageningen University

This research was conducted under the auspices of the Graduate School of Socio-Economic and Natural Sciences of the Environment (SENSE)

Modelling and monitoring of Aquifer Thermal Energy Storage

Impacts of heterogeneity, thermal interference and
bioremediation

Wijbrand Sommer

Thesis

submitted in fulfilment of the requirements for the degree of doctor
at Wageningen University

by the authority of the Academic Board

in the presence of the

Thesis Committee appointed by the Academic Board

to be defended in public

on Thursday 4 June 2015

at 11 a.m. in the Aula.

Wijbrand Teunis Sommer

Modelling and monitoring of Aquifer Thermal Energy Storage

Impacts of soil heterogeneity, thermal interference and bioremediation

204 pages

PhD thesis, Wageningen University, Wageningen, NL (2015)

With references, with summaries in English and Dutch

ISBN 978-94-6257-294-2

Contents

Chapter 1	Introduction	7
Chapter 2	Thermal performance and heat transport in aquifer thermal energy storage	17
Chapter 3	The impact of aquifer heterogeneity on the performance of aquifer thermal energy storage	49
Chapter 4	Efficiency of and interference among multiple aquifer thermal energy storage systems; a Dutch case study	73
Chapter 5	Optimization and spatial pattern of large-scale aquifer thermal energy storage	95
Chapter 6	Reactive transport modelling of TCE bioremediation combined with aquifer thermal energy storage	135
Chapter 7	Opportunities and challenges for implementation of ATES in urban areas	157
	Bibliography	169
	Summary	187
	Samenvatting	191
	List of publications	197
	Acknowledgements	199
	Curriculum Vitae	201

Chapter 1

Introduction

Global energy consumption has increased by 57% between 1973 and 1998 [1] and is expected to increase by another 57% between 2002 and 2025 due to increasing population and economic growth [2]. At the same time fossil fuels are depleting [3] and there is increasing concern about the impact of the use of fossil fuels on our climate [4, 5] and the environment [6]. Furthermore, security of energy supply is a major concern related to economic development and geopolitical stability [7]. Considering the increasing energy demand worldwide, these issues are expected to become even more pertinent in the future [8]. Therefore, over the past decades there has been a growing interest in energy saving technologies as well as renewable energy sources such as solar or wind energy.

A less well-known sustainable energy technology is the use of the subsurface to provide heating and cooling to buildings, greenhouses and industrial processes [9, 10]. This is achieved by using the subsurface as a heat source or sink, or as a storage medium for thermal energy. Multiple technologies are being applied to utilize the subsurface for these purposes. This thesis is concerned with one particular application called aquifer thermal energy storage (ATES). In ATES systems, storage and recovery of thermal energy in the subsurface are achieved by injection and extraction of groundwater into and from water saturated subsurface formations (aquifers). ATES is suitable to store large amounts of thermal energy and has developed into a cost-effective technology for heating and cooling of utility buildings such as offices, hospitals, universities and greenhouses [10-13]. Moreover, it is a sustainable energy technology that can reduce greenhouse gas emissions by replacing fossil fuel dependent heating and cooling systems [10, 11]. As approximately 40% of the global energy consumption is used in buildings [14, 15], mostly to provide heating and cooling [15], large-scale application of ATES can contribute significantly to a more sustainable energy use in urban environments.

1.1 Aquifer thermal energy storage

In its basic form, an ATES system consists of two groundwater wells (called a doublet) and operates in a seasonal mode. One well is used for the storage of cold, the second for storage of heat. In summertime, cold groundwater is extracted from the aquifer using the cold storage well and directed through a heat exchanger to provide cooling to a building or industrial process. This heats up the groundwater, which is subsequently injected back into the aquifer through the warm storage well, typically at a distance of 100 or 200 meters. In wintertime, the flow direction is reversed such that the warmer groundwater is extracted and can be used for heating. At the same time, this creates a storage of cold groundwater (Figure 1.1). Depending on the stored volume, the thermal properties of the aquifer and hydrological conditions [16, 17], the thermal storage retains its temperature for months to years [18], such that typically between 50 and 90% of the injected energy is recovered (chapter 4). ATES systems can also consist of multiple doublets.

One of the larger ATEs systems in Europe, located at Eindhoven University of Technology in the Netherlands, consists of more than 30 groundwater wells [19]. In some cases, the heat and cold storage are not placed side by side in the same aquifer, but one below the other. In this case, pipes or tubing can be installed through a single borehole. These systems are referred to as mono-well systems.

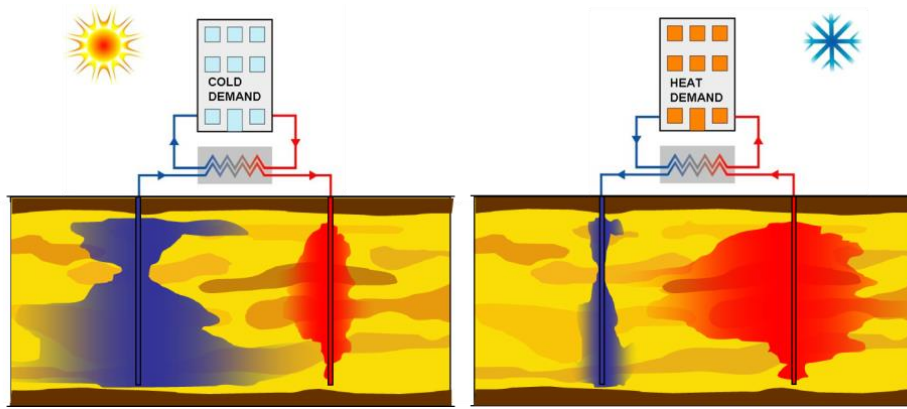


Figure 1.1 Principle operation of an ATEs doublet system in summer (left) and winter (right) (adapted from [20])

Typical well depths vary between 20 and 200 m below ground level, depending on regulations and the presence of a suitable aquifer. Undisturbed temperatures at these depths resemble the annual mean surface temperature. Typical storage temperatures are 5-12 °C for cold storage and 14-30 °C for heat storage [21, 22]. However, there are also practical applications where excess heat from power plants is stored at temperatures between 60 and 80 °C [23-27].

Thermal impact and performance

Injection of groundwater with a temperature that is different from the undisturbed aquifer temperature gives rise to a thermal plume in the subsurface. As the groundwater is injected, part of the thermal energy is transferred from the groundwater to the aquifer matrix. Typically, the volumetric heat capacity of the porous material (1.7 MJ/m³/K for quartz) is approximately half the volumetric heat capacity of groundwater (4.18 MJ/m³/K) [28], but the volume of porous material is twice the volume of groundwater (for a porosity of 0.33), such that roughly half of the thermal energy is stored in the groundwater and the other half in the porous matrix. When the amount of heat that is extracted in winter is equal to the amount of cold in summer, the net aquifer temperature remains constant and the ATEs system operates under thermally balanced conditions. However, when the system is, for example, used more for cooling than for heating, the aquifer gradually heats up. Under such circumstances, the warm plume expands and may

reach the cold storage well, which has a negative influence on the system performance. In case of regional groundwater flow, the excess heat is transported with the groundwater and thereby makes the aquifer downstream less suitable for cooling purposes due to higher temperatures. Plume development depends mainly on site specific hydrogeological conditions and historic thermal storage activities. Assessment and forecasting of thermal plume shape, size and development usually involves numerical heat transport modelling and subsurface temperature measurements [29-32].

1.2 Other types of subsurface thermal applications

Besides ATES there are several other technologies that use the subsurface as a source or storage medium for thermal energy. The main representatives are borehole heat exchangers (BHE) [33, 34] and geothermal energy production [35]. We present here a short overview of the distinctive features of these energy concepts as compared to ATES.

Borehole heat exchangers

Like ATES systems, borehole heat exchangers are also used to provide heating and cooling from the shallow subsurface (<200 m below ground level). However, unlike the case in ATES, no groundwater is extracted or injected. Instead, BHE involve circulating a fluid through a buried heat exchanger, which usually consists of a pipeline that is installed via trenches or boreholes [33, 36]. Heat exchange with the subsurface in this case occurs through thermal conduction through the pipe wall and surrounding formation. Because thermal conduction is less effective in transferring heat than advective transport in ATES, the thermal impact of BHE is limited to several meters around the borehole [10]. An advantage of BHE over ATES systems is that they can be applied in low permeable strata such as clay or tight rocks, whereas ATES requires the presence of a suitable aquifer that is able to yield and receive water [14]. However, under suitable conditions, ATES is the most economical type of ground-coupled heat exchange system [14], and is typically applied for large installations [33]. When BHE are used to deliberately store thermal energy with the aim to recover it later, they are also referred to as borehole thermal energy storage (BTES) systems, and when coupled with a heat pump they are known as ground source heat pumps (GSHP) or geothermal heat pumps (GHP).

Geothermal energy production

Geothermal energy utilizes heat that is present in the Earth's interior by extraction of steam or hot water through wells [35]. Although geothermal energy can be harnessed from any depth and temperature level, geothermal energy production usually refers to systems that are much deeper (1-3 km) [37] than ATES systems (20-200 m) and produce thermal energy at a higher temperature. The hottest geothermal well that has been reported is located in Japan, where a

temperature of 500 °C was measured at a depth of 3.7 km [35]. Geothermal utilization is divided into direct use of heat and electricity production. Direct utilizations of geothermal energy are for example space heating, snow melting, industrial drying or heating, bathing and balneology [37]. Electricity production from such installations commonly involves driving a turbine with steam at temperatures above 150 °C. In contrast, so called binary cycle plants, can produce electricity using fluid temperatures as low as 85 °C [35].

1.3 History of ATEs

It is reported that deliberate storage of thermal energy in aquifers originated in China around 1960 [9, 10]. There, excessive withdrawal of groundwater for an industrial cooling application caused substantial land subsidence. To cope with the subsidence, cold surface water was injected into the aquifer. Subsequently, it was observed that the stored water remained cold for months after injection and could be used for industrial cooling [10]. Storage of thermal energy in aquifers was further suggested in the 1970s which led to field experiments and feasibility studies in France, Switzerland, US and Japan as described in Tsang et al. [38]. First, research was mainly focussed on the behaviour and recoverability of heat stored in the subsurface [38, 39]. Later, research expanded to include also subsidence, water chemistry and economic feasibility [38]. To coordinate various ATEs related studies, the International Energy Agency (IEA) initiated a research program in 1987 entitled: '*Environmental and chemical aspects of thermal energy storage in aquifers and development of water treatment methods*' [40]. The program was focussed on environmental and chemical aspects of ATEs such as bacterial growth and biogeochemical precipitation reactions and effects on groundwater quality [40]. Currently, ATEs is used worldwide in many applications such as for air-conditioning of a supermarket in Turkey [41] and for heating and cooling of a hospital in Belgium [11], a college in the USA [42] and a governmental building in Germany [43]. There are no official statistics on the number and size of ATEs systems worldwide. However, the Netherlands and Sweden are considered to dominate the market in terms of implementation [10, 44]. For Sweden, Anderson [44] estimated that, in 2012, there were approximately 104 ATEs systems with a total capacity of 110 MW. Based on yearly reports of the Dutch Central Bureau of Statistics (CBS), the number of ATEs systems in the Netherlands in the same year was 2740, with a total estimated capacity of 1103 MW [45]. Current developments and research focus mainly on economic performance and sustainability [11, 46], interference between systems [47, 48], governmental and regulatory issues [22, 49] and environmental impact [21, 50].

1.4 Development of ATEs in the Netherlands

Implementation of ATEs in the Netherlands started with demonstration projects in the 1980s [39, 51-53]. However, it was not until 1990 that the number of ATEs systems in the Netherlands began to increase rapidly from 5 in the year 1990 to over 3000 in 2013 (Figure 1.2). The Dutch government wishes to further stimulate this growth to meet targets concerning energy savings, reduction of carbon emissions and implementation of sustainable energy technologies [54]. The number of systems in the Netherlands is expected to increase to a total of 3500 (autonomous growth) or 18000 (accelerated growth) installations in 2020. This is estimated to results in a CO₂ emission reduction of respectively 2% (0.5 Mton CO₂/yr) and 11% (2.9 Mton CO₂/yr) of the total CO₂ emission in the built environment [54].

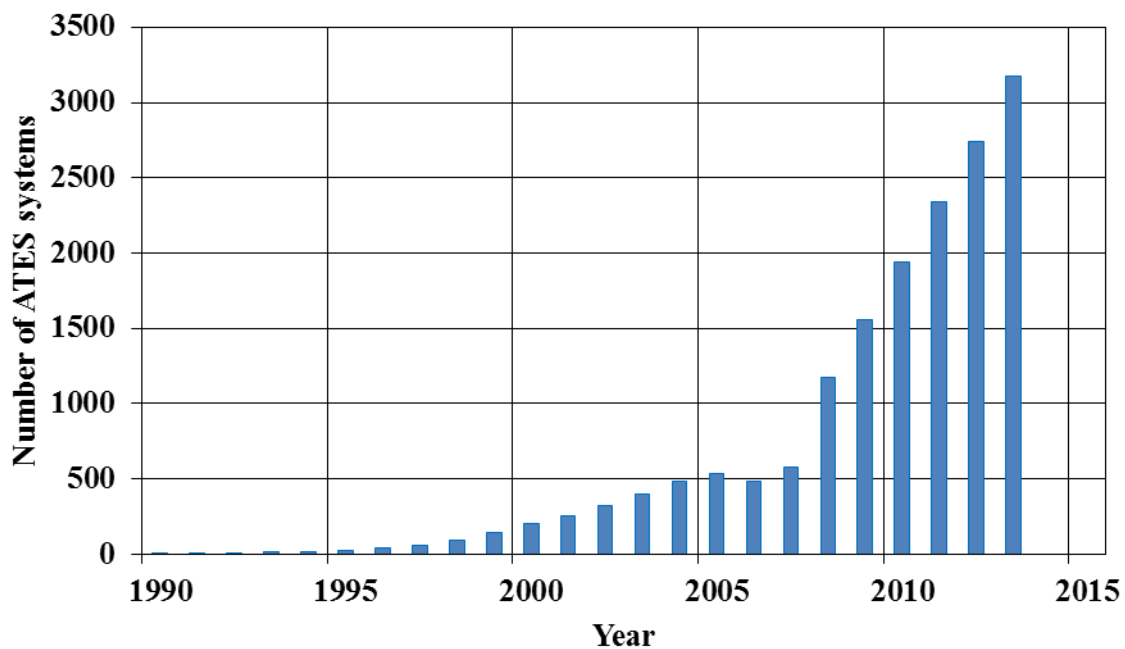


Figure 1.2 The number of ATEs systems in the Netherlands in the utility sector (compiled from yearly reports of the Dutch Central Bureau of Statistics [45, 55-64])

All systems in the Netherlands combined displaced a groundwater volume of 261 million m³ in 2013 [64]. The main other groundwater usages in the Netherlands are drinking water preparation (756 Mm³/yr), industry (148 Mm³/yr) and agriculture (89 Mm³/yr) [65]. This shows that ATEs has become the second largest groundwater user in the Netherlands. An important difference with the other mentioned usages is that in case of ATEs, the majority of the groundwater is re-injected in the aquifer from which it was drawn, and therefore, ATEs does not lead to a depletion of groundwater reserves.

Large-scale application

The rapid increase in the number of ATES systems in the Netherlands over the past 20 years (Figure 1.2), has led to the situation that wells are placed at such small well-to-well distances that their thermal plumes in the subsurface interact [66-69]. When this concerns multiple plumes with similar temperature, this can have a positive effect on the system efficiency. For plumes with different temperature, on the other hand, the efficiency may decrease. Therefore, the size and behaviour of thermal plumes is relevant for the design of ATES systems (i.e. the distance between the cold and warm storage wells) and for the planning of multiple ATES systems in the same area. Because of the increasing number of ATES systems in urban areas, interference is expected to play an important role in the development of these areas. Generally, for installing and operating an ATES system, a permit is required from the regulating authority [49, 70]. Permit applications often involve an environmental impact assessment to show (amongst others) that the system does not negatively influence other ATES systems in the area. However, this does not necessarily lead to optimal use of available aquifer volume [49]. To facilitate optimal use of the subsurface, municipalities in the Netherlands have issued master plans that regulate the positioning of the wells for storing thermal energy [71, 72].

Application of ATES in contaminated aquifers

Since ATES is mostly used to supply energy for offices and homes, its main application is in urban areas. Many of these areas suffer from historic contaminations of soil and groundwater. Contaminants that are frequently encountered are chlorinated aliphatic hydrocarbons (CAH) [73-77]. These substances were used in (former) industrial activities such as dry cleaning, chemical and metal processing factories. Since CAHs are potentially carcinogenic, especially the intermediate degradation product vinyl chloride [78], their presence in groundwater is a threat to subsurface drinking water resources and public health through penetration into water infrastructure and vapour intrusion into indoor air [79-81]. The presence of groundwater contaminants in the capture zone of an ATES system is of concern, because groundwater movement induced by the ATES system can result in a larger contaminant flux to the aqueous phase due to increased dissolution of pure product and a larger volume of contaminated groundwater [82]. Also, temperature changes induced by ATES can impact redox processes, microbial communities [83] and geochemistry [84], and therefore the behaviour of contaminants. In contrast to risks of spreading groundwater contamination, ATES may offer new opportunities to remove pollutants such as CAH from the subsurface environment.

Because of extensive contaminant plumes and recalcitrant behaviour, physical remediation techniques such as pump-and-treat, soil vapour extraction and soil excavation are generally

either too costly or inefficient to properly remediate CAH contaminated subsurface systems [85, 86]. However, in the late 1970s it was recognized that, under certain conditions, CAH are degraded by naturally occurring bacteria to presumably non-toxic compounds as ethene and ethane by reductive dechlorination [73]. Under natural conditions, reductive dechlorination is usually limited by availability of electron donor or nutrients, absence of specific microorganisms or unsuitable redox conditions, resulting in absent or incompletely biodegradation of CAH [87-91]. In these cases, enhanced reductive dechlorination (ERD) through addition of electron donor and nutrients (biostimulation) or addition of specific CAH degrading micro-organisms (bio-augmentation) is required to achieve complete in situ reductive dechlorination [92-96].

During recent years, there is a growing interest in combining ATEs with ERD [97, 98]. In 2012, two pilot locations were studied, where, for the first time, ATEs was combined with monitored natural attenuation [99, 100]. Even without ERD, it was hypothesized that dilution, mixing of water qualities and temperature changes associated with ATEs may have a positive effect on in situ degradation rates, and thereby stimulate natural attenuation. In both pilots no active biostimulation or bio-augmentation was applied, although this has been suggested as an adequate method to be applied when natural biodegradation appears to be insufficient [101]. Hence, the well-designed combination of ATEs with natural attenuation or biostimulation could be a promising integrated technique for remediation of CAHs [101, 102] and broadening the window of opportunity for ATEs.

1.5 Thesis objectives and research questions

The rapid increase in the use of ATEs in the Netherlands has given rise to concerns on the influence of ATEs on its surroundings in terms of spreading of groundwater contaminants, groundwater levels, mixing of fresh-salt water gradients, subsidence, effect on groundwater temperature (that may disturb natural chemical and biological processes), influence on other ATEs systems and also on the thermal performance of the systems themselves [103, 104]. This PhD project aims to improve understanding of heat transport around the wells of ATEs systems related to their thermal efficiency and interference between systems, as well as opportunities to combine ATEs with soil- and groundwater remediation. The research can be divided into three parts:

Part 1: Heat transport and thermal performance of ATEs systems (chapters 2 and 3)

The thermal impact and amount of thermal energy that can be recovered in ATEs depend on hydrogeological conditions as well as the stored volume and presence of other subsurface thermal applications [105-110]. Regarding the number of installed systems it is remarkable how little is reported in scientific literature on the actual thermal impact and performance of these

systems. This thesis addresses this lack of knowledge by providing answers to the following research questions:

- ▶ What is the thermal impact of ATES?
- ▶ What is the storage performance of ATES?

Part 2: Thermal interference and spatial pattern of large-scale application (chapters 4 and 5)

Regarding the increasing number of ATES systems, thermal interference between systems is the main concern for large-scale application of ATES. In Part 2 we aim at quantifying energetic advantage and disadvantage of thermal interference and identification of the factors by which that is influenced. This knowledge can be used in maximizing the amount of energy that can be stored in a particular aquifer volume and suggestions are made on the planning and well placement of large scale ATES. The following research questions are addressed:

- ▶ What is the role of thermal interference in large-scale application of ATES?
- ▶ How can large-scale application of ATES be optimized?

Part 3: Combining ATES with bioremediation of aquifers contaminated with chlorinated hydrocarbons (chapter 6)

The presence of soil and- and groundwater contaminants narrow the opportunity window for ATES and hamper redevelopment of contaminated sites. Hence, the well-designed combination of ATES with biostimulation could be a promising integrated technique, improving groundwater quality while recovering sustainable energy. In this PhD-project, the potential synergy of ATES and measures to stimulate CAH biodegradation in contaminated aquifers are explored. Recommendations for the application of ATES in contaminated aquifers are provided by addressing the central research question:

- ▶ What are the anticipated effects and possibilities of combining ATES and in situ bioremediation in a CAH contaminated aquifer?

1.6 Thesis outline

Chapter 2 presents a detailed thermal assessment of an ATES system over 7 years of operation (2005-2012). The system consists of eight wells and supplies heating and cooling to several office buildings with an annual flow rate of approximately 500 000 m³. Thermal recovery and energy balance are determined from operational data that are logged by the building management system. Detailed monitoring of subsurface temperature development is achieved by a unique application of Distributed Temperature Sensing (DTS) using glass fibre optical cables that are

installed around the wells of the system. Finally, subsurface temperature measurements are interpreted by comparison with a numerical heat transport model.

Temperature measurements (chapter 2) revealed the presence of aquifer heterogeneity and transport by preferential flow paths. In **Chapter 3**, the influence of aquifer heterogeneity on thermal recovery of a doublet ATES system is studied through heat transport modelling. A sensitivity analysis is performed to demonstrate the impact of well-to-well distance, the degree of heterogeneity and regional groundwater flow.

Chapter 4 presents an analysis of a case study on efficiency and thermal interference among multiple ATES systems in The Hague. With 76 ATES wells situated in an area of 4 km², the study area has one of the highest densities of ATES systems worldwide.

The increasing demand for sustainable heating and cooling calls for efficient use of aquifer volume that is available for ATES. **Chapter 5** describes a method to optimize large-scale application of ATES. Investment and operational costs of large-scale application of ATES are estimated for various degrees of thermal interference and compared to the costs of conventional heating and cooling systems. Criteria and indicators are introduced to assess the thermal performance of ATES systems and the usage of subsurface potential.

Since many urban areas deal with groundwater contaminants, a combination between ATES and groundwater remediation is considered a promising new concept that enables both energy savings and improvement of groundwater quality. **Chapter 6** presents a hypothetical case study in which ATES is combined with biostimulation in an aquifer contaminated with chlorinated hydrocarbons. The role of temperature changes, biostimulation measures such as addition of electron donor or specialized CAH degrading microorganisms to the re-injected water streams are discussed, as well as effects of microbial growth and transport.

Chapter 7 addresses the research questions and discusses implications of the previous chapters in a broader perspective.

Thermal performance and heat transport in aquifer thermal energy storage

Abstract

Aquifer thermal energy storage (ATES) is used for seasonal storage of large quantities of thermal energy. Due to the increasing demand for sustainable energy, the number of ATES systems has increased rapidly, which has raised questions on the effect of ATES systems on their surroundings as well as their thermal performance. Furthermore, the increasing density of systems generates concern regarding thermal interference between the wells of one system and between neighbouring systems. An assessment is made of (1) the thermal storage performance, and (2) the heat transport around the wells of an existing ATES system in the Netherlands. Reconstruction of flow rates and injection and extraction temperatures from hourly logs of operational data from 2005 to 2012 show that the average thermal recovery is 82% for cold storage and 68% for heat storage. Subsurface heat transport is monitored using distributed temperature sensing. Although the measurements reveal unequal distribution of flow rate over different parts of the well screen and preferential flow due to aquifer heterogeneity, sufficient well spacing has avoided thermal interference. However, oversizing of well spacing may limit the number of systems that can be realized in an area and lower the potential of ATES.

This chapter is published as: Sommer, W.T., Doornenbal, P.J., Drijver, B.C., van Gaans, P.F.M., Leusbrock, I., Grotenhuis, J.T.C. and Rijnaarts, H.H.M. (2014). *Thermal performance and heat transport in aquifer thermal energy storage*. Hydrogeology Journal, 22(1), 263-279.

2.1 Introduction

The subsurface is increasingly being used to provide cooling and heating for buildings and industrial processes [111]. Suitability for heating and cooling is determined by the groundwater temperature. In the Netherlands, subsurface temperature increases approximately 3 °C with every 100 m increase of depth. At 50 m depth, the subsurface temperature is approximately 12 °C [112] and increases to approximately 25 °C at 500 m depth, 40 °C at 1 km depth and 70 °C at 2 km depth [113]. Subsurface temperatures between 12 and 40 °C make shallow aquifers (<500 m) suitable for both cooling and heating of buildings. To provide heat at higher temperature than the groundwater temperature, a heat pump is required. Due to its higher temperature, the deep subsurface (>500 m) can be used for direct heating. Among the different types of shallow subsurface thermal energy storage concepts, aquifer thermal energy storage (ATES) is suitable for seasonal storage of large quantities of thermal energy. The principle of seasonal ATES is that in summer, groundwater is extracted to provide cooling. The heated groundwater is injected back into the aquifer to create a heat storage. In winter, the flow direction in the system is reversed such that the heated groundwater is extracted to provide heating and create a cold storage [68, 114]. Re-using stored thermal energy can increase the performance of the system with respect to mono-directional systems that simply use the prevailing groundwater temperature for heating or cooling [115].

Due to the increasing demand for sustainable energy, the number of ATES systems in the Netherlands has increased rapidly from five systems in 1990 to more than 1300 in 2010 [61, 116]. The increasing application of ATES has raised questions on the thermal influence of ATES on its surroundings as well as their thermal performance. Furthermore, the increasing density of systems generates concern on thermal interference between systems [117, 118].

The thermal performance of an ATES system can be expressed in thermal recovery, defined as the fraction of stored energy that is recovered. Modelling studies show that part of the injected energy is not recovered due to regional groundwater flow [119], heat conduction and interaction with the solid matrix [16, 106, 120]. In multi-well systems, thermal interference between the cold and warm water storage may decrease thermal recovery when they are built too close together [68, 69, 121, 122]. An example of a group of geothermal systems where extraction temperatures are negatively influenced due to insufficient well spacing is given by Ferguson and Woodbury [47]. On the other hand, thermal recovery may increase due to thermal interference between wells with similar storage temperatures [117]. Modelling studies show that aquifer heterogeneity can influence the thermal recovery of ATES. Ferguson [107] considers a single ATES well in two selected heterogeneous aquifers and shows that the amount of extracted energy can be 5.5 and 8.2% lower than in a homogeneous aquifer. Modelling of a doublet ATES

system in a heterogeneous aquifer [123] confirms that, on average, thermal recovery is lower in heterogeneous aquifers. Furthermore, considerable uncertainty exists in expected thermal recovery due to uncertainty in the thermal interference. The design and use of the system also determine how much energy is recovered, for example the volume of groundwater used for storage, the temperature difference between the storage and the natural aquifer temperature, well screen length and duration of the storage.

In this study, an assessment is made of (1) the thermal storage performance, and (2) the heat transport around the wells of an existing ATES system. Subsurface heat transport is monitored using distributed temperature sensing (DTS) in glass fibre optic cables. Application of DTS enables continuous monitoring with high temporal and spatial resolution. The cables are installed over the full thickness of the aquifer to be able to observe the temperature evolution at different parts of the well screen. To assess the current approach for designing ATES systems and estimating their thermal influence, measured temperatures are compared to the results of a heat transport model. By applying two scenarios, it is possible to differentiate between the effect of incorrect assumptions on operational flow rates and injection temperatures and the effect of aquifer heterogeneity.

2.2 Materials and methods

ATES system considered in this case study

The ATES system considered in this case study is located on the campus of Utrecht University, Utrecht, the Netherlands (Figure 2.1a). The system uses eight groundwater wells to provide heating and cooling to several office buildings on the campus (Figure 2.1c). The wells that are used to store cold energy (C1–C4) and heat (H1–H4) are grouped in four clusters (C12, C34, H12, H34). The aquifer used for thermal energy storage is located at a depth of 3–50 m below ground level (bgl) and has an average temperature of 12.3 °C. The average injection temperature is 7.5 °C for cold storage and 14.5 °C for heat storage. All wells are connected to a central heat exchanger, where the energy is exchanged and subsequently distributed over the buildings. Since its construction in 2002, the system extracts approximately 520 000 m³ of groundwater per year. The average energy supply to by the ATES system is 1681 MWh of heating and 1668 MWh of cooling and per year, with a maximum cooling load of 3 MW.

Flow rates and injection temperatures in the system are controlled by the (net) heat and cold demand of the buildings. The system is fully automated and controlled by a building management system (BMS). A BMS is computer software that controls the ATES system and registers operational parameters. Depending on the thermal power that is needed, the flow rates of the wells are automatically adjusted. Switching from pumping to injection also occurs

automatically. The wells operate at full capacity when the maximum heating or cooling capacity is needed for the buildings or when storage of heat or cold at full capacity is needed (storage of thermal energy for the next season and/or for the required thermal balancing of the system). When the thermal power that is required is lower, the flow rates are reduced equally, to (1) secure the desired injection temperature and (2) reduce the amount of water that is being pumped and consequently reduce the related energy use and environmental (hydraulic) impact. To be able to do this, advanced submersible pumps are used that can operate at variable speed (known as adjustable speed drive or variable speed drive). The pumping speed can be controlled by adjusting the frequency of the alternating electrical current.

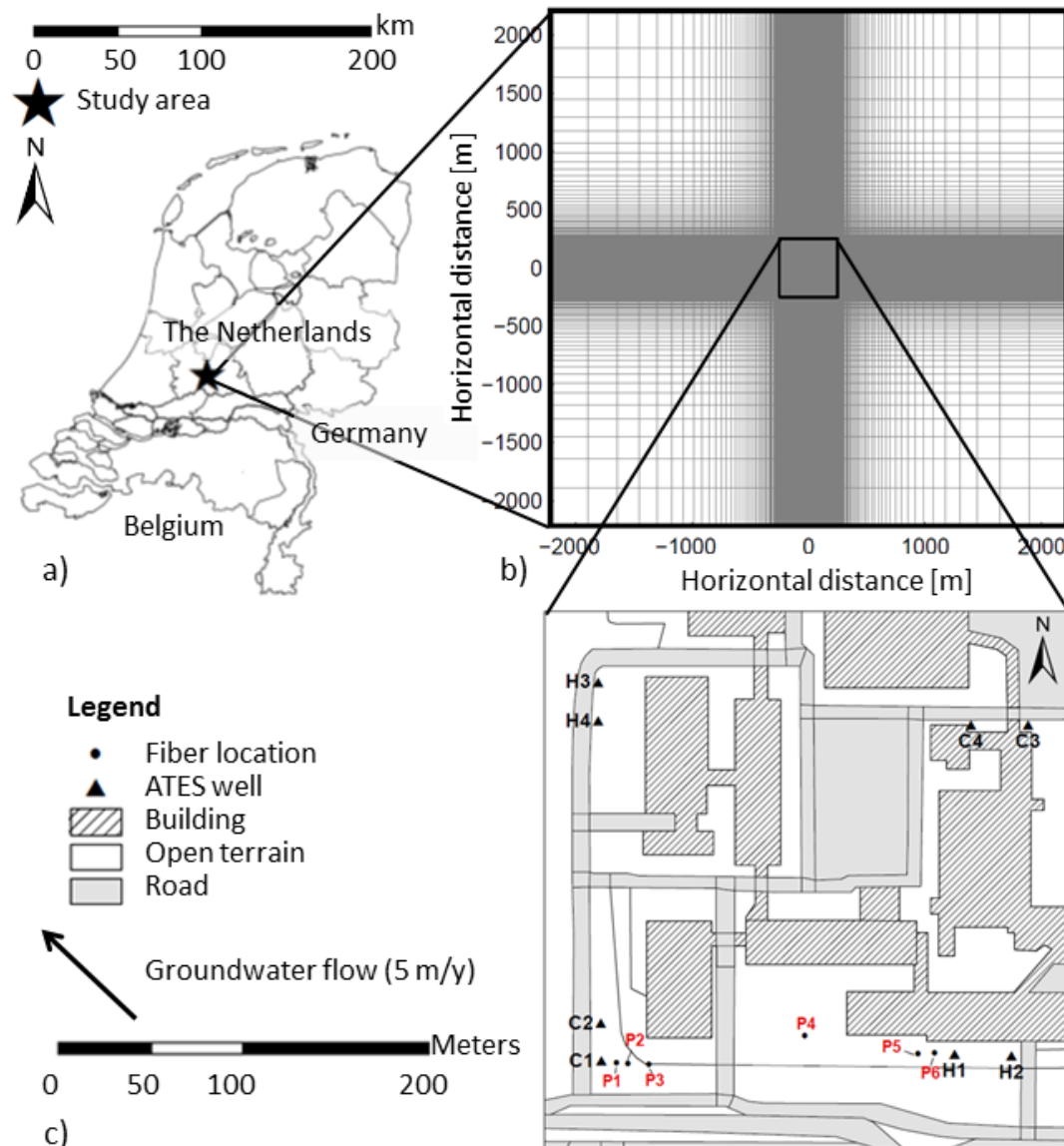


Figure 2.1 (a) Location of the study area in the Netherlands. (b) Model domain showing grid refinement towards the centre of the domain and constant head and constant temperature boundaries along the edge of the domain. (c) Map of the study area indicating the location of geothermal wells (C1-C4 and H1-H4) and fibre optical cables (P1-P6)

Local hydrogeology

The local geological structure (Figure 2.2) is derived from drillings, geophysical well logs and two available geological models [124-127]. The top layer (Table 2.1) consists of 2 to 3 m thick peat and clays. Below this top layer, the aquifer used for thermal storage reaches to a depth of approximately 50 m bgl where it is bounded by a 13 m thick clay layer. The aquifer is fully saturated and consists of several formations with different lithoclasses. The top part of the aquifer (2.8–7.5 m bgl) is formed by fine to medium coarse sands (medium grain size 105–300 μm) from the Boxtel formation, deposited by local and small-scale processes during a periglacial environment in the Weichselian. Below this layer, down to a depth of 20 m bgl, the Kreftenheye formation consists of coarse sands and gravels, deposited by braided rivers. The formation of Urk stretches to a depth of approximately 27.5 m and mainly consists of medium to coarse sands (150–2 000 μm) deposited by a fluvial system in the mid Pleistocene. The bottom part of the aquifer belongs to the formation of Sterksel and consists mainly of medium to coarse sand.

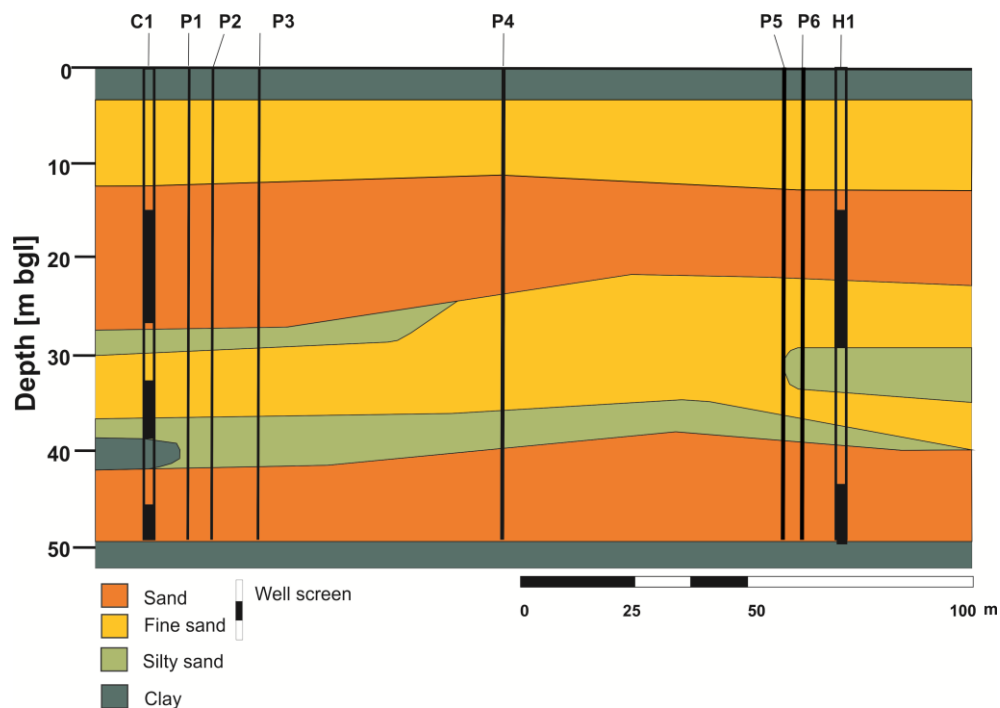


Figure 2.2 Interpreted hydrogeological cross-section with main lithoclasses. The positions of the wells (C1) and (H1) and fibre optical cables (P1 – P6) is indicated with black lines

Hydraulic properties are estimated by coupling lithoclasses to hydraulic conductivities. The horizontal hydraulic conductivity in the aquifer is between 20 and 50 m/day [126]. Regional groundwater flow in the aquifer is estimated at 5 m/yr in a north-west direction [128].

Table 2.1 Hydrogeological stratigraphy of the study site

Depth (m bgl)	Lithoclasses
0.0 - 2.8	Peat and clay
2.8 - 7.5	Fine to medium course sand
7.5 - 20.0	Course sand and gravel
20.0 - 27.5	Medium to course sand
27.5 - 57.5	Medium to course sand
57.5 - 70.0	Clay

All well screens are placed between 15 and 50 m bgl. The exact position of the screens is different for each well. Based on the drilling logs and borehole measurements, well screens are generally placed in the most permeable parts of the aquifer. This resulted in two or three screened sections per well [129].

Reconstruction of flow rates and well temperatures

To assess the thermal storage performance of the system and provide input for the heat transport model, flow rates and injection and extraction temperatures are reconstructed for each well using operational parameters as logged by the BMS. From 2005 onwards, operational parameters are logged every hour. Due to a lack of data, the first 3 years after the start of the system (2002 to 2004) are excluded from this analysis. The parameters that are logged by the BMS are: (1) water level in each well (an overview of recorded levels is available in the electronic supplementary material of [130]), (2) cumulative volume of water injected into each cluster, (3) current pumping rate for all wells combined and (4) water temperature at both sides of the heat exchanger. Operation of the ATES system is implemented such that the following rules can be used to determine the hourly averaged pumping rate for each well from the data that are logged by the BMS:

1. The clusters are connected (C12 with H12 and C34 with H34) such that when there is only injection in one cluster, all injected water (as logged by the BMS) is extracted from the cluster connected to that one. For example, when the record shows only injection into cluster C34, the same amount of water is extracted from H34.
2. The pumps in the extraction wells are controlled in parallel, such that when a cluster is used for extraction, the two wells in this cluster have the same flow rate.
3. The flow rate of each injection well is deduced from the levels in the wells and their specific capacity.

4. When two clusters are used for injection, the same amount of water is extracted from the other two clusters combined (water balance). The extraction rate for each cluster is deduced from the levels in the wells and their specific capacity.

Flow rates in a well are determined using the specific capacity of the well and the measured drawdown. Specific capacity for extraction is determined for each well during regular maintenance (once every year, except in 2007 and 2008). The specific capacity for injection is assumed to be proportional to the specific capacity for extraction for the same well. The drawdown in each well is determined by subtracting the level in each well while the system was inactive from the measured well levels. Measured levels during the well tests show that pumping in a well also influences the observed level in the other well of the same cluster. The other clusters are at sufficient distance from each other not to be of influence. To get drawdown in a well due to pumping in this well, observed drawdowns are corrected for mutual hydraulic interference using Equation 2.1.

$$\begin{pmatrix} D_1^* \\ D_2^* \end{pmatrix} = \begin{pmatrix} 1 & f \\ f & 1 \end{pmatrix} \cdot \begin{pmatrix} D_1 \\ D_2 \end{pmatrix} \quad (2.1)$$

Here D_1^* and D_2^* are the measured drawdowns in the two wells of a cluster, D_1 and D_2 are the drawdowns due to pumping in this well, and the factor f gives the hydraulic influence of pumping in one well on the other well in a cluster.

The drawdown in a well due to pumping in this well is calculated by solving for D_1 and D_2 in Equation 2.1. The influence factors f (Table 2.2) are determined from the measured drawdowns during the maintenance tests when each well is pumped individually, following Equation 2.2.

$$f = \frac{D_{\text{neighboringwell}}}{D_{\text{pumpedwell}}} \quad (2.2)$$

Regular maintenance tests in the period 2005 to 2012 resulted in 5 to 7 separate estimations of f per cluster. The capacity tests showed a linear response of drawdown to extraction flow rate (40, 60, 80 and 90 m³/h per well, sustained for 30 min each), which indicates a linear well loss.

Table 2.2 Hydraulic influence factors (f) between wells in a cluster

Cluster	f
C12	0.172 ± 0.066
C34	0.158 ± 0.027
H12	0.170 ± 0.030
H34	0.235 ± 0.025

After correction for hydraulic interference, the estimated drawdown is used to determine the flow rate distribution over the individual injection wells according to Equation 2.3.

$$Q_i = \frac{Q_{total}}{\sum_{i=1}^n Q_i^{sp} D_i} Q_i^{sp} D_i \quad (2.3)$$

Here Q_i is the flow rate in well i , Q_i^{sp} is the specific capacity for well i , D_i the drawdown due to pumping in well i and n is the number of wells over which the total flow rate Q_{total} is divided. Instead of Equation 2.3, one could also have directly used $Q_i = Q_i^{sp} D_i$ to determine the flow rate per well. However, adding the scaling term in Equation 2.3 ensures that the total measured flow rate (Q_{total}) matches exactly and reduces the influence of noise in the estimated drawdowns.

The injection and extraction temperatures of the system are measured at the two sides of the heat exchanger. It is assumed that heat loss during transport of the water between the heat exchanger and the wells is negligible, such that the injection temperature for all wells that are injecting is equal to the water temperature coming out of the heat exchanger. For extraction however, the measured extraction temperature at the heat exchanger is a flow rate average of the temperatures from all extracting wells. By selecting moments when only one cluster is used for extraction, it is possible to discriminate between the extraction temperatures of each cluster. Since the two wells in a cluster are always used together, it is not possible to discriminate between the extraction temperatures of the two individual wells in each cluster. For cluster H34 it appeared that there were too few moments that only this cluster is used for extraction to accurately determine its time varying extraction temperature. For this cluster, extraction temperatures (T_{H34}) are determined from the flow rate averaged extraction temperature of H12 and H34 measured at the heat exchanger (T_{HE}) and individual extraction temperatures of H12 (T_{H12}) using Equation 2.4.

$$T_{H34} = \frac{(Q_{H12} + Q_{H34}) \cdot T_{HE} - Q_{H12} \cdot T_{H12}}{Q_{H34}} \quad (2.4)$$

The flow rates in cluster H12 and H34 are given by Q_{H12} and Q_{H34} . The extraction temperature from cluster H12 (T_{H12}) is interpolated from the moments that only this cluster is used for extraction.

Thermal recovery

Using the injection and extraction flow rates and temperatures, thermal recovery of each cluster is determined over the period 2005–2012. Thermal recovery (TR) is defined as the ratio between thermal energy that is extracted from the subsurface ($E_{extracted}$) and what was injected in the previous period ($E_{injected}$) with respect to the natural temperature of the aquifer (Equation 2.5). A thermal recovery equal to zero means that none of the stored energy is retrieved.

$$TR = \frac{E_{extracted}}{E_{injected}} = \frac{\int_{\text{begin extraction}}^{\text{end extraction}} Q_t \cdot (T_{\text{extraction}} - T_{\text{natural}}) \cdot dt}{\int_{\text{begin injection}}^{\text{end injection}} Q_t \cdot (T_{\text{injection}} - T_{\text{natural}}) \cdot dt} \quad (2.5)$$

Here Q_t is the pumping rate, $T_{\text{extraction}}$ and $T_{\text{injection}}$ are the extraction and injection temperatures, T_{natural} is the natural temperature of the aquifer and dt is a time increment.

Thermal recovery can be calculated for an individual well or a group of wells. Because the operational data logged by the BMS do not allow discrimination between the extraction temperatures of the individual wells in a cluster, thermal recovery values are calculated for each cluster.

If only a small portion of the volume of injected water is extracted during the recovery phase, this will result in a low thermal recovery. This does not necessarily mean that there are significant heat losses, but merely that, for a specific reason, it was chosen not to extract the stored energy. To take into account the injected and extracted volumes, volume recovery (VR) is defined analogous to thermal recovery (Equation 2.6).

$$VR = \frac{V_{\text{extracted}}}{V_{\text{injected}}} \quad (2.6)$$

Thermal balance

A thermally balanced ATES system provides the same amount of cold in summer as heat in winter. However, energy demand from the building often results in different amounts of energy extracted for cooling than for heating [131]. An imbalanced system can result in lower performance. For example, if the aquifer is predominantly used for cooling a building and this is not balanced by cold storage, there is a net heating of the aquifer. As the warm storage expands, at a certain point this heat may reach the well used for cold storage, reducing the suitability of this well for cooling [47]. To avoid systematic heating or cooling of the subsurface, Dutch regulators often require a thermally balanced system [132].

The thermal balance is expressed in the energy balance ratio (EBR). The EBR gives the difference between the amounts of energy that are extracted in cooling and heating mode over a certain period of time, normalized by the total extracted energy (Equation 2.7). An EBR equal to zero means that there is no net heating or cooling of the subsurface.

$$EBR = \frac{E_{\text{cold}}^{\text{extracted}} - E_{\text{warm}}^{\text{extracted}}}{E_{\text{cold}}^{\text{extracted}} + E_{\text{warm}}^{\text{extracted}}} \quad (2.7)$$

Here the amount of cold energy that is extracted from the subsurface ($E_{\text{cold}}^{\text{extracted}}$) is given by:

$$E_{\text{cold}}^{\text{extracted}} = \int_{\text{Heating mode}} c_{\text{water}} \cdot Q \cdot \text{abs}(T_{\text{extraction}} - T_{\text{injection}}) \cdot dt \quad (2.8)$$

where $T_{\text{extraction}}$ is the temperature of the cold water that is being extracted and $T_{\text{injection}}$ is the temperature of the warm water that is injected. For the amount of heat extracted ($E_{\text{warm}}^{\text{extracted}}$), the same equation is used, but then it is integrated over the time that the system is in heating mode.

To relate the EBR to the volumes that are pumped during the cooling and heating mode, a volume balance ratio (VBR) is defined, similar to Equation 2.7. Here, $V_{\text{cold}}^{\text{extracted}}$ is the groundwater volume extracted during cooling mode and $V_{\text{warm}}^{\text{extracted}}$ is the volume extracted during heating mode.

$$VBR = \frac{V_{\text{cold}}^{\text{extracted}} - V_{\text{warm}}^{\text{extracted}}}{V_{\text{cold}}^{\text{extracted}} + V_{\text{warm}}^{\text{extracted}}} \quad (2.9)$$

Distributed temperature sensing (DTS) with fibre optics

To assess heat transport around the ATES wells, temperature monitoring using DTS is applied. Temperature monitoring using DTS is based on temperature dependent back scattering of a laser pulse sent through a fibre optic cable. By analysing the reflected pulse, the distance is determined from where the light was reflected. Part of the energy which is sent into the cable is absorbed and re-emitted at shorter and longer wave lengths known as the Raman-backscatter. By analysing the Raman-backscatter, it is possible to deduce the temperature along the cable [133, 134].

Six fibre optic cables (Optofil-0 ZGGT HighP) were installed vertically from the surface to the base of the aquifer (50 m bgl). Three cables (P1, P2 and P3) are located at respectively 10, 15 and 25 m from well C1 to observe the temperature evolution near the wells used for cold storage (Figure 2.1 and Figure 2.2). One cable (P4) is installed in the middle between wells C1 and H1 (at a distance of respectively 88 and 100 m) to observe whether the thermal front is extending beyond this point. Based on design calculation this observation point is expected to show only small temperature fluctuations. Temperature evolution near the wells used for heat storage is monitored with two cables (P5, P6), which are installed at 15 and 10 m from well H1.

To install the cables, 80 mm diameter boreholes were drilled using flush drilling (Figure 2.3). After inserting the fibre optic cables, the holes are backfilled with material of similar grain size as the aquifer material at each depth (according to SIKB protocol for mechanical drillings, [135]). At the surface, all cables are collected in a mobile cabin where they are connected to a DTS system. Temperature measurements were taken from 10 December 2010 until 31 March 2012.



Figure 2.3 Installation of glass fibre optic cables for distributed temperature sensing (DTS)

Raman-backscatter DTS along the multimode fibre optic cable was alternatively employed using the Halo HL4 and ORYX OX4-SR system [136]. Both machines are equipped with four channels, so they can measure four cables sequentially. To focus on different stages of the injection and retrieval of thermal energy, occasionally a different set of four cables was selected for monitoring from the total of six available cables.

Spatial resolution is 2 m for the Halo and 1 m for the ORYX system. Acquisition time was varied between 240 and 900 s, resulting in a measurement frequency between 1 and 4 measurements per hour for each cable that is monitored. This is sufficient to capture the frequency of subsurface temperature changes due to aquifer thermal storage at the location of the observations, which is expected to be on the order of days to weeks. The temperature resolution depends on cable length and acquisition time [136]. In our case, a precision of 0.5 °C is achieved.

Calibration of the temperature data of each cable was achieved by averaging over a loop of at least 6 m inside the cabin where they are connected to the DTS system. The temperatures are calibrated on absolute temperature using two reference temperature sensors (PT100). The temperatures in cables P5 and P6 have an additional correction to correct for signal loss over a splice between the DTS system and the buried cable.

It was observed that different temperature corrections are needed when switching between the two DTS systems (Halo and ORYX) or changing between the channels of a DTS system. Within these periods constant temperature corrections were applied.

Numerical modelling

It is common practice (in the Netherlands) to assess the thermal influence of an ATEs system by numerical heat transport modelling. The model results are used to determine optimal well placing and to check whether the system does not interfere with other functions (such as other ATEs systems). To assess the accuracy of current design practice of ATEs, measurements of extraction temperature (2005–2012) and subsurface temperatures (December 2010–March 2012) are compared with temperatures predicted by the heat transport model that was used at the design stage.

Two scenarios are considered: (1) the design model that was originally used to estimate the thermal influence of the system before it was built (SC1), and (2) an adapted design model, in which flow rates and injection temperatures are adjusted to the flow rates and temperatures as reconstructed from the operational data reported by the BMS (SC2). In the first scenario, the difference between modelled and measured temperatures reflects the combined uncertainty in the

estimated use of the system (flow rates and injection temperatures) and in the estimated thermal and hydraulic properties of the subsurface and the wells. In the second scenario, the difference between modelled and measured temperatures reflects only the uncertainty in the estimated thermal and hydraulic properties of the subsurface and the wells.

HSTwin [137] was used to simulate heat transport in the aquifer. HSTwin is a modified version of HST3D [138], a finite difference code for simulation of heat and solute transport in groundwater flow systems. Modifications were made to improve the software interface for ATEs design. Density differences due to non-isothermal conditions can be incorporated in HSTwin. However, due to the small temperature differences in this study (maximum 6 °C), the tendency for density driven flow is very small compared to forced flow by pumping of the wells and, therefore, allows density driven flow to be neglected [82, 139].

The aquifer is modelled by a single layer with homogeneous hydraulic conductivity. Conductive heat transport through the base of the aquifer and the overburden are incorporated by two additional model layers. To resolve heat transport at the scale of subsurface temperature measurements, the original grid spacing of 5 m is reduced to 2 m around the locations of the wells. Near the edges of the model, grid spacing is allowed to increase to reduce calculation time while retaining detail at the location of the temperature measurements (Figure 2.1b).

In scenario 1 (the original design), every year consists of two stress periods: cold injection for 182.5 days followed by heat injection for 182.5 days. In scenario 2 (using reconstructed flow rates and injection temperatures), the stress period length is 2 days. To generate input for scenario 2, the hourly BMS data is summed over periods of 4 days. All injection into a well during these 4 days is assigned to one stress period, and all extraction is assigned to the next stress period. This averaging method ensures that the flow rates and injection temperatures reported by the BMS are exactly incorporated in the model. The reason for averaging the hourly BMS data is to avoid cumbersome input files and long calculation times. It was tested that further reducing the stress period length did not influence the modelled temperature evolution at all observation locations.

Total model extent is 4460 m in both north–south and east–west directions. Grid sizes range from 2×2 m around the wells of the ATEs system to 341×341 m near the edges of the model. Fixed head boundaries are applied to result in a regional groundwater flow velocity of 5 m/yr in the aquifer. All sides of the model have a constant temperature boundary condition. An overview of hydraulic and heat transport input parameters is given in Table 3.

Table 2.3 Parameters used in the numerical model

Model parameter	Value
Thermal diffusivity cap and base rock [m ² /s]	0.9×10^{-6}
Thermal conductivity cap and base rock [W/m/C]	2.4
Initial aquifer temperature [°C]	12.3
Aquifer permeability [m ²]	53.3×10^{-12}
Porosity	0.35
Aquifer heat capacity [J/m ³ /C]	2.5e6
Water heat capacity [J/kg/C]	4189
Thermal conductivity of the aquifer [W/m/C]	2.4
Longitudinal dispersivity [m]	2.5
Transversal dispersivity [m]	0.25
Aquifer thickness [m]	30

2.3 Results

Flow rates and well temperatures

Using operational data logged by the BMS for the period 2005 to 2012 it was possible to reconstruct hourly averaged flow rates for each well. To improve visibility, flow rates are presented as daily totals for two heating and cooling cycles (Nov 2009 to Nov 2011; Figure 2.4). Flow rates are stacked for the two wells in each cluster. An overview of flow rates over the period 2005 to 2012 is presented in Figure 2.5. Extraction from a well is defined as negative. Figure 2.4 and Figure 2.5 show a clear seasonal trend, with extraction from the cold wells in summer to provide cooling and extraction from the warm wells during winter to provide heating. Furthermore, the average duration of the cooling season (summer: 221 days) is longer than the heating season (winter: 144 days). The highest flow rates are observed in the middle of the winter and summer and lower flow rates in autumn and spring when climate is more moderate.

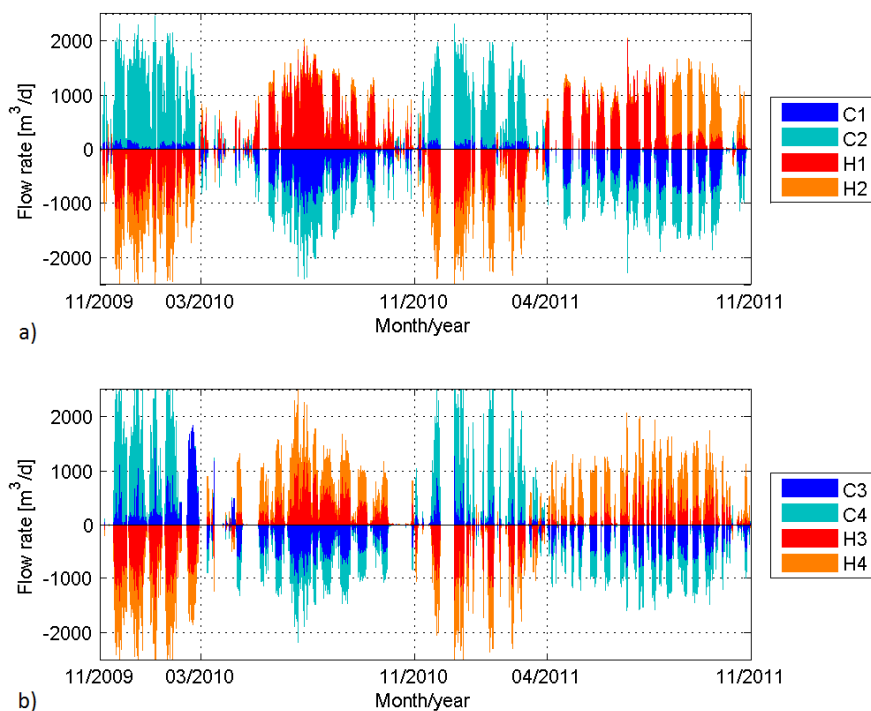


Figure 2.4 Estimated well fluxes for stacked for the two wells of each cluster, a) C12 and H12 and b) C34 and H34. A positive flow rate indicates injection into a well, negative flow rate is extraction. The dates on the x-axis indicate the approximate switch of the system between heating and cooling mode

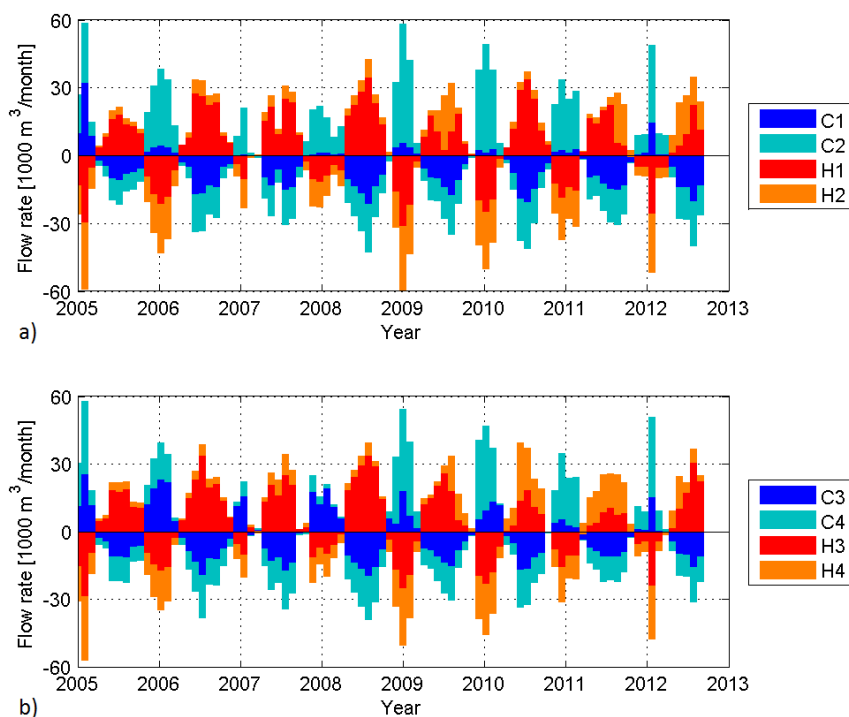


Figure 2.5 Estimated well fluxes for stacked for the two wells of each cluster, a) C12 and H12 and b) C34 and H34. A positive flow rate indicates injection into a well, negative flow rate is extraction

As mentioned before, frequency operated pumps are controlled to extract the same flow rate from each of the two wells in a cluster. For injection, the wells in each cluster are also intended to receive similar injection flow rates. Figure 2.5, however, shows that injection flow rates are generally not the same for the two wells in each cluster. Injection of cold water in cluster C12 occurs predominantly in well C2. Injection in cluster H12 occurs mainly through well H1 until 2009, after which injection switches between H1 and H2. Also for cluster C34, the distribution of injection flow rate changes around 2009, from C3 to C4. Injection of warm water in cluster H34 occurs mainly through well H3, except for the years 2010 and 2011. The explanation for this unequal distribution of flow rate among the wells of a cluster is that at the injection wells, valves are controlled in such a way that they can result in unequal distribution of injection flow rate. The purpose of these valves is to maintain a pre-set water pressure in the pipelines in order to (1) to prevent clogging by degassing, (2) prevent intrusion of oxygen in case of leakage which may cause clogging by precipitation of iron oxides or deteriorated heat exchange due to air in the heat exchanger and (3) provide pressure to regulate flow rates. Regular maintenance reports show that the wells that receive the highest injection load (C2, H1, H3) show more clogging than wells with lower injection loads (Figure 2.6). Even so, after the main injection load switches from H3 to H4 in 2010, well H3 shows increasing specific capacity while the specific capacity of well H4 decreases. Increased clogging for the wells with the highest injection load could be generated by the higher load of suspended particles that pass through the well screen, which is a common phenomenon for recharge wells [140].

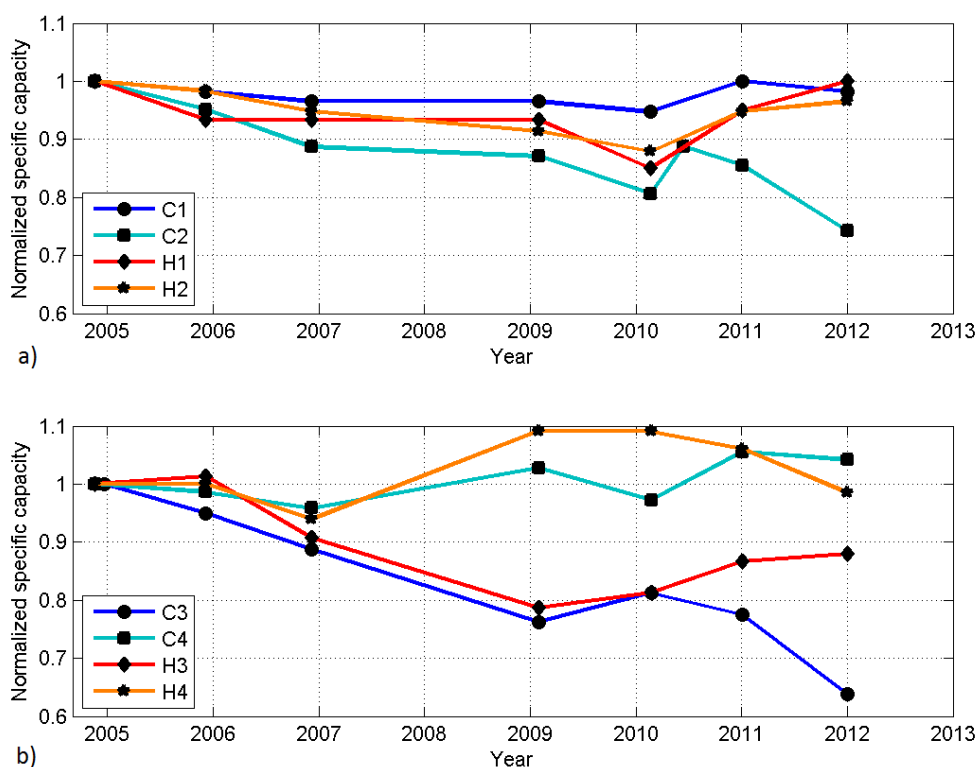


Figure 2.6 Normalized specific capacity the wells in clusters C12 and H12 (a) and C34 and H34 (b). Decreasing specific capacity for wells C2, C3 and H3 illustrates that the wells that receive the highest injection load show most clogging

Comparison with the numerical model shows that extraction temperatures are well resolved by scenario SC2 (Figure 2.7). Only for cluster C34, the measurements show a faster increase of temperature during extraction of cold water. Injection temperatures over the period 2005 to 2012 show high variability compared to the extraction temperatures (Figure 2.8). Injection temperatures during cooling mode vary between 11 and 18 °C, and injection temperatures during heating range from 6.5 to 9.5 °C. Due to depletion of the thermal storage, extraction temperatures approach the natural aquifer temperature near the end of a recovery phase. Because for cold storage generally more water is extracted than injected (Figure 2.9a), this effect is stronger for retrieval of cold than for retrieval of heat. Although the VR of C12 is generally larger than the VR of C34, extraction temperature in C34 approaches the natural aquifer temperature faster than in C12.

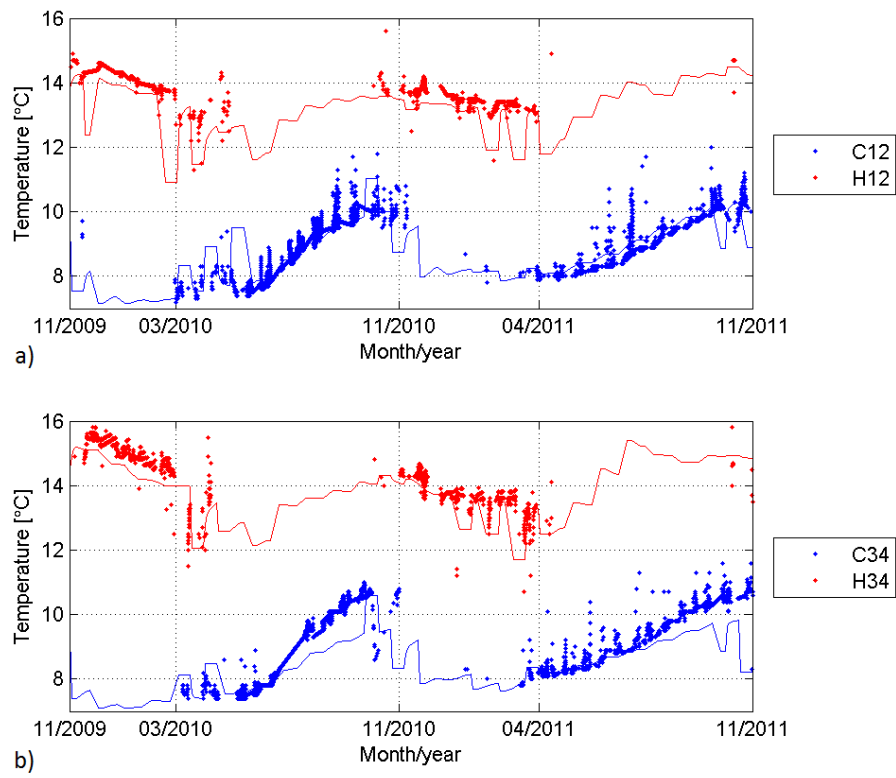


Figure 2.7 Comparison between measured extraction temperatures (dots) and modelled injection/ extraction temperatures (solid line) for clusters C12 and H12 (a) and C34 and H34 (b)

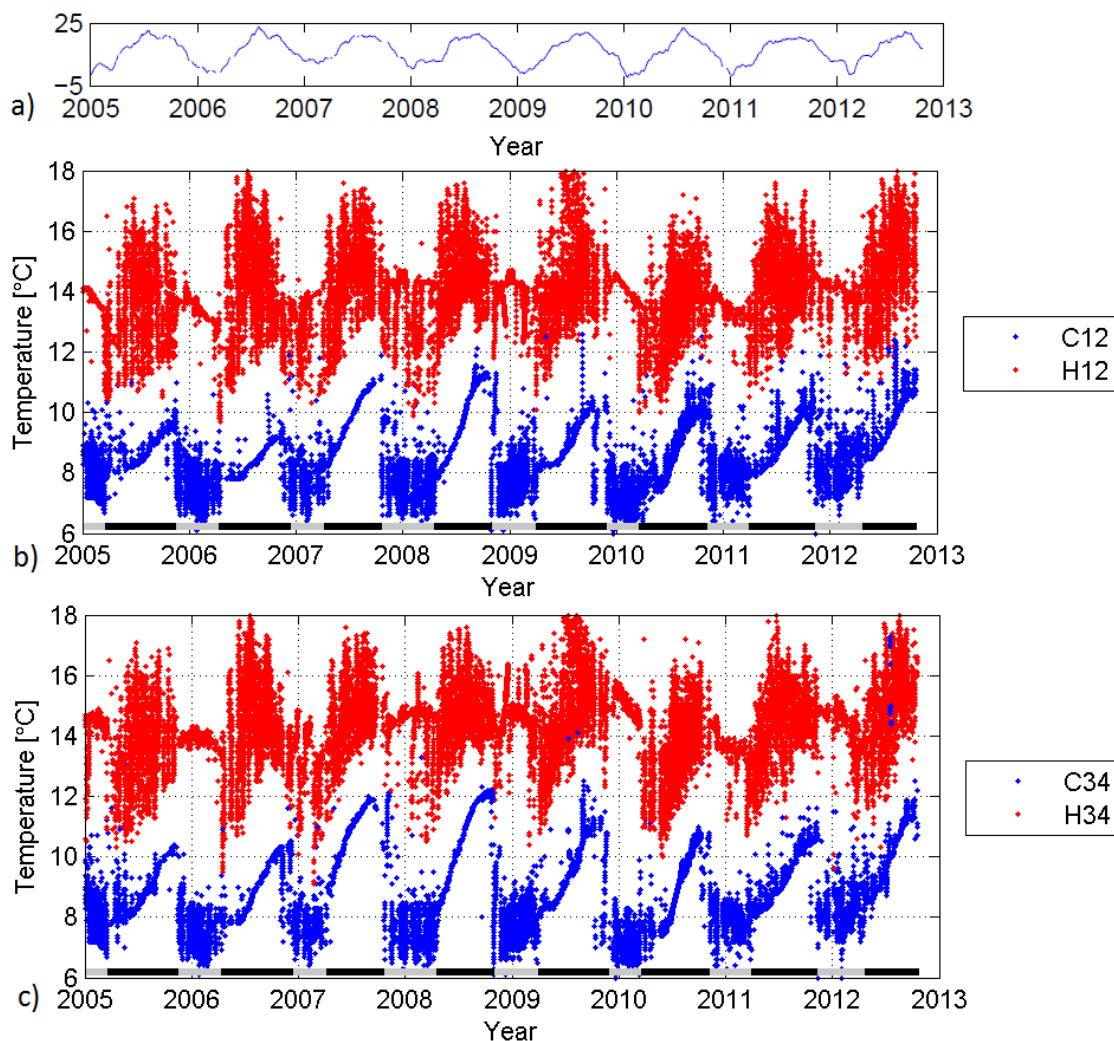


Figure 2.8 Average outdoor temperature during office hours (8–17 h) (a), injection and extraction temperatures for clusters C12 and H12 (b) and clusters C34 and H34 (c). The mode of the system is indicated below each figure (grey = heating mode, black = cooling)

Thermal recovery

Thermal recovery is determined for each cluster for each storage and recovery cycle (Figure 2.9b). The beginning and end of every storage and recovery cycle is determined from the moment when the system switches between heating and cooling mode (Table 2.4). Note that in spring and autumn, the system may switch several times between heating and cooling mode according to climate variability. Pumped water volumes in these periods are small compared to the total extracted volumes during the whole heating and cooling season, such that the calculated thermal recovery values are not sensitive to the exact date that is used to define the beginning and end of the storage and recovery cycles.

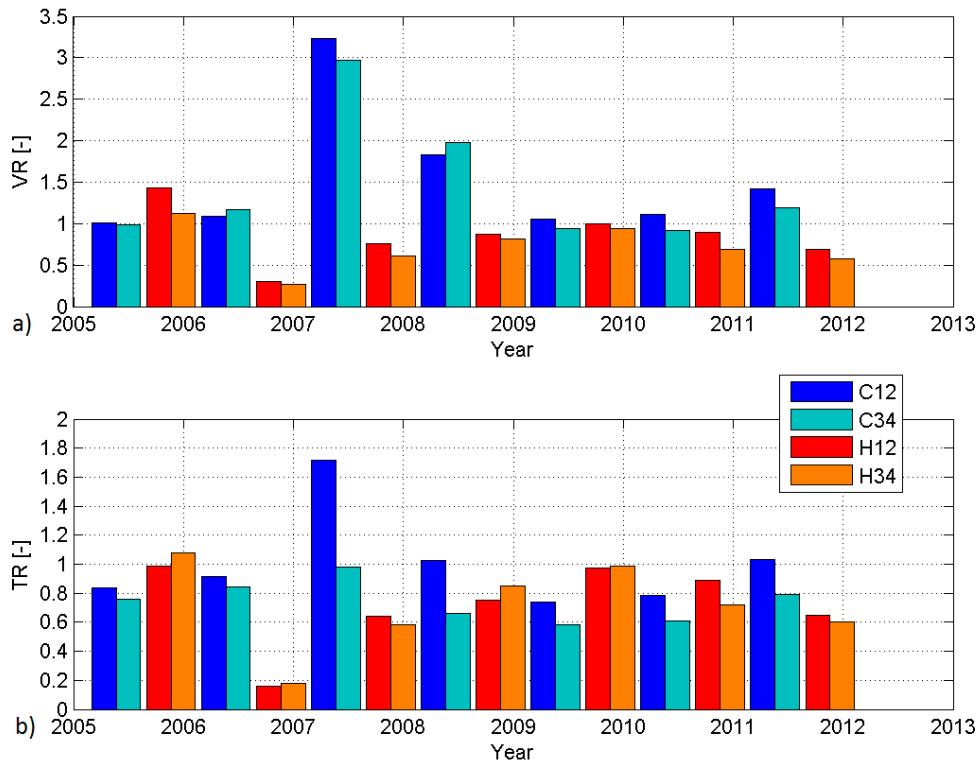


Figure 2.9 Volume recovery (a) and thermal recovery (b) for each cluster

The average thermal recovery for cold storage is 0.82 and for heat storage 0.68. However, from year to year, thermal recovery varies between 0.2 and 1.7. The explanation for this large variation in thermal recovery values is that, in some years, only a small portion of the injected water is extracted, while in other years much more water is extracted than what was injected in the preceding season (Figure 2.9a). For example in winter 2006/2007, a thermal recovery of only 0.17 is observed. Average outdoor temperature during office hours in winter 2006/2007 was high (7.44 °C) compared with the average (5.16 °C) for the years 2005 to 2012. Therefore, the demand for heating was less than in other years. Because only a small part of the injected water was extracted (VR=0.28; Figure 2.9a), only a small part of the injected heat is recovered. The small volume extracted for heating automatically means that also only a small volume of cold water is injected. While extracting a normal amount of water in the summer of 2007 for cooling, the volume ratio becomes very large (VR=3.23 for C12). The thermal recovery for cluster C12 at the end of this summer is 1.72. It was possible to achieve a thermal recovery larger than 1 because not only the small amount of cold that was injected in winter 2006/2007 is extracted, but also remnant cold from previous years.

Table 2.4 Effective dates that the system switches between heating and cooling mode, length of each mode and energy balance ratio (EBR) calculated for each year, starting with a cooling season, followed by a heating season

Date	System mode	Length of mode [d]	EBR
2005-03-19	Cooling	239	
2005-11-13	Heating	151	-0.22
2006-04-13	Cooling	243	
2006-12-12	Heating	117	0.54
2007-04-08	Cooling	195	
2007-10-20	Heating	182	-0.05
2008-04-19	Cooling	192	
2008-10-28	Heating	155	-0.14
2009-04-01	Cooling	240	
2009-11-27	Heating	111	-0.15
2010-03-18	Cooling	234	
2010-11-07	Heating	146	-0.01
2011-04-02	Cooling	223	
2011-11-11	Heating	165	0.13
2012-04-24	Cooling		

The ability to retrieve thermal energy from the subsurface is assessed by dividing thermal recovery by volume recovery (Figure 2.10). TR/VR values for the warm clusters (H12 and H34) show an increasing recovery for subsequent storage/recovery cycles during the first 10 years after start-up of the system. The reason for this is that part of the energy that is not recovered reduces energy loss in following storage/recovery cycles. Due to the high variability in VR, this increase is not well visible by considering only TR values (Figure 2.9b). As a result of the high VR for cold storage (C12 and C34) in summer 2007, the cold storage is fully depleted and ambient temperature around these wells is close to the natural aquifer temperature (12.3 °C). Figure 2.10 shows that the years following this event are characterized by high energy losses since the surroundings of the wells have to adapt again to the injection temperatures. The same effect can be observed in the extraction temperatures of C12 and C34 (Figure 2.8) where extraction temperatures in summer 2007 approach the natural aquifer temperature, while in the following years, extraction temperature decreases due to smaller energy losses.

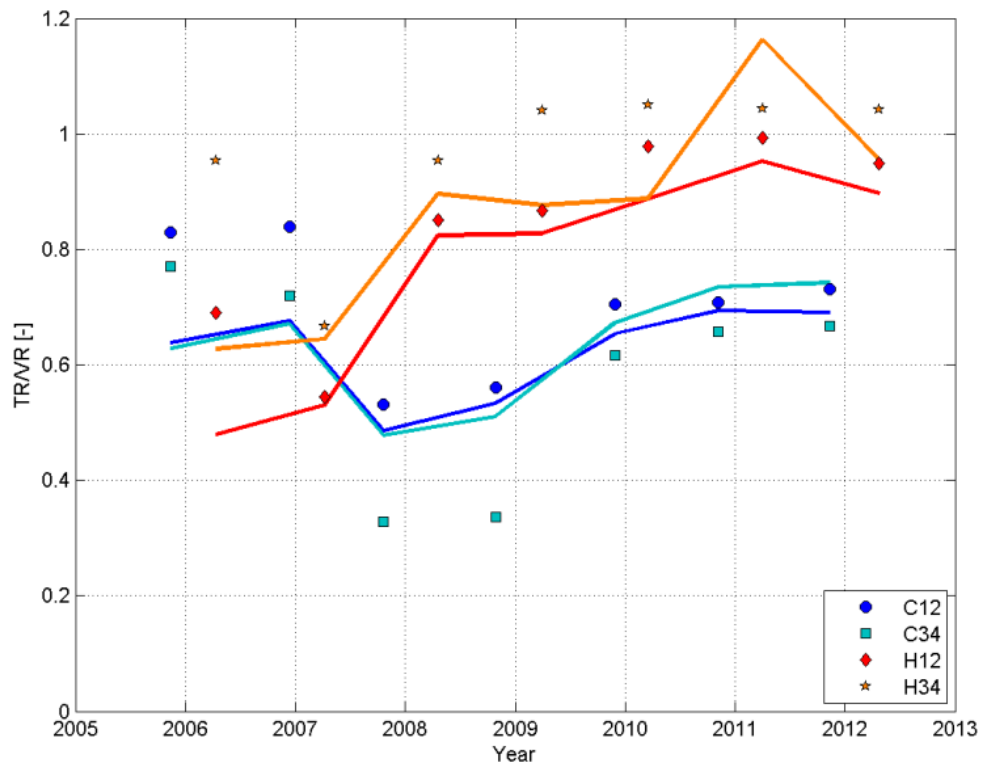


Figure 2.10 Comparison of estimated TR/VR values (symbols) with TR/VR determined by the numerical model, scenario SC2 (solid lines)

Since for heat storage generally more water is injected than extracted ($VR < 1$), extraction temperatures remain close to the injected temperature (Figure 2.8) resulting in a value TR/VR close to 1 (Figure 2.11). For VR larger than 1, the extracted water temperature approaches the natural aquifer temperature and TR/VR decreases.

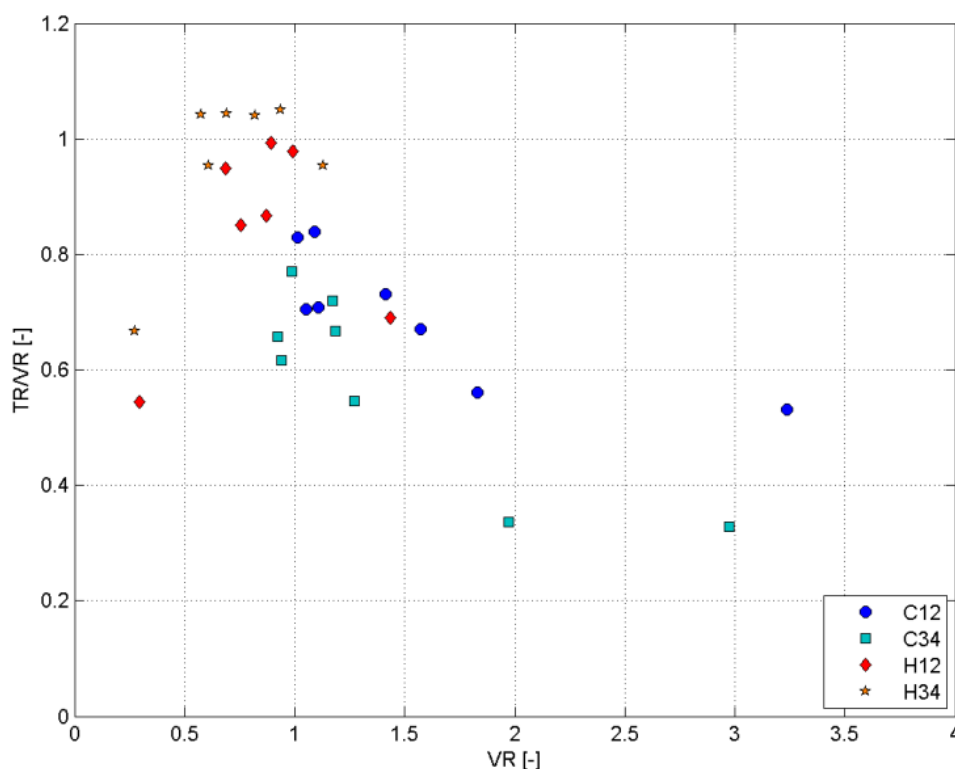


Figure 2.11 TR/VR is close to 1 for small VR since extraction temperatures remain close to the injection temperature. For larger VR the ratio TR/VR decreases as extraction temperature approaches the natural aquifer temperature

Thermal balance

Over the period 2005 to 2012, approximately the same amount of heat and cold is extracted from the subsurface, resulting in a cumulative energy balance ratio below 0.1 (Figure 2.12). Yearly EBR values, however, vary between -0.22 and 0.54 (Table 4). The yearly EBR values are determined from the start of the cooling season to the end of the subsequent heating season. The large EBR in 2006 is a result of the small amount of heat extracted in winter 2006/2007, while in summer 2006, a normal amount of cold energy is extracted. As can be seen from Figure 2.12, this imbalance is compensated by a negative EBR in the years following 2006 (Table 2.4).

The cumulative VBR varies between 0.05 and 0.15. This shows that since 1 January 2005 between 11 and 35% more water is extracted during the cooling season than in the heating season. The cumulative EBR on the other hand varies between 0 and -0.1 , meaning that on average, between 0 and 18% less cold energy is extracted than heat. This is possible because the average temperature difference between extraction and injection in cooling mode ($4.9\text{ }^{\circ}\text{C}$) is

smaller than in heating mode (6.4 °C). Every moment that the cumulative EBR is equal to zero, the system is exactly balanced, meaning that there is no net heating or cooling of the subsurface.

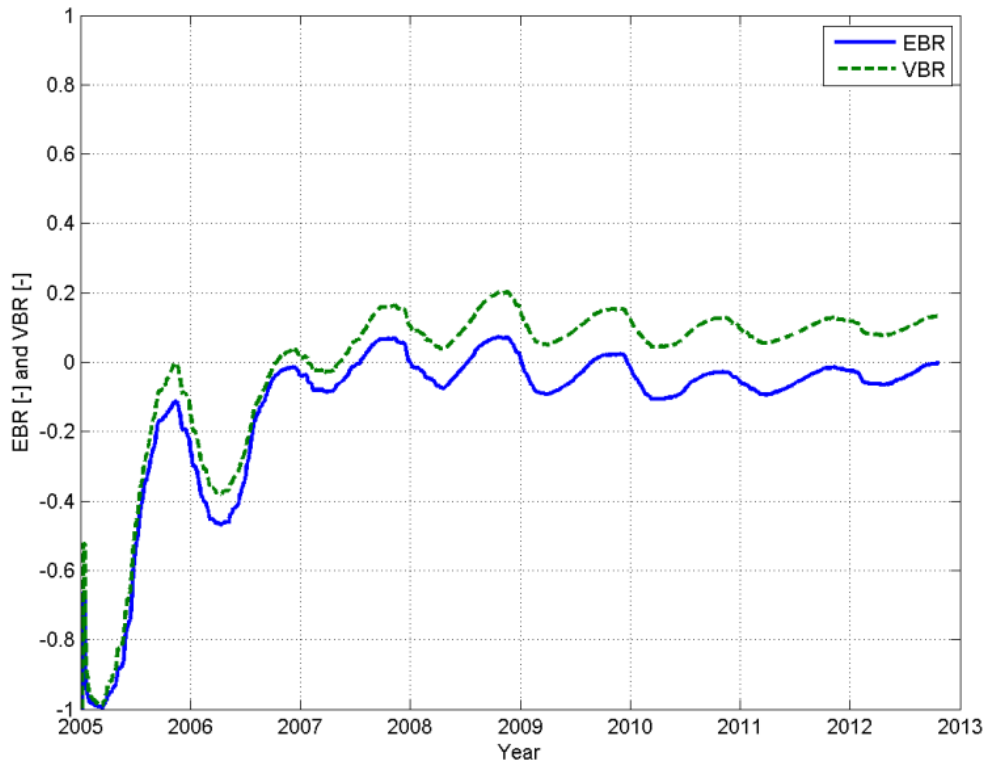


Figure 2.12 Cumulative EBR and VBR of the system

Subsurface temperature profiles

With DTS, one can obtain detailed insight in the thermal behaviour of the subsurface. Storage and recovery of thermal energy is demonstrated in Figure 2.13, where measured temperatures are averaged over the depth range of the well screens (15–48 m bgl). In December 2010, cables P1, P2 and P3 show a rapid decrease in temperature following injection of cold water in cluster C12. As the thermal front of this injected cold water successively passes the monitoring cables, temperature remains constant and equal to the injection temperature of 7.8 °C until the end of the heating mode, 2 April 2011 (Table 2.4). After switching to the cooling mode, temperatures rise gradually to the natural aquifer temperature as the cold storage is being depleted in November 2011. With the system in heating mode (injection of cold water), temperature at P1 decreases; however, reacting to the relatively warm winter until mid-January (Figure 2.13), the thermal front does not reach cable P2 until the second half of January when heating demand and associated flow rates increase following colder weather conditions.

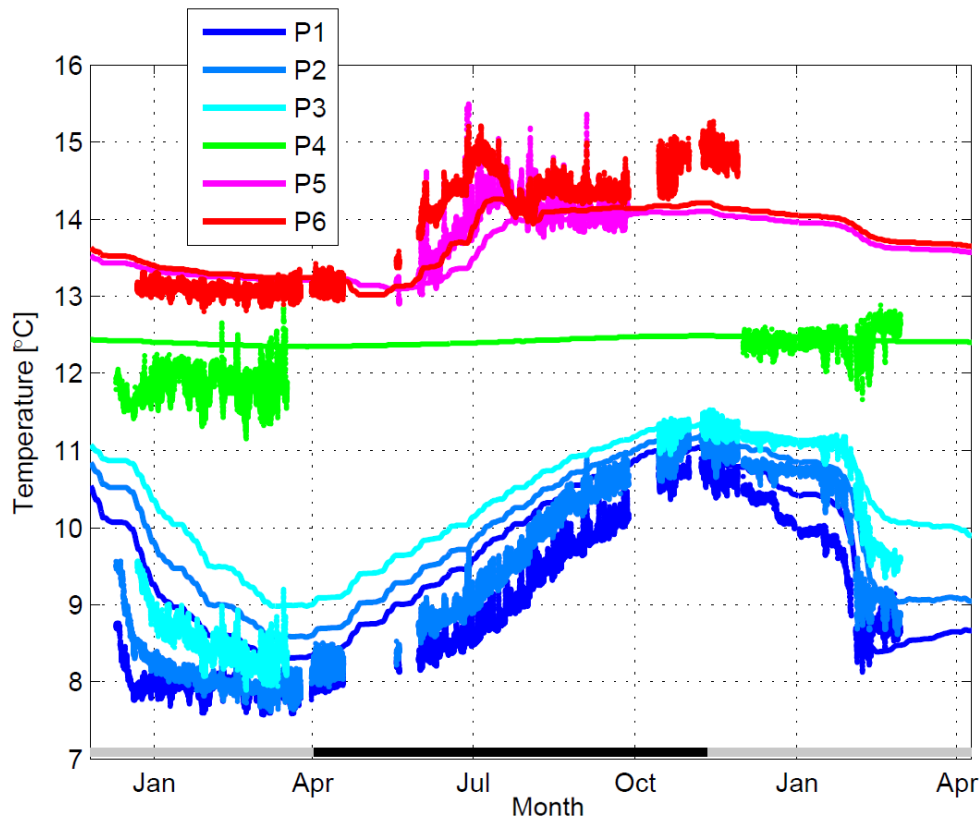


Figure 2.13 Comparison of measured subsurface temperatures averaged between 15 and 48 m bgl (dots) and modelled temperatures with scenario SC2 (solid line) from December 2010 to March 2012

Irregular injection temperatures in the warm wells of cluster H12 during summer 2011 (Figure 2.8) result in irregular subsurface temperatures at cables P5 and P6. Still, there is clear heating of the subsurface to 15 °C (equal to the average injection temperature) during injection of heat in the summer of 2012.

A slight heating from 12.3 in 2005 to 12.8 °C in 2012 of the subsurface is observed around cable P4. Considering the uncertainty in temperature measurements, it is not clear whether this is an artefact of the temperature calibration or whether the subsurface is really heating up. Operational data show that, since 2005, the total volume of hot water injected is larger than the volume of hot water that was extracted, which could result in a gradual expansion of the thermal plume near the wells used for heat storage and a gradual increase in temperature at cable P4. Model results using the reconstructed flow rates and injection temperatures (SC2) indicate a much smaller temperature increase of only 0.15 °C at cable P4. The observed temperature increase at P4 seems independent of depth, which could indicate that this is rather a calibration error than a true effect.

Evolution of the temperature profile in cable P1 is shown in Figure 2.14 for the cooling season (2 Apr 2011 to 11 Nov 2011) and heating season (11 Nov 2011 to 24 Apr 2012). The positions of the well screens in C1 are indicated by black lines at the left side of Figure 2.14. At the start of the cooling season, the cold storage is charged maximal and temperatures at P1 are around 7.8 °C over the whole length of the well screen. As water is extracted from cluster C12 during the cooling season, temperature at P1 rises as the cold storage is being depleted. The temperature increase is largest at the depth of the upper well screen. At the end of the cooling season (11 Nov 2011), temperature at P1 is at its maximum. Following injection of cold water, temperature decreases again to approximately 8.2 °C at the end of the heating season. As in the cooling season, the largest temperature change occurs at the depth of the upper well screen. Over the depth of the upper well screen, the part between 21 and 24 m bgl shows the fastest decrease in temperature. Temperature at the depth of the other well screens also changes during the season, but the amplitude of temperature changes is smaller and changes occur more slowly. Therefore, the temperature profiles show that the two lower screens show an inferior performance compared to the upper screen. This can be explained for the second screen, because this filter is located in fine sand (Figure 2.2). The lowest screen, however, is in a sand layer and should perform similar to the upper screen.

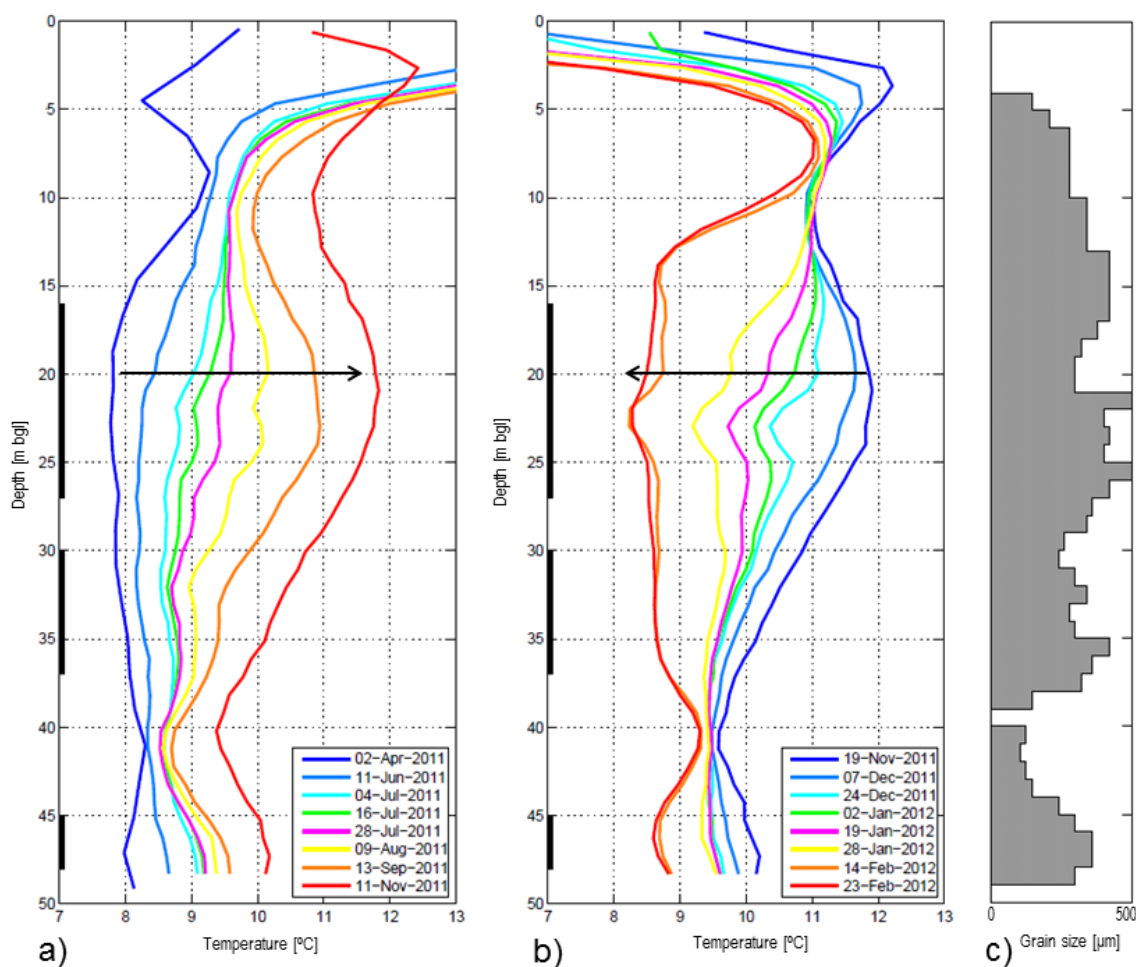


Figure 2.14 Subsurface temperatures in cable P1 during cooling mode (a), heating mode (b) and average grain size (μm) along well C1. Screen sections in well C1 are indicated by the black line at the left of the figure

The temporal evolution of temperature at different depths was investigated with DTS. Comparing the temperature evolution at several depths in cable P6 (Figure 2.15a) and cable P2 (Figure 2.15b) shows the different behaviour at different depths. At P6, the results of model scenario SC1 systematically overestimate subsurface temperatures. Taking into account actual well fluxes and injection temperatures, scenario SC2 reproduces more closely the temperature increase in P6 due to injection of hot water (Figure 2.16a). At location P2 (Figure 2.15b), the results of model scenario SC1 show that, in the design, temperature was expected to decrease to lower values during injection; and, during extraction, temperature would not rise as much as it does in the measurements. In the design, the cooling and heating season were both assumed to be 182.5 days. From the reconstructed flow rates, it becomes clear that the cooling season (221 days) is on average longer than the heating season (144 days) such that the timing of observed

temperature changes is different from than in scenario SC1. Using the reconstructed flow rates and injection temperatures (SC2) improves not only the fit with the data but, also in this case, the high dynamics at 21 m bgl are not reproduced. At this depth, the thermal front shows a much sharper breakthrough curve in the measurements, both for injection as for extraction. Accuracy of the models is demonstrated by comparing measured and modelled subsurface temperatures at P2 and P6. The vertical temperature variations shown by the measurements are represented by a band around the average temperature difference $T_{measured} - T_{modelled}$.

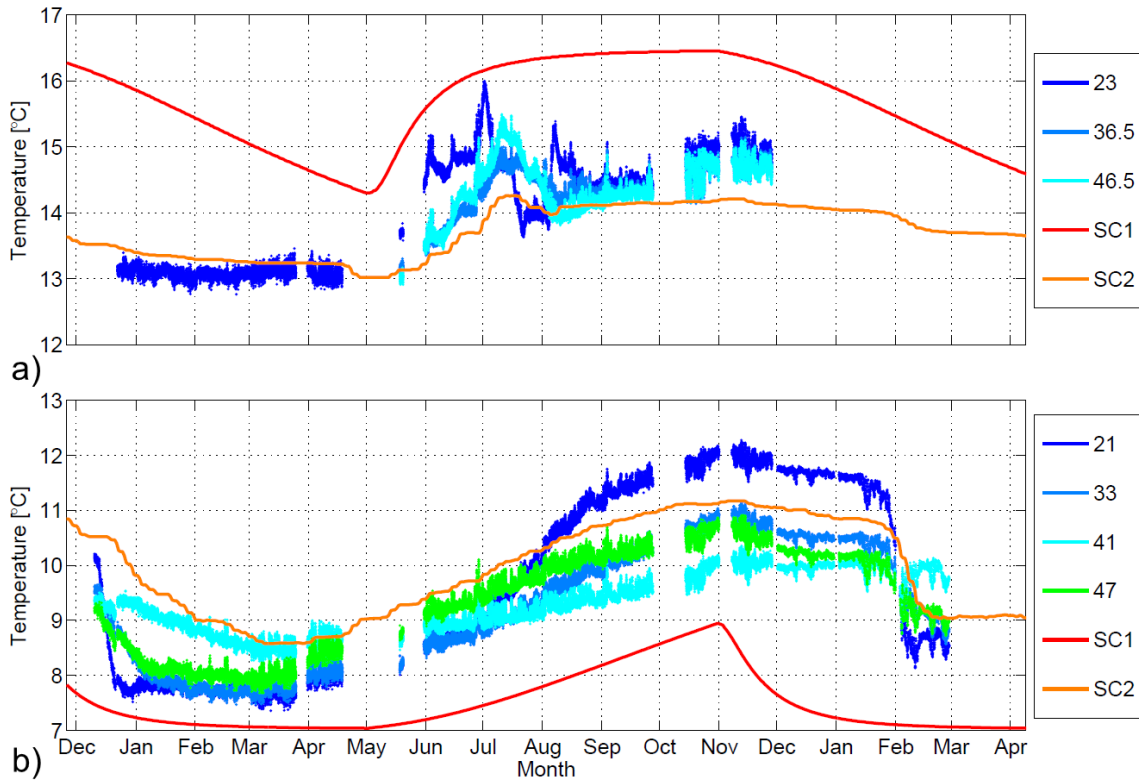


Figure 2.15 Comparison of temperature evolution at (a) P6 at the depth of the filter screens (23 and 46.5 m bgl), in between two filters (36.5 m bgl) and at (b) P2 at the depth of the filter screens (21, 33 and 47 m bgl), in between two filters (47 m bgl). Temperature evolution at P6 and P2 according to model scenarios SC1 and SC2 from December 2010 to March 2012

At location P6 (Figure 2.16a), the difference between SC1 and measured temperatures is between 1 and 3 °C. The fit is improved by taking into account measured fluxes and injection temperatures (SC2). At location P2 (Figure 2.16b), the temperature difference of SC1 compared to measured temperatures is particularly large during thermal breakthrough (Nov 2011 to Jan 2012), whereas for P6, SC2 improves the fit with the data. Average differences between measured and modelled temperature at each of the observation locations are given in Table 5. In general, the measured breakthrough curves of the thermal front at P2 and P6 are steeper than shown by both models, which could indicate an overestimation of thermal diffusion or

dispersion. Vertical temperature variations are between 1 and 3 °C and are highest during thermal breakthrough.

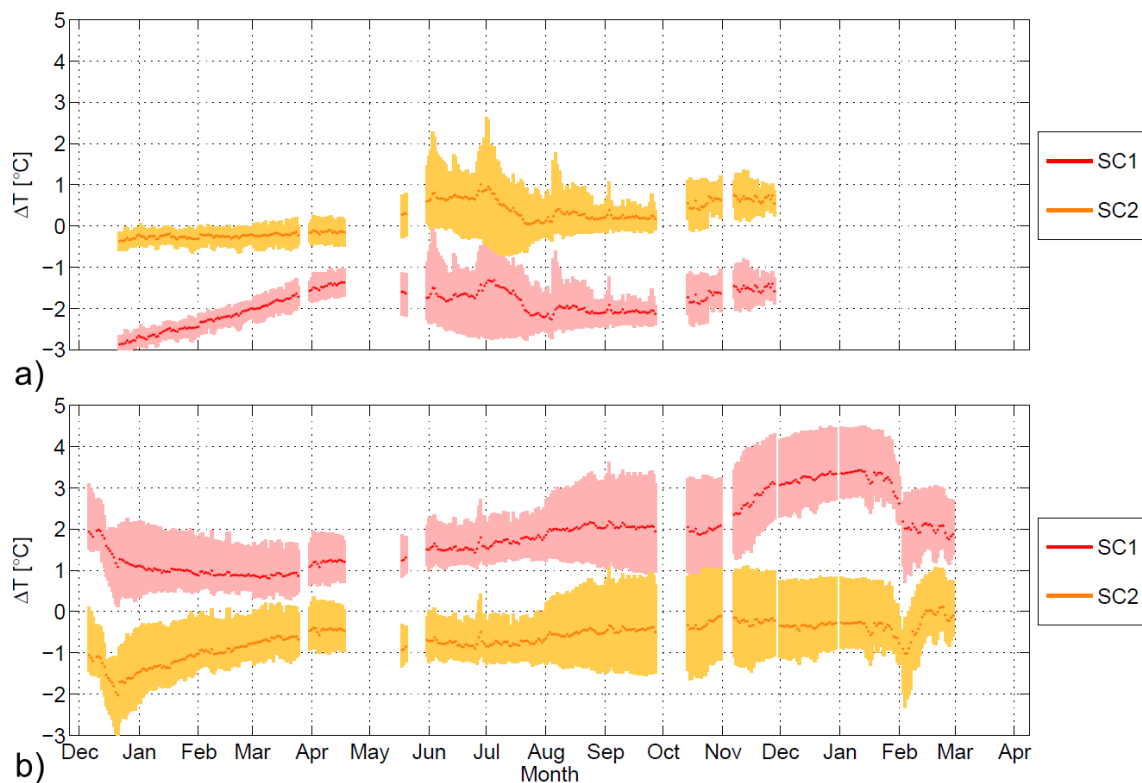


Figure 2.16 Difference between measured aquifer temperature and modelled aquifer temperature for scenarios SC1 and SC2 at location P6 (a) and P2 (b) from December 2010 to March 2012. The observed variation in aquifer temperature in the range 20 to 50 m bgl is presented by the band around the average difference $T_{\text{measured}} - T_{\text{observed}}$

Table 2.5 Average difference between measured and modelled subsurface temperatures (°C) at location P2 and P6 over the vertical extent of the aquifer used for thermal storage (20 – 50 m bgl)

	P1	P2	P3	P4	P5	P6
SC1	1.56	1.85	1.91	0.27	-1.93	-1.91
SC2	-0.75	-0.62	-0.52	-0.40	0.26	0.26

2.4 Discussion

Thermal recovery

Analysis of injection and extraction flow rates and temperatures shows that there is considerable variability in thermal recovery values (Figure 2.9). In the period 2005 to 2012, thermal recovery values range between 0.2 and 1.7. The thermal recovery, normalized to volume recovery, reproduces the increasing trend for subsequent storage cycles (Figure 2.10), which is shown in

several modelling studies [16, 69, 120] and in a field experiment [141]. However, it must be noted that when energy is extracted until the extraction temperature reaches the natural aquifer temperature (as is the case in summer 2007; Figure 2.8), the aquifer returns to its natural temperature and it will take several storage cycles until thermal recovery increases again to what it was before this event. When equal volumes of water are extracted as injected, approximately 75% of the injected energy is retrieved. Previous field experiments show thermal recovery values between 18.9 and 68% for several small-scale field experiments [142]. For a larger field experiment, where 55 000 m³ water of 55 ° C is injected and recovered during a 6-month cycle, Molz et al. [141] report thermal recovery values of 66 and 76% for two successive storage and recovery cycles. For a similar field experiment, recoveries of 56 and 45% were achieved [143]. The high values for thermal recovery presented in this study are expected to result from the low regional groundwater velocity (5 m/yr) and improvement of thermal recovery over several years since the start of the system in 2002.

Thermal balance

Analysis of the energy balance shows that the yearly EBR varies between 0.54 and -0.22. Despite yearly fluctuations, the system is able to achieve a cumulative EBR smaller than 0.1 within 3 years after start of the assessment. To achieve an EBR equal to zero every year would in general require additional input of heat or cold energy. Financially and environmentally, it seems more economical to achieve a thermal balance over multiple years, such that the variable energy demand of a building (under influence of climatic variability) is allowed to level out over several years.

Subsurface temperatures

Distributed temperature sensing (DTS) was applied to monitor temperature development around the wells of the ATES system. The permanent setup enabled monitoring of temperature with a high temporal and spatial resolution. With the high temporal resolution, it was observed that thermal breakthrough at the observation locations close to the injection wells occurs within a week (Figure 2.15). For slower temperature fluctuations at longer distance from the wells, less frequent measurements (for example with a mobile DTS setup) would already be useful in the assessment of the thermal influence of the ATES system. The spatial resolution allowed for observation of heat transport by preferential flow paths and through different parts of the well screen. Care must be taken to properly calibrate DTS data. Although most devices have internal calibration, additional calibration (for example by looping one or more sections of the cable through a bath with constant or controllable temperature [144, 145]) is needed to arrive at

absolute temperatures with high precision. Absence of calibration baths resulted, in this case, in a precision in the order of 0.5 °C (Figure 2.13).

Measurements of subsurface temperatures indicate that the majority of the water (and energy) is injected through the upper screen and is not equally distributed over the total thickness of the aquifer (30 m) as is the case in the design model. The reason for this unequal flow rate distribution cannot be deduced from the temperature measurements alone. Description of drilling materials during flush drilling show the largest average grain size to be between 21 and 27 m bgl (Figure 2.14c), which could indicate a region of higher hydraulic conductivity, resulting in higher flow rates in this part of the well screen. However, the techniques used to drill and develop the wells could also result in higher productivities in shallower parts of the well screen. The strong response to injection and withdrawal of heat observed in the zone from 22 to 24 m bgl does indicate the presence of preferential flow paths. The drilling description characterizes this section as very coarse sand with pebbles, suggesting higher hydraulic conductivity values and a higher contribution to the total flow rate. It is unlikely that development of the wells focuses on such a discrete part of the upper well screen. Movement of heat and cold in discrete zones is also reported by Bridger and Allen [146] for a group of ATEs systems in a sand/gravel aquifer.

The consequence of higher than average flow rates in discrete parts of the well screen is that this increases the radius of thermal influence at these depths. This may influence optimal well-to-well distances in areas with a high density of ATEs systems. To reduce the risk of thermal interference, Dutch design practice is to use a distance between wells of three thermal radii [147]. Thermal radius (R_{th}) is defined as the maximum distance of the thermal front from the injection well in a homogeneous medium, neglecting advection by regional flow, thermal conduction and dispersion (Equation 2.10).

$$R_{th} = \sqrt{\frac{c_{water} \cdot V}{c_{aquifer} \cdot \pi \cdot H}} \quad (2.10)$$

Here, c_{water} and $c_{aquifer}$ are the volumetric heat capacities of respectively water and the aquifer, V is the volume of water that is injected in one storage cycle and H is the length of the well screen.

Comparing designed (970 000 m³/yr) and actual flow rates (520 000 m³/yr) shows that the actual use of the system is approximately half of what it was designed for. Likewise, observed temperature changes in the subsurface are well within the maximum changes predicted by the design model (SC1). An oversized system has the advantages that (1) even in years with exceptionally high energy demand, the thermal influence of the system on the subsurface is

smaller than predicted by the design, (2) the use of the system can be increased in the future and (3) there is a low risk of thermal interference. However, the large volume claim also limits the number of ATES systems that can be realized in this area.

2.5 Conclusion

Assessment of flow rates and injection and extraction temperatures over the period 2005 to 2012 demonstrates successful storage and recovery of thermal energy at an ATES system. Average thermal recovery is 82% for cold storage and 68% for heat storage. Analysis of hourly logs of operational data revealed an unexpected distribution of flow rates over the different wells in the multi-well system. While extraction load is equally distributed over the wells, injection occurs preferentially through only some of the wells. These wells show more clogging than the wells that receive a lower injection load. Optimization of the distribution of flow rates over the wells is expected to further increase thermal recovery and reduce clogging of the wells.

Subsurface heat transport around the wells of the ATES system was monitored with high spatial and temporal resolution by applying distributed temperature sensing in fibre optic cables. Although the measurements show unequal distribution of flow rate over different parts of the well screen and preferential flow due to aquifer heterogeneity, no thermal interference is observed. Comparison with a numerical model shows that the distribution of thermal energy around ATES wells is to some extent uncertain due to (1) uncertainty in estimated energy demand of a building and associated uncertainty in projected flow rates, and (2) preferential movement of heat through distinct parts of the well screen and due to aquifer heterogeneity. To reduce the risk of thermal interference, the system in this case study is designed using an overestimation of expected flow rates and safety margins on chosen well-to-well distance. This is desirable for the individual system, but also limits the number of ATES systems that can be realized in this area and consequently the amount of energy that can be saved using ATES. A risk-based cost-benefit analysis that incorporates the risk of thermal interference should determine optimal well-to-well distance from an energetic sustainability perspective.

The impact of aquifer heterogeneity on the performance of aquifer thermal energy storage

Abstract

Heterogeneity in hydraulic properties of the subsurface is not accounted for in current design calculations of aquifer thermal energy storage (ATES). However, the subsurface is heterogeneous and thus affects the heat distribution around ATES wells. In this chapter, the influence of heterogeneity on the performance of a doublet well system is quantified using stochastic heat transport modelling. The results show that on average, thermal recovery decreases with increasing heterogeneity, expressed as the lognormal standard deviation of the hydraulic conductivity field around the doublet. Furthermore, heterogeneity at the scale of a doublet ATES system introduces an uncertainty in the amount of expected thermal interference between the warm and cold storage. This results in an uncertainty in thermal recovery that also increases with heterogeneity and decreases with increasing distance between ATES wells. The uncertainty in thermal balance due to heterogeneity can reach values near 50 percent points in case of regional groundwater flow in excess of 200 m/y. To account for heterogeneity whilst using homogeneous models, an attempt was made to express the effect of heterogeneity by an apparent macro-dispersivity. As expected, apparent macro-dispersivity increases with increasing heterogeneity. However, it also depends on well-to-well distance and regional groundwater velocity. Considering the increasing density of ATES systems we conclude that thermal interference limits the number of ATES systems that can be implemented in a specific area, and the uncertainty in the hydraulic conductivity field related to heterogeneity should be accounted for when optimizing well-to-well distances.

This chapter is published as: Sommer, W.T., Valstar, J., van Gaans, P.F.M., Grotenhuis, J.T.C., and Rijnaarts, H.H.M. (2013). *The impact of aquifer heterogeneity on the performance of Aquifer Thermal Energy Storage*. Water Resources Research 49(12), 8128-8138.

3.1 Introduction

Due to increasing energy demand and concern about emission of greenhouse gasses, groundwater based heating and cooling systems are receiving attention worldwide. Among the different types of energy storage systems, aquifer thermal energy storage (ATES) is suitable for large scale applications like residential areas, shopping malls and utility buildings. Aquifer thermal energy storage is a technology in which sensible heat is temporarily stored in the subsurface through injection and withdrawal of groundwater [114, 121]. The heat capacity of the groundwater is used to transfer heat between a building and the aquifer. Application of ATES results in savings on conventional resources used for heating or cooling, and leads therefore to a reduction of (1) dependence on these resources, (2) costs and (3) CO₂ emissions.

ATES systems in regions with a cold-warm periodicity, like the Netherlands, commonly operate in a seasonal mode [114, 131]. In summertime, cool groundwater is extracted and used to cool down a building. The heated groundwater is injected back into the aquifer through a different well creating a storage of heated groundwater (i.e. warm wells). In wintertime, the flow direction in the system is reversed: the heated groundwater is extracted, used to heat the building and create a cold storage (i.e. cold wells).

The storage efficiency of each ATES well is expressed as thermal recovery (TR), defined as the ratio between thermal energy that is extracted from the subsurface and what was stored (Equation 3.1).

$$TR = \frac{\int_{\text{extraction}} c_{\text{water}} \cdot Q \cdot (T - T_{\text{natural}}) \cdot dt}{\int_{\text{injection}} c_{\text{water}} \cdot Q \cdot (T - T_{\text{natural}}) \cdot dt} \quad (3.1)$$

Here, c_{water} is the volumetric heat capacity of water, Q is the pumping rate, T is the temperature of the water that is injected or extracted, T_{natural} is the natural temperature of the aquifer and dt is a time increment. The integrals in Equation 3.1 can be evaluated over any time period. In our analysis we will consider each cycle of storage and subsequent recovery separately.

Modelling studies of a single ATES well show that thermal recovery is always lower than 100% as a result of heat loss by regional groundwater flow [17] and heat conduction [120, 148, 149]. When the wells for storing cold and warm water are built close together, thermal recovery may be further reduced by thermal interference between the wells [68, 69, 121, 122]. On the other hand, thermal recovery of wells in multi-well systems may increase due to thermal interference between wells with similar storage temperature [150].

Reports of thermal recoveries for actual systems are scarce. Sauty et al. [142] report thermal recoveries between 18.9% and 68% for several small scale field experiments. The lower value for thermal recovery was attributed to the fact that energy was stored close to the surface, leading to high heat loss to the surface. For a larger field experiment, where 55 000 m³ water of 55 °C was injected and recovered during a 6-month cycle, Molz et al. [151] report thermal recovery values of 66% and 76% for two successive storage and recovery cycles. For two similar field experiments, where water of 58.5 and 81 °C was injected, recoveries of 56% and 45% were achieved [152]. The lower value is explained by increased buoyancy flow due to higher storage temperature. More recently, Sommer et al. [130] reported a 7-year average thermal recovery of 82% for cold storage and 68% for heat storage for an operational ATES site in the Netherlands.

Since its introduction in the 1970's, use of ATES has experienced large growth worldwide. Due to increasing demand for sustainable energy, this trend is expected to continue [114]. In the Netherlands, ATES is already used as a standard technique for utility buildings such as offices, hospitals and public buildings [153]. Due to limited space in urban areas, thermal interference between wells is a major concern for large-scale application of ATES. An example of an ATES system where extraction temperatures are negatively influenced by thermal interference in the subsurface is given by Ferguson and Woodbury [47]. To avoid thermal interference, guidelines exist on well-to-well distance [147, 154]. For ATES systems, it is convenient to express well-to-well distance in terms of thermal radii. The thermal radius (R_{th}) is defined as the maximum distance of the thermal front from the injection well in a homogeneous medium and neglecting vertical flow, advection by regional flow, thermal conduction and dispersion (Equation 3.2).

$$R_{th} = \sqrt{\frac{c_{water} \cdot V}{c_{aquifer} \cdot \pi \cdot H}} \quad (3.2)$$

Here, $c_{aquifer}$ is the volumetric heat capacity of the aquifer (groundwater and aquifer matrix), V is the volume of water that is injected in one storage cycle and H is the length of the well screen.

Literature shows diversity in recommended well-to-well distances. Kim et al. [121] report on the basis of numerical modelling that the recovery of thermal energy is not significantly affected when the wells are separated by more than one thermal radius. Kowalczyk and Havinga [122] report an optimal well-to-well distance between 1 and 2 thermal radii for heat storage and as far as possible for cold storage. The Dutch society for subsurface heat storage (NVOE) advises a well-to-well distance of at least three thermal radii to avoid thermal interference [147].

These guidelines and design calculations are based on the assumption of a homogeneous subsurface, while studies for unconsolidated aquifers report widely varying degrees of hydraulic

heterogeneity, of up to 2.1 in terms of the logconductivity standard deviation (σ) [155-160]. Reported correlation lengths of aquifers are in the order of cm to km [156]. Especially heterogeneity in the horizontal direction at the scale of an ATES system or larger may create preferential pathways, reducing ATES performance due to increased advective heat loss or thermal interference between ATES wells.

The role of hydraulic heterogeneity of the subsurface related to ATES performance has received little attention in literature. Previous research includes the modelling of a single ATES well in a heterogeneous aquifer under stagnant flow conditions [161] and the influence of heterogeneity on thermal recovery of a group of ATES systems [162]. Ferguson [2007] uses the geostatistical properties from the Borden aquifer [163] and a carbonate rock aquifer [164] to determine the influence of heterogeneity on the recoverability of thermal energy. For the Borden aquifer ($\sigma = 0.261$) he calculated a reduction of 5.5% in energy recovered with respect to the homogeneous model while for the more heterogeneous carbonate rock aquifer ($\sigma = 1.6$) a reduction of 8.2% is reported. Temperature measurements around ATES wells [130, 146, 165] indicate that heterogeneity gives rise to preferential pathways and short-circuiting between ATES wells. This may not only result in a different thermal efficiency than expected based on design calculations, but also in an increased spatial extent that is used by an individual ATES system, which is not available for other systems in the surrounding [161]. To avoid thermal interaction, wells in heterogeneous media should be placed farther apart than in homogeneous media, leading to a larger spatial claim in the subsurface.

This research elaborates on the effect of heterogeneity on the storage performance of ATES. Heat transport modelling is applied to simulate operation of a doublet ATES system in a subsurface with 3D heterogeneous hydraulic conductivity. Sensitivity analyses are conducted to assess the influence of heterogeneity under different design condition (well-to-well distance, orientation of the doublet with respect to regional groundwater flow) and hydrogeological conditions (groundwater velocity). Since the number of non-interfering ATES systems that can be realized in an area depends on well-to-well distance, this research supports assessment of the potential contribution of ATES to sustainability goals.

3.2 Method

To address the statistical uncertainty in groundwater flow and heat transport in heterogeneous media, a Monte Carlo approach was applied [166]. Ensembles of synthetic 3D heterogeneous hydraulic conductivity fields were generated, in which the operation of a doublet ATEs system was simulated for a period of 10 years. The heterogeneous conductivity fields were generated using GSLIB [167]. Spatial correlation was defined as an exponential covariance function, described by a horizontal and vertical correlation length. The 3D fields that were generated with GSLIB have a zero-mean and unit standard deviation. These were converted to lognormal hydraulic conductivity fields using Equation 3.3.

$$k = e^{\mu + \sigma \cdot r} \quad (3.3)$$

Here k is hydraulic conductivity and r is the spatially correlated random variate generated by GSLIB. The values μ and σ define the mean and standard deviation of the lognormal hydraulic conductivity field. An example is given in Figure 3.1. Preliminary tests showed that the median thermal recovery of an ensemble converges between 10 and 30 members. Therefore, it was decided to limit the ensemble size to 50 members. In addition to the ensemble median, the 10th and 90th percentiles were calculated to show the spread in the results. These percentiles were chosen as being more robust estimators than the minimum and maximum values. The method of Helsel and Hirsch [168] was applied to check the precision at which the percentiles could be estimated.

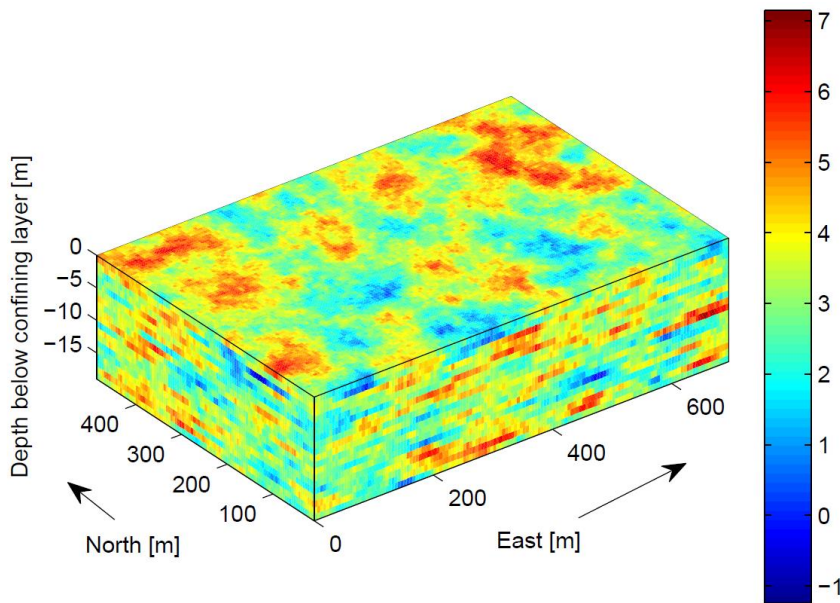


Figure 3.1 Example of a heterogeneous subsurface ($\mu=3.2$, $\sigma=1$, $\lambda_h=104.1$ m, $\lambda_v=2$ m). The colours indicate log conductivity in log(m/d)

Modflow [169] and MT3DMS [170] were used to model water and heat transport. MT3DMS was originally designed to model solute transport. Due to similarity between the solute and energy transport equation MT3DMS can be applied to model heat transport by adopting the following transformations [28, 171]. The thermal diffusion coefficient (D_T) = $k_{bulk}/(n \cdot \rho \cdot c_{p,water})$, where k_{bulk} is the bulk thermal conductivity of the aquifer, n is porosity, ρ is the density of water and $c_{p,water}$ is the specific heat capacity of water; the thermal distribution coefficient (K_d) = $c_{p,solid}/(c_{p,water} \cdot \rho)$, where $c_{p,solid}$ is the specific heat capacity of the solid phase. The dimensions of the ATES system have been chosen to represent ATES systems typically applied for utility buildings [114, 172, 173]. The horizontal grid size was set at 1/10 of the thermal radius, (5.2 x 5.2 m). The 3D heterogeneous conductivity field generated through GSLIB describes the aquifer in which ATES is applied. The aquifer consists of 20 layers with a thickness of 1 m each. The aquifer is bounded on the top and bottom by aquitards. Both aquitards are discretized by 8 layers with thicknesses increasing by a factor 1.5 starting from 1m at the edge of the aquifer. Test calculations showed that further reducing the grid size or increasing the aquitard thicknesses does not influence the calculated thermal performance of the ATES system. The length of the well screens is equal to the thickness of the aquifer layers in the model. To simulate regional groundwater flow, a constant discharge boundary condition was applied to the south boundary and a constant head to the north boundary. The east and west have no-flow boundaries. The north boundary also has a constant temperature equal to the initial aquifer temperature of 10 °C. In the reference model scenario, the doublet was oriented perpendicular to the regional groundwater flow (if present), so that both wells would be affected equally by advective heat loss (wells C1 and W2 in Figure 3.2). The wells were modelled using the MULTI NODE WELL (MNW) package [174, 175]. For wells that are screened over multiple layers, the MNW package distributes the total prescribed well flow rate over the different nodes according to the calculated pressure. Furthermore, a flux weighted extraction temperature in the well has been calculated.

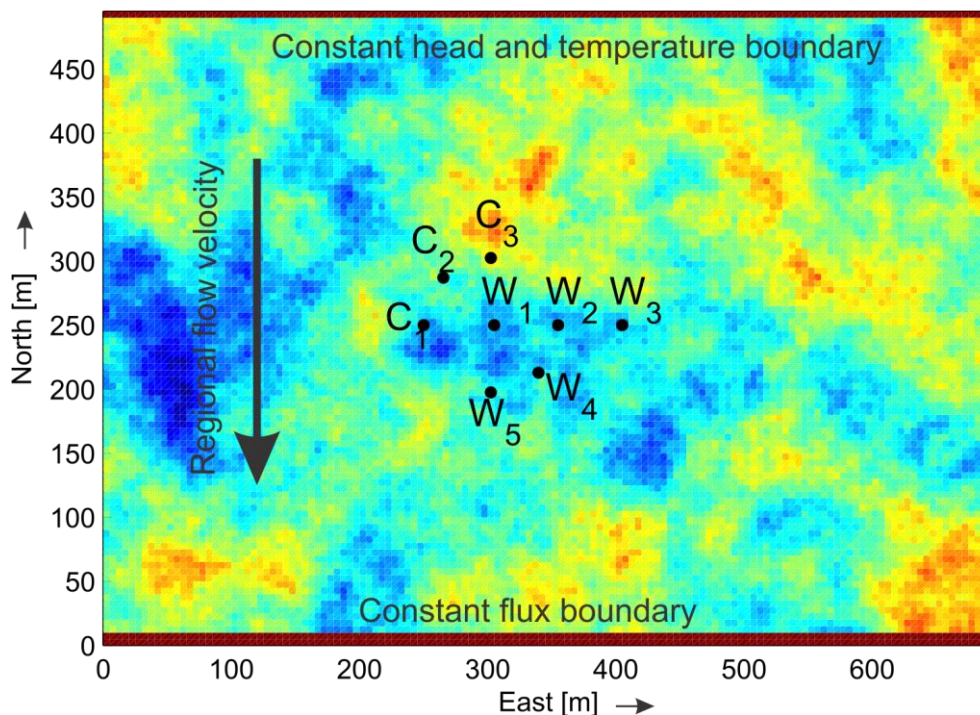


Figure 3.2 Top view of model, with well locations for several scenarios and boundary conditions indicated. The colours indicate log conductivity (see Figure 3.1, for scale). All scenarios use only two wells (or one to simulate infinite well-to-well distance). The reference case combines C1 (cold well) and W2 (warm well). The distance between wells is varied by changing the location of the warm well to W1 or W3. The angle with regional flow is varied by selecting wells C2 and W4 (45°) or C3 and W5 (0°)

The ATES system was modelled using fixed injection temperatures and a closed water volume balance, i.e. equal injection and extraction rates (Q). Injection temperatures were set at 14 °C (summer) and 6 °C (winter). The initial aquifer temperature was fixed at 10 °C throughout the whole domain. The temperature differences due to thermal storage are small enough to neglect the temperature dependency of density and viscosity [146, 173, 176]. Each storage and recovery cycle consists of four months of constant operation of the ATES system during summer and winter, with a two-month passive storage phase in between (Figure 3.3). This mimics the operational strategy commonly observed in actual systems [114, 173].

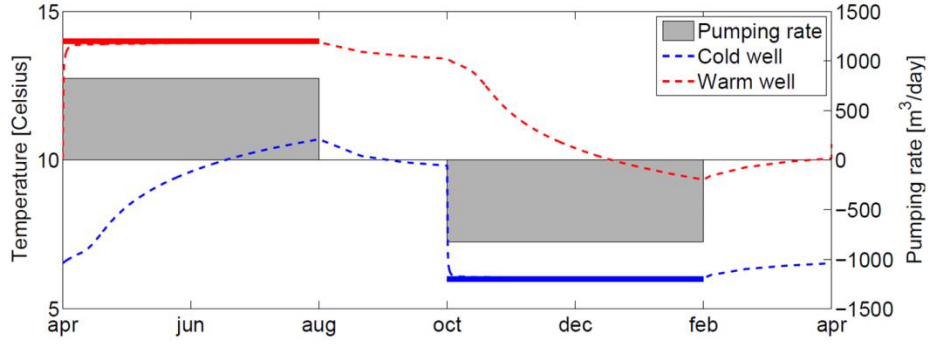


Figure 3.3 Yearly time evolution of pumping rate and temperature in the wells for a typical model run. Injection temperatures are indicated with a solid line. The pumping rate out of the cold well and into the warm well (summer operation) is defined positive, and the pumping rate out of the warm well and into the cold well (winter operation) is defined negative

The results were analysed for thermal recovery (TR , Equation 3.1) and thermal balance (Equation 3.4), expressed in the energy balance ratio (EBR) [131].

$$EBR = \frac{E_{cold}^{extracted} - E_{warm}^{extracted}}{E_{cold}^{extracted} + E_{warm}^{extracted}} \quad (3.4)$$

The amount of cold energy that is extracted from the subsurface ($E_{cold}^{extracted}$) is given by:

$$E_{cold}^{extracted} = \int_{\text{cold extraction}} c_{water} \cdot Q \cdot abs(T_{extr} - T_{inj}) \cdot dt \quad (3.5)$$

Here, T_{extr} is the temperature of the water being extracted, T_{inj} is the temperature of the injected water and the integration is over the period of cold water extraction (cooling of the building). For the amount of warm energy extracted, the same equation was used, now integrating over the period of warm water extraction (heating).

As mentioned before, the dimensions of the reference ATES system (Table 3.1) are representative of a typical ATES system in the Netherlands. However, the effect of heterogeneity on the performance of the ATES system may depend not only on the degree of heterogeneity but also on the configuration of the ATES system and hydrological conditions. To explore the effect of these conditions on ATES performance, local sensitivity analyses were performed by varying the following parameters separately with respect to the reference case: (1) horizontal correlation length, (2) logconductivity standard deviation, (3) well-to-well distance, (4) regional

groundwater flow velocity, and (5) orientation of the doublet system with respect to the regional flow (Table 3.2).

Finally, the possibility of representing heterogeneity by an apparent macro-dispersivity is investigated. This could enable the use of homogeneous models, which are less computationally demanding. To this end, for each heterogeneous scenario, a series of homogeneous models was generated with longitudinal dispersivity ranging from 0 to 50 m, where the reference value is a dispersivity of 0 m (Table 3.1). The hydraulic conductivity field for the homogeneous models is obtained by setting σ to zero in Equation 3.3. Model results for each series were used to derive a relation between model dispersivity and calculated thermal recovery. Apparent values for macro-dispersivity were determined by fitting the thermal recovery of the ATES system as calculated by the heterogeneous model with the thermal recoveries of the series of homogeneous models with varying dispersivity. The practical applicability of an apparent macro-dispersivity to assess the uncertainty in thermal recovery associated with aquifer heterogeneity is discussed in some detail.

Table 3.1 Model parameter values for the reference case

Grid cells (rows x columns x layers)	140 x 100 x 36
Cell size [m]	5.2x5.2 ($0.1 \cdot R_{th}$)
Cell thickness Layers 1 to 36 [m]	17.1; 11.4; 7.6; 5.1; 3.4; 2.3; 1.5; 1; 20 x 1; 1; 1.5; 2.3; 3.4; 5.1; 7.6; 11.4; 17.1
Distance between wells [m]	104.1 ($2 \cdot R_{th}$)
Pumping rate [m^3 /storage cycle]	100 000
Ensemble size	50
Horizontal correlation length [m]	104.1 ($2 \cdot R_{th}$)
Vertical correlation length [m]	2
Average horizontal hydraulic conductivity [$\log(m/d)$]	3.2
Logconductivity standard deviation	1
Vertical hydraulic conductivity [m/d]	Horizontal hydraulic conductivity/10
Porosity [-]	0.3
Regional flow velocity [m/y]	0
Dispersivity [m]	0
Water density [kg/m^3] ^a	999.7
Water heat capacity [J/kg/K] ^a	4192.1
Water thermal conductivity [W/m/K] ^a	0.58
Solid density [kg/m^3] ^b	2643
Solid heat capacity [J/kg/K] ^b	652
Solid thermal conductivity [W/m/K] ^b	7.69
Thermal distribution coefficient [m^3/kg]	0.000156
Thermal diffusion coefficient [m^2/d]	0.382

Water and aquifer properties from ^aLide [177] and ^bThorne et al. [28]

Table 3.2 Overview of scenarios considered for sensitivity analysis

Parameter (unit)	Range in parameter value	Reference case
Horizontal correlation length (R_{th})	0.2, 1, 2, 5, 20 (=10.4, 52.0, 104.1, 156.1, 1040.7 m)	2 (= 104.1 m)
Standard deviation	0, 0.5, 1, 2	1
Well distance (R_{th})	1, 1.5, 2, 3, ∞^a (=52.0, 78.1, 104.1, 156.1, ∞ m)	2 (=104.1 m)
Regional flow velocity (m/yr)	0, 50, 100, 200	0
Angle between regional flow ^b and doublet system ($^\circ$)	0, 45, 90	90

^a Infinite well separation is simulated by modelling only one well

^b for a regional flow velocity of 50 m/y

3.3 Results

First the effects of heterogeneity on the performance of a typical doublet ATEs system are presented (the reference case, Table 3.1), followed by the results of the sensitivity analysis (Table 3.2) and the apparent dispersivity estimations.

Reference case

Figure 3.4 shows the thermal recovery for the first 10 storage and recovery cycles for the reference model. Plotted are the thermal recovery of an ATEs system in a homogeneous subsurface and the median thermal recovery of the ensemble of heterogeneous models together with the 10 and 90 percentiles. For both the homogeneous and heterogeneous case, thermal recovery increases with every storage and recovery cycle. This has also been observed in previous modelling studies [69, 120, 149] and in field experiments [130, 151]. During the first cycle, part of the thermal energy is lost due to thermal diffusion and dispersion. In the following cycles, the amount of lost energy gets smaller as the surroundings have already warmed up or cooled down because of energy dissipation in the previous cycles. Figure 3.4 shows that for the reference system, thermal recovery in a homogeneous aquifer reaches 75.7% in the tenth recovery cycle.

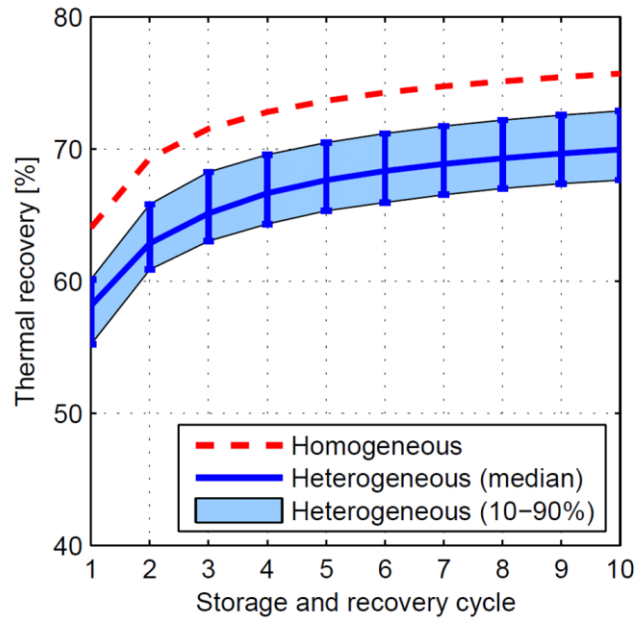


Figure 3.4 Development of thermal recovery of the cold well during the first 10 storage and recovery cycles for the reference case (Table 3.2)

The median thermal recovery in a heterogeneous aquifer is 5.8 pp (percent point) lower than in a homogeneous aquifer. Moreover, uncertainty in the exact conductivity field in case of a heterogeneous aquifer results in an uncertainty in thermal recovery between 67.7 and 72.9% indicated by the 10th and 90th percentiles. Precision of the percentiles is within 1 pp (Table 3.3).

Table 3.3 68% uncertainty intervals [178] for the relevant statistics of the thermal recovery in the 10th year, for the reference case

Heterogeneous ensemble	P10	0.671 – 0.678
	median	0.692 – 0.706
	P90	0.727 – 0.731
Homogeneous case		0.757

Sensitivity analysis: thermal recovery

Results of the sensitivity analysis for thermal recovery, as reached after 10 storage cycles, are shown in Figure 3.5. The results for horizontal correlation length (Figure 3.5a) show that uncertainty increases with increasing correlation length, until the correlation length is equal to the well-to-well distance. For larger correlation lengths, the situation reduces to a layered subsurface and the uncertainty converges. With increasing logconductivity standard deviation (Figure 3.5b), the median thermal recovery decreases from 75.7% in the homogeneous case to 59.0% at a standard deviation of 2. The width of the 10/90-percentiles uncertainty range

increases to 15.0 pp. Due to thermal interference (Figure 3.5c), thermal recovery decreases with decreasing distance between the wells. At the same time, the uncertainty related to heterogeneity increases for small well-to-well distance. At a well-to-well distance equal to 1 thermal radius, some of the heterogeneous realizations show slightly higher TR values than obtained for the homogeneous case. In this case, thermal interference is probably reduced due to a low hydraulic conductivity zone between the wells. Figure 3.5c shows that increasing the well-to-well distance beyond $3 R_{th}$ does not further increase thermal recovery or decrease uncertainty. Due to increased advective heat loss, thermal recovery declines with increasing regional flow velocity. Furthermore the uncertainty range increases from 5.2 pp in case of stagnant groundwater to 15.7 pp with a regional flow velocity of 200 m/yr (Figure 3.5d). The effect of the orientation of the doublet system (see Figure 3.2) with respect to a regional flow velocity of 50 m/yr is shown for the cold well (Figure 3.5e) and the warm well (Figure 3.5f). Here, 0° corresponds to the situation with the cold well upstream of the warm well, and 90° with the doublet perpendicular to the regional flow (Figure 3.2). For the situation where the doublet is oriented parallel with the regional flow the recovery of the downstream well reduces by 8.9 pp with respect to the situation when the wells are oriented perpendicular to the regional flow. The uncertainty range increases from 7.5 pp to 10.5 pp.

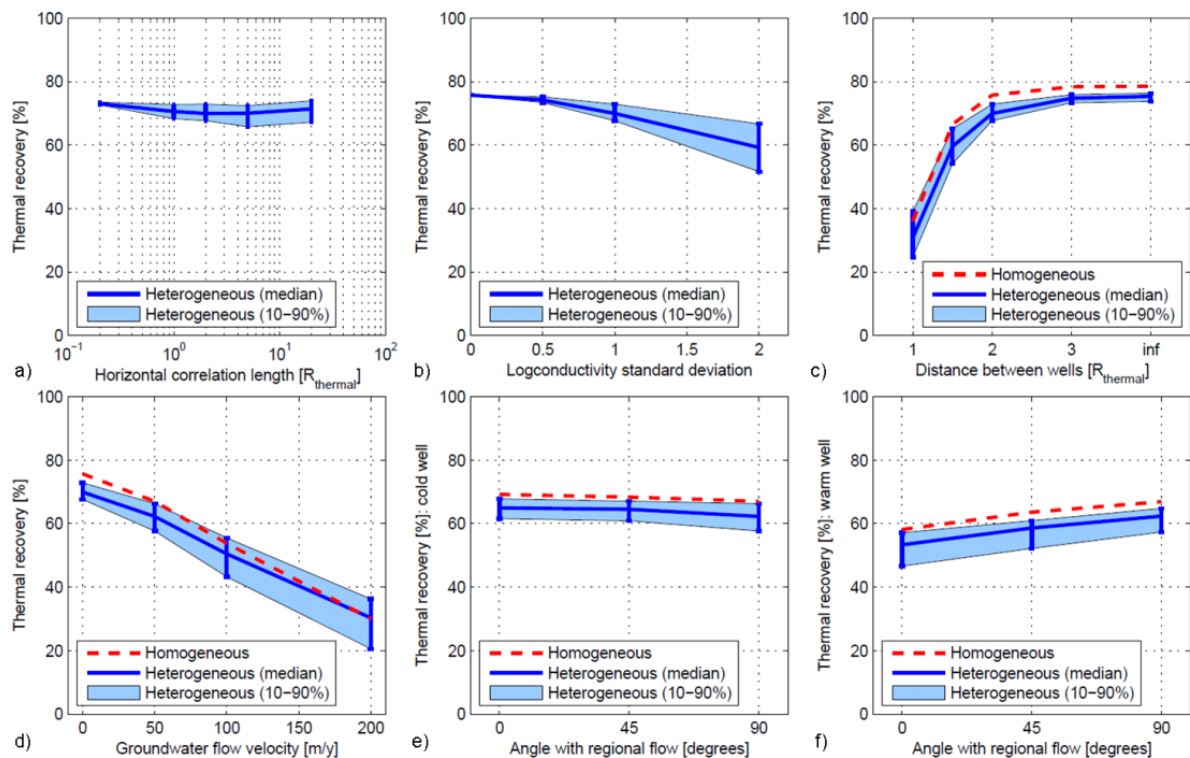


Figure 3.5 Sensitivity analysis of thermal recovery (TR) after 10 storage cycles for (a) horizontal correlation length, (b) log conductivity standard deviation, (c) well-to-well distance, (d) groundwater velocity, and (e) and (f) the orientation of the doublet system with respect to the regional flow for the cold and warm well (for a groundwater flow of 50 m/yr)

Sensitivity analysis: thermal balance

The influence of heterogeneity on thermal balance is shown in Figure 3.6. Other than for thermal recovery, the median thermal balance for the heterogeneous simulations is similar to the homogeneous case. The median energy balance ratio (*EBR*) is mostly close to zero, meaning that there is no net heating or cooling of the subsurface. Only when the well doublet is at an angle to the groundwater flow direction, a systematic thermal imbalance is observed (Figure 3.6e). Maximum uncertainty is observed when the horizontal correlation length is equal to the well distance (Figure 3.6). The uncertainty increases with increasing logconductivity standard deviation (Figure 3.6) and specifically with increasing groundwater flow (Figure 3.6d). Because of the large spread observed in *EBR* for the ensemble with a flow velocity of 200 m/y, the median value does not significantly differ from zero (at the $p = 0.05$ level). The effect of increasing well distance on uncertainty is small (Figure 3.6c).

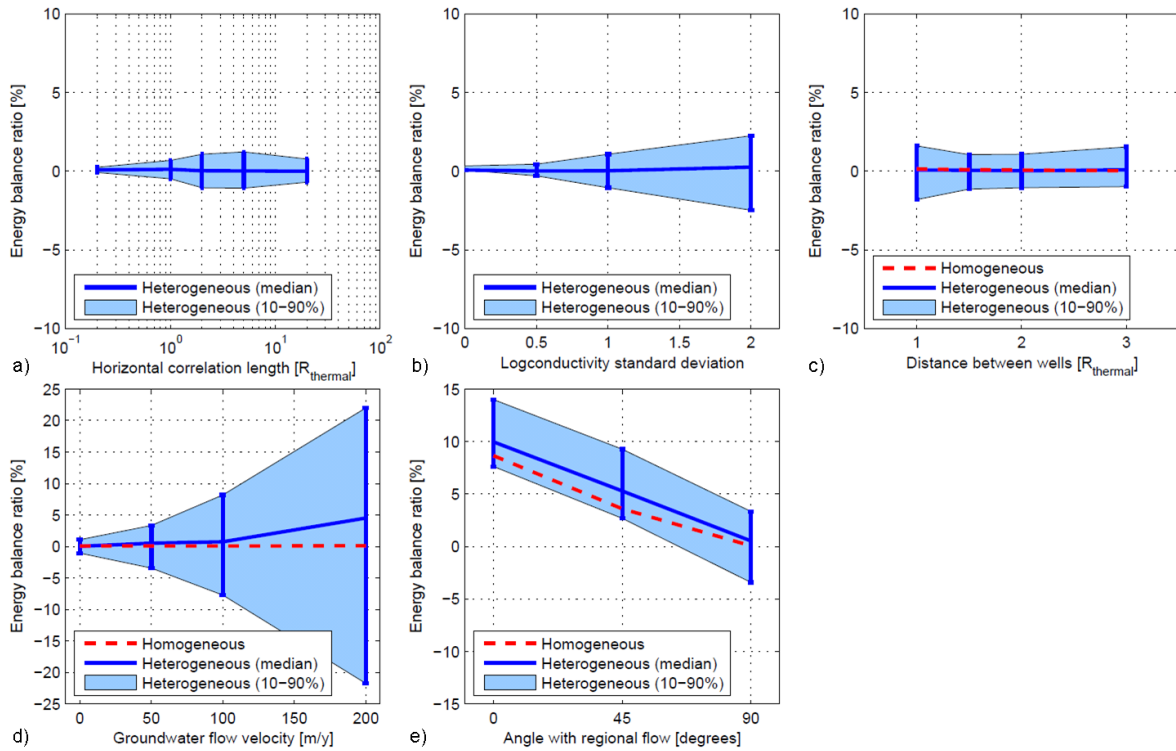


Figure 3.6 Sensitivity analysis of the energy balance ratio (EBR) after 10 storage cycles for (a) horizontal correlation length, (b) log conductivity standard deviation, (c) well-to-well distance, (d) groundwater velocity, and (e) the orientation of the doublet system with respect to the regional flow

Sensitivity analysis: apparent dispersivity

For all heterogeneous model runs in the sensitivity analysis, an apparent macro-dispersivity was determined (Figure 3.7). The median apparent dispersivity increases with increasing logconductivity standard deviation (Figure 3.7b) and is relatively insensitive to changes in the other parameters. The apparent decrease in median apparent dispersivity observed at 200 m/yr (Figure 3.7d) with respect to the median value at 0 m/yr is not significant at the $p = 0.05$ level. As for thermal recovery, the spreading in the ensemble does not increase further when the correlation length becomes larger than the well distance (Figure 3.7a) and increases with increasing logconductivity standard deviation (Figure 3.7b), decreasing well-to-well distance (Figure 3.7c) and especially with increasing groundwater flow velocity (Figure 3.7d). The effect of the orientation of the doublet system with respect to the groundwater flow on both median and uncertainty range is small (Figure 3.7e and Figure 3.7f).

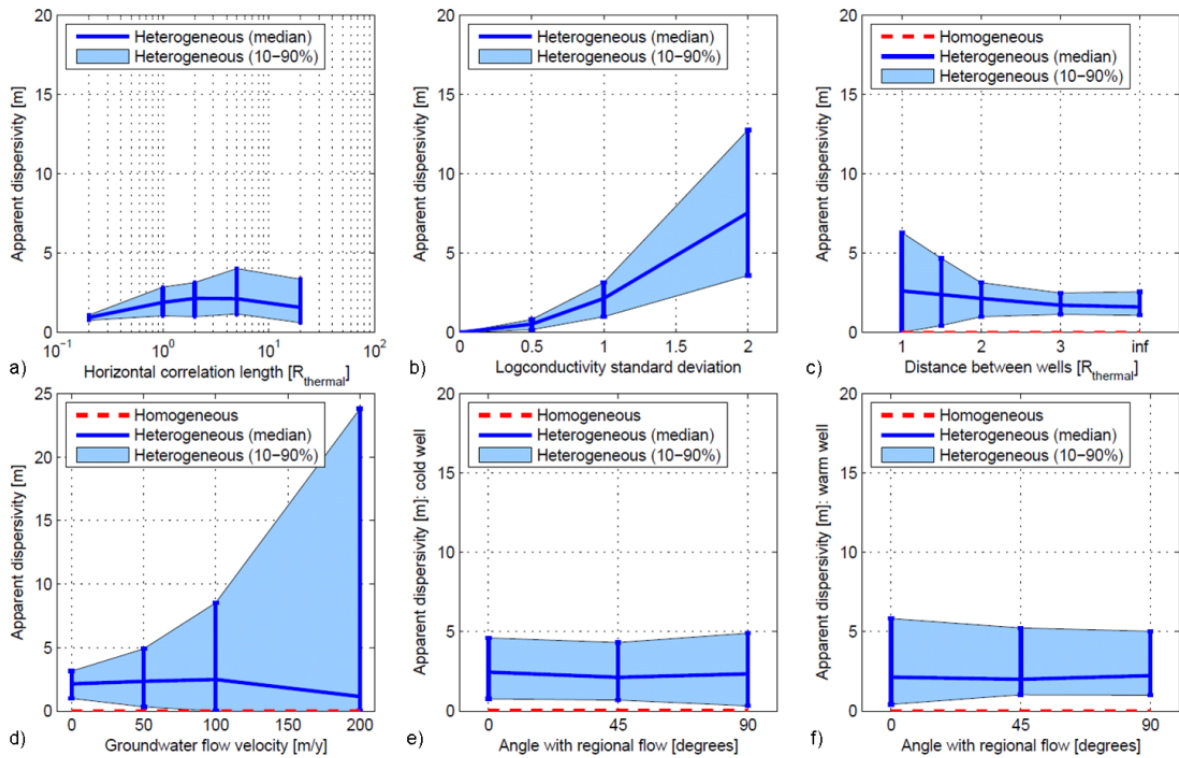


Figure 3.7 Sensitivity of apparent macrodispersivity after 10 storage cycles for (a) horizontal correlation length, (b) log conductivity standard deviation, (c) well-to-well distance, (d) groundwater velocity, and (e) and (f) the orientation of the doublet system with respect to the regional flow for the cold and warm well

3.4 Discussion

From our simulations it becomes clear that the median thermal recovery of an ATES system decreases with increasing heterogeneity (Figure 3.5b). Yet, when thermal interference is reduced due to a low hydraulic conductivity zone between the wells, thermal recovery in a heterogeneous aquifer can be higher than in the homogeneous aquifer, for example at small well-to-well distances (Figure 3.5c) or with high regional groundwater flow (Figure 3.5d).

By comparing our results with similar model simulations for a single ATES well in a heterogeneous medium [161], the effect of two wells operating concurrently is illustrated. Considering two heterogeneous aquifers ($\sigma = 0.261$ and $\sigma = 1.6$), Ferguson [161] also finds a reduction in the amount of extracted thermal energy with respect to the homogeneous case (respectively 5.5% and 8.2% after one cycle). To compare our results, extracted energies are determined for every ensemble member in the first storage/ recovery cycle ($\sigma = 0, 0.5, 1, 2$). Interpolating these values to $\sigma = 0.261$ and $\sigma = 1.6$ gives an average reduction of respectively 13.6% and 20.2%. Our simulations are more sensitive to σ , most likely due to the fact that we consider a doublet well system where preferential pathways result in energy loss due to thermal interference.

Regarding the thermal balance, Figure 3.6 shows that the uncertainty in EBR is most sensitive to heterogeneity at the scale of the ATES system itself. For much smaller correlation lengths, the effect of hydraulic conductivity variations around the wells averages out, such that both wells are affected similarly by the heterogeneous medium. Likewise, for correlation lengths that are much larger than the scale of the ATES system, the 3D heterogeneous medium reduces to a 2D system consisting of homogeneous layers at the scale of the ATES system, thereby influencing the wells equally. In these cases, where both wells are affected similarly by the heterogeneous medium, EBR is close to zero (a balanced system). In a comparative study on 67 systems in the Netherlands [131] it is shown that 67% of the systems have an absolute EBR larger than 15%. Considering that the groundwater flow velocity at these sites is generally below 50 m/yr and doublets are constructed preferably perpendicular to the groundwater flow, non-zero EBR observed in practice, can only for a minor part be attributed to heterogeneity. Our simulations are based on equal volumes of groundwater extracted during heating and cooling mode and fixed injection temperatures. In principle, extracted energy during heating and cooling mode could be changed individually to compensate for observed thermal imbalance during operation of the system. In contrast to this, operational ATES systems frequently experience fluctuating extraction and injection temperatures, as well as imbalances in extracted and injected groundwater volumes, in response to changing cooling and heating demands of the attached

building. These changes in demand are in turn caused by changing outdoor conditions and are assumed for a large part to be responsible for ATES energy imbalances.

Considering the computation time needed to perform a Monte Carlo type simulation using heterogeneous hydraulic conductivity fields, it would be convenient to express the effect of heterogeneity in a single, a priori determined parameter such as macro-dispersivity, enabling the use of homogeneous models. Analytical solutions for the relationship between macro-dispersivity and heterogeneity have been derived for both solute transport [156, 179, 180] and heat transport [181]. The solutions differ in the method that is used to derive them (e.g. homogenization / spectral analysis) and the assumptions used (e.g. parallel/ radial flow fields, isotropic/ anisotropic conditions, spatial correlation function and in-/ or excluding diffusion and local dispersivity). Although no solution was found that exactly matches the conditions of our simulations, a comparison is presented here to illustrate the specific features for the case of an ATES system.

A comparison is provided with the solutions of Attinger et al. [179], Chang and Yeh [181] and Gelhar [156] for which formula and main assumptions are given in appendix 3.1. The numerical solutions are all derived for large displacement conditions ($\int q/n \cdot dt \gg \lambda_h$), whereas in our case the transported distance is of the same order of magnitude as the correlation length (λ_h). Since local temperature differences do not average out at this length scale, we observe an uncertainty in thermal recovery which calls for a range in macro-dispersivity values instead of a single value. The solutions in Chang and Yeh and Gelhar are derived for isotropic conditions. For these cases our numerical results are compared with the analytically derived apparent macro-dispersivity for both the horizontal correlation length ($2 \cdot R_{th}$, 104.1 m for the reference case; Figure 3.8a) and the vertical correlation length (2 m; Figure 3.8b) as used in our simulations. As the main flow direction is in the horizontal plane, the first (horizontal comparison) could be considered as most relevant. However, using either the anisotropic solution of Attinger et al. or the horizontal correlation length in the isotropic solutions of Chang and Yeh and Gelhar, these analytical solutions calculate much higher dispersivity values than the apparent macro-dispersivities found in this study. On the other hand, the small vertical correlation length could generate preferential pathways and thereby promote the tendency for horizontal interaction between the wells. Using the vertical correlation length in the solutions of Chang and Yeh and Gelhar results in similar dispersivity values as found in this study. We can, however, not show if this is also true for other ratios between λ_h and λ_v .

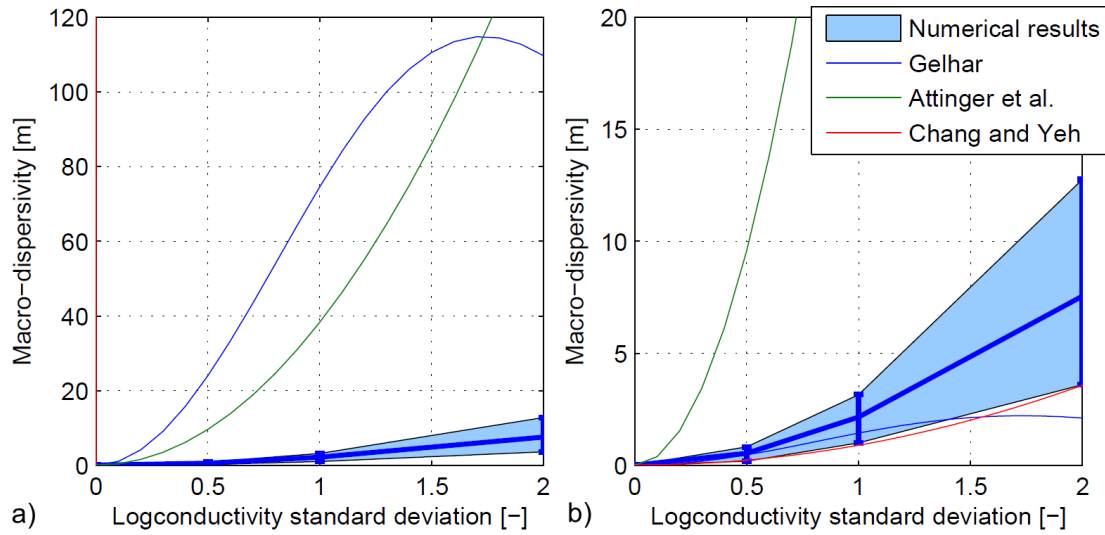


Figure 3.8 Comparison of numerical results for macrodispersivity with closed-form analytical solutions. Gelhar [1993] and Chang and Yeh [2012] are derived for isotropic conditions. These solutions are calculated using (a) the horizontal correlation length (104.1 m) and (b) the vertical correlation length (2 m) as used in this study. Note that in Figure 8a the Chang and Yeh solution results in a steep curve near the y axis. The solution from Attinger et al. [2001] is derived for anisotropic conditions and is calculated using $\lambda_v=2$ m and $\lambda_h=104.1$ m

In previous studies [108, 161, 182] it has been suggested that thermal diffusion is able to smooth temperature differences due to preferential flow and thereby reduce the effect of heterogeneity. This concept is tested by comparing the magnitude of thermal conduction with the expected size of temperature fluctuations due to heterogeneity. In the modelled scenarios, as in most actual aquifers, the horizontal correlation length is much larger than the vertical correlation length [156]. Comparison of vertical diffusion time ($\tau = \lambda_v^2 / D_{th} = 10.5$ days) with the average residence time (182.5 days for one storage cycle) shows that there is ample time for thermal diffusion to level out temperature differences due to preferential flow, resulting in a macro-dispersivity only slightly larger than the local dispersivity. Because the diffusion coefficient for heat, $0.382 \text{ m}^2/\text{d}$ (Table 3.1), is several orders of magnitude larger than for chemical tracers like Cl^- ($1.4\text{E-}5 \text{ m}^2/\text{d}$) [183, 184], this effect is much stronger in the case of heat transport than for solute transport. Running our simulations for non-reactive solute tracer transport, showed more distinctive fingering and increased spreading of the tracer front than in the case of heat transport (animations of the evolution of temperature as well as tracer concentrations around the wells are attached as auxiliary material of [185]; simulation results are provided as horizontal and vertical cross-sections for the homogeneous case and one heterogeneous case ($\lambda = 2 \text{ R}_{th}$, $\sigma = 2$, well distance = 2 R_{th} , regional groundwater velocity = 0 m/y).

A second difference between our case and the conditions used in deriving the analytical solutions for macro-dispersivity is that the injected heat is extracted back over the same flow paths. In this case, the dispersive effect of heterogeneity is partly reversed while extracting (i.e. the more permeable parts that transported heat more effectively during injection also transport it back when extracting), also resulting in a lower value for macro-dispersivity. A last important difference between the analytical solutions and our simulations is that we consider the flow field around a dipole well system. Where for a single well, flow and advective transport are reversible, this is not the case in a doublet well system. Due to thermal interference, stored energy that reaches the other well is not extracted. Because of thermal interference, apparent macro-dispersivity for a doublet well system does not depend only on the statistical and actual properties of the subsurface, but also on well-to-well distance and the configuration of the wells (Figure 3.7).

3.5 Conclusions

Heterogeneity in hydraulic conductivity affects the distribution of thermal energy around ATES systems. This in turn has an effect on the thermal recovery and the thermal balance of the system. Using a Monte Carlo approach, the sensitivity of ATES performance to heterogeneity was determined. Simulations of a doublet well system, with a well-to-well distance equal to two thermal radii, show that the median thermal recovery in moderately heterogeneous media (logconductivity standard deviation of 1 to 2) is 6 to 15 percent point (pp) lower than in a homogeneous medium. Even without significant regional groundwater flow, uncertainty in the degree of thermal interference for heterogeneous aquifers results in an uncertainty in predicted thermal recovery up to 15 pp.

In regulations for ATES, balanced conditions are important, which means a volume balance and equal temperature offset between the warm and cold well and the natural aquifer temperature. When the ATES system is operated under such conditions, sensitivity of the energy balance to heterogeneity is only minor. All modelled cases with a regional groundwater flow of less than 50 m/yr show an absolute energy balance ratio smaller than 4%. However, in the case of high regional groundwater flow uncertainty in expected EBR is larger (up to 22% for a flow velocity of 200 m/y).

The results indicate that it is possible to capture the effect of heterogeneity on thermal recovery in homogeneous models by applying a range of macro-dispersivities. However, the appropriate range of dispersivities not only depends on the correlation length and logconductivity standard deviation, but also on groundwater velocity and well-to-well distance.

Considering the increasing demand for ATES systems we conclude that thermal interference limits the number of ATES systems that can be built in a specific area. Furthermore, uncertainty in the hydraulic conductivity field related to heterogeneity should be accounted for when optimizing well-to-well distance for the wells within a single system and between systems. This study is limited to thermal interference between two wells and the effect of heterogeneity on the performance of a single doublet well ATES system. ATES performance reduction due to interference in regional, multi-system situations might be partly compensated by interference between wells with similar temperature [150].

Appendix 3.1

Closed-form solutions of macro-dispersivity as a function of correlation length (λ) and logconductivity standard deviation (σ).

Gelhar [156]

Main assumptions:

1. Isotropic log conductivity field
2. Steady parallel flow field
3. Including local dispersive mixing (no diffusion)
4. Ideal tracer conditions (non-reactive solute and constant density and viscosity)
5. Transport scale \gg correlation length

Formula (modified from Equation 5.2.13 Gelhar, 1993)

$$\alpha_{L,app} = \sigma^2 \lambda / e^{\sigma^2/3} \quad (A1)$$

$\alpha_{L,app}$ longitudinal macro-dispersivity
 σ logconductivity standard deviation
 λ correlation length

Attinger et al. [186]

Main assumptions:

1. An-isotropic Gaussian correlation function
2. Steady radially diverging flow field
3. Including vertical diffusion (no dispersion)
4. Ideal tracer conditions (non-reactive solute and constant density and viscosity)
5. Transport scale \gg correlation length

Formula (modified from Equation 51 Attinger et al. 2001):

$$\alpha_{L,app} = \sigma^2 \lambda_h \int_0^{r/\lambda_h} e^{-\hat{r}^2} / \sqrt{1 + \frac{Dn\lambda_h^2}{Q\lambda_v^2} (r/\lambda_h \hat{r} - \hat{r}^2/2)} \cdot d\hat{r} \quad (A2)$$

$\alpha_{L,app}$ longitudinal macro-dispersivity
 σ logconductivity standard deviation
 λ_h horizontal correlation length
 λ_v vertical correlation length
 D (thermal) diffusion coefficient
 Q Discharge of the well/meter of well screen

n porosity
r radial distance

Chang and Yeh [181]

Main assumptions:

1. Isotropic Gaussian log conductivity field
2. Steady parallel flow field
3. Including diffusion (no dispersion)
4. Constant density and viscosity

Formula (Equation 24 Chang and Yeh 2012):

$$\alpha_{L,app} = \sigma^2 \lambda \left\{ \begin{aligned} & -\frac{16}{P^3} - \frac{8}{3P} + \frac{16\sqrt{\pi}}{P^4} e^{P^2/4} \left[\psi(\Lambda) - \psi\left(\frac{P}{2}\right) \right] \\ & + \left[\left(\frac{4}{P^2} + \frac{1}{2} \right) \eta^2 - \frac{3}{4} \right] \frac{\Lambda}{\eta^4} e^{-\eta^2} \\ & + \sqrt{\pi} \left[\left(\frac{16}{P^4} + \frac{4}{P^2} + \frac{1}{2} \right) \eta^4 - \left(\frac{2}{P^2} + \frac{1}{2} \right) \eta^2 + \frac{8}{3} \right] \frac{\Lambda \varphi(\eta)}{\eta^5} \\ & - \frac{\sqrt{\pi}}{4} \frac{P}{\tau} \left(\frac{3}{4} \frac{1}{\eta^4} - \frac{1}{\eta^2} + 1 \right) \varphi(\eta) - \frac{1}{4} \frac{P}{\tau} \left(-\frac{3}{2} \frac{1}{\eta^3} + \frac{1}{\eta} \right) e^{-\eta^2} \end{aligned} \right\}$$

$$P = \rho_w c_w q \lambda / k_a$$

$$\Lambda = \sqrt{P(P+4\tau)} / 2 - \eta$$

$$\tau = \nu q t / \lambda$$

$$\nu = \rho_w c_w / (\rho_a c_a)$$

$$\eta = \sqrt{P\tau^2 / (P+4\tau)}$$

$$q = Q / (2\pi r)$$

$\alpha_{L,app}$ longitudinal macro-dispersivity

σ logconductivity standard deviation

λ correlation length

D (thermal) diffusion coefficient

Q Discharge of the well/meter of well screen

q specific discharge

r radial distance to the well

ρ_w density of water

c_w heat capacity of water

ρ_a density of aquifer

c_a heat capacity of aquifer

k_a	thermal conductivity of aquifer
φ	error function
ψ	complementary error function

Efficiency of and interference among multiple aquifer thermal energy storage systems; a Dutch case study

Abstract

This chapter describes the analysis of a real case of multiple Aquifer Thermal Energy Storage systems. The Hague, the capital city of the province of South Holland in the Netherlands, is densely populated with many ATES systems. A total of 19 ATES systems are installed in an area of 3.8 km² with a total of 76 functioning wells. The analysis focuses on the development of a coupled groundwater flow and heat transfer model that simulates these systems over a period of 10 years. Results are then post-processed to evaluate efficiency of each individual well and system. Efficiency of the ATES systems has ranged between 40% and 89%. The analysis showed that efficiency tends, in general, to increase over time and stabilize at an asymptotic value after few years. Analysis of interference among individual wells of an ATES system and wells of other systems showed that interference could, in fact, have a positive impact on the efficiency of a well and system. Interference can increase efficiency of an ATES system since it can help in trapping energy (cold or warm) within the capture zone of all operating ATES systems. In the study area, the interference phenomenon affects efficiency, in general, positively where it increases the efficiency of individually operating wells by a maximum of 10%. However, the phenomenon also affects efficiency of some wells negatively where it reduces the efficiency of individually operating wells also by a maximum of 10%. On average, systems in the study area are positively affected by interferences among each other with an overall average of 2.5% for all wells.

This chapter is based on: Bakr, M., van Oostrom, N., and Sommer, W.T. (2013). *Efficiency of and interference among multiple Aquifer Thermal Energy Storage systems; A Dutch case study*. Renewable Energy 60, 53-62. Revisions to the model and analysis used in this chapter are outlined in Appendix 4.1.

4.1 Introduction

Aquifer Thermal Energy Storage (ATES) systems have recently received considerable attention as one of the most promising renewable energy utilization methods. This comes at no surprise to an increased global demand for energy and growing environmental concerns over fossil fuel consumption and CO₂ emissions. ATES has proven to be an economical, commercially viable and energy efficient technology [187, 188]. In its simplest form, ATES involves heating or cooling groundwater using low grade thermal energy (e.g., solar energy), and store it during periods of low demand into a suitable aquifer. During periods of high demand, this water is extracted where its energy can be used for a variety of applications (e.g., air conditioning). Numerous successful ATES projects are currently in operation in Europe, Asia, and North America. Design components of an ATES system include a suitable aquifer system, injection/extraction well(s), a heat exchanger, and a cheap or free source of thermal energy (e.g., solar energy or cold outside air temperature). ATES systems that operate on low temperature can store usually heated (13-25 °C) or cooled (6-12 °C) water [189, 190]. Such systems usually operate on seasonal (e.g. summer and winter) frequency, although they can also operate on shorter periods depending on demand for thermal energy.

Selecting an aquifer to be used for thermal energy storage is a crucial step towards a successful ATES system. For example, the capacity of an aquifer to accept or yield water limits the flow rate that can be used in an ATES plant. Also, the effective porosity of the aquifer affects the volume of aquifer required to store a given volume of heated or cold water. This in turn affects the size of an ATES well field. Also, the direction and rate of groundwater flow, as well as thermal properties of water and aquifer materials similarly affect the size, shape, and operation of the ATES systems. So, for example, sand and gravel aquifers located below the maximum depth of annual cyclic temperature are considered suitable for ATES installations. Such aquifers will ensure reasonable well yields and will minimize thermal losses by conduction. In addition, a low regional hydraulic gradient is considered necessary for a successful ATES to minimize heat losses by convective transport. Sommer et al. [123] shows that for a doublet system with dimensions typical for ATES application in the Netherlands thermal recovery drops below 50% when there is a regional groundwater flow of 150 m/yr. Moreover, Kangas [191] shows that, using multi-well systems, low temperature ATES systems can be feasible with regional flow up to 500-600 m/yr. In addition, aquifers of low iron (Fe), calcium (Ca), and magnesium (Mg) content are desirable to reduce risks of clogging and corrosion of well casings.

Significant uncertainties in our ability to predict states of aquifer systems, such as fluid and thermal fluxes, complicate the design process of ATES systems (e.g. [161]). Overdesigning ATES systems, to compensate for these uncertainties, reduces their potential optimum

utilization. The role of heterogeneity in advective-conductive heat transport has received comparatively little attention. Previous work shows that heterogeneity increases the thermal influence radius of an ATES well [161] and results in an uncertainty in the thermal recovery of a doublet well system [123]. In addition to the uncertainty introduced by heterogeneity, hydrodynamic dispersion is also contributing to modelling of mass transport in porous media [192]. This link is well established for solute transport, but there is still some controversy on the importance of thermal dispersion to heat transport [193]. The hydrodynamic component of thermal dispersion is often neglected because thermal diffusion is more efficient than molecular diffusion by several orders of magnitude [194]. Analysis of heat transport under natural gradients has commonly neglected hydrodynamic dispersion; only few studies have considered hydrodynamic dispersion (e.g., [142, 195]). Sauty et al. [142] suggested that there was a correlation between the apparent thermal conductivity and Darcy velocity putting a strong argument to consider the hydrodynamic dispersion in any advective-conductive transport study in porous media. De Marsily [196] suggests that the thermal dispersivity and the hydrodynamic dispersivity may be equal. Based on a field experiment of thermal energy storage in a confined aquifer, Molz et al. [197] concluded that the hydrodynamic thermal dispersion within the storage aquifer was probably an important dissipation process. They, also, observed that additional mixing due to clogging and unclogging of the formation could have played an important role. Moreover, Shen et al. [198] have also examined effects of variations in thermal parameters which they concluded of important role on conductive heat flow. Consequently, a good system characterization is therefore required to achieve an efficient ATES system. In the literature, methods combining conventional hydrologic testing with thermal tracer tests are reported (e.g. [182, 199-203]).

In this chapter, a real case study of ATES systems is presented. This case was simulated as a part of the Dutch research program on ATES called “Meer met bodemenergie” (i.e. “More with Subsurface Energy”). This 2 years research program was conducted by 4 partners and funded and supported by 36 governmental and private organizations. This program resulted in 11 reports on several topics concerning ATES, with one report focusing on interference [204]. Here, we consider the analysis of efficiency and interference among systems installed in the city of The Hague, the Netherlands. In this city a total of 19 ATES systems are installed within an area of about 3.8 km² with a total of 76 operating wells. Efficiency of individual systems, efficiency of individual wells, and interference among wells and systems are analysed. The methodology for modelling heat transfer in porous media is briefly described with all relevant related physical processes. As a prerequisite for simulating heat transfer, groundwater flow should be identified. The groundwater flow model for the study area is a window of a larger model developed in another study [205].

4.2 Modelling heat transfer in porous media

Heat is transported through porous media by conduction, advection, and dispersion. Conductive transport occurs even in static groundwater. It is controlled by thermal conductivity of the geological formations and the contained pore water. The equation describing the relation between conductive heat flux (H_c) and the temperature gradient (∇T) is the constitutive Fourier law:

$$H_c = -\lambda_b \nabla T \quad (4.1)$$

where λ_b is bulk thermal conductivity (Energy/Time/Length/Temperature). The bulk thermal conductivity is expressed as:

$$\lambda_b = \lambda_w \theta + \lambda_s (1 - \theta) \quad (4.2)$$

where λ_w is the thermal conductivity of water [$\text{ML}^2\text{T}^{-2}\text{T}^{-1}\text{L}^{-1}\text{C}^{-1}$], λ_s is the thermal conductivity of the aquifer materials [$\text{ML}^2\text{T}^{-2}\text{T}^{-1}\text{L}^{-1}\text{C}^{-1}$], θ is the effective porosity [-]. Advective transport occurs only in moving groundwater. It is the heat that is carried along with the flowing groundwater. In most systems advective transport exceeds conductive transport. The advective heat flux (H_a) can be written as:

$$H_a = q \rho_w c_w T \quad (4.3)$$

where q is specific discharge [LT^{-1}], ρ_w is the density of water [ML^{-3}], and c_w is the specific heat capacity of water [$\text{L}^2\text{T}^{-2}\text{C}^{-1}$]. Thermal dispersion is a scale-dependent transport process due to heterogeneity of the subsurface. The dispersive heat flux (H_d) can be written as:

$$H_d = -\rho_w c_w \alpha q \nabla T \quad (4.4)$$

where α is the thermal dispersivity [L]. Considering a source/sink mixing term and applying an energy balance, the partial differential equation governing heat transport in porous media can be expressed as:

$$(\rho c)_b \frac{\partial T}{\partial t} = \nabla \left[(\nabla \rho_w c_w \alpha q + \lambda_b) \nabla T \right] - \rho_w c_w \nabla q T - \rho_w c_w q_s T_s \quad (4.5)$$

where q_s is a source or sink term [T^{-1}] of water with density ρ_w and specific heat capacity c_w , T_s is the source temperature [$^{\circ}\text{C}$]. Here, $(\rho c)_b$ is given by:

$$(\rho c)_b = \rho_w c_w \theta + \rho_s c_s (1 - \theta) \quad (4.6)$$

where ρ_s is the density of the solid (i.e., mass of the solid divided by the volume of the solid) $[\text{ML}^{-3}]$, ρ_b is the (dry) bulk density (i.e., mass of the solid divided by the total volume) $[\text{ML}^{-3}]$, c_s is the specific heat capacity of aquifer materials $[\text{L}^2\text{T}^{-2}\text{C}^{-1}]$. The left-side of Equation 4.5 reflects the fact that heat travels over time through both fluid-filled pores and the geological formations, and is therefore retarded relative to fluid velocities. Equation 4.5 can be simplified such that:

$$\left(1 + \frac{\rho_s c_s (1 - \theta)}{\rho_w c_w \theta}\right) \frac{\partial T}{\partial t} = \nabla \left[\left(\frac{\lambda_b}{\rho_w c_w \theta} + \alpha \nu \right) \nabla T \right] - \nabla(\nu T) - \frac{q_s}{\theta} T_s \quad (4.7)$$

where ν $[\text{LT}^{-1}]$ is pore water velocity which is given by dividing specific discharge (q) by porosity (θ). This equation can be further reduced to the following form:

$$R_T \frac{\partial(\theta T)}{\partial t} = \nabla \cdot (D_T \cdot \nabla T) - \nabla(\nu T) - \frac{q_s}{\theta} T_s \quad (4.8)$$

Here, the thermal retardation factor R_T [-] and the thermal dispersion coefficient (tensor) D_T $[\text{L}^2\text{T}^{-1}]$ are given by:

$$R_T = 1 + \frac{1 - \theta}{\theta} \frac{\rho_s c_s}{\rho_w c_w} \quad (4.9)$$

and,

$$D_T = D_m + \alpha \nu \quad (4.10)$$

The thermal molecular diffusion coefficient D_m $[\text{L}^2\text{T}^{-1}]$ is given by:

$$D_m = \frac{\lambda_b}{\theta \rho_w c_w} \quad (4.11)$$

Note that Equation 4.9 can be expressed in terms of the thermal distribution factor K_d , such that:

$$R_T = 1 + \frac{\rho_b}{\theta} K_d \quad (4.12)$$

where,

$$K_d = \frac{c_s}{\rho_w c_w} \quad (4.13)$$

and

$$\rho_b = \rho_s (1 - \theta) \quad (4.14)$$

Equation 4.8 has similar structure as the equation governing mass transport in porous media [28]. This means that codes developed for mass transport (e.g. MT3DMS [170]) can be used to simulate heat transfer in porous media.

4.3 Efficiency and interference

The thermodynamic analysis of ATES systems in this study is based on an annual cycle of two periods (winter and summer). During winter seasons, pumping wells extract warm water while injection wells inject back cold water and vice versa for summer seasons. In this chapter, the application of energy analysis to ATES systems is investigated. Hence, efficiency and interference of systems are based on the energy concept.

To calculate energy efficiency of a well in an ATES system, two consecutive periods of injection and recovery are considered. This means that efficiency of a well is function of time with annual variability. It should be noted that this is valid for both warm and cold water wells. So, injecting water colder than ambient groundwater temperature is considered cold energy which should be recovered in summer periods. In general, energy (E [ML^2T^{-2}]) can be obtained using:

$$E(\tau) = \int_{\tau} \dot{E}(t) dt \quad (4.15)$$

where the integration is performed over a groundwater flow stress period of length (τ) for the extracted or injected energy rate \dot{E} which is given by:

$$\dot{E}(t) = c_w \rho_w Q [T(t) - T_0] \quad (4.16)$$

Here, Q [L^3/T] is well injection/extraction rate (assumed to be constant through each stress period), T [$^{\circ}\text{C}$] is temperature of groundwater at well location, and T_0 [$^{\circ}\text{C}$] is the ambient groundwater temperature.

The difference between the injected and the extracted energy (in two consecutive stress periods) indicates un-retrieved energy. The percentage of the two terms (i.e., the extracted and the injected energy) in two consecutive stress periods (the injection is at the first stress period) gives the efficiency (η_w) of a well of an ATEs system. This can be mathematically expressed as:

$$\eta_w(\tau+1) = \frac{E(\tau+1)}{E(\tau)} \quad (4.17)$$

Similarly, efficiency of a system can be obtained by dividing summation of extracted energy of all wells by summation of injected energy of all wells. Here, it should be noted that energy has positive values; this is regardless of warm or cold water wells (i.e. injected water temperature is higher or lower the ambient groundwater temperature, respectively).

Interferences among individual wells and systems are also quantitatively evaluated. This is done by comparing the efficiency of each well with all systems operating with the efficiency of the well while other systems are assumed off and the case in which all other wells are assumed off.

4.4 Modelling flow and heat transfer in the study area

The study area is located in the city of The Hague, the Netherlands. Figure 4.1 shows a location map of the study area. The key map of the figure shows the boundary of the local groundwater flow and heat transport models used in this study.

To develop a groundwater flow model, geological depositions are classified into aquifers and confining (aquitard) layers. Such hydro-geological-units description, do not necessarily coincide with the geological formations. The top layers of the hydrogeological model consist mainly of Holocene aquitard materials. They consist of fine sand containing silt, clay, and peat deposits. However, poorly permeable coarse sediments from beach-sand and stream channels also exist. The combined thickness of these top layers varies from a few meters to 20 m, where the hydraulic properties (transmissivity and vertical resistance) are determined from an extensive data set [205].

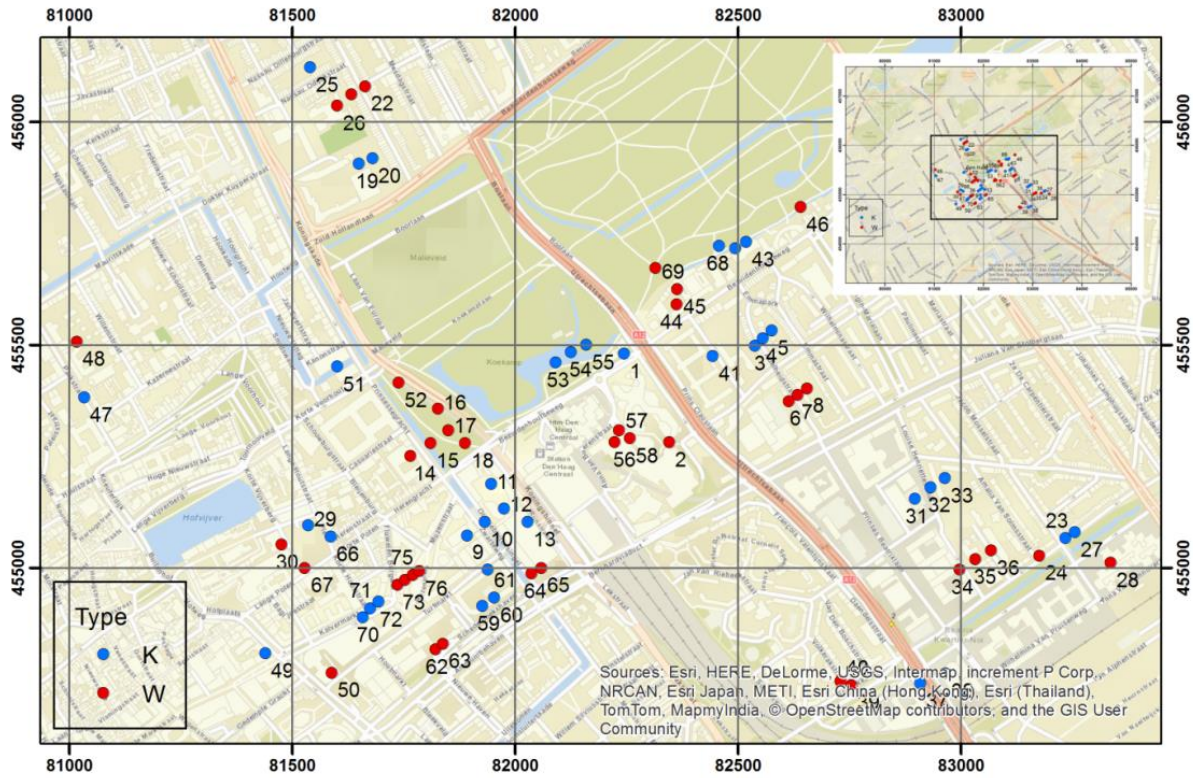


Figure 4.1 Location map of the study area; internal map shows the model boundary while the main map is a zoomed area of the rectangle in the internal map containing the ATES wells which are numbered according to Table 4.2

The first aquifer is formed by fluvial deposits of the Formations of Urk and Kreftenheye. The top of this aquifer tilts westward and its thickness ranges from 30 to about 45 m inside the model domain. The first aquitard layer in the full plan area is formed by clay and silt deposits from the Formation of Waalre. The top of this formation varies between NAP -55 m to NAP -65 m, and the thickness of this layer varies from a few meters to 10 m. Below this aquitard is a sequence of sand and clay layers that belong to the Formation of Peize and Waalre, with thicknesses ranging between 5 and 30 m. The lower part of the model consists of sandy deposits of the Maassluis Formation that extend up to between NAP -237 m and NAP -260 m.

The groundwater flow model of the study area is a window of a larger calibrated groundwater flow model of the Delfland region in the Netherlands [205]. Figure 4.1 shows a zoomed area (black box in the key map) to give a better view of the distributions of the ATES wells. The figure shows well numbers (Table 4.2). The original Delfland model consists of 24 model layers with thicknesses ranging between 0 and 140 m. To accurately model flow and heat transport, a new layer discretization is made using a rectilinear grid as described in Zheng and Wang [170]. The developed model consists of 352 rows, 464 columns, and 20 layers with 12.5 m cell size in

x- and y-directions. The first model layer follows the topography, has a thickness of 2 m and contains the recharge, river and drainage packages. The second model layer has variable thickness and extends to a constant depth of NAP -10 m. Subsequent model layers have a constant thickness of 5 m up to a depth of NAP -75 m. Below that depth layer thickness is allowed to increase with a factor 2 per layer to reduce computational demand. Influence of model discretisation was demonstrated by systematically reducing layer thickness and grid size (see appendix 4.2). Vertical well screen length, position and flow rate are determined from the permit for each system from the regulating authority. The well screen length of the 76 wells ranges between 20 and 40 m. In case a well screen extended over multiple model layers, the flow rate was divided according to the well screen length in each layer. All wells are positioned between NAP -21.9 m and NAP -65.0 m. The total number of stress periods considered for the flow and heat transfer models is 21 of half a year length each. Groundwater flow is simulated using steady state conditions assuming that the system reaches the steady state condition after a short time of switching the direction of pumping.

Parameters controlling heat transfer in the aquifer system of this case study are considered uniformly distributed and are listed in Table 4.1 [204]. Here, we follow the assumption often made in the literature where the hydrodynamic component of thermal dispersion is neglected [194]. Finally, Table 4.2 lists wells operating within all systems with their permitted pumping/injection rates. The total permitted yearly pumping volume for each system is distributed evenly over the wells of that system. The total permitted yearly pumping volume for a system is often dimensioned on the maximum expected cooling/ heating demand. Therefore, average pumping rates are generally much smaller. The Dutch Central Bureau of Statistics estimates that in 2007 all systems in the Netherlands combined pumped 56% of their permitted volume [59]. Other estimates range from 50% [206] to 60% [49]. We consider two scenarios: (SC1) all systems operate at 2/3 of their permitted capacity, and (SC2) all systems operate at their total permitted capacity.

Table 4.1 Input values for modelling heat transfer in the study area

Parameter	Value	Unit
Effective porosity (θ)	0.35	-
Specific heat capacity of water (C_w)	4183	J/(kg °C)
Density of water (ρ_w)	1000	kg/m ³
Bulk thermal conductivity (λ_{bulk})	2.55	W/(m °C)
Molecular diffusion coefficient (D_m)	0.125	m ² /d
Longitudinal dispersivity (α_L)	0	m
Transverse dispersivity (α_T)	0	m
Thermal retardation factor (R_T)	2	-

Initial conditions for temperature (Figure 4.2) are based on borehole temperature logs within the model area, provided by IF Technology. Constant temperature boundary conditions are applied to the top and bottom model layers as well as constant head cells along the lateral model boundaries. The ambient temperature at the average well screen depth of NAP -44.5 m is 13.0 °C. Injection temperatures are set to 10.0 °C and 16.0 °C for the cold and warm storage respectively.

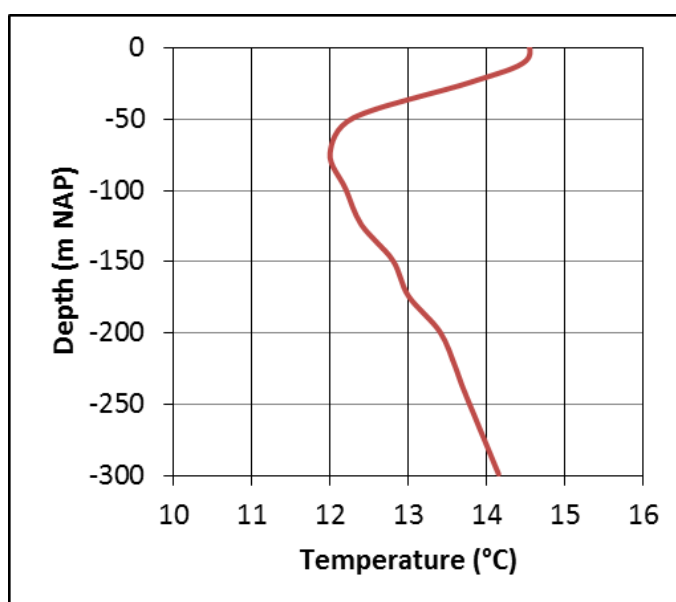


Figure 4.2 Temperature log within the study area (provided by IF Technology)

To demonstrate the results for the coupled model of flow and heat transfer in the study area, Figure 4.3 and Figure 4.4 show temperature distribution ($^{\circ}\text{C}$) at the end of stress periods 20 (summer), and 21 (winter). Also, Figure 4.5 shows evolution of temperature over time at different wells of one of the ATEs systems in the study area. Figure 4.3 and Figure 4.4 show interference among temperature distributions of several wells where the two figures show merging temperature contours of neighbouring wells either below or above the ambient groundwater temperature (i.e. 13.0°C). The phenomenon will be discussed in the next section. Figure 4.5 shows the persisting injected temperature of 10.0°C and 16.0°C during winter and summer seasons, respectively. This, in fact, indicates one of the assumptions made here that extracted water is either heated up or cooled down to 16.0°C and 10.0°C , respectively, before being injected back into the aquifer. The figure also shows a trend of decreasing difference between injected and extracted water temperature of each individual well over time. This is an indication of enhanced system efficiency over operation time. Similar behaviour is observed in other modelling studies (e.g., [69, 123]). In the next section we discuss the efficiency of different ATEs systems within the study area. Also, interference among systems and wells is discussed and results are used to highlight the need for effective design procedure for efficient ATEs systems.

Table 4.2 List of wells and their maximum permitted pumping/extraction rates

System ID	Well ID	Type	Q (m ³ /yr)	System ID	Well ID	Type	Q (m ³ /yr)
S01	W01	Cold	200 000	S10	W39	Warm	195 000
S01	W02	Warm	200 000	S10	W40	Warm	195 000
S02	W03	Cold	150 000	S11	W41	Cold	205 000
S02	W04	Cold	150 000	S11	W42	Cold	205 000
S02	W05	Cold	150 000	S11	W43	Cold	205 000
S02	W06	Warm	150 000	S11	W44	Warm	205 000
S02	W07	Warm	150 000	S11	W45	Warm	205 000
S02	W08	Warm	150 000	S11	W46	Warm	205 000
S03	W09	Cold	155 000	S12	W47	Cold	83 750
S03	W10	Cold	155 000	S12	W48	Warm	83 750
S03	W11	Cold	155 000	S13	W49	Cold	390 000
S03	W12	Cold	155 000	S13	W50	Warm	390 000
S03	W13	Cold	155 000	S14	W51	Cold	375 000
S03	W14	Warm	155 000	S14	W52	Warm	375 000
S03	W15	Warm	155 000	S15	W53	Cold	164 000
S03	W16	Warm	155 000	S15	W54	Cold	164 000
S03	W17	Warm	155 000	S15	W55	Cold	164 000
S03	W18	Warm	155 000	S15	W56	Warm	164 000
S04	W19	Cold	150 000	S15	W57	Warm	164 000
S04	W20	Cold	150 000	S15	W58	Warm	164 000
S04	W21	Warm	150 000	S16	W59	Cold	200 000
S04	W22	Warm	150 000	S16	W60	Cold	200 000
S05	W23	Cold	55 000	S16	W61	Cold	200 000
S05	W24	Warm	55 000	S16	W62	Warm	150 000
S06	W25	Cold	144 000	S16	W63	Warm	150 000
S06	W26	Warm	144 000	S16	W64	Warm	150 000
S07	W27	Cold	37 500	S16	W65	Warm	150 000
S07	W28	Warm	37 500	S17	W66	Cold	260 000
S08	W29	Cold	9 100	S17	W67	Warm	260 000
S08	W30	Warm	9 100	S18	W68	Cold	220 000
S09	W31	Cold	200 000	S18	W69	Warm	220 000
S09	W32	Cold	200 000	S19	W70	Cold	96 667
S09	W33	Cold	200 000	S19	W71	Cold	96 667
S09	W34	Warm	200 000	S19	W72	Cold	96 667
S09	W35	Warm	200 000	S19	W73	Warm	72 500
S09	W36	Warm	200 000	S19	W74	Warm	72 500
S10	W37	Cold	195 000	S19	W75	Warm	72 500
S10	W38	Cold	195 000	S19	W76	Warm	72 500

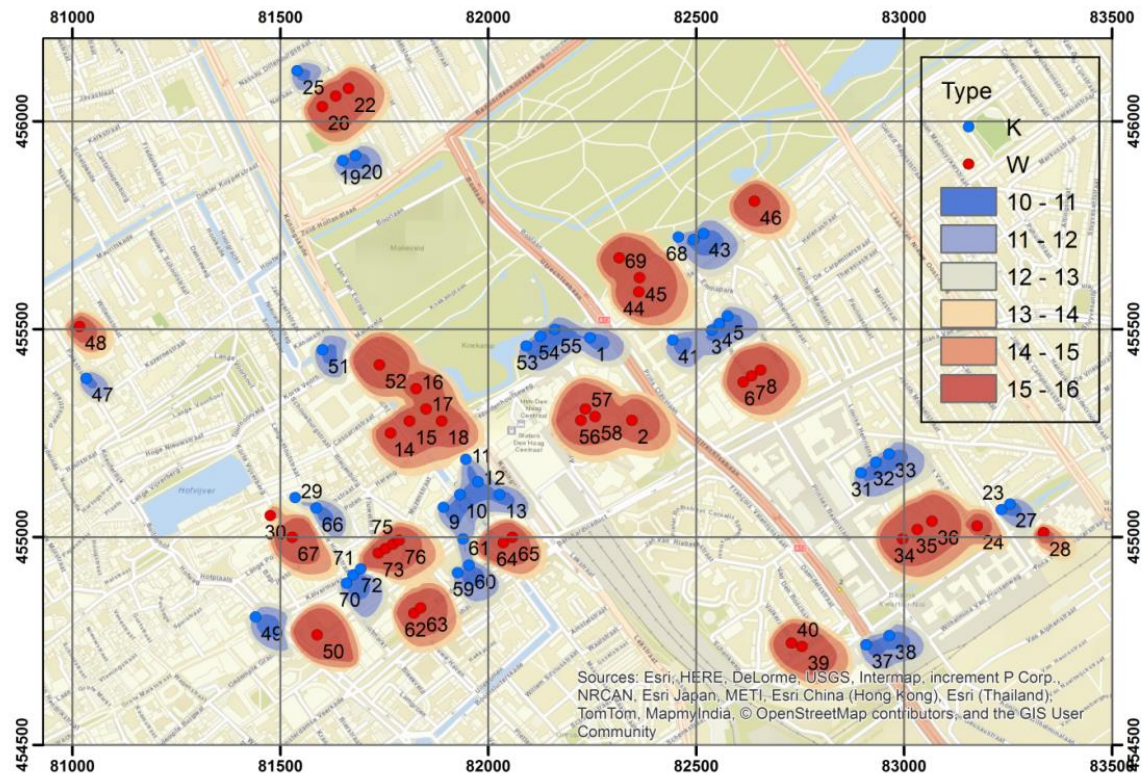


Figure 4.3 Temperature distribution (°C) at end of stress period 20 (summer); well labels show Well ID

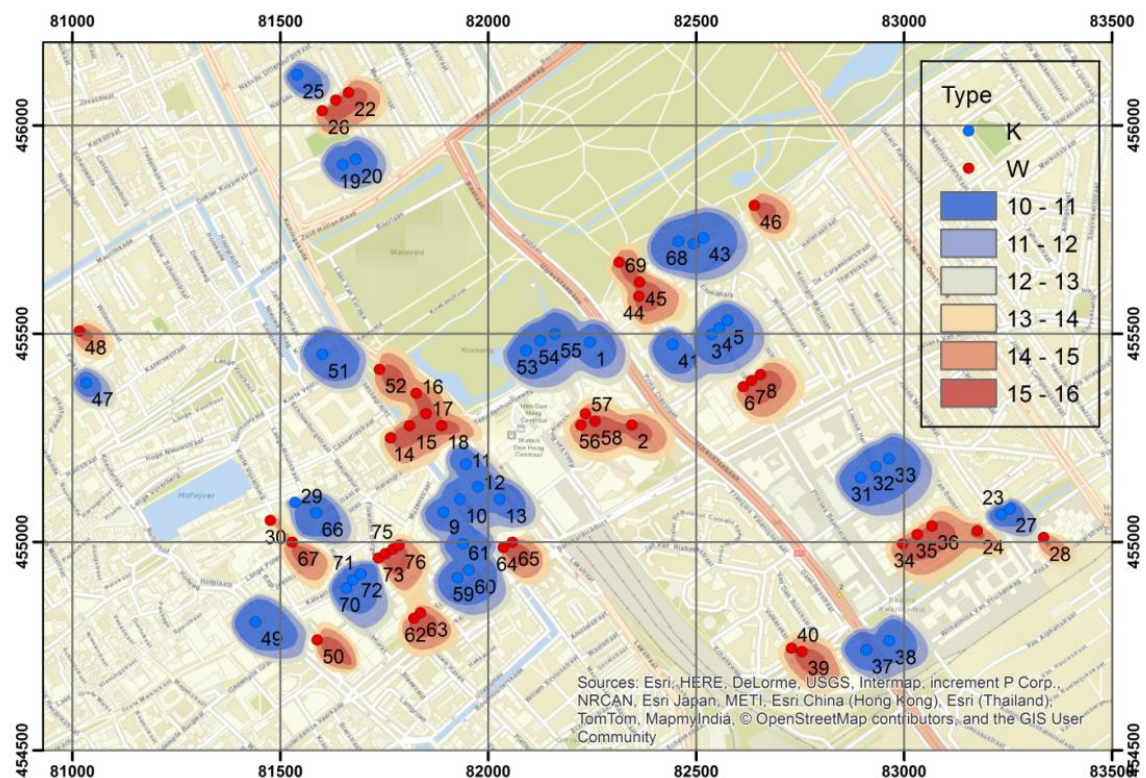


Figure 4.4 Temperature distribution (°C) at end of stress period 21 (winter); well labels show Well ID

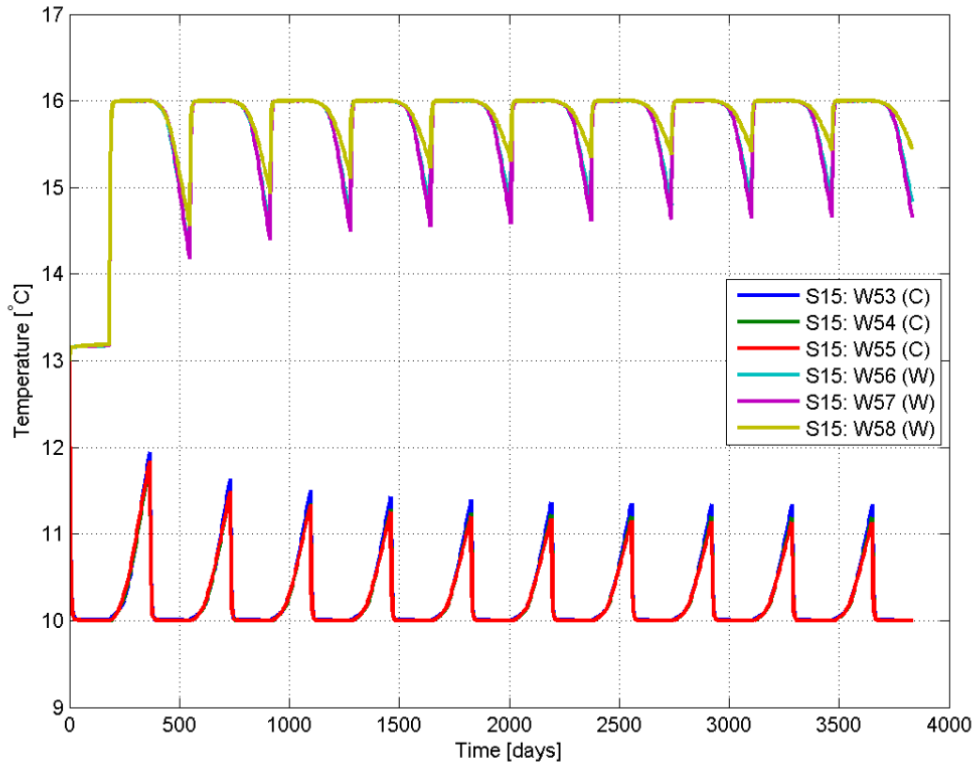


Figure 4.5 Temperature evolution in the wells of system S15

4.5 Efficiency and interference of the Hague ATES systems

As described in section “Efficiency and Interference”, efficiency of each ATES well is calculated using Equation 4.17. Similarly, efficiency of an ATES system is calculated by summing energy of the system’s wells extracted at time $\tau+1$ and divide it by sum of energy of these wells injected at time τ . Figure 4.6 shows that efficiency (scenario SC1) ranges from a minimum of 40% (year 1 for system 8) to a maximum of 89% (year 10 for system 11). The general trend of efficiency curves is to increase over time (to reach a sill value) as already anticipated from Figure 4.5. System numbers 8, 7, 5, 12 and 19 show the lowest efficiency among all systems. It appears that the system efficiency in this case is mainly coupled to the average storage volume per well (Figure 4.7). In Figure 4.7, we also plotted the energy efficiency of each well as it operates individually (with all other wells switched off shows) for SC1 and SC2, to show that the same relation between the seasonal annual flow rate and the energy efficiency of each well, holds for the case in which there is no thermal interference between wells. We hypothesise that the wells with a larger flow rate have higher energy efficiency because they are less sensitive to heat loss due to regional groundwater flow and also have less

dissipative heat loss due to a larger volume to area ratio. For large systems, a maximum energy efficiency around 90% seems to be possible.

To study the behaviour of individual wells of systems 1, 8, 11 and 16, Figure 4.8 shows the efficiency of individual wells of these systems. The figure shows that well W45 of system 11 has the highest energy efficiency. The high efficiency results probably from the large flow rate (Table 4.2) and close proximity to other wells used for heat storage (Figure 4.3). Well W29 of the system with the lowest performance (S8) shows similar improvement of energy efficiency over time, but starts at a lower value in year 1 because of the low flow rate. The other well of this system (W30) shows even a lowering of the energy efficiency from year 7, which could be due to expansion of the thermal plume around well W67 (Figure 4.3). The figure also shows a different performance among individual wells of each of the systems. In particular, efficiency of system number 16 is decreased significantly by the bad performance of one of the warm wells. This indicates higher interferences among wells of each system and/or among wells of other systems. System S1 shows a high energy efficiency and similar performance for both cold and warm wells. This indicates the least interference between the two operating wells of the system and the least interference with wells of other systems.

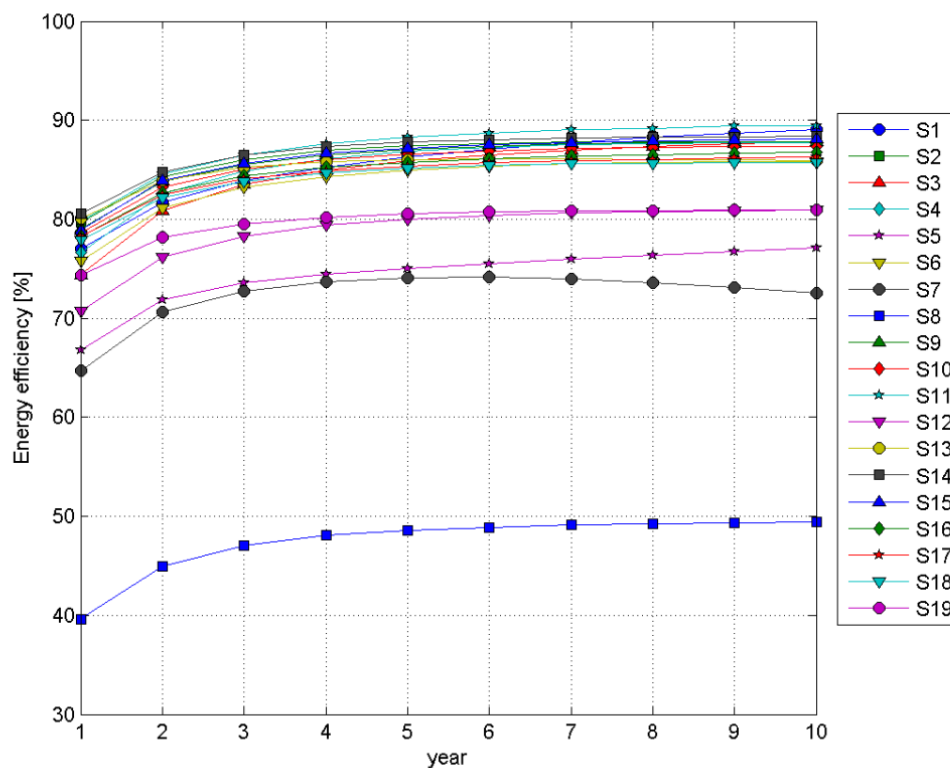


Figure 4.6 Efficiency of all systems; the legend shows system number

With multiple wells in one ATEs system and several ATEs systems operating in an aquifer, two hypothetical reference cases are used to study the interference phenomenon. The first reference case assumes a well operating individually in the field while all other wells have been assumed inactive. The second reference case assumes a system operating individually in the field while all other systems have been assumed inactive. The simulation of these reference cases has enabled us to calculate the efficiency of each well for that specific case and compare it to the original case where all wells have been assumed operating normally. The difference between efficiency values of original and reference cases defines the effect of interference for a given well. We discriminate between (1) total interference (the difference in energy efficiency between the case in which all wells are active and the case in which each well is modelled individually), (2) thermal interference within a system (the difference in energy efficiency between the case in which each system is modelled individually and the case in which each well is modelled individually) and (3) thermal interference between systems (the difference in energy efficiency between the case in which all systems are active and the case in which each system is modelled individually).

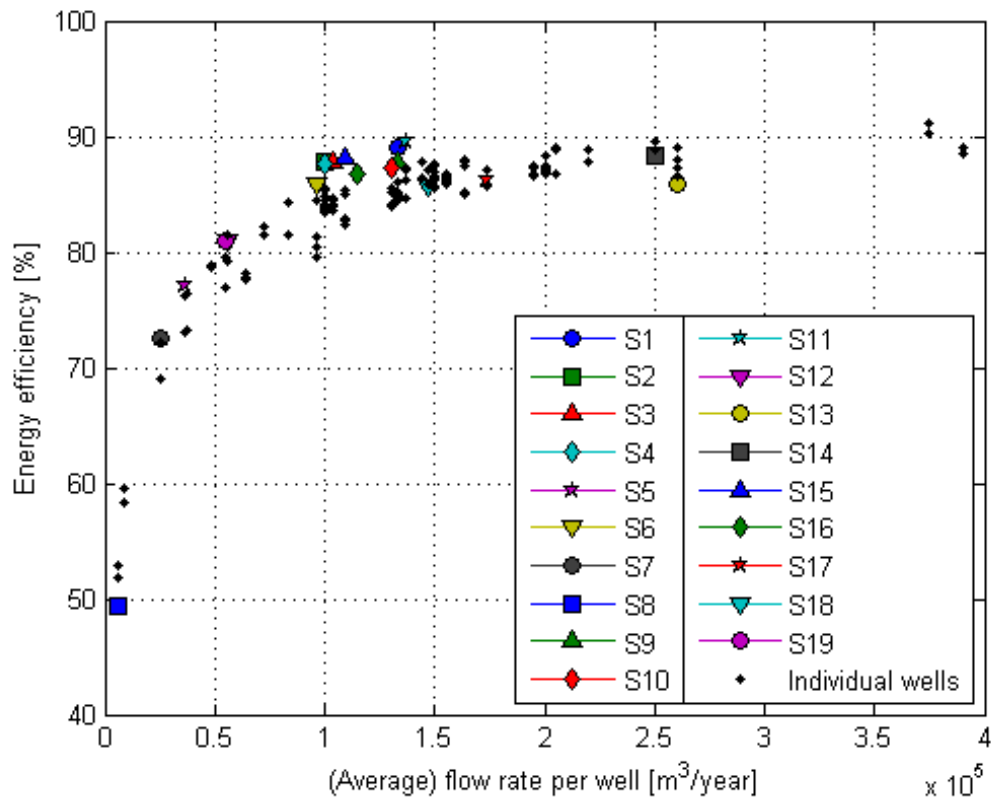


Figure 4.7 Energy efficiency in year 10 for each system (SC1) and for all individual wells while all other wells are switched of (SC1 and SC2)

Simulation of these cases enabled us to indicate whether interference occurs with other wells of the same system, or wells of other systems. All simulations: all systems active (1 model run), each system individually (19 model runs) and each well individually (76 model runs), have been performed for the scenario in which wells pump 2/3 of their permitted yearly flow rate (SC1), and the scenario in which they pump 100% of their permitted yearly flow rate (SC2).

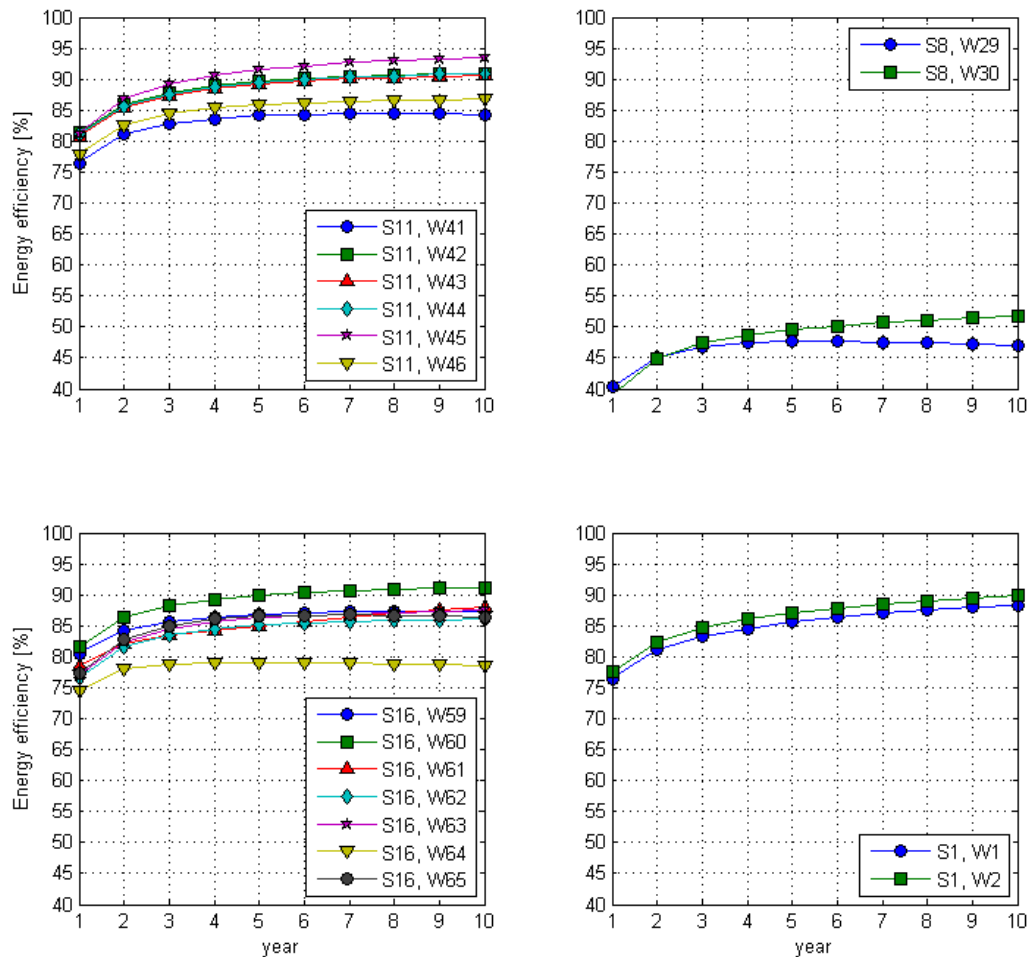


Figure 4.8 Efficiency of individual wells of some selected systems

Figure 4.9 shows the histograms of thermal interference for the 10th year of operation for scenario SC1. Average, minimum and maximum interference values for each case are given in Table 4.3 (SC1 and SC2). Positive sign interferences indicate that the well efficiency has increased due to interference with other wells. In addition, negative sign interferences indicate negatively affected well efficiency (reduced) due to interference with other wells. It is obvious in the figure that most wells experience only minor thermal interference (between -1 and +1%). In

case of larger interference, positively affected wells are dominating. Here, it should be stressed again that a well with positive sign of thermal interference means that the well efficiency has increased due to thermal interference. This could be a surprising result since one could expect no interference at all for the individually operating wells case and hence a well is best operating when it does individually. However, when wells with similar storage temperature are placed close to each other such that their thermal plumes meet, this reduces conductive heat loss to their surroundings (similar to the influence of storage volume in Figure 4.7). Energy efficiency of downstream wells also increases when they are positively influenced by the thermal plume of their upstream neighbours with similar storage temperature.

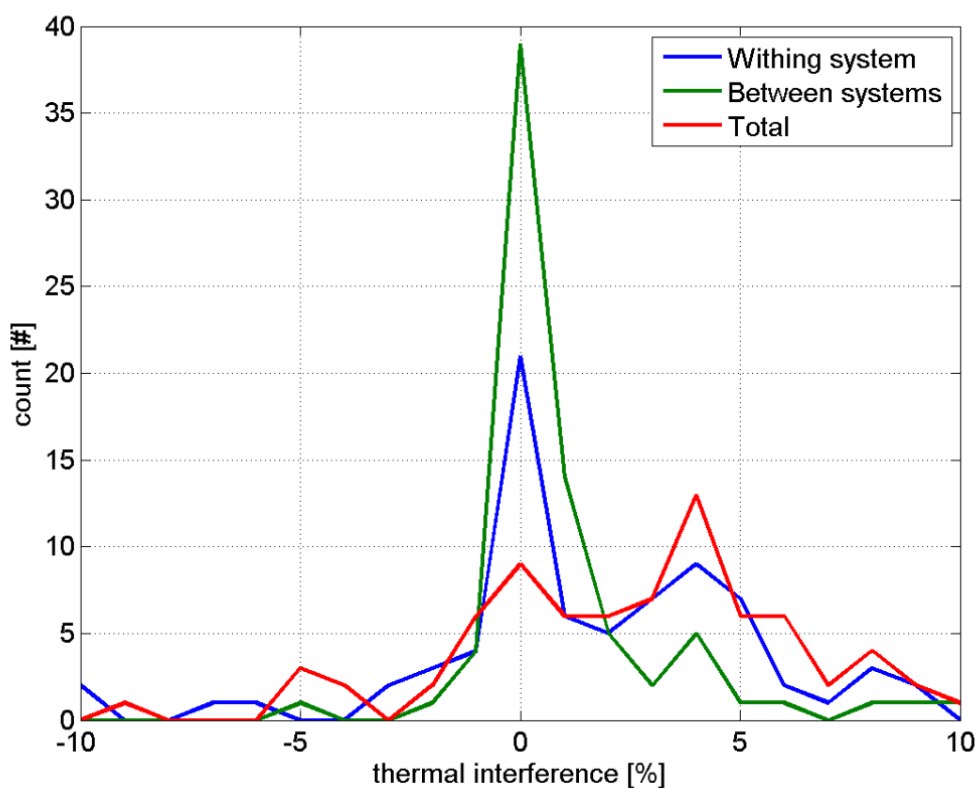


Figure 4.9 Thermal interference for scenario SC1 in year 10

For both scenarios, (absolute) thermal interference is strongest between wells within a system. This is reasonable, since wells within a system are in general closer to each other, than to the wells of other systems. Wells with similar storage temperature (i.e. cold or warm) in multi-well systems are often placed close to each other (see Figure 4.1). For scenario SC1 this results on average in a 1.3% higher energy efficiency. Thermal interference between systems increases average system performance with a similar amount (1.1%). In total, thermal interference increases average energy efficiency by 2.5%. Individual wells, however, may be affected by -10

or +10%. When wells operate at their full permitted capacity (SC2), wells within a system show more negative interference, while interference between systems actually becomes more positive. In scenario SC2 the average positive effect on energy efficiency is somewhat reduced due to increased negative interference within the systems. Ideally, Figure 4.9 would be all in the positive interference side to be positively affected by interference. This would require replacing some of the well locations to maximize retrieved energy.

Table 4.3 Energy efficiency and thermal interference in year 10

Scenario	Energy efficiency [%] (min-max)	Thermal interference within system [%] (min-max)	Thermal interference between systems [%] (min-max)	Total thermal interference [%] (min-max)
SC1	85.2 (47.0 - 94.4)	1.3 (-21.4 - 9.2)	1.1 (-5.1 - 12.1)	2.5 (-9.3 - 9.6)
SC2	86.4 (53.0 - 95.1)	-0.2 (-49.5 - 7.4)	1.4 (-5.4 - 20.9)	1.2 (-28.6 - 8.1)

Finally, it should be noted that the analysis carried out here assumes a fully deterministic approach, and ignores uncertainty associated with different input parameters of flow and heat transport. However, it is recommended to adapt a stochastic framework for the optimum ATEs system design. This is because many of the input parameters introduce uncertainties in estimated well efficiencies. Such uncertainties are due to, mainly, parameters heterogeneity, as well as uncertainty in flow rates of pumping/injection wells.

4.6 Conclusions

This chapter has described in detail a procedure of modelling a coupled flow and heat transport processes in porous media and application to Aquifer Thermal Energy Storage (ATES) systems. The three main processes of heat transfer through porous media namely conduction, advection, and dispersion are discussed. Simulation of coupled flow and heat transport in the area showed that for each well a trend of decreasing difference between injected and extracted water temperature over time for both winter and summer seasons is observed. This, in fact, indicates enhanced system efficiency over time of operation. In the study area, efficiency of ATES systems has ranged between 40% (year 1 for system 8) and 89% (year 10 for system 11).

Performance of the ATES systems in the study area varies among systems due to either negative impact (least favourite) or positive impact (favourite) of interference among wells of the same system or wells of other systems. Several factors may contribute to consequences of interference on efficiency of an ATES system including distributions of wells and their proximity to each other, their pumping/injection rates, and hydraulic and thermal characteristics of hosting aquifers. It was found that final energy efficiency (represented by model results in year 10) increases from 50% for a well with a low flow rate ($9\ 100\ \text{m}^3/\text{yr}$) to 90% for wells with larger flow rate ($250\ 000\ \text{m}^3/\text{yr}$). For the worst performing systems in the study area, it has been noticed that these systems show lower initial efficiency, as well as different performance among their individual wells. For systems with positive impact of interference, wells of these systems are allocated (location and rate) more optimally to trap energy within their capture zones. This, in fact, leads to an increased efficiency of a well working simultaneously with other wells in a well field (of the same system or other systems). Achieving an overall higher efficiency for ATES systems by maximizing positive interference can be obtained in several ways by adjusting design variables of ATES systems including, for example, well separation distances and discharge/injection rates. Developing methodologies to achieve such optimum setups can be valuable.

To get a better understanding of the interference phenomenon among all wells, interferences for each well have been calculated. It has been shown that both maximum positive as negative interference in the study area are 10%. Average interference is 2.5% and can be attributed equally to interference between wells within a system as interference with wells of other systems. The latter indicates that interference among wells in the study area has positively increased efficiency in average by 2.5% per well.

Appendix 4.1

This chapter is based on Bakr, M., van Oostrom, N., and Sommer, W.T. (2013). *Efficiency of and interference among multiple Aquifer Thermal Energy Storage systems; A Dutch case study*. Renewable Energy 60, 53-62. This appendix lists revisions to the model and interpretations that were used in that publication with respect to the model that was used in this chapter.

1. Layers are defined using a rectilinear grid (Fig. 4.4b Zheng and Wang [170])
2. Well screen positions and flow rates are updated according to permits issued by the regulating authority
3. Initial temperature distribution is adapted to available borehole temperature logs performed within the model area
4. Constant temperature boundary conditions are set for the upper, lower and lateral boundaries of the model domain, including source terms (river infiltration and recharge)
5. The grid size and layer thickness are refined
6. The method that is used to calculate energy efficiency is improved
7. Additional simulations are performed to determine which part of the observed thermal interference occurs between the multiple wells of a single system, and which part between wells of different systems
8. An additional scenario is defined in which all wells act at 100% of their permitted flow rate
9. Figures and tables are adapted according to the updated model
10. Figures 4.2, 4.7 and 4.9, Table 4.3 and Appendix 4.1 and 4.2 were not present in the original publication

Appendix 4.2

A grid refinement study was performed to determine the influence of discretization errors on the relevant heat transport processes in the model. As shown in Table 4.4 the chosen grid did not affect average and maximum thermal interference values for a grid size below 12.5x12.5 m and layer thickness of 5 m. The minimum thermal interference, however, increases as the grid size becomes smaller. This is expected mainly to be caused by less negative thermal interference which results from the difference in well-to-well distances that arises from the finer discretization. Because wells are defined in the middle of a model grid cell, specific well-to-well distances may change upon grid refinements.

Table 4.4 Effect of grid refinement on model results (SC1; year 10)

Grid size [m]	Aquifer layer thickness [m]	Total thermal interference [%] (min – max)
25x25	5	2.55 (-11.27 – 16.62)
12.5x12.5	5	2.47 (-9.29 – 9.58)
6.25x6.25	5	2.44 (-5.90 – 8.99)
12.5x12.5	1	2.22 (-8.08 – 10.35)

Optimization and spatial pattern of large-scale aquifer thermal energy storage

Abstract

Aquifer thermal energy storage (ATES) is a cost-effective technology that enables the reduction of energy use and CO₂ emissions associated with the heating and cooling of buildings by storage and recovery of large quantities of thermal energy in the subsurface. Reducing the distance between wells in large-scale application of ATES increases the total amount of energy that can be provided by ATES in a given area. However, due to thermal interference the performance of individual systems can decrease. In this study, a novel method is presented that can be used to (a) determine the impact of thermal interference on the economic and environmental performance of ATES and (b) optimize well distances in large-scale applications. The method is demonstrated using the hydrogeological conditions of Amsterdam, the Netherlands. Results for this case study show that it is cost-effective to allow a limited amount of thermal interference, such that 30 to 40% more energy can be provided in a given area compared to the case in which all negative thermal interference is avoided. Sensitivity analysis indicates that optimal well distance is moderately insensitive to changes in hydrogeological and economic conditions. Maximum economic benefit compared to conventional heating and cooling systems on the other hand is sensitive, especially to changes in the gas price and storage temperatures.

This chapter is published as: Sommer, W.T., Valstar, J., Leusbrock, I., Grotenhuis, J.T.C. and Rijnaarts, H.H.M. (2015). *Optimization and spatial pattern of large-scale aquifer thermal energy storage*. Applied Energy, 137, 322-337.

5.1 Introduction

The subsurface is increasingly being used as a storage medium for thermal energy, generally referred to as underground thermal energy storage (UTES) [207, 208]. Heat is exchanged with the subsurface either by circulating a fluid through a circuit of buried pipes (closed systems) or via direct withdrawal and injection of groundwater through groundwater wells (open systems). Systems generally operate in a seasonal mode to provide cooling in summer and heating in winter and are applied both for industrial processes as for space heating and cooling at different scales (such as households, offices and greenhouses). An overview of different system types and applications is available in [68, 114, 207-209]. Among the different system types, aquifer thermal energy storage (ATES) is particularly suitable to store large amounts of thermal energy and has developed into a cost-effective technology for heating and cooling of utility buildings such as offices, hospitals, universities and greenhouses, and to reduce greenhouse gas emissions by replacing fossil fuel dependent heating and cooling systems [11, 111, 210]. In its simplest form, a bi-directional doublet ATES system consists of two groundwater wells and operates in a seasonal mode. In summertime, cool groundwater is extracted from the aquifer and used to cool down a building or facility. The heated groundwater is re-injected into the aquifer through the other well at typically 100 or 200 meters distance. In wintertime, the flow direction is reversed such that the heated groundwater is extracted and can be used for heating purposes and simultaneously create a storage of cool groundwater [114]. Cold storage is generally applied at 5-12 °C and heat storage at 14-30 °C, although there are also examples where heat is stored at temperatures between 60 and 80 °C [23-26]. Larger systems consist of more than two wells. One of the larger ATES systems in Europe, located at Eindhoven University of Technology, the Netherlands consists of more than 30 groundwater wells [19]. The amount of energy that is recovered from the aquifer is generally lower than the amount that was stored because part of the energy is lost due to dissipation of heat to the surroundings of the storage and advection with regional groundwater flow. This is expressed in the thermal recovery (η_{rec}) of a well [117] (Equation 5.1).

$$\eta_{rec} = \frac{E_{extracted}}{E_{injected}} \quad (5.1)$$

Here the injected ($E_{injected}$) and extracted ($E_{extracted}$) energies are related to the undisturbed temperature of the aquifer. Numerical modelling of a doublet ATES system shows that thermal recovery in a stagnant aquifer can be higher than 75% and drop to 40% with a regional groundwater flow velocity of 150 m/yr [123]. Field studies report thermal recovery values between 65 and 82% [130, 151]. Selection of a suitable aquifer is an important step in the design of an ATES system. In general, suitable aquifers should readily yield water and have a low

hydraulic gradient to prevent the stored energy to be transported outside the capture zone of the well [117, 208, 209]. Dissipative heat loss can be reduced by selecting an aquifer with a temperature close to the storage temperature and below the zone that is influenced by seasonal temperature fluctuations. Care should also be taken to select appropriate materials according the chemical composition of the soil and groundwater to prevent well clogging [23]. Rapid increase in the number of ATEs systems in the Netherlands over the past 20 years (Figure 5.1) has led to the situation that in areas such as dense populated city centres, wells are placed at such small well-to-well distances that they influence each other's extraction temperature [117]. Furthermore, for mono-directional systems, Ferguson and Woodbury [47] report thermal interference between wells due to insufficient well spacing. In case of wells with similar storage temperature (e.g. both wells storing water warmer than the ambient aquifer temperature), thermal interference can improve the system performance. However, in case of wells with non-similar storage temperature thermal interference can deteriorate the system performance [48, 117, 121]. Thermal interference limits large scale application of ATEs when energy demand is high considering the available aquifer volume. Due to the increasing demand for sustainable heating and cooling, the impact of thermal interference on the overall performance and optimal usage of the subsurface potential are important issues for the development and integration of large-scale ATEs systems.

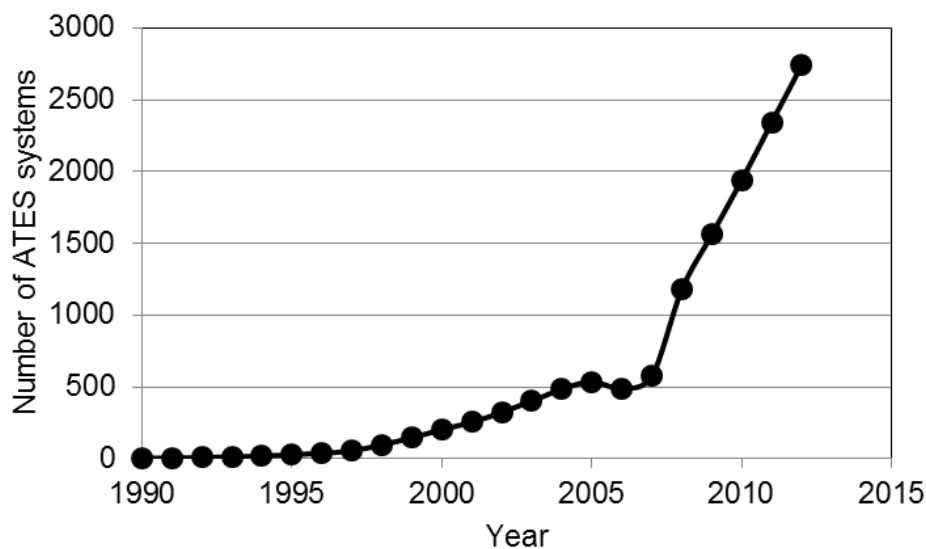


Figure 5.1 The number of ATEs system in the Netherlands in the utility sector (compiled from yearly reports of the Dutch Central Bureau of Statistics [45, 55-63]. The apparent decrease in 2006 may result from the use of a different method to estimate the number of systems. Accuracy of this data is estimated to be 25% [45]

Generally, for installing and operating an ATEs system, a permit is required from the regulating authority [22, 49]. Permit applications often involve an environmental impact assessment to show (amongst others) that the system does not negatively influence other ATEs systems in the area. However, this does not necessarily lead to the most optimal use of the subsurface [49]. To facilitate optimal use of the subsurface, some municipalities in the Netherlands have issued master plans that regulate the positioning of the wells for storing thermal energy [71, 72, 211]. Common zonation patterns used for positioning wells for cold and heat storage are the ‘checkerboard’ and ‘lane’ pattern (Figure 5.2). These patterns can be applied for multiple ATEs systems or the wells of individual systems. From superposition of the drawdown at each well, it follows that the checkerboard pattern minimizes the impact of the well field on hydraulic head. The lane pattern, with $R_2/2 < R_1$, is thermally more efficient, because neighbouring wells that store a similar temperature reduce dissipative heat loss to their surroundings (positive thermal interference). Note that the checkerboard pattern is actually a special case of the lane pattern when R_1 is equal to $R_2/2$. In case of regional groundwater flow, the lanes are aligned with the prevalent groundwater flow direction to minimize thermal interference between the cold and warm lanes (negative thermal interference).

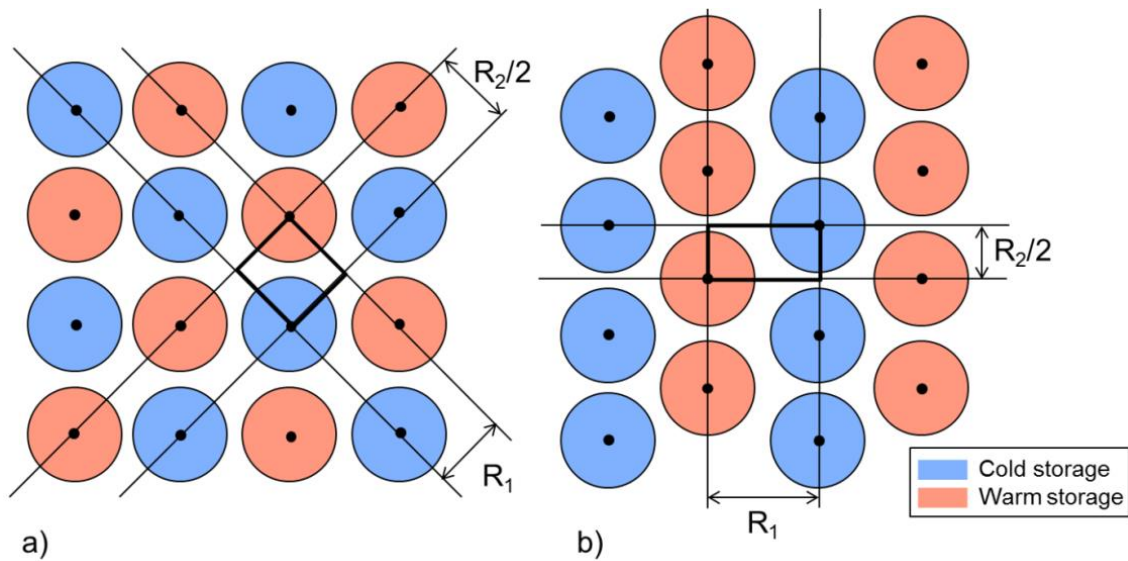


Figure 5.2 a) Checkerboard and b) lane zonation patterns to arrange ATEs wells. The circle around each well indicates $1 R_{th}$ distance for heat storage and cold storage. By using axes of symmetry, each pattern can be modelled by considering the square (indicated in bold) in each respective subfigure

Decreasing the well distance in either pattern allows for more systems in a certain area to be realized and therefore leads to more total energy delivered by all systems combined. However, because of thermal interference the performance of individual wells can decrease. Previous

studies have shown the effect of well distance on thermal interference for doublet systems by scaling the well distance with the thermal radius [121, 123]. The thermal radius (R_{th}) of an ATES well is defined as the maximum distance of the thermal front from the injection well in a homogeneous medium, neglecting vertical flow, advection by regional flow, thermal conduction and dispersion. The thermal radius can be calculated by setting the injected energy ($c_w \cdot V \cdot \Delta T$) equal to the energy stored in a cylinder, centred on the injecting well ($c_a \cdot H \cdot \pi \cdot R_{th}^2$), resulting in Equation 5.2. This serves as a first order approximation of the thermally affected area around an ATES well. Note that the actual affected area may be different from this first order approximation due to thermal conduction, dispersion, heterogeneities and the presence of other than radial flow components.

$$R_{th} = \sqrt{\frac{c_w \cdot V}{c_a \cdot \pi \cdot H}} \quad (5.2)$$

Here, c_w and c_a are the volumetric heat capacity of water and the aquifer (groundwater and aquifer matrix) respectively, V is the volume of water that is injected in one storage cycle and H is the length of the well screen [123].

From numerical modelling studies, Kim et al. [121] report that the recovery of thermal energy is not significantly affected when the wells are separated by more than one thermal radius, while Sommer et al. [123] show that in both homogeneous as heterogeneous aquifers the thermal recovery decreases for well distances below 2 thermal radii. The different conclusions from these studies can partly be attributed to the dependency of thermal recovery on other aspects than the (scaled) distance between the wells, such as the volume of storage and hydrological and thermal conditions, but also by the lack of a well-defined criterion by which thermal interference should be evaluated. The Dutch Society for Subsurface Heat Storage (NVOE) advises a well distance of at least three thermal radii to avoid thermal interference [147]. This design rule includes uncertainties related to the available aquifer thickness, aquifer heterogeneity, and uncertainty and variability in future energy demand.

In this chapter, the thermal performance of large-scale application of ATES is determined using a simplified hydrogeological model. We compare the different zonation patterns and determine the influence of well-to-well distances. The role of aquifer thickness, thermal radius and heat loss through the upper and lower confining aquitards are discussed. Also, we provide a method to determine the amount of thermal interference that is acceptable from an economical and environmental perspective. The method is demonstrated using hydrogeological conditions that are roughly representative for the aquifer used for thermal storage in Amsterdam, the Netherlands, a city with one of the highest concentrations of ATES systems reported. In such

situations, thermal interference between ATES wells is expected to become even more critical in the near future, due to a further increase in the number of ATES systems. Using a sensitivity analysis we identify key factors that determine optimal well-to-well distances and quantify the impact of these factors on the amount of energy that is supplied and on the reduction of costs and CO₂ emissions. Actual design of individual well locations in a large-scale application of ATES at a specific site will probably benefit from a site-specific model that includes detailed characteristics of that site. In a specific urban area not all locations will be available for installation of groundwater wells due to presence of buildings and infrastructure and conflicting uses of the subsurface. These types of considerations are not included in our calculations. Rather we aim to increase insight in the key factors that determine optimal design, operation and management of large-scale ATES systems.

5.2 Materials and methods

Using a simplified hydrogeological model, the thermal efficiency of a doublet ATES system in a large-scale application of ATES is determined by modelling the solid rectangles in Figure 5.2. In this model the aquifer used for storage is simplified to a homogeneous horizontal aquifer that is confined on the lower and upper side by aquitards (geological layers of low hydraulic conductivity in comparison to the adjacent aquifer). The well is screened over the full thickness of the aquifer. The distance between lanes (R_1) and the distance between wells within a lane (R_2) are varied to determine their influence on the thermal performance of the doublet system. Following the thermal assessment, equivalent annual cost and CO₂ emission associated with the installation and operation of the doublet system are calculated. A comparison is made with cost and CO₂ emissions of a conventional heating and cooling system that would provide the same amount of energy. We hypothesise that for very large well distances, ATES will only generate a limited amount of energy per area, and therefore also the reduction in cost and CO₂ emissions per area with respect to the conventional system will be limited. For very small well distances on the other hand, the amount of energy provided per area will be larger, but due to severe thermal interference, the cost and CO₂ emission reduction with respect to the conventional system will be small or even negative. However, for intermediate well distances ATES is expected to be a cost-effective technology [111], for which optimal well-to-well distances can be determined.

Hydrogeological model

The dimensions of our model are based on geohydrological conditions of the aquifer used for ATES in Amsterdam, the Netherlands. Analysis of 36 permitted ATES systems (105 wells) in Amsterdam [212] shows that well screens are generally constructed at a depth between 70 and 180 m. The average well screen length is 64.8 meters. The aquifer at these depths belongs to the Peize formation that consists of coarse sand (grain size 210-2000 µm) [213]. The aquifer is

simplified to a confined aquifer with a thickness of 60 meters with its base at 180 m. Aquifer hydraulic conductivity is set to 30 m/d [213]. Based on regional hydraulic head contours [213], and a porosity of 0.35, the groundwater flow velocity in this aquifer is estimated to be around 5 m/y, but is neglected in the current groundwater model. Using symmetry axes, the performance of a doublet system in a large-scale application of ATEs can be modelled with the boxed volume in Figure 5.3. Boundary conditions comprise of no flow and zero heat flux along the boundaries of the boxed volume. The wells are modelled with a fixed flow rate and injection temperature.

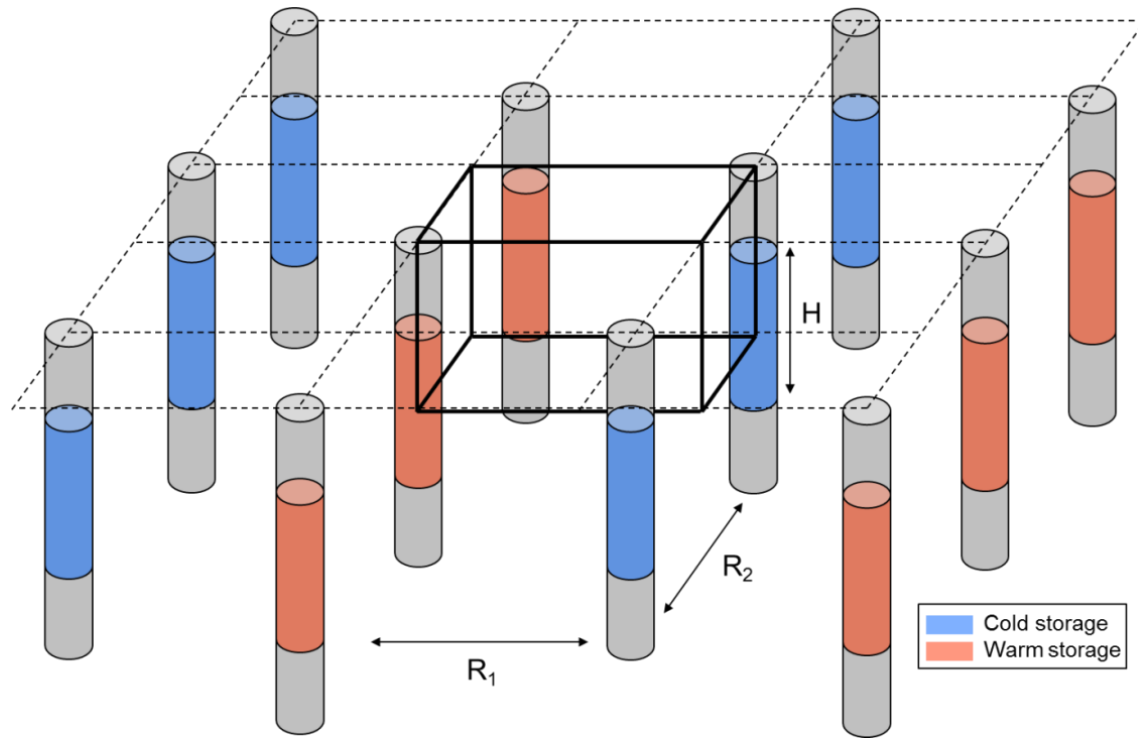


Figure 5.3 Schematic layout of wells used for warm and cold storage, positioned in lanes. Using symmetry axes, performance of a doublet system in a large-scale application of ATEs can be represented by modelling the boxed volume

Subsurface heat transport was modelled with Modflow [169] and MT3DMS [170]. Modflow and MT3DMS are widely used computer codes for simulation of groundwater flow and solute and heat transport. References and validation are available in [28, 169-171, 214, 215]. MT3DMS was originally designed to model solute transport. Due to similarity between the solute and energy transport equation, MT3DMS can be applied to model heat transport by adopting the following transformations [28, 171]. Thermal diffusion coefficient (D_T) is given by $D_T = k_b / (n \cdot c_w)$, where k_b is the bulk thermal conductivity of the aquifer and n is porosity, and thermal distribution coefficient $K_d = c_s / c_w$, where c_s is the specific heat of the solid phase. Using quartz as the main constituent of the aquifer material, the thermal distribution coefficient, bulk density and thermal

diffusion coefficient are set to $1.56\text{E-}4 \text{ m}^3/\text{kg}$, 1718 kg/m^3 and $0.306 \text{ m}^2/\text{d}$ [28]. Thermal dispersion is assumed negligible compared to thermal diffusion [193, 194, 216] and therefore set to zero. Model accuracy related to the choice of numerical tolerance criteria is addressed in Appendix 5.1.

Zonation pattern

The distance between the lanes (R_1) and between the wells within a lane (R_2) are independently varied between 0.3 and 5 thermal radii. These boundaries are chosen to explore much smaller as well as larger well distances than the current design rule of $3 R_{th}$ [147]. A larger well distance than $5 R_{th}$ is considered not realistic, because of practical limitations, such as property boundaries or the scale of urban redevelopment. The aquifer volume that is used for thermal storage in our model domain is approximated by $\pi \cdot R_{th}^2 \cdot H / 8$, while available aquifer volume in the model is equal to $R_1 \cdot R_2 \cdot H / 4$. Storing a larger volume than the available aquifer volume is not sensible, since the excess would be extracted at the extraction well due to short circuiting. With one well distance (R_1 or R_2) at its maximum value ($5 R_{th}$) this leads to a minimum of $0.31 R_{th}$. Therefore, the minimum well distance in our simulations is set to $0.3 R_{th}$. Another reason for a minimum distance between wells within a lane is that the combined drawdown and pumping head can become too large due to superposition of the drawdowns for the individual wells. Due to application of insulated pipes, energy loss between the building and the wells is considered negligible for well distances below $5 R_{th}$.

Discretization

The number of grid cells is 30 in direction of R_1 and 15 in direction of R_2 . The number of grid cells is chosen such that for maximum distance ($5 R_{th}$), the approximate thermal influenced distance of $1 R_{th}$ is covered by at least 6 grid cells. A grid refinement to 50 (R_1) and 25 (R_2) cells showed that the grid was fine enough to accurately simulate the thermal behaviour of the ATES system (RMS of thermal efficiency $< 0.5\%$, Appendix 5.1). The distance between the wells is varied by changing the size of the grid cells. To accurately resolve conductive heat transfer with the aquitard above (and below) the aquifer, a layer thickness of 1 m is chosen for the aquifer-layer closest to the aquitard. Towards the middle of the aquifer (where the vertical temperature gradient is smaller), the layer thickness is allowed to increase with a factor of 1.5 per layer. For the same reason, the aquitard is divided in layers which are finer close to the aquifer, similar to Sommer et al. [123]. An overview of the discretization of the model layers is given in Table 5.1. To test the layer discretization, the number of model layers was increased to 30 and the aquitard thickness was increased up to 113.33 m. Both refinements did not significantly influence the model results (RMS values $< 0.03\%$, Appendix 5.1).

Table 5.1 Discretization of model layers

Layer nr	Layer type	Thickness [m]	Layer nr	Layer type	Thickness [m]
1	Aquitard	17.09	9	Aquifer	1.00
2	Aquitard	11.39	10	Aquifer	1.50
3	Aquitard	7.59	11	Aquifer	2.25
4	Aquitard	5.06	12	Aquifer	3.38
5	Aquitard	3.38	13	Aquifer	5.06
6	Aquitard	2.25	14	Aquifer	7.59
7	Aquitard	1.50	15	Aquifer	9.22
8	Aquitard	1.00			

Heating and cooling loads

In general, seasonal ATEs systems are in heating mode in the winter and in cooling mode in the summer. However, due to variability in energy demand, a specific system may switch on and off several times per day and vary the pumping rate. Furthermore, in spring and autumn, systems may switch between heating and cooling mode, for example to provide heating in the morning and cooling in the afternoon. Short-term variations in flow rates are assumed not to influence the overall thermal impact and thermal efficiency of the system and are commonly averaged over time periods of 3 to 6 months [114, 121, 123, 161]. Heating and cooling loads in our simulations are simplified to a 4 month heating period in winter and a 4 month cooling period in summer, with a period of 2 months in between when the system is not running, similar to the seasonal variation observed in an existing ATEs system in the Netherlands [130]. Flow rate and injection temperature are constant during each period and chosen to represent a typical system as applied in the utility sector [114, 130, 217]. The robustness of this approximation was tested by running our model also using shorter and longer production periods, while preserving the total seasonal flow rate. Calculations show that thermal efficiency is not affected while varying the production period length between 73 and 164.25 days (RMS < 0.55%, Appendix 5.1). The maximum pumping rate is determined from guidelines on maximum velocity on the borehole wall [218] and the length of the well screen and set to 200 m³/h. For a system that has an average use of 1500 full load hours/season, this gives a seasonal flow rate of 300 000 m³ for each well. In our model only 1/8 of each well is modelled, such that during the heating period 308.6 m³/d is extracted from the warm well and injected into the cold well, with an injection temperature of 7 °C. During the cooling period the same extraction flow rate is assigned to the cold well and injected in the warm well, with an injection temperature of 13 °C. The natural aquifer temperature is 10 °C [114, 130]. The model was run for 30 years, which is the expected lifetime of the ATEs system.

Thermal efficiency

From the modelled extraction temperature, the extracted energy for each 4 month cooling or heating period during the lifetime of the system is determined following Equation 5.3.

$$E_{\text{extracted}} = \int_{\text{extraction}} c_w \cdot Q \cdot |T_{\text{extraction}} - T_{\text{injection}}| \cdot dt \quad (5.3)$$

Here, Q is the (positive) total pumping rate, $T_{\text{extraction}}$ is the temperature of the water that is extracted from the production well, $T_{\text{injection}}$ is the temperature of the water that is injected in the injection well and dt is a time increment. The total pumping rate in our model is divided over the well nodes proportional to the layer thickness. Extraction temperature is determined from a volume averaged extraction temperature for each layer. The thermal efficiency (η_t) is defined by normalizing the extracted energy by the energy that would be extracted if there would not be any subsurface heat loss ($E_{\text{extracted}}^{\text{no heat loss}}$). In our simulations pumping rate (Q) and injection temperatures in summer and winter are constant during the operational modes, such that $E_{\text{extracted}}^{\text{no heat loss}} = c_w \cdot Q \cdot \Delta T \cdot \Delta t$. Here ΔT is the difference between the injection temperature of heated water during cooling mode (summer) and cooled water during heating mode (winter) and Δt is the duration of the operational mode (in our case 4 months). Then, η_t reduces to:

$$\eta_{t,i} = \frac{\int_{\text{extraction},i} |T_{\text{extraction}} - T_{\text{injection}}| \cdot dt}{\Delta T \cdot \Delta t} \quad (5.4)$$

The subscript i indicates the year since start of the system, $\eta_{t,i}$ is the thermal efficiency for year i . Another way to interpret η_t is that it gives the average temperature difference between the wells during operation, normalized with the temperature difference in case there is no subsurface energy loss. η_t can vary between 0 and 1. If $\eta_t = 1$, no subsurface energy losses occur and the average temperature difference between the extraction and injection well is equal to $T_{\text{injection}}^{\text{hot}} - T_{\text{injection}}^{\text{cold}}$. For $\eta_t = 0$, the extraction temperature is equal to the injection temperature at any moment during the production phase such that in fact no energy is provided by the ATES system. In practice, subsurface energy losses (i.e. thermal interference, advective and conductive heat loss) result in a thermal efficiency between 0 and 1. In the definition of the thermal efficiency, energy is related to the temperature difference between the extraction and injection well. Note that this is different from thermal recovery, where energy is related to the temperature difference between the extracted water and the ambient temperature of the aquifer. Thermal recovery is an indicator of the thermal performance of a single well. In our case it is more convenient to use thermal efficiency because (1) it is proportional to the energy delivered by the

ATES system, and (2) the concept of thermal recovery is not usable when the extraction temperature of the cold well becomes higher than the ambient aquifer temperature (or lower in case of the warm well), which can occur in case of thermal interference.

During the first years after the start of an ATES system, the surroundings of the storage wells adapt to the temperature of the injected water, resulting in a gradual increase of the thermal efficiency [117, 123, 130, 151]. A thermal response time is defined as the time needed to arrive at a thermal efficiency larger than 95% of the final thermal efficiency during the expected life time of the system (30 years). The thermal response time is calculated by interpolation of the thermal efficiency values for each year.

The injection temperatures that are normally applied in ATES systems are between 6 and 20 °C [219]. In this range, the effect of temperature dependency of groundwater viscosity and density on the performance of the ATES can be neglected [139, 146, 173, 176] such that the heat transport processes (advection, conduction and dispersion) are linear with temperature. As long as the difference between the injection temperatures in summer and winter with the ambient aquifer temperature are equal, η_t becomes independent of injection temperatures.

Volume ratio

For a pattern of wells, the total volume of aquifer that is occupied (i.e. not available for other thermal applications) is usually much bigger than the actual volume that is used to store the thermal energy. For design of large-scale ATES, a volume ratio (η_v) is defined as a simple design tool to approximate the relative aquifer volume that is used for thermal storage.

$$\eta_v = \frac{V_{storage}}{V_{occupied}} \quad (5.5)$$

$V_{storage}$ is the estimated aquifer volume that is used for thermal storage, neglecting thermal diffusion and dispersion and is given by $c_w/c_a \cdot V$. The total aquifer volume that is occupied by the ATES system and therefore not available for other ATES systems is given by $V_{occupied}$. For the lane pattern, the volume ratio can be calculated for each doublet, such that η_v reduces to:

$$\eta_v = \frac{1}{2} \frac{c_w}{c_a} \frac{V}{H} \frac{1}{R_1 \cdot R_2} = \frac{\pi \cdot R_{th}^2}{2 \cdot R_1 \cdot R_2} \quad (5.6)$$

The volume ratio can be used as a design tool, similar to thermal radius and can be calculated during the design when flow rates and well distances are being set.

Energy ratio

By increasing the injected volume (V) or reducing well distances (R_1 and R_2), it is possible to increase the volume ratio (Equation 5.6), even to values higher than 1. However, this does not always mean that more energy is provided. For example for $\eta_v > 1$ we expect that the injected thermal front reaches the extraction well, such that it is not possible to extract more energy. As a measure for how efficient the available aquifer volume is used for energy storage, we introduce the energy ratio (η_e) (Equation 5.7). The energy ratio is defined as the extracted amount of energy in a year (cooling or heating) divided by the energy that would be provided when all aquifer volume that is occupied would be heated or cooled by ΔT , which is the maximum amount of energy that can be supplied by this volume of aquifer.

$$\eta_e = \frac{E_{\text{extracted}}}{V_{\text{occupied}} \cdot \Delta T \cdot c_a} \quad (5.7)$$

In case of the lane pattern, the energy ratio reduces to:

$$\eta_e = \frac{E_{\text{extracted}}}{2 \cdot R_1 \cdot R_2 \cdot H \cdot \Delta T \cdot c_a} = \eta_v \cdot \eta_t \quad (5.8)$$

The energy ratio can be estimated using model calculations in the design stage, or from monitoring in case of field applications. The concept of energy ratio is introduced to show how much energy can (economically) be produced from the subsurface and how this is influenced by the well zonation pattern.

Economic and environmental performance

Two important reasons for applying ATES are (1) to reduce costs for heating and cooling, and (2) to reduce CO₂ emissions with respect to conventional heating and cooling systems. This section describes the approach that is used to calculate the equivalent annual cost and CO₂ emission associated with the energy provided by the ATES system and by a conventional heating and cooling system that would produce the same amount of energy. The ATES system is operated to supply heating with a heat pump and direct cooling, which is representative for application in the utility sector in a moderate climate and the most frequently used configuration for ATES systems in the Netherlands [45]. The conventional system consists of a gas boiler heating system (efficiency 85%) and electrical compression cooling (with a coefficient of performance (COP) value of 3.5) [11]. In our analysis we assume that all energy provided by the ATES system is used and should otherwise be produced by the conventional system. Energy, costs and CO₂ emissions in our analysis are calculated for a doublet in a large-scale application

of ATES. Because the systems in our simulations operate under balanced conditions (equal amounts of heat and cold are extracted from the subsurface), there is no net heating or cooling of the subsurface. Then, the amount of energy (cooling in summer, and heating in winter) that is extracted from the subsurface (E_i) can be expressed as:

$$E_i = c_w \cdot V \cdot \eta_{t,i} \cdot \Delta T \quad (5.9)$$

Here, V can be expressed by $q_{max} \cdot u_{eq} \cdot H$, with q_{max} is the maximum flow rate per meter well screen and u_{eq} is the equivalent number of full load hours per season. Because the surroundings of each well and the confining aquitards adapt to the temperature of the thermal storage via thermal conduction, $\eta_{t,i}$ increases during the first cycles after the start of the system. This has previously been shown by calculating thermal recovery in both modelling [117, 123] and field studies [130, 151]. When a heat pump is used, the amount of heat provided to the building is larger than E_i , because of the additional input of electrical energy. Given the coefficient of performance of the heat pump (COP_H), the electricity use of the heat pump is $E_i / (COP_H - 1)$, such that the total heat delivered to the building each year is $E_i \cdot COP_H / (COP_H - 1)$. Cooling can be delivered without use of a heat pump (free cooling) such that the amount of cooling delivered is equal to E_i . Current heat pumps operate with a COP_H between 3 and 5 [220-222], such that in our case approximately 43% of the total energy that is supplied by the ATES system each year is cooling and 57% is heating. When this does not match with the ratio between heat and cooling demand of a building we assume the surplus to be provided by an additional (conventional) system which would generate the same costs and CO₂ emissions regardless whether an ATES system was applied or the conventional system.

Electricity use

Total electricity use of the ATES system consists of electricity used for pumping of the groundwater for each well, and electricity used to drive the heat pump (Equation 5.10).

$$E_{i,ATES} = 2 \cdot q_{max} \cdot u_{eq} \cdot H \cdot E_p + E_i / (COP_H - 1) \quad (5.10)$$

The subscript *ATES* indicated the ATES system, while the conventional system is indicated by the subscript *conv*. E_p is the electrical energy needed to pump 1 m³ of groundwater (kWh/m³). In the conventional system, electricity is used to drive a heat pump for cooling, with a COP value equal to COP_C (Equation 5.11).

$$E_{i,conv} = E_i / COP_C \quad (5.11)$$

Gas use

There is no gas use when the ATEs system is used.

$$G_{i,ATES} = 0 \quad (5.12)$$

For the conventional system, the amount of heat delivered to the building is generated by a gas boiler with efficiency B .

$$G_{i,conv} = E_i \cdot COP_H / (COP_H - 1) / B \quad (5.13)$$

CO₂ emission

CO₂ emissions are calculated from the electricity and gas use in combination with emission factors for electricity production C_{elec} and gas use C_{gas} .

$$C_{i,ATES} = E_{i,ATES} \cdot C_{elec} \quad (5.14)$$

$$C_{i,conv} = E_{i,conv} \cdot C_{elec} + G_{i,conv} \cdot C_{gas} \quad (5.15)$$

Costs

Costs for each doublet are calculated combining (1) investment and (2) operational costs such as: maintenance and costs for electricity use, gas use and for CO₂ emissions. Total investment costs for ATEs (I_{ATES} , Equation 5.16) include fixed costs (P_{fix}) per project for constructing the well housing at the surface, transport pipes in the building, supply and installation of a heat exchanger and heat pump, electrical and technical control systems and permit applications (1st term on the right hand side of Equation 5.16), costs for drilling and construction of the wells (2nd term) and costs for digging and installing pipelines toward the wells (3rd term). Drilling costs are determined from the maximum drilling depth (D) and cost of drilling and well installation per meter (P_{well}). The total length of pipelines towards the wells is estimated from the distance between lanes (R_1) and distance between wells within a lane (R_2) with a price of P_{pipe} per meter.

$$I_{ATES} = P_{fix} + 2 \cdot P_{well} \cdot D + P_{pipe} \cdot (R_1 + R_2 / 2) \quad (5.16)$$

Total operational costs per year ($P_{i,ATES}$) are given by Equation 5.17 and consist of maintenance costs (1st term), electricity use (2nd term) and cost for emitting CO₂ (3rd term).

$$P_{i,ATES} = M_{ATES} \cdot I_{ATES} + P_{elec} \cdot E_{i,ATES} + P_{CO2} \cdot C_{i,ATES} \quad (5.17)$$

M_{ATES} expresses the maintenance costs in relation to the investment costs and P_{elec} , and P_{CO2} give the price of electricity and emitting CO₂. The expected lifetime of a heat pump (16 years [223]), is generally shorter than the lifetime of the ATES system (L), that may vary between 20 and 40 years. Replacement of the heat pump is not included in the normal maintenance costs but is added as extra investments after 16 years, while a residual value after the lifetime of the ATES system is subtracted. The investment costs for the conventional system are calculated from the peak energy load (W_{max}) that can be delivered by the ATES system (Equation 5.18).

$$W_{max} = q_{max} \cdot H \cdot \eta_{max} \cdot \Delta T \cdot c_w \quad (5.18)$$

The maximum groundwater extraction flow rate (q_{max}) depends primarily on the diameter of the well, hydraulic conductivity of the aquifer, the type of the pump that is used and maximum allowable drawdown in the well and velocity on the borehole wall [218]. η_{max} is the maximum thermal efficiency during the lifetime of the ATES system. Investment costs for the conventional system (I_{conv} , Equation 5.19) are estimated from indicator prices per kWh for cooling (P_{cool}) and heating (P_{heat}) that represent investment cost of the cooling system (1st term) and heating system (2nd term).

$$I_{conv} = P_{cool} \cdot W_{max} + P_{heat} \cdot COP_H / (COP_H - 1) \cdot W_{max} \quad (5.19)$$

Similar to ATES, operational costs ($P_{i,conv}$, Equation 5.20) consist of maintenance costs (M_{conv}) and prices for electricity, gas and CO₂ emissions. The terms on the right hand side give respectively costs for: maintenance of the cooling system, maintenance of the heating system, electricity use, gas use and CO₂ emissions.

$$P_{i,conv} = P_{cool} \cdot M_{conv} \cdot W_{max} + P_{heat} \cdot M_{conv} \cdot COP_H / (COP_H - 1) \cdot W_{max} + P_{elec} \cdot E_{i,conv} + P_{gas} \cdot G_{i,conv} + P_{CO2} \cdot C_{i,conv} \quad (5.20)$$

P_{gas} is the price of gas. The lifetime of the cooling system and heating system is set to respectively 15 and 21 years [223]. Replacement of these components is not included in the normal maintenance costs but is added as extra investments after respectively 15 and 21 years, while a residual value after the total calculated lifetime is subtracted. Equivalent annual cost (EAC) is calculated following Pirouti et al. [224] by summing investment and yearly costs after converting them to net present values using a discount rate (j) of 4% [225] and dividing by the lifetime.

$$EAC_s = \left[I_s + \sum_{i=1}^L \frac{P_{i,s}}{(1+j)^i} \right] / L \quad (5.21)$$

Because we are interested in the optimal amount of energy that can be supplied by ATES for large-scale applications, cost reduction is divided by the area (A) that is needed by the ATES system to arrive at an equivalent annual cost reduction per area (Equation 5.22). Similarly, also an equivalent annual CO₂ emission reduction is defined (Equation 5.23). Relative cost and CO₂ emission reduction are given in Equations 5.24 and 5.25.

$$\text{cost reduction} = [EAC_{conv} - EAC_{ATES}] / (A \cdot H \cdot \Delta T) \quad (5.22)$$

$$\text{CO}_2 \text{ emission reduction} = \sum_{i=1}^L (C_{i,conv} - C_{i,ATES}) / (L \cdot A \cdot H \cdot \Delta T) \quad (5.23)$$

$$\text{Relative cost reduction} = 1 - EAC_{ATES} / EAC_{conv} \quad (5.24)$$

$$\text{Relative CO}_2 \text{ emission reduction} = 1 - \sum_{i=1}^L (C_{i,ATES} / C_{i,conv}) \quad (5.25)$$

Investment costs for a medium size (1500 kW) ATES project and other site-specific parameters are estimated from information provided by two consulting companies that are actively involved in the design of ATES systems in the Netherlands (Bam Nelis De Ruiter bv and IF Technology). For the case study Amsterdam, well screen length and depth are confirmed by analysis of permits for 105 ATES wells in the municipality of Amsterdam [212]. Nomenclature and an overview of parameter values used in this study are given in Table 5.2.

Table 5.2 Nomenclature and parameters values and variation (min-max)

Abbreviation [unit]	Description	Value (min-max)
R_1	Distance between lanes [R_{th}]	0.3-5
R_2	Distance between wells within a lane [R_{th}]	0.3-5
H	Aquifer thickness [m]	60 (50-70)
D	Aquifer depth [m]	180 (160-200)
q_{max}	Maximum pumping rate [$m^3/m/h$]	3.33
u_{eq}	Full load hours [h/season]	1500 (1000-2000)
c_w	Water volumetric heat capacity [$MJ/m^3/^\circ C$]	4.2
c_a	Aquifer volumetric heat capacity [$MJ/m^3/^\circ C$]	2.6 (2.2-2.7)
ΔT	$T_{injection}^{hot} - T_{injection}^{cold}$ [$^\circ C$]	6 (4-8)
L	Lifetime ATES system [yr]	30 (20-40)
E_{pump}	Water pump efficiency [kWh/m^3]	0.15 (0.1-0.2)
COP_H	COP heat pump ATES [-]	4 (3-5)
COP_C	COP cooling [-]	3.5 (3-5)
B	Boiler efficiency [%]	85 (75-95)
I_{ATES}	Fixed investment ATES [€]	245000 (245000-275000)
P_{pipe}	Investment pipelines [€/m]	275 (275-288)
P_{well}	Investment wells [€/m]	333 (333-400)
M_{ATES}	Maintenance costs ATES [%]	4 (2-6)
P_{cool}	Investment conventional cooling [€/kWh]	200 (150-250)
P_{heat}	Investment conventional heating [€/kWh]	100 (75-125)
M_{conv}	Maintenance costs conventional [%]	3 (2-4)
C_{elec}	Emission factor electricity [$kg\ CO_2/MWh$]	460 (370-550)
C_{gas}	Emission factor gas [$kg\ CO_2/MWh$]	277
P_{elec}	Electricity price [€/MWh]	102 (51-204)
P_{gas}	Gas price [€/MWh]	32.3 (16.2-64.6)
P_{CO_2}	CO_2 emission price [€/ton CO_2]	14 (0-28)
j	Discount rate [%]	4 (2.5-5.5)

Optimization and sensitivity analysis

The amount of energy that is provided by ATEs varies with distance between the lanes and between wells within a lane. Close positioning of wells leading to negative interference can be acceptable when this is cost-effective for the specific area. To determine optimal well distances for increasing energy demand, iso-energy ratio contours are selected from the modelling results and on these contours the positions with the highest cost reduction with respect to the conventional system are determined. Optimal use of the subsurface is defined by the well positions that result in the highest cost reduction with respect to the conventional system. Sensitivity of optimal well positions, and corresponding energy ratio and cost and CO₂ emission reduction is determined by computing total-effect and first order indices using a Monte-Carlo method [226]. Here the variance in model output is related to a variance in input parameters. The parameter space is filled using quasi-random numbers using the Matlab function LPTAU51 [227], with a sample size of 100 000. An overview of model parameters is given in Table 5.2. For the parameters that are included in the sensitivity analysis, the range of the uniform distribution is specified by the minimum and maximum values (min-max). In the following we give a short motivation for the selected range in each parameter. Variation in aquifer thickness and depth are based on the variability observed in 36 permits for ATEs systems (with a total of 105 wells) in Amsterdam. The equivalent number of full load hours per season is varied between limited use of the system (1000 hours) and intensive use (2000 hours). Note that the thermal efficiency of an ATEs system depends on the size of the storage. The size of a storage can be approximated by the height of the well screen (in our case equal to the aquifer thickness) and the thermal radius (in our case mainly determined by the number of full load hours). Large systems will generally have a higher thermal efficiency due to a more favourable (smaller) surface over volume ratio that results in smaller heat loss. To incorporate this in the model results, simulations are repeated using an aquifer thickness of 50 and 70 meter and a number of full load hours of 1000 and 2000, resulting in a thermal radius between 40 and 60 m. Intermediate results are determined using piecewise linear interpolation. The variation in thermal efficiency considering these ranges in aquifer thickness and number of full load hours is small (<2 pp (percent points)). Variation in aquifer heat capacity is based on a variation in porosity between 0.2 and 0.4. Although a review of 67 ATEs systems in 2007 in the Netherlands showed that the average temperature difference over the wells is around 4 °C, present-day systems are designed for a temperature difference around 8 °C [219]. Therefore, a range in ΔT between 3 and 8 °C seems reasonable. System lifetime, water pump efficiency, investment and maintenance costs of the conventional system are based on information provided by IF Technology. Boiler efficiency was varied between 75 and 95% [228-230]. The average COP of the heat pump for heating in case of the ATEs system, or cooling in case of the conventional system was varied between 3 and 5

[220-222, 231]. The range in cost parameters (I_{ATES} , P_{pipe} , P_{well} and M_{ATES}) is chosen according to the cost estimations for a medium sized (1500 kW) ATES system (Bam Nelis De Ruiter bv and IF Technology). Variation in the CO₂ emission factor for electricity production in the Netherlands is derived from linear extrapolation of the emission factors in 2000 and 2010 [232] to 2020. The emission factor of gas use was fixed according to the European standard EN 15603:2008 [233], however, total emissions vary with the boiler efficiency. The range in electricity and gas price is set from half to double of the current price according to price developments that show a doubling between 1997 and 2007 [234]. The CO₂ emission price was varied between 0 and a doubling of the current price of 14 €/ton [235].

5.3 Results

Thermal performance

Thermal efficiency of a doublet ATES system in the lane pattern (Figure 5.2b) is determined for a distance between lanes (R_1) and wells within a lane (R_2) that are independently varied between 0.3 and 5 R_{th} . As an example, the simulated well temperature is presented for the first year of simulation in Figure 5.4 for the specific case where $R_1 = 3 R_{th}$ and $R_2 = 0.5 R_{th}$. The simulation starts at $t = 0$ d with injection of cold water in the cold storage well for 121.5 d. During this period the temperature in the well is equal to the injection temperature (6 °C). The temperature in the warm well remains equal to the initial aquifer temperature (10 °C) until breakthrough of the cold water appears around $t = 100$ d. After the initial injection phase there is a 61 d period in which the system is inactive. At $t = 182.5$ d the system switches to cooling mode (extraction from cold storage well) and the temperature in the warm storage well becomes equal to the injection temperature (14 °C). Again after approximately 100 d breakthrough of warm injected water at the cold storage well appears, apparent from the increase in temperature in the cold storage well from 6.5 to 11.5 °C at $t = 280$ d.

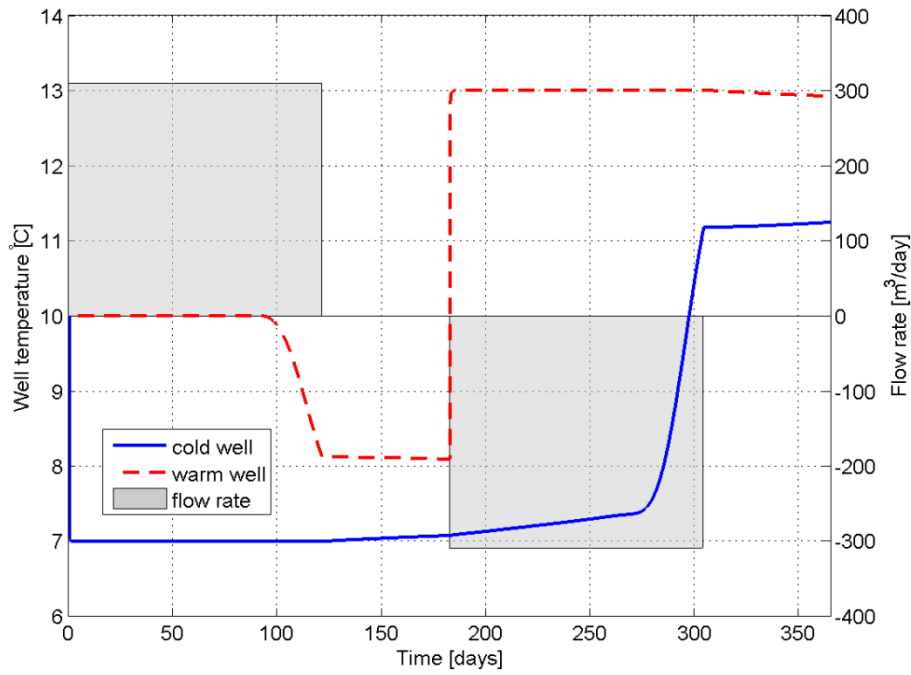


Figure 5.4 Modelled well temperatures during the first year of operation ($R_1=3 R_{th}$, $R_2=0.5 R_{th}$)

Using the modelled extraction temperature, thermal efficiency is calculated following Equations 5.3 and 5.4 and averaged over the lifetime of the system (30 years) and presented in Figure 5.5a. In case of large well distances $(R_1, R_2) = (5, 5) R_{th}$, there is negligible thermal interference between the wells leading to a high thermal efficiency ($\eta_t = 94\%$) averaged over the lifetime of the system. This means that the amount of energy that is yearly supplied by the system is on average 6% lower than the amount of energy that would be supplied if there would be no thermal losses in the subsurface. Due to positive thermal interference, η_t increases by reducing the distance between the wells within a lane up to 96% at $R_2=0.75 R_{th}$. Placing wells with similar storage temperature at this distance from each other reduces conductive thermal losses to the surroundings of the storage, leading to a higher thermal efficiency. Further decreasing this distance changes the flow field around the wells from radial to linear. This increases thermal interaction between the lanes, and therefore reduces the thermal efficiency. When wells within a lane are placed at $R_2=0.3 R_{th}$ the flow field between the lanes is near linear. In this case, thermal efficiency decreases almost linearly when the distance between lanes is decreased. Due to increased thermal interference when placing the wells closer to each other, the thermal efficiency decreases to 6% at $(R_1, R_2) = (0.3, 0.3) R_{th}$. Note that the results for $R_1 < R_2/2$ are similar to the results for $R_1 > R_2/2$ according to the transformation $R_1^* = R_2/2$ and $R_2^* = 2 \cdot R_1$. This can be understood from Figure 5.5b, where the lanes that are in north-south direction for $R_1 > R_2/2$ can be

identified west-east for $R_1 < R_2/2$. In case of non-zero regional groundwater flow this is obviously not the case.

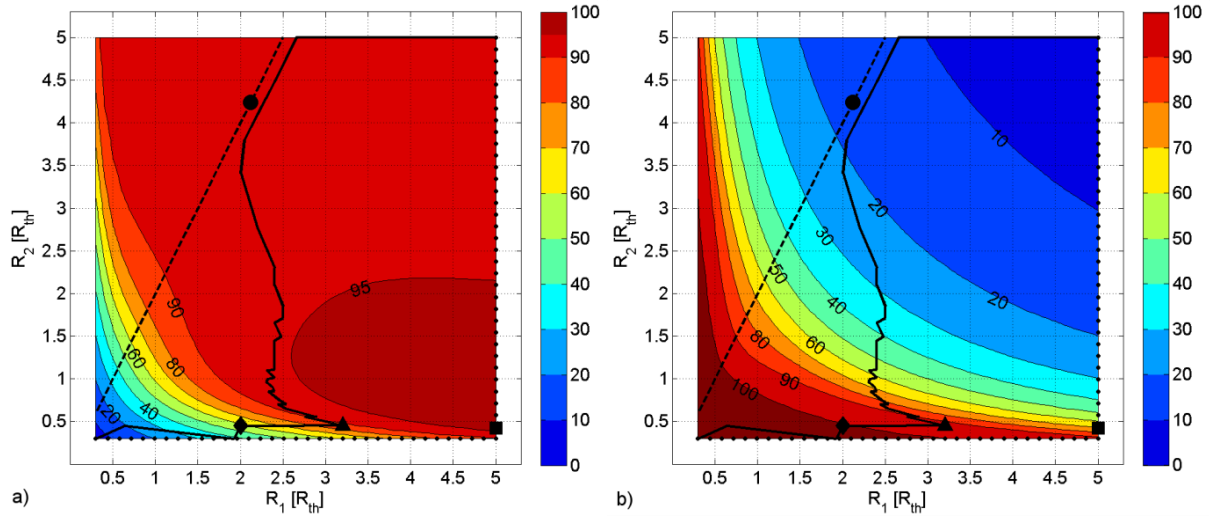


Figure 5.5 a) average thermal efficiency (η_t) [%] and b) average energy ratio (η_e) [%]

The black lines in Figure 5.5, Figure 5.8 and Figure 5.9 indicate different ways to decrease well distances R_1 and R_2 : checkerboard (dashed), minimal negative thermal interference (dotted) and following the maximum cost reduction (solid) and are discussed in section 3.2. The black markers indicate the current 3- R_{th} design criterion (circle), highest cost reduction without negative thermal interference (square), maximum cost reduction (triangle) and maximum CO_2 emission reduction (diamond) and correspond to markers in Figure 5.9.

Although the thermal efficiency for each doublet decreases with decreasing well distances, the total amount of energy delivered by ATEs in a given area increases because more systems can be realized. This is expressed in the energy ratio. The 30 year average energy ratio is presented in Figure 5.5b. Remarkable is that the energy ratio can become higher than 1 for small well distances. This is a result of thermal exchange with the confining aquitards. This is further investigated by running our simulations without thermal exchange with the aquitards. The difference in thermal efficiency is shown in Figure 5.6. For large well distances, heat exchange with the confining aquitards results in a net thermal loss (lower thermal efficiency) with a maximum of 3.8 pp. For very small well distances, however, heat that is stored in these aquitards is transported back to the well by thermal diffusion because the thermal gradient between the aquifer and aquitard inverts owing to severe thermal interference. This effect has a maximum of 1.2 pp on thermal efficiency.

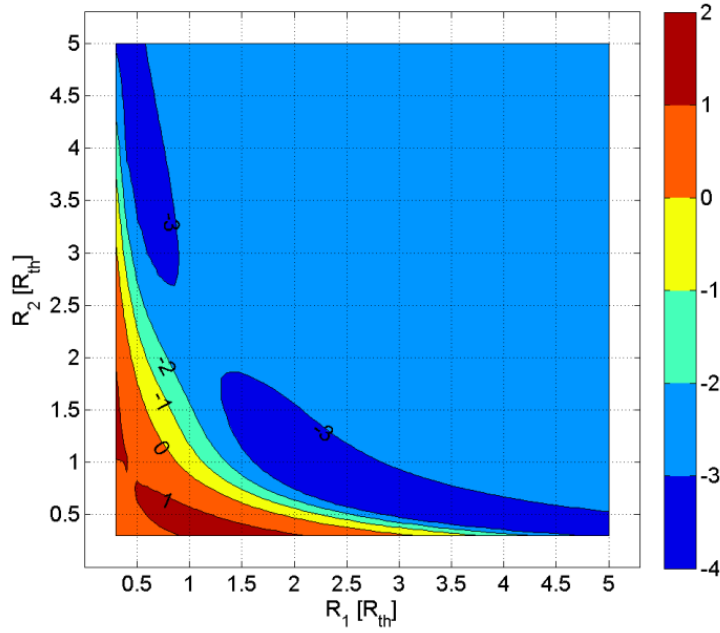


Figure 5.6 Effect of heat transfer with the confining aquitards on the thermal efficiency of a doublet system in large-scale application of ATEs ($\eta_t - \eta_{t, \text{no top/bottom}}$) [pp]

The response time for the system to reach an efficiency larger than 95% of the final thermal efficiency (Figure 5.7) is below 3 years for all well patterns, but depends on the well pattern. In case of strong thermal interference between the lanes, the associated heat loss is much larger than that of diffusive heat loss to the surrounding of the storage, and hardly any improvement of the thermal efficiency with time occurs. The maximum response time of 2.4 years is found at $(R_1, R_2) = (5, 1.8) R_{th}$. This shows that the simulated period (30 years) is sufficient to reach asymptotic values for thermal efficiency.

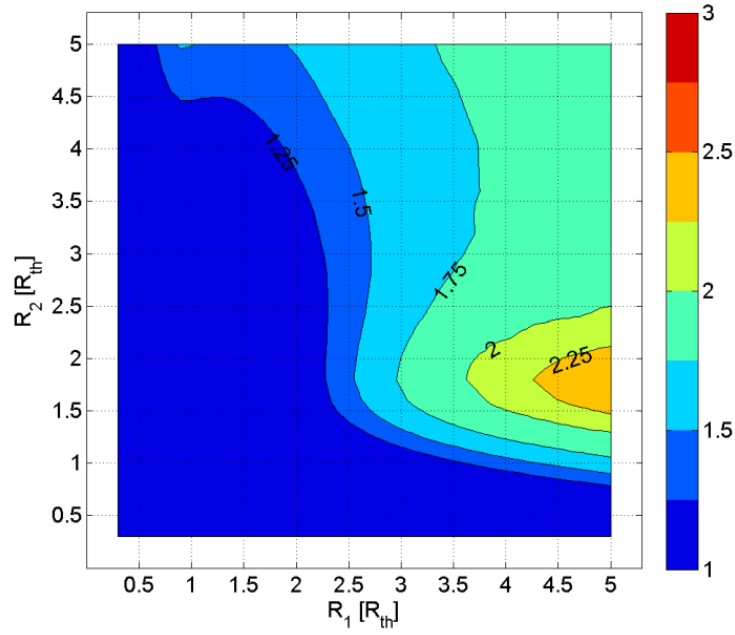


Figure 5.7 Time [years] needed to reach 95% of the final thermal efficiency

Economic and environmental performance

Following the thermal performance, the total costs and CO₂ emissions of the system are calculated. The same is done for a conventional system that would supply the same amount of energy. The difference in costs is shown in Figure 5.8a and the difference in CO₂ emissions in Figure 5.8b. As described in Equations 5.22 and 5.23, results are expressed per year per m² surface area per m aquifer thickness per °C difference in injection temperatures. Cost reduction increases from 0.0012 €/yr/m²/m/°C at maximum well distance $(R_1, R_2) = (5, 5) R_{th}$ to a maximum of 0.019 €/yr/m²/m/°C at $(R_1, R_2) = (3.2, 0.45) R_{th}$. For very small well distances severe thermal interference reduces the well performance such that it is not economically feasible to apply ATEs (a cost reduction smaller than 0).

Reduction in CO₂ emissions compared to a conventional heating/cooling system range from 0.017 kg/yr/m²/m/°C at $(R_1, R_2) = (5, 5) R_{th}$ to a maximum value of 0.27 kg/yr/m²/m/°C at $(R_1, R_2) = (3.4, 0.3) R_{th}$.

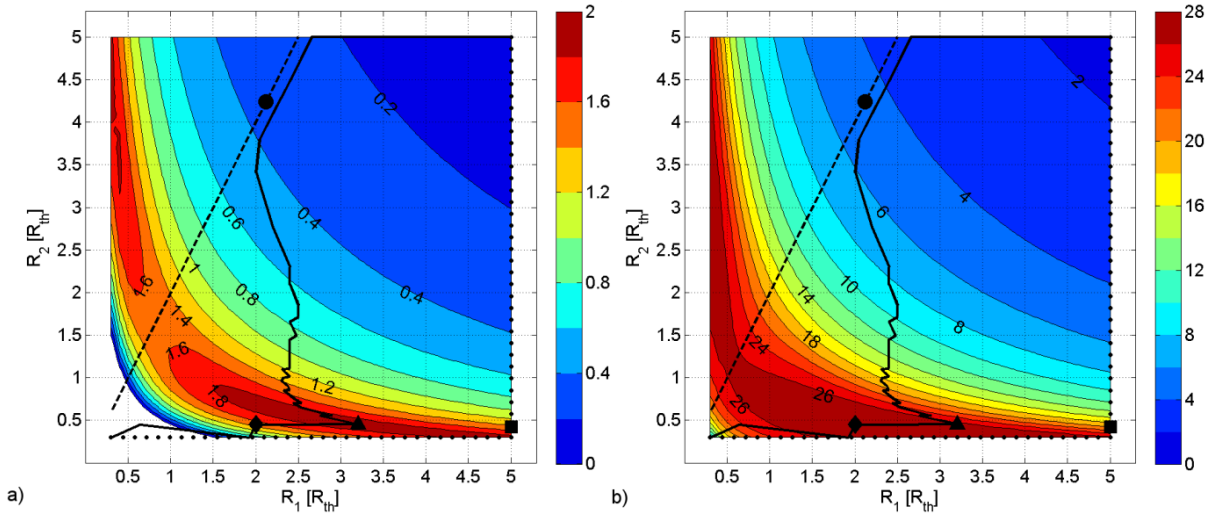


Figure 5.8 a) cost reduction [$0.01 \text{ €/m}^2\text{/yr/m/}^\circ\text{C}$], and b) CO_2 emission reduction [$0.01 \text{ kg/m}^2\text{/yr/m/}^\circ\text{C}$]

For large distance between the wells, the amount of energy that is supplied by ATEs is low (Figure 5.5b), resulting in a low cost reduction (Figure 5.8a). As wells are placed closer together, more energy is supplied by the ATEs systems. The cost reduction grows until thermal interference reduces the performance of each well such that it is not cost-effective to further decrease well spacing. Providing more energy is only functional if it matches energy demand. Therefore, it is reasonable to optimize well positions, given a certain energy ratio that is needed to satisfy the energy demand. This is achieved by selecting iso-energy ratio lines from Figure 5.5b and determining the well distances R_1 and R_2 on this line that result in the highest cost reduction with respect to the conventional heating/cooling system. Connecting the optimal positions for increasing energy ratio defines a path that gives the most economic well pattern for increasing energy demand (solid line in Figure 5.5, Figure 5.8 and Figure 5.9). For comparison also two other paths are plotted that give well patterns according to: (1) the checkerboard pattern (dashed), and (2) minimum negative thermal interference (dash-dotted). Minimum negative thermal interference is achieved by selecting the maximum distance between lanes that is able to provide the demanded energy. This path starts at $(R_1, R_2) = (5, 5)$ and for increasing energy ratio follows first the right boundary, than the lower boundary of the model domain. For low energy ratio ($\eta_e = 0$ to 20%), the optimal path follows the checkerboard pattern because this pattern minimizes the costs for pipelines from and to the wells, which in this case determine the difference in cost reduction for the different combinations R_1 and R_2 . For larger energy demand ($\eta_e > 90\%$) the amount of thermal interference becomes the dominant process to determine total cost reduction and the optimal path approaches the path of minimum thermal interference. The slightly erratic shape of the optimal path results from interpolation errors in the optimization routine (MATLAB v4 griddata method [236]).

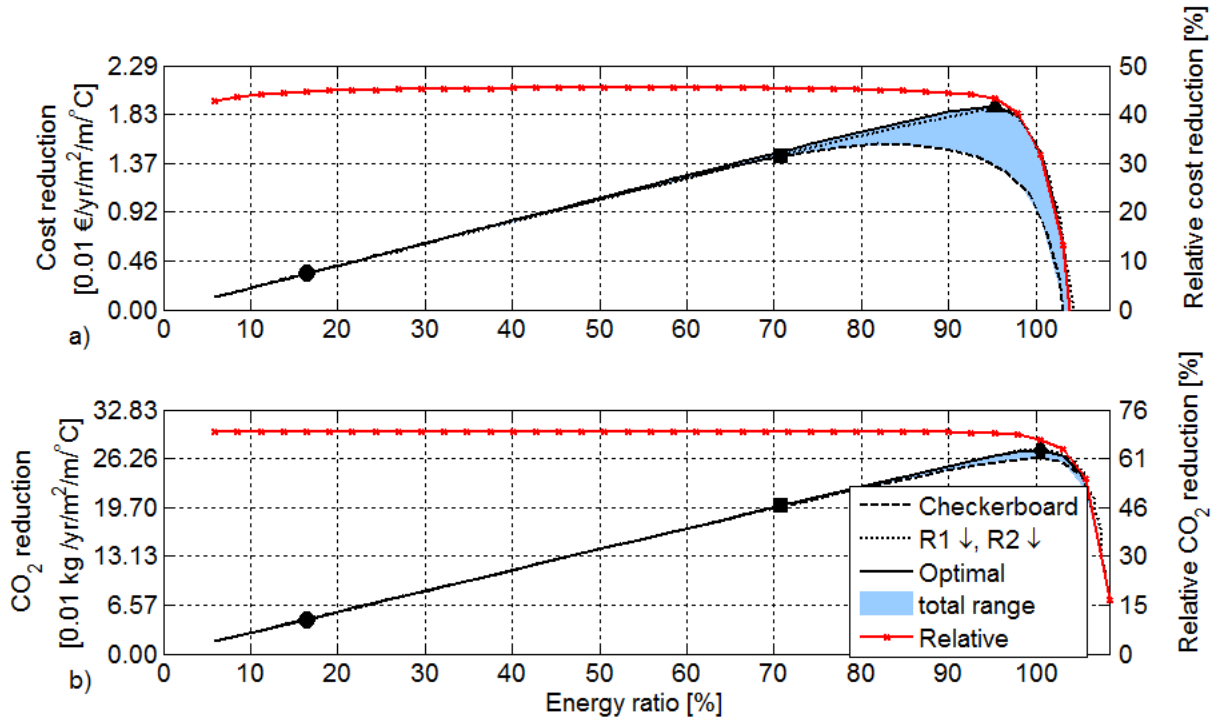


Figure 5.9 a) Cost reduction [€/yr/m²/m/°C] and b) CO₂ emission reduction [kg/yr/m²/m/°C]. The markers indicate the current 3-R_{th} design criterion (circle), highest cost reduction without negative thermal interference (square), maximum cost reduction (triangle) and maximum CO₂ emission reduction (diamond) and correspond to markers in Figure 5.5 and Figure 5.8

The black markers in Figure 5.5, Figure 5.8 and Figure 5.9 indicate the location of maximum cost reduction (triangle), maximum CO₂ emission reduction on the optimal path (diamond), the highest cost reduction achievable without significant negative thermal interference (thermal efficiency $\geq 99\%$ of the maximum thermal efficiency) (square) and the equivalent of the current design norm of 3 R_{th} distance [147] between doublet wells (circle). The 3 R_{th} design norm is developed for doublet systems. The equivalent for large-scale application of this norm is derived considering the checkerboard pattern with a minimum well-to-well distance of 3 R_{th}, thus $(R_1, R_2) = (2.1, 4.2) R_{th}$.

The different paths are compared by plotting reduction of cost (Figure 5.9a) and CO₂ emissions (Figure 5.9b) for increasing energy ratio. Figure 5.9a shows that up to an energy ratio of 71%, the specific well pattern that is used has no significant influence on the corresponding cost reduction. Thus, although the optimization is able to find the most cost-effective well pattern for $\eta_e < 71\%$, the differences in cost reduction between the different patterns below this energy ratio do not differ significantly compared to the increase in cost reduction for higher energy ratio. When energy demand is higher and the energy ratio is further increased, we observe a difference

in cost reduction between the different paths. Cost reduction for the optimal path increases to 0.019 €/yr/m²/m/°C at an energy ratio of 95%. The cost reduction at this point is 40% larger than in case of the checkerboard pattern. The path with minimum negative thermal interference performs almost as well as the optimum path as the curves largely overlap in Figure 5.9. The checkerboard pattern is the least favourable pattern as thermal interference is larger and therefore economic benefits are lower than for the other patterns. In case of maximum cost reduction (black triangle) 35% more energy can be provided than in the case that all negative thermal interference would be avoided (black square). The amount of CO₂ emission reduction is less sensitive to the specific path. When all negative thermal interference would be avoided, emission reduction is 0.20 kg/yr/m²/m/°C. This increases to 0.27 kg/yr/m²/m/°C by selecting maximum CO₂ emission reduction on the optimal path. Because of thermal interference, CO₂ emission reduction decreases fast when well distances are further decreased. The reason for this decrease is that for small well distances, the amount of energy supplied by each doublet in the well field decreases (Figure 5.5), while the flow rate in each well, and therefore electricity use with corresponding CO₂ emissions remains the same as for larger well distances. An overview of the performance and pattern at the economic optimum is given in Table 5.3.

Table 5.3 Optimal performance and pattern for the case Amsterdam and mean \pm 1 standard deviation from the sensitivity analysis

	Case Amsterdam	Sensitivity analysis
Thermal efficiency [%]	87	88 \pm 2
Volume ratio [%]	109	106 \pm 7
Energy ratio [%]	95	94 \pm 4
Cost reduction [€/yr/m ² /m/°C]	0.019	0.020 \pm 0.010
CO ₂ reduction [kg/yr/m ² /m/°C]	0.27	0.25 \pm 0.03
Lane distance [R _{th}]	3.2	3.1 \pm 0.2
Distance within lane [R _{th}]	0.45	0.48 \pm 0.08

The relative reduction in cost is 45%, and does not depend much on the amount of energy that is provided by the ATEs system until the point of maximum cost reduction. The relative reduction in CO₂ emissions is 69% and also independent on the amount of energy supplied for systems smaller than the point of maximum emission reduction.

In the design stage, it is more convenient to express the thermal performance in terms of the volume ratio, because the volume ratio can be easily calculated from the aquifer properties and planned flow rates and well positions, analogues to the use of current guidelines on well distance

that are based on the concept of thermal radius [6, 10, 26]. Energy ratio on the other hand is a result of heat transport simulations or monitoring data. In appendix 5.2, results are presented for increasing volume ratio. The results show that for a given volume ratio, the thermal efficiency of doublets in the checkerboard configuration is always lower than in the lane configuration where $R_1 > R_2/2$. Maximum thermal efficiency is achieved by selecting the maximum distance between lanes and minimum distance between wells within a lane for each given volume ratio. Maximum cost reduction is in this case achieved with a volume ratio equal to 109%. It may be surprising to find an optimal volume ratio larger than 100%. This means that actually more energy is injected than the amount that can be stored by the aquifer volume that is available ($V_{\text{storage}} > V_{\text{occupied}}$). However, part of the energy is transported to the aquitard layers above and below the aquifer, which is not accounted for in the expression for V_{occupied} (Equation 5.6). Accounting for the volume used in the aquitard layers would increase V_{occupied} and reduce η_v , however it is not clear how this volume should be estimated, and therefore unfavourable from a practical point of view.

Sensitivity analysis

The sensitivity of the optimization result is determined using a Monte-Carlo method [226] by relating the variation in optimal pattern and performance to a variation in each parameter. The variation in each parameter may reflect uncertainty in this parameter (e.g. future electricity or gas price, life time of the system) or choices in the design stage (e.g. temperature difference over the wells, seasonal flow rate, a more efficient water pump). Sensitivity of the optimization result is expressed by the total-effect and first-order indices (Figure 5.10). The optimization result is most sensitive to the parameter with the highest total sensitivity index. Figure 5.10 shows that the optimal well distances, energy ratio and associated cost and CO₂ emission reduction are all most sensitive to variations in gas price and temperature difference over the cold and warm storage. For cost reduction (Figure 5.10b) first-order and total-effect indices are similar, indicating that parameters act independently on the model output. For the other performance indicators, first-order indices are generally lower than the total-effect indices, indicating parameter interactions. Increasing the sample size to 200 000 resulted in a maximum change in total-effect and first-order indices of 0.037, which demonstrates that a sufficient sample size was used. The spreading in optimization result is given by their mean values and standard deviation (Table 5.3). The sensitivity analysis shows that the thermal efficiency at the point of highest cost reduction is on average 88%. This is 6 pp lower than the thermal efficiency for non-interfering systems $(R_1, R_2) = (5, 5) R_{\text{th}}$ and 8 pp lower than the pattern with maximum positive interference at $(R_1, R_2) = (5, 0.75) R_{\text{th}}$ (Figure 5.5). Apparently this reduction in thermal efficiency due to negative interference is cost-effective considering the smaller area that is occupied by each system. A lower thermal efficiency than 75% is suboptimal in all parameter combinations. The

highest cost reduction and associated energy that is provided by ATES and CO₂ emission reduction show large spreading due to variation in input parameters (mainly in gas price and temperature difference between the cold and warm storage). Optimal distance between lanes and between wells within a lane is mainly sensitive to P_{gas} , ΔT , COP_H and P_{elec} (Figure 5.10d and e), however, their actual variation is small (Table 5.3). The dependency of optimal pattern and performance on the individual input parameters is illustrated with a local sensitivity analysis, fixing all parameters at their representative value (Table 5.2) and varying the parameters of interest within their range. Local sensitivity for the two most sensitive parameters is shown in Figure 5.11. A higher temperature difference between the cold and warm storage (Figure 5.11a) makes ATES more attractive in comparison with conventional heating/ cooling systems. Therefore more thermal interference is cost-effective such that more energy can be provided (higher energy ratio). This is achieved by selecting slightly smaller distance between the wells within a lane, and slightly larger distance between the lanes. Higher gas prices (Figure 5.11b) also make ATES more attractive and therefore result in a higher cost reduction compared to the conventional system. As a result of ATES becoming more attractive, more thermal interference is allowed, resulting in smaller optimal distance between the wells within a lane such that more energy is provided by ATES and also more CO₂ emission is avoided.

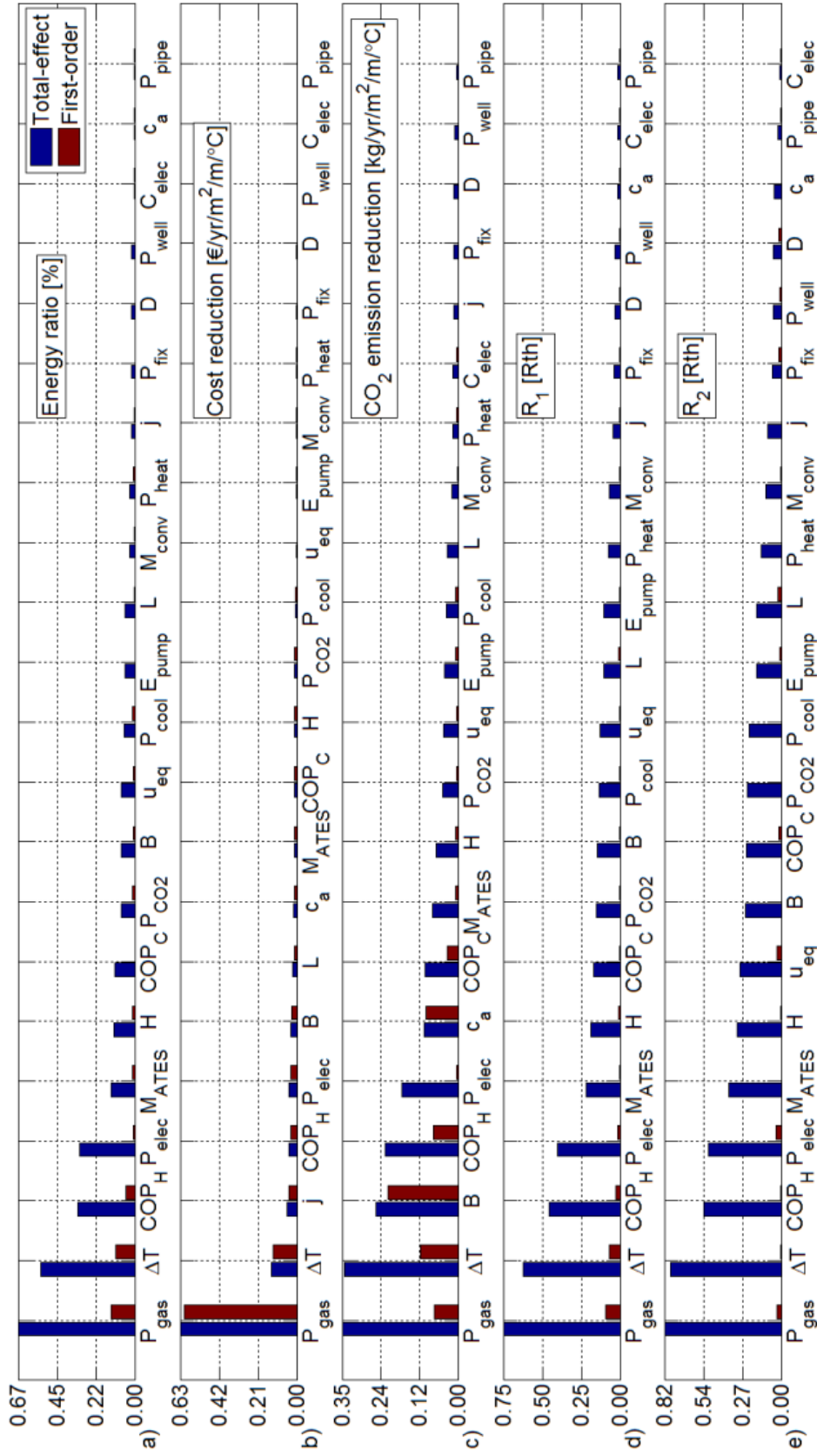


Figure 5.10 Total-effect and first-order sensitivity indices [226] for optimal a) energy ratio, b) cost reduction, c) CO₂ emission reduction, d) distance between lanes and e) distance between wells within a lane

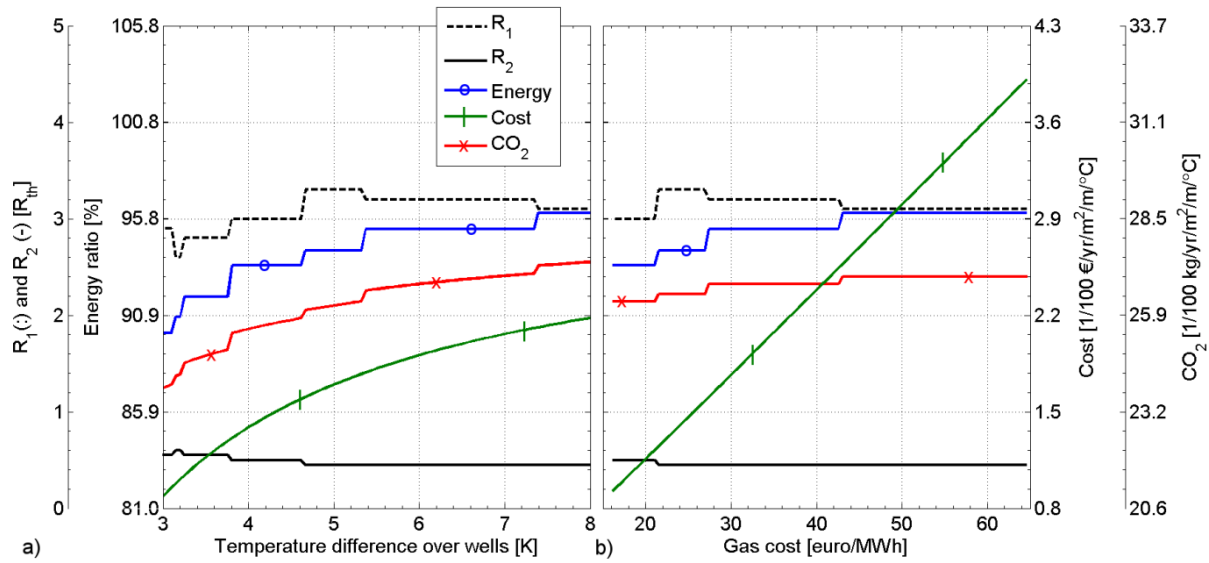


Figure 5.11 Local sensitivities of the two parameters with the highest total sensitivity indices, a) temperature difference between the wells, b) the gas price

5.4 Discussion

Figure 5.9 shows that in our case study it is economically feasible to supply energy with ATES up to an energy ratio of 95%. Several other uncertainties that are not included in our analysis need also to be considered, namely: aquifer heterogeneity creating preferential flow and increased thermal interference [123, 146], or variability in energy demand. Due to these factors, it could be argued to select well distances somewhat larger than the well distances obtained in our optimization. Analysis of 120 ATES permits in the province North-Holland (including Amsterdam, Haarlemmermeer and Amstelveen [212]) shows that in the period 2002 to 2012, systems have pumped on average 50% of their permitted yearly volume. The Dutch Central Bureau of Statistics estimates that in 2007 all systems in the Netherlands combined pumped 56% of their permitted volume [59]. This shows that ATES systems in the Netherlands currently claim a larger aquifer volume than is actually used. This reduces the risk on negative thermal interference, which is sensible when there is enough aquifer volume. However, in case aquifer volume is limiting, oversized volume claims hamper optimal use of the subsurface. More insight in the uncertainties related to the subsurface (aquifer heterogeneity, heat transport properties) and our ability to predict yearly energy demand and its' variability are needed for further improving robust designs of large-scale applications.

Our optimization shows that in case of large-scale application of ATES 30 to 40% more energy can be supplied by allowing negative thermal interference between systems compared to the case in which all negative interference is avoided. This decreases the performance of individual

doublets, but because more doublets can be realized, total energy delivered per aquifer volume, and associated cost reduction is higher than in the case that all negative thermal interference is avoided. When systems in a large-scale application have different owners, it is for the individual owners more favourable to avoid all negative thermal interference. It is therefore important to identify areas with a high energy demand, considering the available aquifer volume, so that the authorities can influence energy savings that can be achieved by introducing regulations. As suggested in Bloemendal et al. [49], another approach is to consider the subsurface as a common resource pool and apply self-organization or self-governance as possible governance tools to approach optimal and sustainable use of the subsurface.

Investment costs for ATES can vary between locations due to different hydrogeological conditions (e.g. presence of clay layers increases drilling cost due to slow drilling, low aquifer hydraulic conductivity requires a larger well diameter, larger well screen length or more wells to produce the same amount of energy), location specific conditions (permits, infrastructure that is present) and economy of scale. Although optimal well distances seem only for a limited degree sensitive to this variation, economic benefits of ATES are. Therefore, future efforts on sustainability and optimization of ATES would benefit greatly from availability of more accurate and extensive data on the economic aspects of ATES. Integrated economic assessments of low temperature ATES systems in literature are scarce. However, the economic analysis presented in Vanhoudt et al. [11] enables comparison of our results. Vanhoudt et al. report on a monitoring study of a low temperature doublet ATES system that supplies cooling and heating to a hospital in Belgium over a three years period. For the ATES system they report total investment (695 k€) and annual fuel costs (28.7 k€). For a reference system, that consist of gas-fired boilers and cooling machines, total investment costs and annual fuel costs are estimated 241 k€ and 82.4 k€ respectively. Assuming a lifetime of both systems equal to 30 years, as in our study, results in an estimated cost reduction by using ATES of 43% compared to the reference system. This is similar to the cost reduction of 45% that is obtained in our study. Over the three-years period Vanhoudt et al. report a reduction of CO₂ emissions between 69 and 77% with respect to the reference system. Again this is surprisingly close to the 69% reduction that is obtained in our study.

In order to put our results on optimal energy ratio for large-scale ATES in relation to actual heating and cooling demand of utility buildings, we investigate under which conditions the available aquifer volume becomes limiting and ATES system performance becomes dependent on the specific well pattern. Literature reports for office heating demand are in the range of 95.6 – 176.1 MJ/m²/yr [237] and 54 – 155 MJ/m²/yr [238] depending on the chosen heating system, while the cooling demand ranges between 45.6 - 121.2 MJ/m²/yr [237] respectively 23.4 - 140.4

MJ/m²/yr [238] depending on the chosen cooling system. In the following, we will use the average of these values for further calculations. As average cooling demand represents the smaller fraction, we assume that the amount of heat extracted from the subsurface is equal to the amount of cooling ($E = 82 \text{ MJ/m}^2/\text{yr}$) in accordance to the earlier assumption that the systems are in thermal balance. Aquifer conditions are chosen to the specifications of the Amsterdam setting as mentioned earlier ($c_a = 2.6 \text{ MJ/m}^3/^\circ\text{C}$; $H = 60 \text{ m}$; $\Delta T = 6 \text{ }^\circ\text{C}$). For an area (A) with multi-storey office buildings, the total amount of energy that should be provided ($E_{\text{extracted}}$) is given by $f \cdot E \cdot A$, where f is the floor space index (i.e. the amount of office floor space with respect to the plot area). The modelling results show that the specific well pattern becomes relevant for $\eta_e > 71\%$. Using Equation 5.7 and the above mentioned conditions this occurs for $f > 8.1$. This analysis shows that under these conditions, the specific well pattern only becomes relevant for concentrated high rise buildings. This is mainly a result of the large aquifer volume that is available (thickness = 60 m). For the specific case Amsterdam this implicates that available aquifer volume in many cases is sufficient to fulfil energy demands for space heating and cooling. Although these results are only valid for the specific conditions in our case study, the presented method can be applied also under different hydrological or economic conditions. For example in case available aquifer thickness is smaller, the spatial pattern will become relevant also for areas with a lower energy demand.

5.5 Conclusion

The energy that can be supplied by large-scale application of ATES is limited by thermal interference between the warm and cold storage. The thermal performance of individual well doublets is optimal when negative thermal interference is avoided. However, in this case, each doublet occupies an unnecessary large aquifer volume, which limits the number of ATES systems that can be realized in a given area, although a larger potential exists. By including more advanced design methods based on local conditions and allowing a limited amount of thermal interference, we have shown that the number of systems can be increased, such that the total benefits of ATES in an area are larger.

By coupling a heat transport model with an economical and environmental analysis of the performance of ATES we developed a method to optimize design of large-scale application of ATES and assess the influence of design parameters on the efficiency of the system. This applies both to multiple wells that belong to a single system as to multiple systems in the same area. A set of dimensionless parameters was introduced that characterize the thermal performance of large-scale ATES. The method can be used to (1) optimize and plan large-scale application of ATES, (2) determine the potential of ATES in a specific area and (3) determine the need for spatial planning considering the expected demand for ATES.

Using hydrogeological conditions of the aquifer used for thermal storage in Amsterdam, we demonstrate that the specific well pattern (checkerboard or lane) does not influence the economic and environmental performance of ATEs up to an energy ratio of 71%. When energy demand is higher, the lane pattern has a higher performance than the checkerboard pattern. In the lane pattern wells with similar storage temperature are placed closer to each other than wells with non-similar storage temperature. Due to positive thermal interference this minimizes subsurface thermal losses. Allowing negative thermal interference between systems allows for more systems to be realized in an area and can cost-efficiently increase the energy ratio to 89-98%, such that 30 to 40% more energy can be provided by ATEs in a given area than in case all negative interference would be avoided. Optimal distance between lanes was between 2.8 and 3.3 R_{th} and optimal distance between the wells within a lane was between 0.41 and 0.56 R_{th} . While optimal well distances are only to a minor extent sensitive to variations in hydrological and economic conditions, the absolute reduction in costs for heating and cooling and reduction in CO₂ emissions show large variation. They are especially sensitive to the gas price and the temperature difference between the cold and warm storage. Therefore, future efforts on sustainability and optimization of ATEs would benefit greatly from availability of more accurate and extensive data on the economic aspects of ATEs and integrated assessment of ATEs as part of the heating and cooling system.

Appendix 5.1: Convergence tests

The sensitivity of our model results for spatial and temporal discretization and numerical tolerance criteria was tested for the following parameters: (1) aquitard thickness, (2) grid size, (3) number of layers, (4) temporal discretization and (5) numerical tolerance criteria. Model refinement tests are performed on the model with optimal well-to-well distance ($R_1=3$ and $R_2=0.5 R_{th}$). For each of these tests we provide a graph of thermal efficiency (%) and the RMS error between the thermal efficiency (%) of the refined model and the model that is used in this manuscript. Thermal efficiency in our results varies between 6 and 96%. We consider an error < 0.5 pp acceptable.

Aquitard thickness

The aquitard thickness in our model is 49.26 m and should be chosen sufficient to accurately represent thermal exchange between the storage aquifer and the confining aquitards. The influence of aquitard thickness is demonstrated by systematically increasing the aquitard thickness between 20.78 and 113.33 m (Table 5.4). As shown in Figure 5.12, energy efficiency deviates for aquitard thicknesses of 20.78 and 32.17 m, but for aquitard thicknesses of 49.26 m and larger the differences become small (<0.05 pp). RMS values are presented in Table 5.4.

Table 5.4 Parametric variation of aquitard thickness

Aquitard thickness (m)	20.78	32.17	49.26	74.89	113.33
RMS value (%)	0.1079	0.0473	0.00	0.0167	0.0214

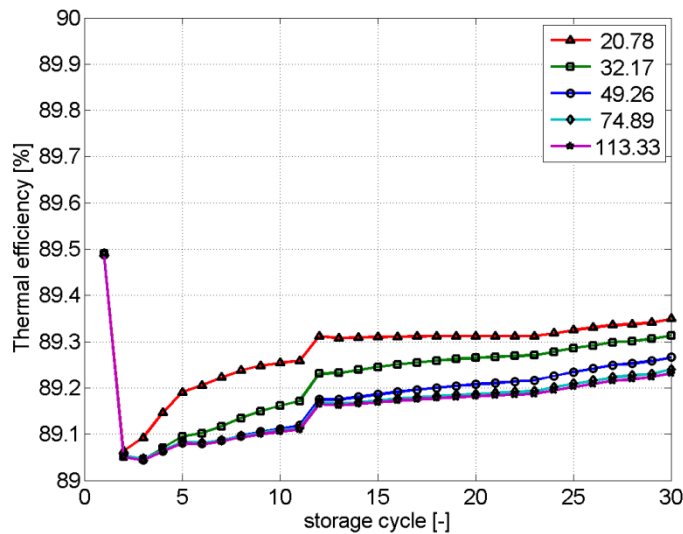


Figure 5.12 Thermal efficiency for increasing aquitard thickness (m) ($R_1 = 3 R_{th}$, $R_2 = 0.5 R_{th}$)

Grid size

Our grid consists of n columns and $n/2$ rows, with $n=30$. This was chosen such that the expected thermal influenced zone of $1 R_{th}$ distance is at least covered by five grid cells. To show that results are not affected by the choice for the grid size, the model was run also using a finer and courser grid by varying n between 10 and 50. Figure 5.13 shows that thermal efficiency is significantly affected by the grid size for $n=20$ or smaller. RMS values between our case ($n = 30$) and the model scenarios are presented in the Table 5.5.

Table 5.5 Parametric variation of the number of grid cells

n	10	20	30	40	50
RMS value (%)	4.15	0.888	0.00	0.339	0.416

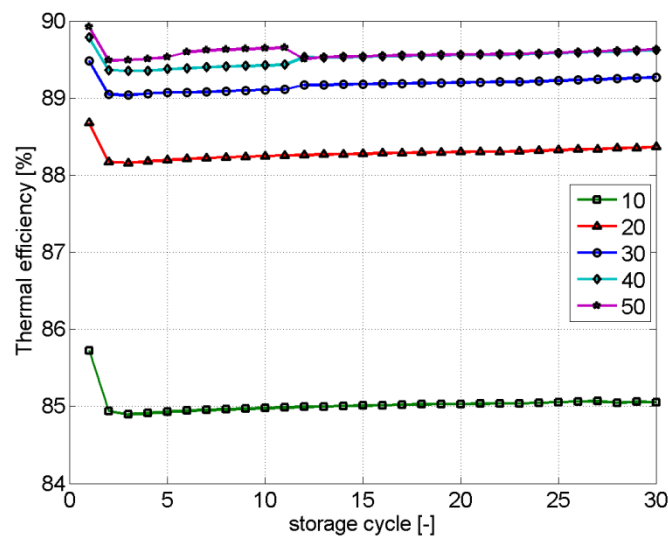


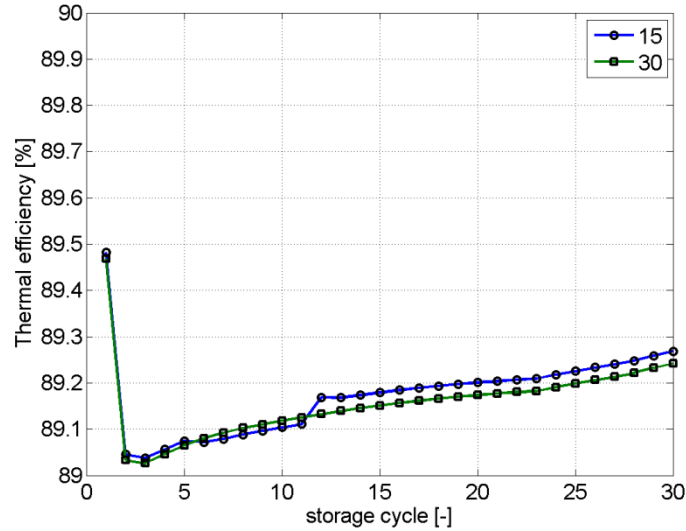
Figure 5.13 Thermal efficiency for various discretization's (n) ($R_1 = 3 R_{th}$, $R_2 = 0.5 R_{th}$)

Number of model layers

The aquifer in our simulations is discretized by 15 layers. To demonstrate that this is sufficient to accurately determine thermal efficiency, the model was also run using 30 layers. Figure 5.14 shows that this affects thermal efficiency by a maximum of 0.036 pp. The RMS values between the model scenarios are given in Table 5.6.

Table 5.6 Parametric variation of the number of aquifer layers

Number of layers	15	30
RMS value (%)	0.00	0.0233

**Figure 5.14** Thermal efficiency ($R_1 = 3 R_{th}$, $R_2 = 0.5 R_{th}$) for a model discretization using 15 and 30 aquifer layers**Temporal discretization**

The length of the heating and cooling season may fluctuate due to a fluctuating energy demand. For the thermal efficiency calculations, the total flow in a season is averaged over a period of 4 months (121.5 d), followed by two months where there is no pumping. We adopt this approximation based on observed flow rates for an existing system [130]. The robustness of this approximation is demonstrated by running the model also by distributing the total flow in a storage cycle over shorter and longer operational periods (Table 5.7). As shown in Figure 5.15, this affects thermal efficiency values below 0.5 pp. RMS values are given in Table 5.7.

Table 5.7 Parametric variation of the length of the production period

Length production period (days)	73	91.25	121.5	146	164.25
RMS value (%)	0.535	0.386	0.00	0.204	0.399

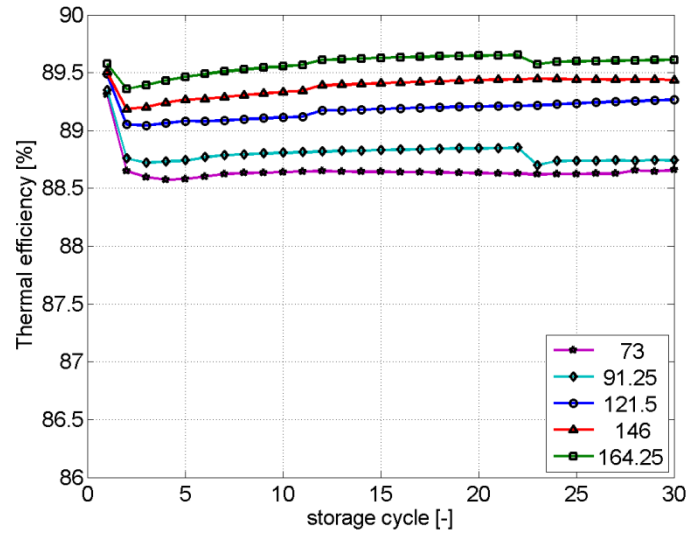


Figure 5.15 Thermal efficiency for various production period lengths (d) ($R_1 = 3 R_{th}$, $R_2 = 0.5 R_{th}$)

Numerical tolerance criteria

In Modflow the preconditioned conjugate-gradient package is used with a maximum head change in one iteration of 0.0001 m (HCLOSE) and a residual criterion for convergence of 0.001 m³/d (RCLOSE). In MT3DMS the generalized conjugate gradient solver package is used with a relative concentration convergence criterion of 0.00001 (CCLOSE). Values were chosen according to the expected head gradients and fluxes in the model and following recommendation in the user manuals. To show that results are not affected by the chosen tolerance criteria, an additional simulation was run in which the tolerance criteria were reduced by a factor 2 (Table 5.8). Figure 5.16 shows thermal efficiency values for both model runs. The curves overlap, indicating that results are not affected by the chosen tolerance criteria. The RMS error between the original model and the model with reduced tolerance criteria is 0.000346.

Table 5.8 Parametric variation of numerical tolerance criteria

Scenario	SC1	SC2
HCLOSE	0.0001	0.00005
RCLOSE	0.001	0.0005
CCLOSE	0.00001	0.000005
RMS value (%)	0.00	0.000346

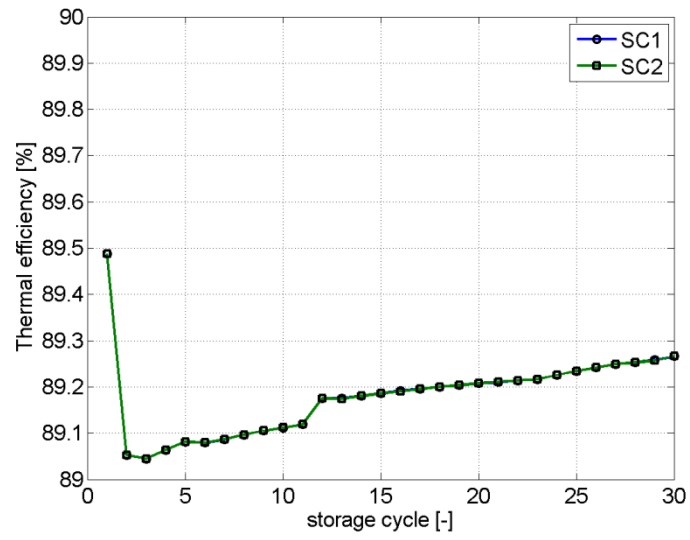


Figure 5.16 Thermal efficiency for two versions choices on numerical tolerance criteria ($R_1 = 3 R_{th}$, $R_2 = 0.5 R_{th}$). Nota bene: the curves exactly overlap

Appendix 5.2

In the design stage, it may be more convenient to express the thermal performance in terms of the volume ratio instead of the energy ratio, because the volume ratio can be easily calculated from the aquifer properties and planned flow rates and well positions, analogues to the use of current guidelines on well distance that are based on the concept of thermal radius [6, 10, 26]. Figure 5.17 shows thermal efficiency (a), energy ratio (b), cost reduction (c) and CO₂ reduction (d) as a function of the applied volume ratio.

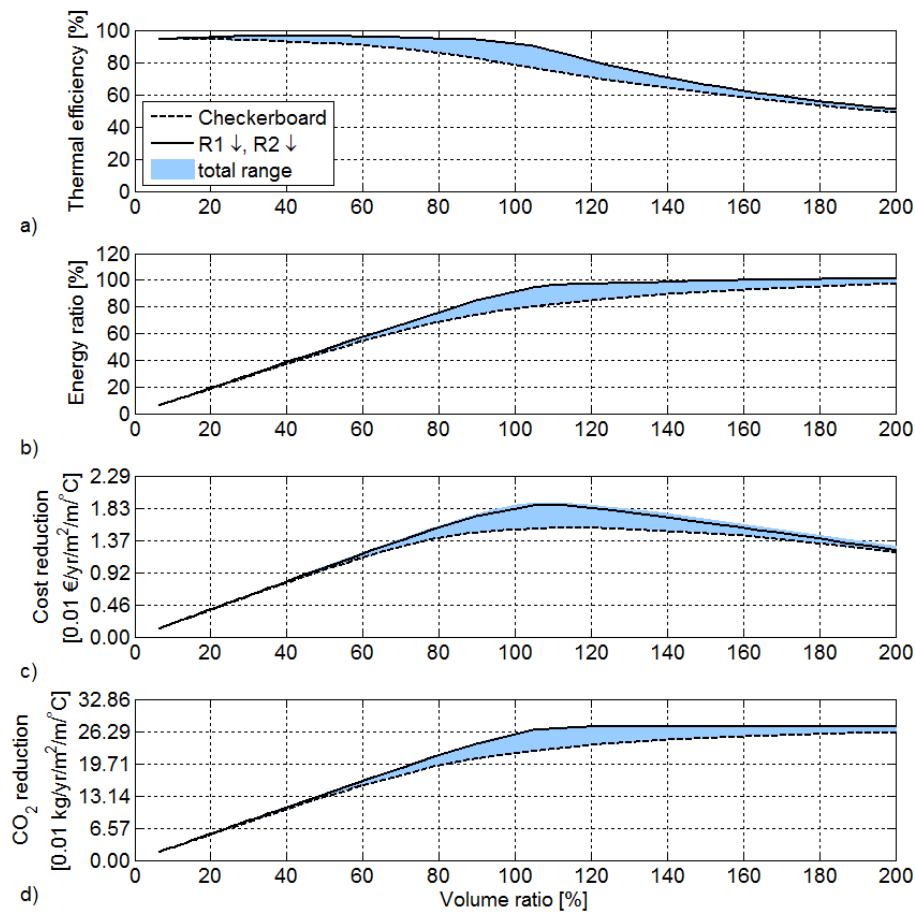


Figure 5.17 Thermal performance and reduction in cost and CO₂ emission compared with conventional heating and cooling

Reactive transport modelling of TCE bioremediation combined with aquifer thermal energy storage

Abstract

Aquifer thermal energy storage (ATES) is increasingly being used to provide heating and cooling for buildings. Because many urbanized centres deal with contaminated soil and groundwater, an increasing number of ATES ambitions is confronted with the presence of contaminants. Hence, a well-designed combination of ATES with biostimulation could be a promising integrated technique, both for remediation of contaminants as for development of ATES. In this study, a reactive transport model was developed to simulate the use of ATES as a continuous biostimulation tool for enhanced reductive dechlorination (ERD) of a hypothetical TCE contaminated aquifer. Model results show that biostimulation by lactate addition reduces iron and sulphate in the capture zone of the ATES wells, after which complete dechlorination is possible. The progress of dechlorination is dictated by lactate dose and amounts of electron acceptors. Although microbial processes are known to be temperature dependent, temperature changes induced by thermal storage do not significantly influence the overall dechlorination process. Simulations also reveal that further study is required on (1) reduction of iron oxide, related to increasing pH of the infiltrated groundwater, and (2) growth and mobility of bacteria related to well clogging, which is a main concern for biostimulation using ATES.

This chapter is submitted as: Sommer, W.T., Ni, Z., Valstar, J., van Gaans, P.F.M., Grotenhuis, J.T.C. and Rijnaarts, H.H.M. *Reactive transport modeling of TCE bioremediation combined with aquifer thermal energy storage*.

6.1 Introduction

The subsurface is increasingly being used to provide heating and cooling for buildings and industrial processes through aquifer thermal energy storage (ATES) [239, 240]. In summer, ATES systems extract groundwater which is used for cooling by passing it through a heat exchanger. The heated groundwater is injected back into the aquifer, typically at a few hundred meters distance. This creates a volume of relatively warm groundwater. In winter, this warm groundwater is extracted and used for heating. This cools down the groundwater, which is again re-injected into the aquifer, such that it can be used for cooling in the next summer [68, 111]. The majority of ATES systems is applied for offices and utility buildings in urban areas [239, 241]. Because many urbanized centres deal with contaminated soil and groundwater [20, 242], an increasing number of ATES ambitions is confronted with the presence of contaminants. Previous research shows that groundwater movement due to application of ATES in a contaminated aquifer can result in a larger contaminant flux to the aqueous phase due to increased dissolution of pure product and a larger volume of contaminated groundwater [82]. Also, temperature changes induced by ATES can impact redox processes, microbial communities [97] and geochemistry [84], and therefore the behaviour of contaminants. Regulations that prohibit extraction, injection or otherwise handling of contaminated groundwater (for example [22, 70, 99]) narrow the opportunity window for ATES as a sustainable energy technology.

At the same time, however, there is a growing interest in combining ATES with bioremediation [97, 98]. In 2012, two pilot locations were studied, where, for the first time, ATES is combined with monitored natural attenuation [99, 100]. In both pilots no active biostimulation or bioaugmentation was applied, although this has been suggested as an adequate method to be applied when natural biodegradation appears to be insufficient [101]. Both pilot locations are contaminated with chlorinated aliphatic hydrocarbons (CAH). Groundwater contaminated with CAH, in particular perchloroethene (PCE), trichloroethene (TCE), dichloroethene (DCE) and vinyl chloride (VC) [243-246], is frequently encountered in urban areas [73-77]. Commonly applied as degreasers at dry cleaners and in chemical and metal processing factories, PCE and TCE, with DCE and VC as degradation products, have entered the groundwater after leakage or improper disposal [78, 247]. Since CAHs are potentially carcinogenic, especially VC [78], their presence in groundwater is a threat to subsurface drinking water resources and public health through penetration into water infrastructure and vapour intrusion into indoor air [79-81]. When present as dense non aqueous-phase liquid (DNAPL), pure product CAH can travel vertically through the subsurface and reach similar depth as where ATES is applied (20-200 m below ground level) [78, 82, 248]. Due to its low solubility, pure product may act as a source of dissolved contaminant and give rise to contaminant plumes [13] with typical lengths that range

from 300 m [245, 249] to 1500 m [250]. This makes physical remediation techniques such as pump-and-treat, soil vapour extraction and soil excavation either too costly or inefficient to properly remediate CAH contaminated subsurface systems [85, 86]. Since biodegradation of chloroethylene compounds was recognized in the late 1970s [251], there is much attention on in situ reductive dechlorination as an effective way to remove organic contaminants [75, 248, 252-256]. Hence, the well-designed combination of ATES with natural attenuation or biostimulation could be a very promising integrated technique, both for remediation of CAHs [101, 102] as for broadening the ATES window of opportunity.

Under natural conditions, reductive dechlorination is usually limited by for example unsuitable redox conditions or lack of electron donor or microorganisms, resulting in absent or incomplete biodegradation of CAHs [87-91]. In these cases, addition of auxiliary electron donor combined with bio-augmentation is required to achieve complete in situ reductive dechlorination [92-96]. Using ATES to deliver electron donor in a biostimulation approach, however, is different from conventional in situ biostimulation for two reasons. First, as temperature is known to be a significant factor for the activity of microorganisms [83, 257], temperature changes induced by storage of cold and warm water may be expected to influence microbial growth and dechlorination. Secondly, ATES involves seasonal displacement of a large volume of groundwater (30 000-150 000 m³) between the cold and warm storage. Therefore, potentially a large aquifer volume can be impacted by ERD activities. Thirdly, flow rates in typical ATES systems (20-100 m³/hour) are much higher than those applied in normal ERD practices (around 2 L/min [94, 95]). As a consequence, crucial for the influence of ATES on biodegradation is whether the microorganisms are transported by the large volumes of groundwater that are displaced by the ATES system, or remain attached to the aquifer matrix, and secondly, how planktonic or attached state affects the activity of the bacteria.

Therefore, optimization and an adequately engineered design of combined ATES and biostimulation as an enhanced bioremediation technique requires comprehensive study of both the biogeochemical aspects as well as characterization of subsurface conditions. Sophisticated modelling is a crucial step to explore the feasibility of the combined technique and direct future laboratory and field experiments. As shown by Chambon et al. [254] and Kouznetsova et al. [258] an increasing number of processes and interactions can be incorporated in numerical models. Although parameterization, especially for field applications, remains a challenge [254], these models can be used to study the relevance and sensitivity of interacting processes. In this study, a reactive transport model was developed to simulate the use of ATES as a continuous biostimulation tool for enhanced bioremediation of a hypothetical TCE contaminated aquifer. With this model we aim to explore the relation between transport and biogeochemical processes

in the capture zone of an ATES system. In several scenarios, the influence of design conditions, i.e. storage temperatures and electron donor dose, were studied for their effect on bioremediation. Furthermore the effects of spreading of biomass upon assumptions regarding biomass mobility and therefore spreading of biodegradation potential in the affected area were simulated.

6.2 Method

Modelling approach

In our hypothetical case, ERD was achieved through lactate addition in both wells of an ATES system in a homogeneous confined aquifer. The reactive transport model was based on Malaguerra et al. [259], who successfully modelled competition between terminal electron acceptors and reactions kinetics in an ERD laboratory batch experiments presented in Scheutz et al. [95]. The model was implemented in the chemical reaction and transport code PHREEQC [260]. PHREEQC is a computer program that incorporates a wide range of biogeochemical reactions, such as kinetic and equilibrium reactions, surface complexation, chemical speciation and 1D transport processes. The constructed model included fermentation of lactate and propionate, iron reduction, sulphate reduction, methanogenesis and sequential reductive dechlorination of TCE, DCE and VC, as well as precipitation of iron minerals and calcite dissolution. Biomass growth and biochemical reactions were fully described by modified Michaelis-Menten kinetics. Competition between terminal electron acceptor processes was incorporated through inhibition factors. The main processes, inhibition and biomass species are presented in the Appendix 6.1 (Table 6.2). The reaction kinetics have been described in detail in Malaguerra et al. [259]. First the batch model presented by Malaguerra et al. [259] was reproduced. Model results (Appendix 6.3, Figure 6.6) were consistent with the results presented in Malaguerra et al. [259], demonstrating correct reproduction of the original model. This batch model was modified to incorporate flow and transport for representing ERD using a typical doublet-well ATES system.

Double axi-symmetric flow tube model

Radial flow around the two wells of the ATES system was simulated using a double axi-symmetric flow tube model (DAFT) [84]. Using the DAFT model, we assume a) sufficient distance between the two wells to exclude interference, b) radial symmetry of flow around the wells, and c) direct infiltration of the volume of water extracted from one well into the other well (Figure 6.1). The equality between extracted and injected water volume is completely in line with how ATES systems function. However, as in this model approach there is no above surface system, we thereby implicitly also assume that d) no significant kinetic reactions occur in the

above surface system. In real ATEs systems, extracted water is directed through pipelines to a heat exchanger, where heat is exchanged either from or to the groundwater depending on the need for cooling or heating, after which the groundwater is directed through a different pipeline towards the injection well. Due to the high pumping rate and small volume of the pipeline network, residence time in the surface equipment is short (minutes to hours) compared to the residence time in the aquifer (approximately half a year), making the latter assumption reasonable.

Initial conditions, boundary conditions and discretization

Flux type boundary conditions were applied to the in- and outflow boundaries of the flow tube. To mimic seasonal storage of thermal energy, each year, flow was defined from left to right in Figure 6.1 for 180 days during summer, followed by 180 days in which the flux is defined in the opposite direction. This simulates extraction from the cold storage well and injection in the warm storage well in summer, and extraction from the warm storage well and injection into the cold storage well in winter. In the middle of the flow tube, a small cell (10 cm) was defined in which no kinetic reactions take place, but where addition of sodium lactate was defined at a constant rate. Temperature in this cell was prescribed equal to the injection temperature of the ATEs system. Initial conditions were chosen according to the initial conditions reported in Malaguerra et al. [259] and are summarized in the Appendix 6.2 (Table 6.3). The radial domain was discretized in 81 grid cells that range in size from 4.74 m near the well to 0.38 m at the model boundary as calculated from equations (1) and (2) in Bonte et al. [84]. Each 180 day season was divided into 20 time steps of 9 days. Therefore, during 1 storage cycle, the injected water travels over 20 grid cells, which represents a total distance of 15 m from the injection well. A reference scenario (S1) was defined in which storage temperatures were set at typical values of 5 °C (cold storage) and 15 °C (warm storage) [84] with an initial aquifer temperature of 10 °C. This model was run for a timeframe of 5 consecutive years.

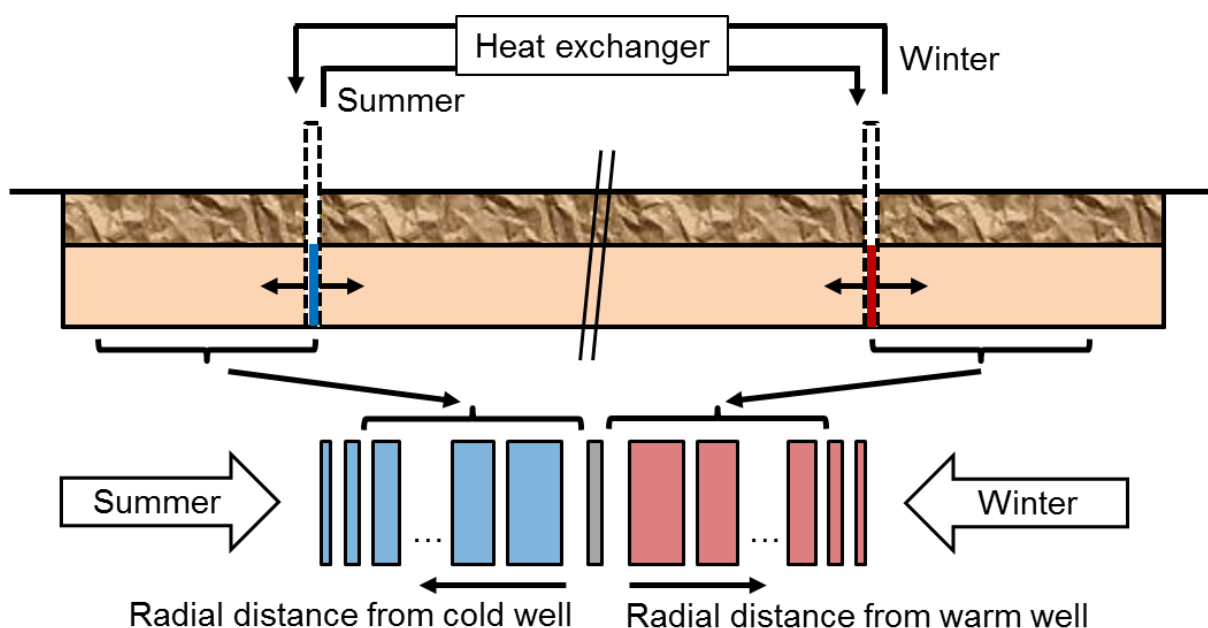


Figure 6.1 Schematic of ATES system (upper part) and how this is represented by the gridding of the double axis-symmetric flow tube (DAFT) model (lower part)

Transport

In the original batch model [259], two types of iron oxide were incorporated, one accounting for the high bio-available fraction (e.g. ferrihydrite and lepidocrocite) and the other accounting for the low bio-available fraction (e.g. goethite). Both iron oxides were defined as aqueous species, such that the intermediate process of iron oxide dissolution is incorporated in the reduction kinetics. To prevent mobility of iron oxides in our transport model both types of iron oxide were defined as mineral phases with low solubility ($\log k = -10$) that are directly used in the reaction network. This ensures that, before reaction, they are considered as primarily associated with the sediment phase. The initial amounts of high and low bioavailable iron in the batch experiment were respectively 10.4 and 1.03 mmol/L [95, 259]. The batch experiment consisted of 100 g wet sediment and 200 ml groundwater. Under aquifer conditions, the sediment to groundwater ratio is approximately 1 kg of dry sediment on every 200 ml of groundwater (considering a quartz aquifer with a porosity of 35% and a quartz density of 2660 kg/m^3). Converting laboratory conditions to aquifer conditions results in 104 and 10.3 mmol per L of pore volume of high and low bio-available iron oxide, according to the higher sediment to groundwater ratio. In the model as presented by Malaguerra et al. [259], siderite, pyrite and ironsulfide were allowed to precipitate. Preliminary model runs showed that more than 97% of the precipitate is siderite. Therefore, in our model runs pyrite and ironsulfide were not included which considerably reduced calculation times. Retardation factors for TCE, DCE and VC were set to 1.4, 1.2 and 1.1

respectively, similar to what was used in earlier modelling studies [261, 262]. Thermal retardation was set to 2, representing a sand aquifer with a porosity of 35% [84].

Temperature dependence

The metabolic activity of microorganisms and their tolerance to geochemical changes are highly influenced by temperature. Optimum biological conversion rates are reported for psychrophilic (-20 to +10 °C) and mesophilic (20 to 45 °C) microbial systems [263-265]. For temperatures above and below the optimum temperature, microbial activity is slower or stops completely. Specifically for lactate-amended reductive dechlorination of TCE, Friis et al. [266] performed laboratory experiments at different temperatures and showed that TCE degradation rates increased approximately by a factor 10 when temperature was increased from 10 to 30 °C. For higher temperature, degradation rates decreased again with a factor 5 at 40 °C. Temperature dependence of the reaction kinetics was incorporated by Malaguerra et al. [259] using an Arrhenius type equation that was fitted to the experimental results of Friis et al. [266]. According to this relation, growth rates in a typical cold storage (5 °C) are approximately 1.7 times smaller than under undisturbed aquifer temperature (10 °C). In a typical warm storage (15 °C) the rates are approximately 1.7 times higher than under undisturbed aquifer conditions, while under maximum storage temperature that is allowed (25 °C) [22, 84], the growth rates are approximately 4.4 times higher.

Biomass mobility

In literature, different views exist on microbial transport and activity. Schaefer et al. [267] report that Dehalococcoides (DHC) concentrations associated with the solid phase are negligible compared to aqueous phase concentrations in a dechlorination column experiment. Amos et al. [268] show different behaviour for Geobacter and DHC in a bio-augmented perchloroethylene (PCE) degradation column experiment. Geobacter bacteria were observed to grow and remain attached in the NAPL source zone but to be largely present in planktonic form in the plume. In contrast, DHC cells were primarily attached to the solid phase throughout the studied column. That bacterial growth and transport is also influenced by pore water flow velocities has been shown by Mendoza-Sanchez et al. [269], who studied the growth and transport of dechlorinating bacteria in a column experiment under different flow conditions. For low and medium flow rates (0.0036 and 0.080 m/d), attached biomass was only observed near the bio-augmentation injection points. In case of a high flow rate (0.51 m/d), a biofilm was observed throughout the whole column. However, whether planktonic or attached bacteria are more relevant in terms of dechlorination activity is yet unclear from the studies mentioned above. Also for other bacterial species, different views on growth and mobility are reported [270, 271]. Activity, attachment and

detachment of bacteria depend on the physical/chemical properties of the sediment as well as the specific bacterial species [272]. To explore the influence of biomass mobility, two extreme cases were considered: (1) completely mobile biomass and (2) completely immobile biomass, while in both cases biomass is initially present throughout the aquifer model domain.

Model scenarios

Several scenarios were defined to study the influence of (1) lactate dose, (2) storage temperature and (3) biomass mobility. In the reference scenario (S1), lactate dose was set at 3.8 mmol/L, equal to the amount that was used in the batch experiments [95]. Storage temperatures were set at 5 °C (cold storage) and 15 °C (warm storage) to represent a typical ATEs system. In the batch experiments, complete dechlorination was observed within 250 days. As ATEs systems are typically designed to operate for 20 to 30 years, it may be considered to apply lactate at a lower dose. This has been studied by running additional simulations using a lactate dose of 1.9 and 0.38 mmol/L. The influence of storage temperatures was explored by setting the storage temperatures for the cold/ warm well to 10/ 10 °C (i.e. no thermal storage, only pumping and addition of electron donor) and 5/ 25 °C (the maximum allowed storage temperature [97]). An overview of the scenarios is presented in Table 6.1.

Table 6.1 Model scenarios

Scenario	Lactate dose (mmol/L)	Injection temperature (°C) cold/ warm storage	Biomass mobility	pH limit on Fe-reduction
S1	3.8	5/15	Mobile	No
S2	1.9	5/15	Mobile	No
S3	0.38	5/15	Mobile	No
S4	3.8	10/10	Mobile	No
S5	3.8	5/25	Mobile	No
S6	3.8	5/15	Mobile	Yes
S7	1.9	5/15	Mobile	Yes
S8	0.38	5/15	Mobile	Yes
S9	3.8	10/10	Mobile	Yes
S10	3.8	5/25	Mobile	Yes
S11	3.8	5/15	Immobile	No
S12	1.9	5/15	Immobile	No
S13	0.38	5/15	Immobile	No
S14	3.8	10/10	Immobile	No
S15	3.8	5/25	Immobile	No

Preliminary model runs showed, remarkably, that pH in the infiltrated groundwater increases from 6.6 to 13.2. Apparently, the amount of buffer capacity available in the model is insufficient to cope with the large amount of protons that is used mainly for iron reduction, and to a lesser extent also for sulphate reduction and methanogenesis. Previous research indicates that iron reduction is hampered at $\text{pH} > 7$ due to lower solubility [273, 274] or blockage of sites available for microbial reduction [275]. Feedback between iron reduction and pH may prevent development of high pH values. Such hypothesis was tested with additional scenarios by incorporating an inhibition factor that limits iron reduction for pH values > 7 . This was achieved by multiplying the iron reduction rate for $\text{pH} > 7$ with $10^{3 \cdot (7 - \text{pH})}$ based on a 3rd order dependence of Fe(III) dissolution on OH^- concentration [274, 276]. Support for and implications of this scenario are further discussed in the results and discussion section.

Presentation of results

Results are discussed on the amount of dechlorination, geochemical conditions and growth and distribution of biomass. The overall progress of dechlorination was expressed by the normalized chlorine number (N_{Cl}) [258] (Equation 6.1).

$$N_{Cl} = \frac{3 \cdot C_{TCE} + 2 \cdot C_{DCE} + C_{VC}}{3 \cdot (C_{TCE} + C_{DCE} + C_{VC} + C_{ETH})} \quad (6.1)$$

Here C_i refers to the concentrations of TCE, DCE, VC and ethene. At the start of the simulation all contaminant is present as TCE and the normalized chlorine number is equal to 1. When TCE, DCE and VC are completely degraded to ethane, N_{Cl} becomes 0.

6.3 Results and discussion

First, results for the reference scenario (S1) and its equivalent with pH limited Fe-reduction (S6) are presented, followed by a discussion of the influence of the various parameters that were considered in the scenario analysis.

Reference scenario

Model results were post processed to represent a cross-section through the doublet well system according to Figure 6.1. Evolution of physical and geochemical conditions in space and time are shown in Figure 6.2. Here, the x-axis represents the horizontal distance from the well for the cold storage (left) and warm storage (right). The y-axis shows the time (years) since the start of the combined ERD-ATES system. Development of thermal plumes due to injection and withdrawal in the cold and warm storage is demonstrated in Figure 6.2a. Concurrent with lactate addition, TCE is degraded to DCE (Figure 6.2c) shortly followed by reduction of high bio-available iron oxides (Figure 6.2g). As degradation of DCE to VC and ethene is inhibited by the presence of iron oxides and sulphate, this only occurs at a later time when methanogenic conditions have been established. Complete reduction of high and low bio-available iron oxides is reached within 2 years (2 storage cycles) in the zone that is affected by the injected electron donor. An expansion of this zone is observed for subsequent storage cycles. Within two storage cycles also the majority of the sulphate in the infiltrated water is reduced to sulphide (Figure 6.2i).

The domain average CAH and ethene concentrations (Figure 6.3) show that the majority of the TCE is fully degraded to ethene, with only a minor amount present as DCE and VC in the injection front (Figure 6.2). The constant total CAH concentration equal to the initial amount of TCE (14.5 $\mu\text{mol/L}$) in Figure 6.3 demonstrates a correct mole balance of contaminant and daughter products in the model.

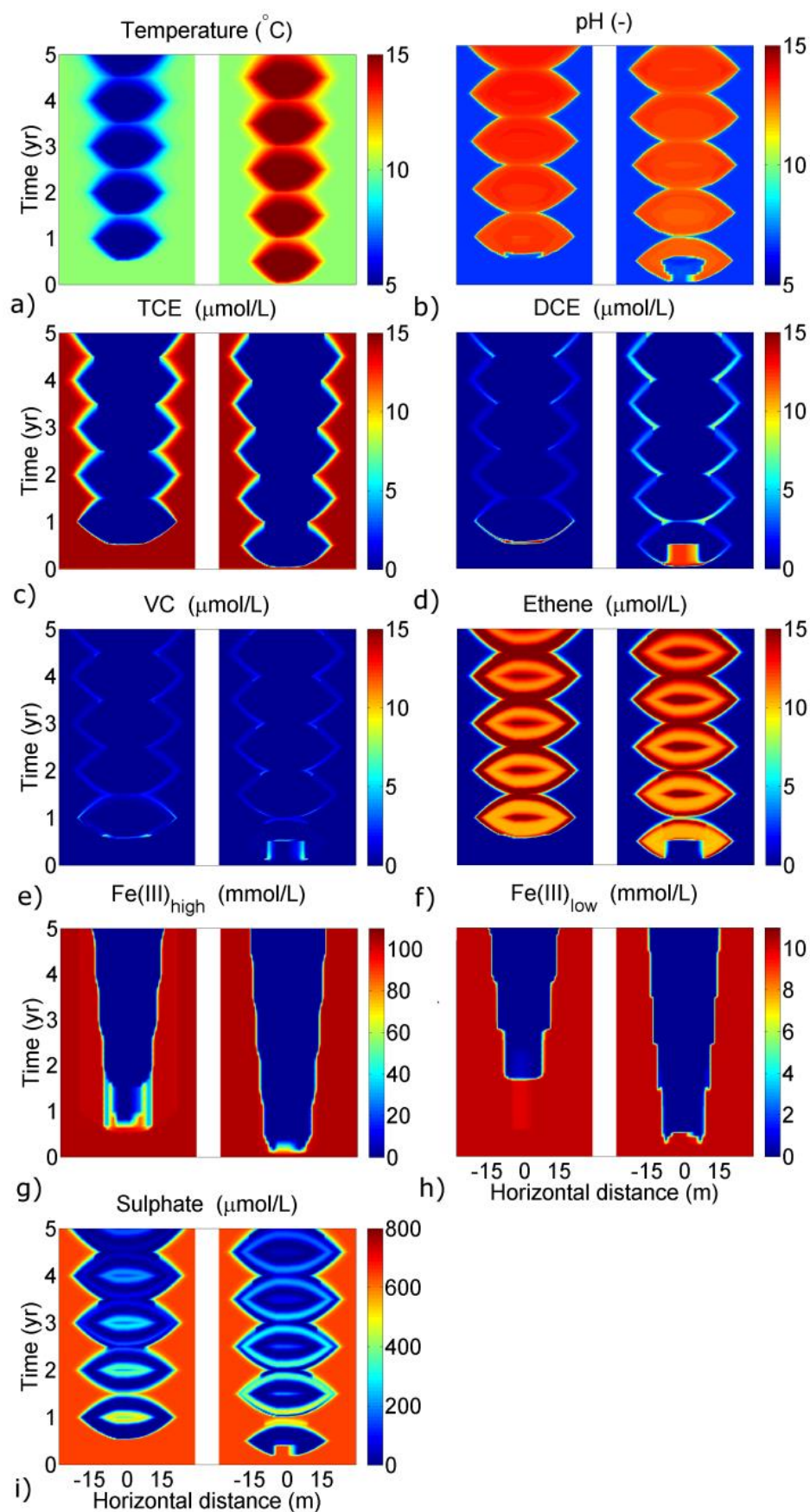


Figure 6.2 Development of aqueous species and minerals for the reference scenario S1. The x-axis depicts horizontal distance from the cold storage well (left) and heat storage well (right)

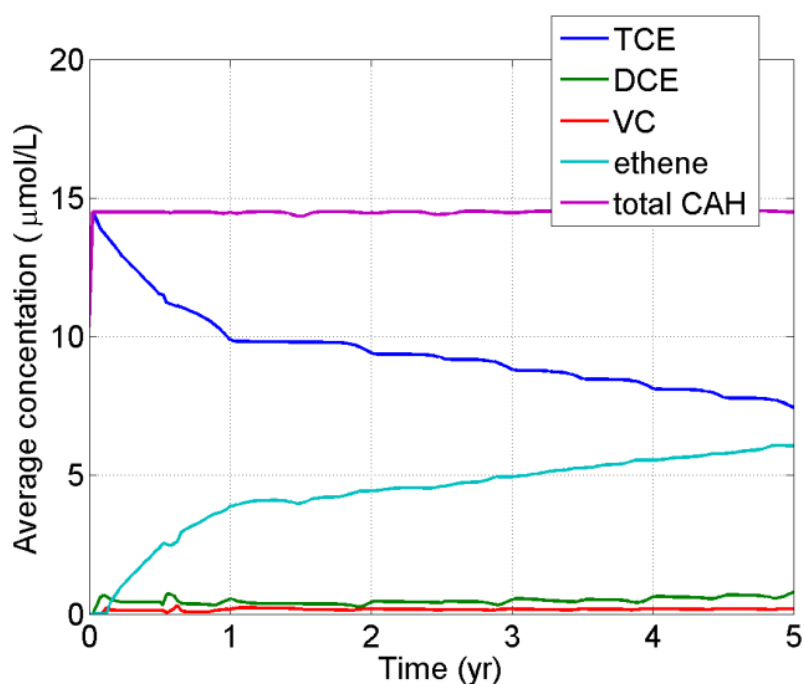


Figure 6.3 Domain average CAH concentrations for scenario S1

Reference scenario with pH limited Fe-reduction

As shown in Figure 6.2b, pH of the infiltrated groundwater in the model increases from 6.6 to 13.2 for scenario S1. This is surprising because dechlorination of CAH releases protons, and HCl formation after dechlorination can actually lower pH [92, 94, 277]. In fact, in some cases a pH buffer is added in ERD to prevent acidification, because reductive dechlorination is less effective at low pH [278]. Considering the relatively high amounts of both high and low bioavailable iron, and the reaction order (Appendix 6.2, Table 6.3), the increase in pH in our model study can largely be attributed to reduction of iron oxides, and to a lesser extent also to sulphate reduction and methanogenesis. In the original batch model [259], pH stabilized at a level of 7.4 (Appendix 6.4, Figure 6.6). However, it must be noted that in the laboratory experiment [95] and batch model [259], the relative amount of bio-available iron was 10 times lower than under aquifer conditions because of the different groundwater to sediment ratio. Increasing pH due to iron reduction has been identified [279], but no report of such considerable pH increase in laboratory or field studies was found. Two hypotheses to explain this discrepancy are (1) that, under field conditions, more buffer capacity is present, for example in the form of ion-exchanging clay minerals [280], or (2) reductive dissolution of Fe(III) is slowed down for increasing pH. The second explanation may be plausible as solubility of iron oxides decreases rapidly for pH levels above 7 [273]. Also, Wu et al. [275] show that microbial reduction of hematite reduces by a factor 10 when pH increases from 7 to 8.7 due to blockage of active surface sites by

accumulation of biogenic Fe(II) and silicate on Fe(III) oxide and Fe(III)-reducing bacterial cell surfaces. As the rates for all the kinetically defined biochemical reactions in our model are independent of pH values, absence or presence of model buffer capacity and consequent model pH have no influence on the simulated dechlorination process. It may, however, be hypothesised that when iron reduction is inhibited, more electron donor becomes available for sulphate reduction and dechlorination, thereby increasing the overall dechlorination rate. This was explored by considering additional scenarios in which iron reduction was inhibited for $\text{pH} > 7$ (scenarios S6-S10). Results of the additional scenario S6 (Appendix 6.4, Figure 6.7), which, apart from the pH inhibition of reductive iron dissolution, is identical to the reference scenario, show that pH in the first storage cycle increases up to 8.7, and in later storage cycles stabilizes around 8. Indeed, dechlorination occurs slightly faster in this case as less electron donor is used by iron reduction (Figure 6.4). Also less electron donor is needed to reach similar dechlorination than in the non pH limiting scenarios. Our simulations indicate that the relation between laboratory and field processes, especially concerning the behaviour and reactivity of iron oxides in bioremediation efforts, and their pH dependency, is an important issue that requires further study. Such kinetic studies should involve laboratory batch or column experiments revealing pH dependencies and detailed pilot field studies related to competition for electron donor and effects of mass transport limitations [254].

Influence of electron donor dose

As addition of electron donor (lactate) and its fermentation products is the key factor in consecutive lowering of the redox conditions and reductive dechlorination, it comes as no surprise that lactate dose influences the dechlorination rate. In the reference scenario (S1) lactate dose was set at 3.8 mmol/L to achieve similar concentrations as in the batch experiments by Scheutz et al. [95]. Adding lactate at a lower dose slows down the reaction (Figure 6.4a). However, because ATEs systems are typically designed to operate for 20 to 30 years, even with slow biodegradation a significant aquifer volume can be remediated. To compare dechlorination per unit of lactate added, scenarios with a lower dose have been run for a longer simulation time: 10 years (S2) and 50 years (S3). Results (Figure 6.4b) show that, although dechlorination is slower at a lower dose, it also increases dechlorination per unit of lactate added. Similar influence of lactate dose is found for the scenarios with pH limitation on iron reduction and scenarios with immobile biomass (Figure 6.4). To cope with competition for electron donor between micro-organisms, a typical ERD approach is to supply an excess electron donor, effectively reducing all sulphate [281]. A similar approach could be suggested for a combined ERD-ATES concept. In addition, upon reaching sufficiently reduced conditions in the capture zone of the ATEs system, the lactate dose can be lowered drastically. Given that typical

groundwater volumes that are pumped by ATES systems are between 30 000 and 150 000 m³/yr per well [117], a continuously added dose of 3.8 mmol/L amounts to respectively 10 and 50 ton/yr of sodium lactate used for the ERD treatment. In a pilot test reported by Lendvay et al. [282], dechlorination of 355 m³ of contaminated aquifer was achieved within 99 days by biostimulation with approximately 23 kg of lactate. For an aquifer volume equivalent to 30 000 and 150 000 m³ of groundwater, the amounts of lactate needed would be 5.6 and 28 ton respectively. However, based on a laboratory experiment performed by Ni et al. [93], the amount of lactate that would be needed to treat an equivalent volume of contaminated aquifer is much larger, respectively 82.5 and 412.5 ton. At a dose of 3.8 mmol/L, the latter would imply that at least 8 years of combined ERD-ATES are required for complete remediation of the volume of displaced water.

Influence of temperature

Although temperature changes do influence the maximum bacterial growth rates [266], temperature changes applied in our model do not have any impact on the overall progress of dechlorination regardless of the assumption on biomass mobility or pH limitation (Figure 6.4). This is partly because increased growth rates in the warm storage are balanced by reduced growth rates in the cold storage. However, even in the scenario with a high storage temperature, virtually no effect is observed. Apparently other factors, such as total available electron donor, have a larger impact on the reaction kinetics.

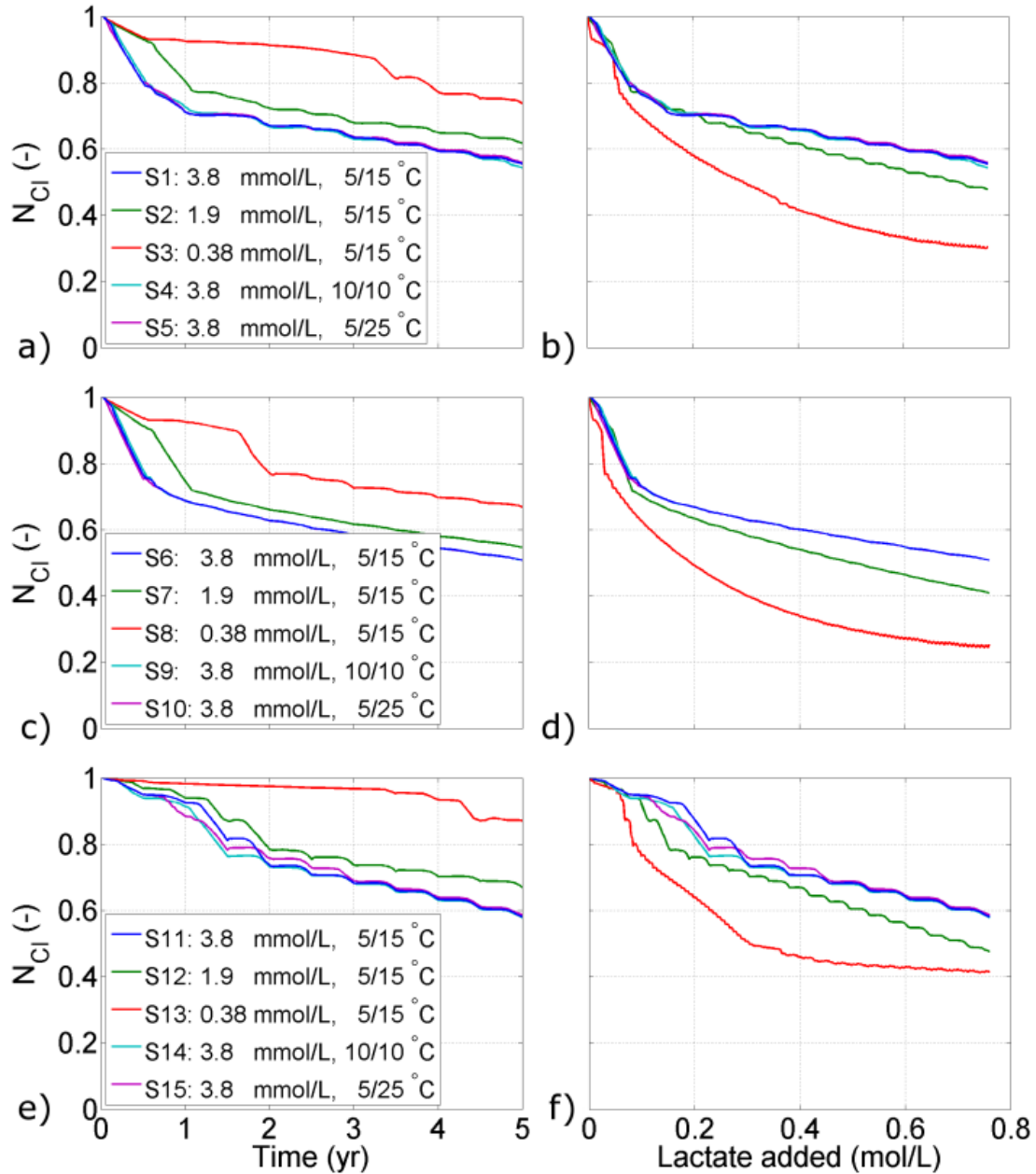


Figure 6.4 Spatially averaged normalized chlorine number in time (left panels) and against the amount of lactate added (right panels) for: (a)-(b) mobile biomass scenarios (S1-S5), (c)-(d) mobile biomass scenarios with pH limitation on iron reduction (S6-S10) and (e)-(f) immobile biomass scenarios (S11-S15)

Biomass mobility

As apparent from Figure 6.4, overall dechlorination is faster when biomass is assumed to be mobile compared to the immobile case. Also the total amount of dechlorination at the end of the simulation period, is slightly higher in case of mobile biomass. In both simulations, the largest biomass growth was observed for iron reducers and secondly for lactate fermenters (Figure 6.5).

Growth of DCE/VC degraders shows that degradation of DCE only occurs at a later time in case of immobile biomass (Figure 6.5a and b) which explains the slower dechlorination progress in this case (Figure 6.4). The average distribution of the different species of biomass during the last year of the simulation period shows that in the immobile case biomass is more concentrated close to the well, than in the mobile case. This is especially the case for lactate fermenters which, in the immobile scenarios, grow close to the well (Figure 6.5d). Large amounts of attached biomass near the wells may lead to well clogging and thereby reduce the performance of an ATES system. Since the largest microbial growth is observed for lactate fermenters, it could be considered to use other electron donors [88, 283, 284]. As shown by Aulenta et al. [281], a mixture of hydrogen and acetate resulted in lower biodiversity and more effective dechlorination compared to lactate amended microcosms. An alternative approach to biostimulation by adding electron donor is bio-augmentation [94, 285]. As shown by Lendvay et al. [282] bioaugmentation with DHC can speed up the dechlorination process compared to biostimulation without bioaugmentation.

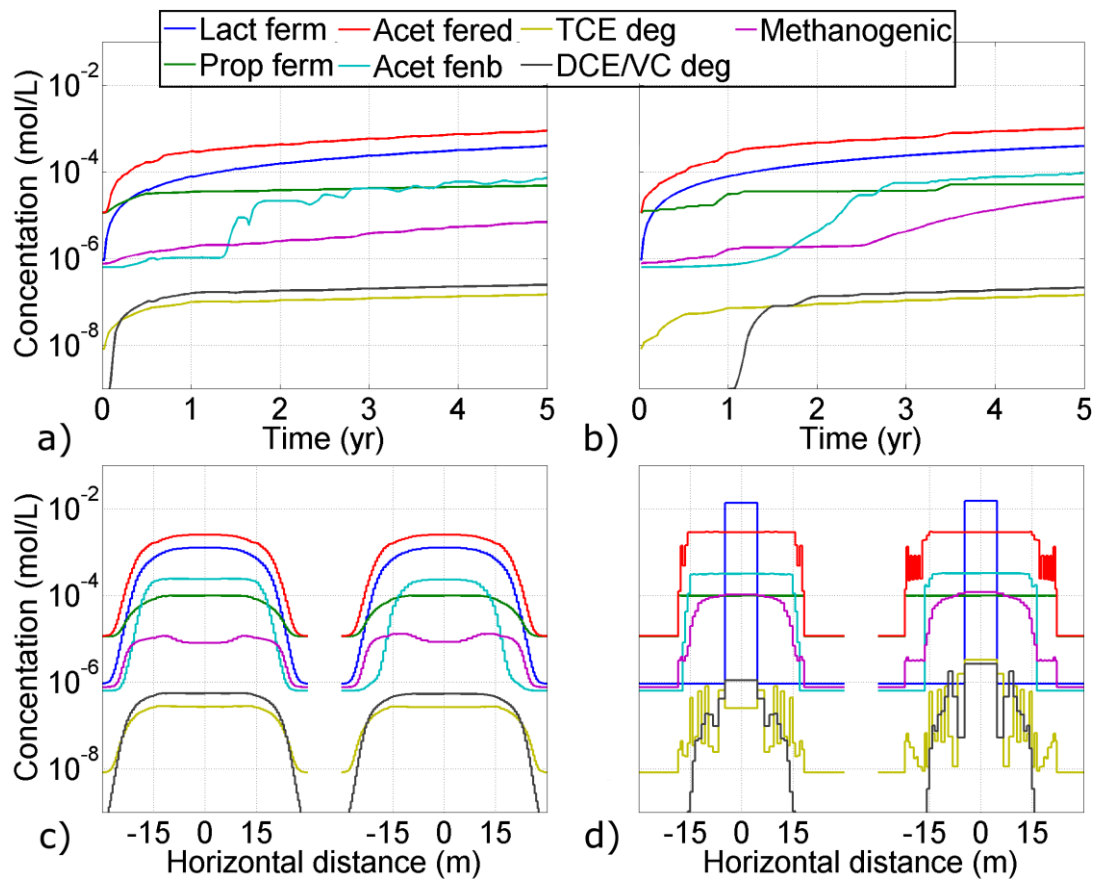


Figure 6.5 Spatially averaged biomass concentration for the mobile case S1 (a) and immobile case S11 (b) and biomass distribution averaged over the last year for the mobile case S1 (c) and immobile case S11 (d)

Knowledge gaps in combined ERD-ATES concepts

Reductive dechlorination is a complex process, especially when competition with different terminal electron acceptors occurs [286], and taking into account transport and growth of microbial populations, mineral dissolution and precipitation and fermentation processes. The numerical model developed in this study provides a comprehensive tool to assess the development of biochemical processes in a combined ERD-ATES concept, which can be used to identify knowledge gaps and guide further research. Our model results suggest that complete dechlorination of TCE in the capture zone of an ATES well is possible when applying biostimulation by addition of electron donor. This is achieved by creating a zone around the wells where iron oxide and sulphate reductions do not occur anymore. After these electron acceptors have been depleted, a larger portion of the electron donor becomes available for dechlorination. Simulations reveal several issues that require further study. Firstly, reduction of iron oxides in our simulation leads to increasing pH values that are not reported for laboratory or field studies. While fermentation of electron donor is widely studied, there is a limited number of reports on iron reduction in reductive dechlorination studies [254]. Also, since well clogging due to microbial growth is a main concern for biostimulation using ATES, growth and mobility are important issues for further study. Study of field pilots is expected to improve the setting of boundary conditions for modelling and therefore model prediction which is needed to advance understanding of the combined ERD-ATES concept.

Appendix 6.1: Overview of the reaction network

Table 6.2 presents the main kinetic processes that are incorporated in the model. Iron in the form of FeOOH is represented by Iron(III)_{high} for the high bio-available component and Iron(III)_{low} for the low bio-available component.

Table 6.2 Biochemical processes and inhibition (after Malaguerra et al. [259])

Process	Reaction equation	Inhibition by	Biomass species
Lactate fermentation	$3\text{CH}_3\text{CH}(\text{OH})\text{COO}^- \rightarrow \text{CH}_3\text{COO}^- + 2\text{CH}_3\text{CH}_2\text{COO}^- + \text{HCO}_3^- + \text{H}^+$	-	Lact ferm
Propionate fermentation	$\text{CH}_3\text{CH}_2\text{COO}^- + 3\text{H}_2\text{O} \rightarrow \text{CH}_3\text{COO}^- + \text{HCO}_3^- + \text{H}^+ + 3\text{H}_2$	maximum biomass Acetate	Prop ferm
Reduction of high bio-available iron with acetate	$\text{CH}_3\text{COO}^- + 8\text{Iron(III)}_{\text{high}} + 15\text{H}^+ \rightarrow 2\text{HCO}_3^- + 8\text{Fe}^{2+} + 12\text{H}_2\text{O}$		Acet fered
Reduction of low bio-available iron with acetate	$\text{CH}_3\text{COO}^- + 8\text{Iron(III)}_{\text{low}} + 15\text{H}^+ \rightarrow 2\text{HCO}_3^- + 8\text{Fe}^{2+} + 12\text{H}_2\text{O}$	Sulphate	Acet fenb
Reduction of high bio-available iron with hydrogen	$\text{H}_2 + 2\text{Iron(III)}_{\text{high}} + 4\text{H}^+ \rightarrow 2\text{Fe}^{2+} + 4\text{H}_2\text{O}$		-
Reduction of low bio-available iron with hydrogen	$\text{H}_2 + 2\text{Iron(III)}_{\text{low}} + 4\text{H}^+ \rightarrow 2\text{Fe}^{2+} + 4\text{H}_2\text{O}$	Sulphate	-
hydrogen sulphate reduction	$4\text{H}_2 + \text{SO}_4^{2-} + \text{H}^+ \rightarrow \text{HS}^- + 4\text{H}_2\text{O}$	Iron(III) _{high}	-
Hydrogenotrophic methanogenesis	$4\text{H}_2 + \text{HCO}_3^- + \text{H}^+ \rightarrow \text{CH}_4 + 3\text{H}_2\text{O}$	-	Methanogenic
TCE acetate dechlorination	$4\text{C}_2\text{H}_3\text{Cl}_3 + \text{CH}_3\text{COO}^- + 4\text{H}_2\text{O} \rightarrow 4\text{C}_2\text{H}_3\text{Cl}_2 + 2\text{HCO}_3^- + 4\text{HCl} + \text{H}^+$	DCE VC	TCE deg
DCE dechlorination	$\text{C}_2\text{H}_3\text{Cl}_3 + \text{H}_2 \rightarrow \text{C}_2\text{H}_3\text{Cl}_2 + \text{HCl}$	TCE VC	DCE/VC deg
VC dechlorination	$\text{C}_2\text{H}_3\text{Cl}_2 + \text{H}_2 \rightarrow \text{C}_2\text{H}_4 + \text{HCl}$	TCE DCE	DCE/VC deg

Appendix 6.2: Initial conditions

Table 6.3 Initial conditions for aqueous components, biomass species and minerals

Initial groundwater conditions in the aquifer:	
pH	6.6
Temperature	10 °C
Acetate	0 mol/L
Propionate	10e-6 mol/L
Fe(+2)	9e-10 mol/L
TCE	14.5e-6 mol/L
Methane	6e-7 mol/L
Sulphate	640e-6 mol/L
Hydrogen	1e-10 mol/L
Cl(-1)	1.94e-3 mol/L
C(+4)	6.7e-3 mol/L
Initial biomass available (calculated per L pore volume)	
Lactate fermenters	9.14e-7 mol/L
Propionate fermenters	1.13e-5 mol/L
Iron reducers (high bio-available)	1.15e-5 mol/L
Iron reducers (low bio-available)	6.34e-7 mol/L
Methanogens	7.65e-7 mol/L
TCE degraders	8.22e-9 mol/L
DCE and VC degraders	5.02e-10 mol/L
Initial mineral species available (calculated per L pore volume)	
Calcite	17.93093 mol/L
Iron oxide (high bio-available)	1.04e-1 mol/L
Iron oxide (low bio-available)	1.03e-2 mol/L
CO ₂ (g)	0.00107 mol/L

Appendix 6.3: Reproduction of batch model results

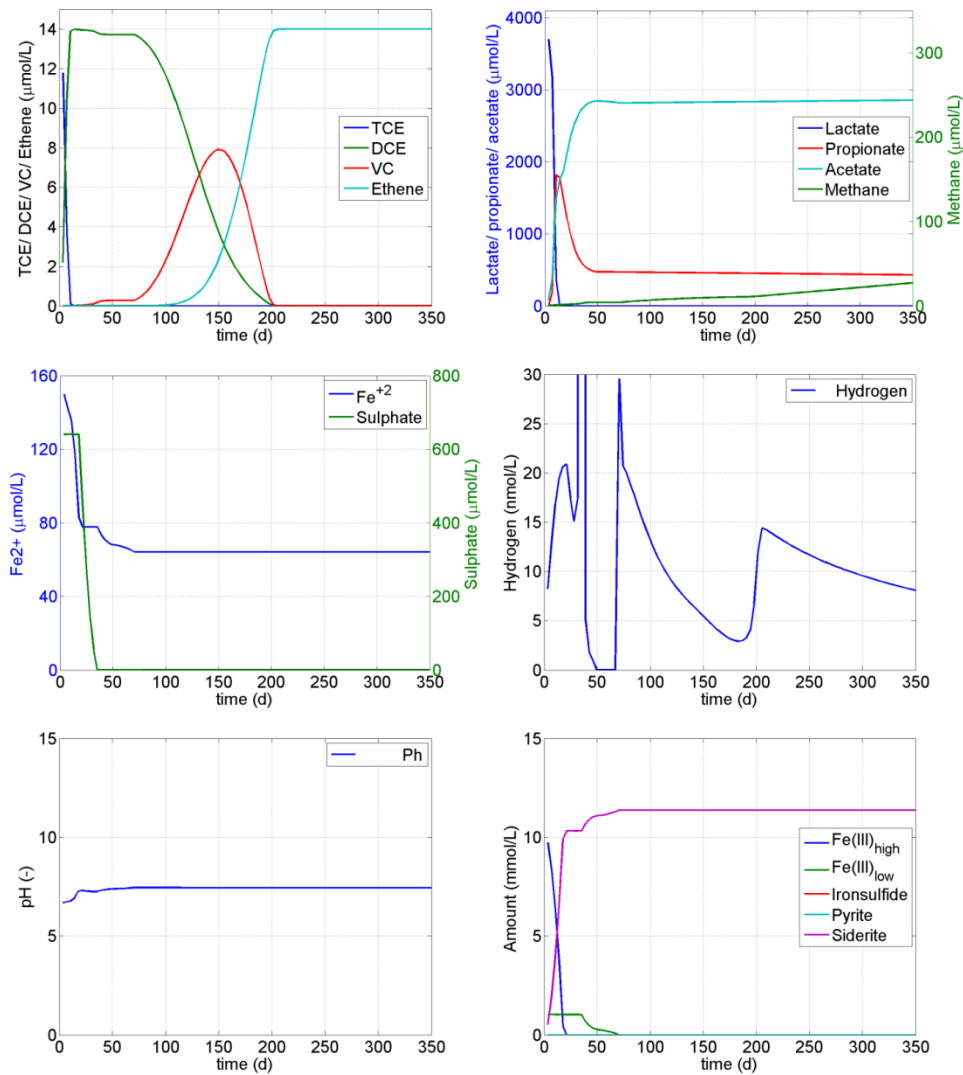


Figure 6.6 Results of the batch model

Appendix 6.4: Results for scenario S6

In model scenario S6 iron reduction is inhibited for $\text{pH} > 7$. In this case, pH increases in the first storage cycle up to 8.7, and in later storage cycles stabilizes around 8.

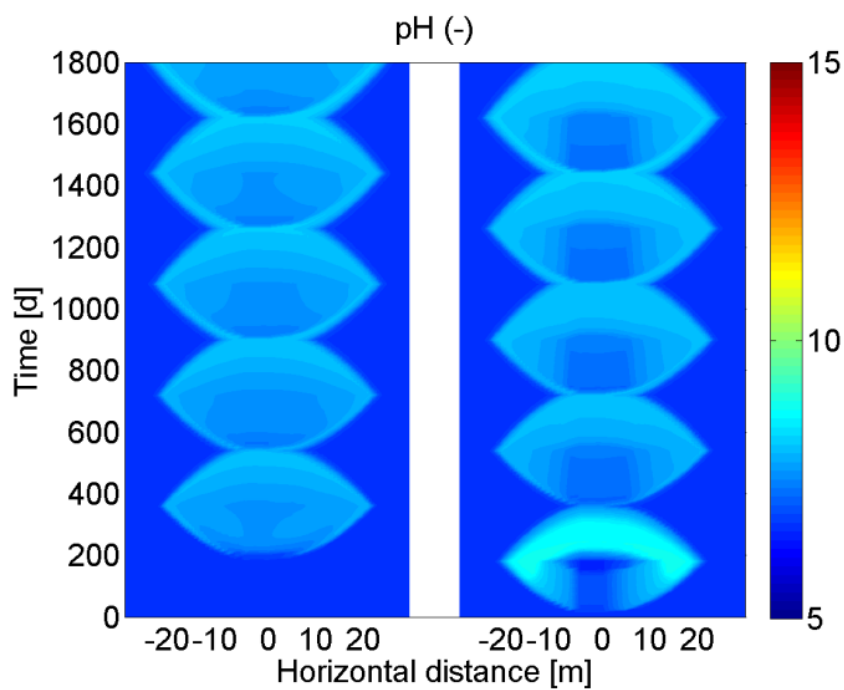


Figure 6.7 Development of pH levels in model scenario S6

Opportunities and challenges for implementation of ATEs in urban areas

Aquifer thermal energy storage (ATES) is applied world-wide to provide heating and cooling and thereby reduce primary energy consumption and related CO₂ emissions. With over 3000 systems installed in the Netherlands, ATES is becoming a standard technology for new and retrofitted buildings such as offices, hospitals and commercial buildings. The intensified use of the subsurface for thermal applications requires more accurate methods to measure and predict the evolution of thermal plumes in the subsurface and to address issues related to subsurface urban planning and the presence of groundwater contaminants. In this thesis, challenges related to intensive use of aquifer thermal energy storage in urbanized areas are treated from various perspectives. From a physical point of view, subsurface heat transport in ATES and the storage performance for thermal energy was assessed. Planning of large-scale application of ATES and optimal use of aquifer volume were studied from an economic and environmental benefits perspective. Finally, opportunities have been explored related to combining ATES with soil and groundwater remediation. In this chapter, the research questions that were presented in the introduction and their implications for practical application are discussed. Furthermore, perspectives for future research are outlined.

7.1 Thermal impact and subsurface heat transport

Research question: What is the thermal impact of ATES?

Detailed measurements and analyses of thermal plumes are rarely reported for existing ATES systems. Presumably, because monitoring of temperature in the subsurface requires additional observation boreholes at least to the depth of a well screen, which is considered expensive and may also be difficult to realize in densely built urbanized areas. A good understanding of the subsurface heat transport in ATES is, however, essential for assessing the environmental impact of ATES, their storage performance and thermal interference between systems. In this research, subsurface temperature monitoring using distributed temperature sensing (DTS) was applied for monitoring of ATES for the first time (chapter 2). Application of DTS (Figure 7.1) enabled continuous automated temperature monitoring at high temporal and spatial resolution. Measurements demonstrated the development of thermal plumes and revealed that not all parts of the well screen contribute equally to the storage and recovery of thermal energy. The measurements also showed preferential flow due to aquifer heterogeneity. This was also observed in a recent study of a different ATES system [29]. There it was found that incorporating fine-scale heterogeneity resulted in a larger thermally impacted area and larger temperature anomalies. Similarly, Bridger et al. [31] observe the effect of geological layering on heat transport for an ATES system in British Columbia, Canada. When not included in the design, the presence of heterogeneity may result in a higher groundwater flux than expected in parts of the well screen. This influences the maintenance requirements of the well, and also

results in a thermal impact that is different than projected (Figure 7.2). Application of borehole logging before installation of the well screens and flow measurements after installation and development of a well could be useful to estimate the presence of preferential flow paths. Furthermore, detailed temperature monitoring is suggested to (1) provide a baseline with respect to which temperature changes can be related, (2) validate the design, (3) improve aquifer characterization and (4) assess the state and development of thermal plumes in the subsurface. This, in turn, is also useful for planning of future ATEs systems in the same area. As shown by Selker et al. [134], DTS has great opportunities for hydrologic systems, mainly due to its accuracy and applicability for a wide range of spatial scales. Although costs for these systems have decreased [134], cost for equipment, but also installation, data acquisition and processing still prevent regular application to monitoring of ATEs systems. Therefore, further reduction of costs, for example by development of a dedicated apparatus, cheaper installation (for example by probing or in conjunction with cone penetration tests) and online data collection and processing protocols are expected to lead to more widespread application.



Figure 7.1 Installation of glass fibre optical cables for distributed temperature sensing (DTS)

Impact assessment and design of ATEs systems

Permit application for ATEs in the Netherlands usually requires an impact assessment of the hydraulic and thermal influence of the proposed system on its surroundings that demonstrates that the system does not negatively influence existing ATEs systems or other subsurface functions. In the current state of practice of planning and design of ATEs, aquifer heterogeneity is generally neglected. Comparison of observed temperatures at an existing ATEs system with

the heat transport model that was used for impact assessment (chapter 2) indicates that, despite the presence of aquifer heterogeneity, the actual thermal impact of this system was smaller than anticipated. This is reasonable, since these models are usually applied as a worst case scenario regarding thermal impact on the environment. A worst case approach allows simplifications of the expected use of the system and hydrogeological conditions, such that models become easier to construct and handle. This is a reasonable approach when there is enough aquifer volume available to accommodate all ATEs ambitions. However, such approach does not lead to optimal use of subsurface potential as in reality only a limited part of the aquifer is actually used for thermal storage. Regarding the rapid increase in the number of ATEs systems (chapter 1) and the desire to intensify application of ATEs [21], more accurate assessment of thermal plume development is needed. This becomes even more relevant as the subsurface is also increasingly being used for other purposes, such as infrastructure and water storage [287] and due to possible effects of ATEs on groundwater quality related to drinking water production [288]. This requires increasing our understanding of subsurface heat transport processes and improving our ability to control and predict this behaviour. Considering the use of simplified models, impact assessments can be improved by incorporating more detailed hydrogeological characterization, for example based on test drillings or application of detailed temperature monitoring as can be achieved with distributed temperature sensing (chapter 2). An alternative approach, that in some cases may be more cost-effective, is to apply a sensitivity analysis that reflects the uncertainty in operational and hydrogeological conditions. In chapter 3 an effort was made to express the effect of heterogeneity in simplified models by an increased value for macro-dispersivity. As expected, effective values for macro-dispersivity did depend on the statistical geological properties of the aquifer formation, i.e. macro-dispersivity increased for more heterogeneous aquifers. However, application of this method in practical situations is challenging, because (1) the heterogeneity of the aquifer should first be characterized, and (2) macro-dispersivity values were shown also to depend on hydrogeological conditions and the spatial distribution of ATEs wells.

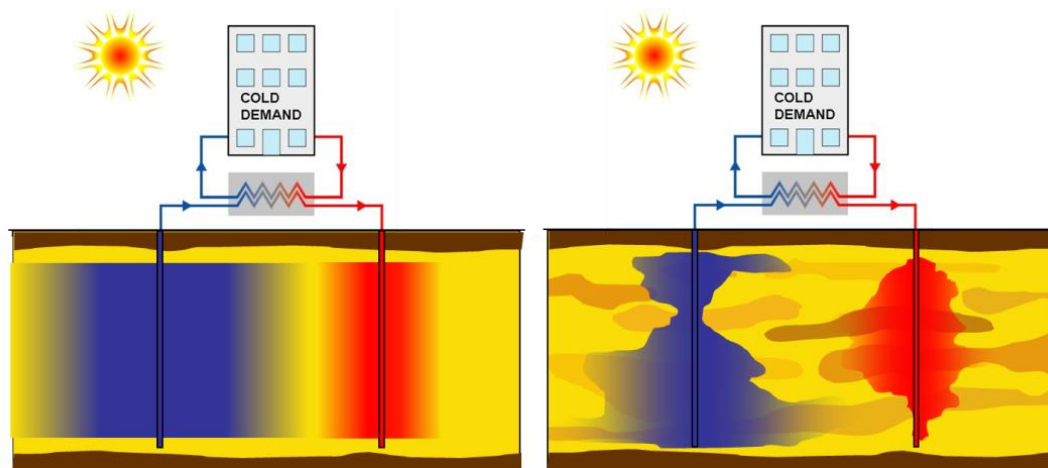


Figure 7.2 Schematic shape of thermal plumes in a homogeneous aquifer (left) and a heterogeneous aquifer (right)

7.2 Thermal storage performance

Research question: What is the storage performance of ATEs?

Detailed assessment of injection and extraction volumes and temperature of an existing system (chapter 2) between 2005 and 2012 showed that on average 82% of the stored cold and 68% of the stored heat was recovered. Besides the properties of the subsurface, also the use of the system plays an important role in the overall performance of the ATEs system. Due to a varying energy demand of the building (under influence of weather conditions), the injected and extracted groundwater volumes showed large variability between the years. As a result, also thermal recovery values showed large variability (18-170%). Values larger than 100% illustrate that thermal energy that is not recovered within the same cycle remains available in the subsurface and can increase the thermal recovery in following years. Likewise, both modelling and monitoring results show that in general, thermal recovery increases during the first few (1 to 10) years after the system starts to operate. It is expected that a better overview of thermal characteristics for existing ATEs systems improves our knowledge on the thermal storage performance of ATEs in general and also helps identify problems when a system is not performing according to expectations. Therefore, assessment of the thermal performance as a standard procedure is recommended. As current ATEs systems are commonly equipped with automated control and logging software, assessment and reporting of thermal behaviour, or at least providing the data to do so, can be achieved with little additional effort.

Factors that impact thermal recovery

Factors that influence the storage performance were further explored using heat transport modelling. For 76 wells that are present in The Hague (the Netherlands), chapter 4 shows that the amount of energy that can be recovered from non-interfering systems is strongly coupled to the stored volume. Thermal recovery varied between 50% for small systems ($9\,100\text{ m}^3/\text{yr}$) up to 90% for larger systems ($250\,000\text{ m}^3/\text{yr}$). It can be concluded that, in general, systems above $100\,000\text{ m}^3/\text{yr}$ are preferred following their good energy performance. When energy demand of a specific application is such that only a small groundwater volume is needed, the possibility should be considered to combine multiple users into a single larger system. The influence of design and hydrogeological conditions on the storage performance were further studied by considering a doublet system of typical dimensions (chapter 3). Results showed that, besides storage volume, regional groundwater flow can also significantly impact the amount of energy that is recovered. In the Netherlands, most ATEs systems are realized in aquifers where groundwater velocity is low ($< 50\text{ m/yr}$). In this case, thermal losses due to regional groundwater flow are modest ($< 10\%$). In case of larger regional groundwater flow (200 m/yr), thermal recovery decreased by 45%. Furthermore, thermal interference between the warm and cold plume reduces the storage performance when wells for heat and cold storage are separated by less than 2 thermal radii (chapter 3). For non-interfering systems, heterogeneity has a minor influence on the storage performance of thermal energy. However, in case of thermal interference, heterogeneity may influence interaction between the thermal plumes and thereby affect the energy that can be recovered from the subsurface. To counteract the effect of aquifer heterogeneity, it could be considered to block parts of the well screen that are adjacent to high permeable layers. This may decrease the specific yield of the well, but also reduce preferential flow and thus result in a more regular plume shape. This has previously been applied at an ATEs system that was constructed in a heterogeneous aquifer in Canada [31, 105]. However, despite this measure, in that case thermal short-circuiting was observed within 7 months of cooling.

Smart control

Regarding the thermal storage performance, it is noted that operating an ATEs system simultaneously serves two goals: (1) to provide energy to a building, and (2) to store energy for future use. Presumably, the system in our case study (chapter 2) mainly operates based on the first principle. In that case, in a relatively warm winter in which the heating demand is below normal, only a limited amount of cold will be stored, such that in the next summer there is also limited amount of cooling available. It may be hypothesized that more advanced operation, which takes into account future projections of climate, energy demand and the status of the thermal storage can improve the overall system performance. Similarly, sustainable exploitation

requires that, in the long-term, the average aquifer temperature remains constant. Therefore, to achieve an energy balance, it may be needed to run the ATES system even when there is no direct need for heating and cooling. To reduce additional costs, it could then be considered to connect the system to cheap energy sources, for example by collecting thermal energy from water streams, ponds, solar collectors or using waste heat. Also in this case, predictive strategies could enable to select the most economic moments to restore the thermal balance, when needed.

7.3 Interference between systems

Research question: What is the role of thermal interference in large-scale application of ATES?

When the distance between multiple ATES wells is below 2 thermal radii, the flow fields and thermal plumes around those wells interact and influence the storage performance of these wells; this is called thermal interference. During the last years, debate is going on mainly on negative interference, leading to a loss of stored energy. However, the influence on thermal recovery can be either positive or negative, depending on the temperature levels of the interfering plumes. In chapter 4, thermal performance and interference among wells was studied for the city of The Hague (the Netherlands), where the subsurface is used intensively for ATES (76 wells in an area of 3.8 km²). On average, thermal recovery was influenced positively by 2.5%. Apparently, wells with similar storage temperature were clustered during the design, leading to a net positive effect. Considering individual storage wells, thermal interference affected thermal recovery both positively and negatively by a maximum of 10%. Ideally, wells would be positioned to maximize positive interference while minimizing negative interference. This would require moving some of the well locations to maximize retrieved energy. Possibly, limited aquifer volume or accessibility at the surface led in some cases to sub-optimal well positioning.

Assessment of thermal interference

In the Netherlands, at several occasions, thermal interference has been claimed to have led to reduced system performance. In these cases, heat transport models are applied to determine whether thermal interference has occurred and to which extent by comparing model scenarios that include and exclude the system that is believed to cause thermal interference. Additional to modelling, strategic positioning of temperature monitoring locations is needed for delineating thermal plumes and calibration or validation of heat transport models. Novel application of DTS (chapter 2) proves to be very useful for this purpose, since it allows continuous automated temperature monitoring at high temporal and spatial resolution. Even more challenging is planning and management of ATES at the regional scale where multiple users are active. This requires the ability to accurately assess thermal plume development. As ATES systems are designed to operate for 20 to 30 years, the state and development of thermal plumes in the

subsurface is difficult to assess, especially when tens or hundreds of wells are realized in a specific area. Monitoring of temperature in the subsurface requires observation boreholes and will therefore be applied only at a limited number of locations, even when using DTS. Therefore, it is expected that assessment of the thermal state of the aquifer often will rely on heat transport models. Accuracy of these assessments relies for a large part on hydrogeological characterization, but also on the availability of historical operational data for each of the wells. Hence, it is recommended to store such data for future use. Furthermore, it was observed that grid refinement was needed to achieve accurate values for thermal interference and performance for large-scale application of ATEs (chapter 4). Especially at the regional scale this results in models that are computationally demanding. In these cases, development of simplified models could reduce computational demand, such that they become usable for uncertainty estimates, sensitivity analysis or well management. An approach could be for example to consider flow path analysis or up-scale local heat transport phenomena to the regional scale. High flow rates and temperature gradients occur mainly close to the wells. Therefore, adaptive mesh refinement or finite element methods could also reduce calculation times, whilst maintaining numerical accuracy.

7.4 Planning and management of large-scale applications

Research question: How can large-scale application of ATEs be optimized?

During the early development of ATEs in the Netherlands, permits for installation were assigned following the ‘first-come, first-served’ principle [54]. However, as the use of ATEs has intensified, at some locations, available aquifer volume is becoming a limiting factor. In that case, pre-designed planning of well locations and thermal plumes may allow for more efficient use of the subsurface [289]. To facilitate optimal use of the subsurface, some municipalities in the Netherlands have issued master plans that regulate the positioning of the wells for storing thermal energy [71, 72, 211]. This can be applied both to multiple ATEs systems and the wells of individual systems. In chapter 5, a method is presented to optimize well spacing in such patterns from an economic perspective. It appears that for large-scale application of ATEs, avoiding all thermal interference does not lead to optimal use of available subsurface potential. Instead, total economic and environmental benefits of ATEs in a certain region should be considered. By allowing a limited amount of thermal interference, more systems can be realized in a given area. Although individual performance of each well is lower, the total benefits in the area (in terms of cost reduction with respect to conventional heating and cooling systems and associated CO₂ emissions) are higher. Optimization showed that it is cost-effective to supply 30-40% more energy than in case all thermal interference is avoided. It is noted that the study in chapter 5 assumes a fully deterministic approach (i.e. flow rates and storage temperatures are

known throughout the simulations). In reality, however, well fluxes and storage temperatures may fluctuate due to changing weather conditions and changing energy requirements of each building. Well locations, once drilled, are not easily replaced, such that planning of well locations requires robust estimates of the expected energy demand. A very useful tool for management of large-scale application of ATES is a calibrated groundwater model that includes all ATES systems and is regularly updated with actual operational data from the respective systems. This model should then be used for the planning of new systems and assessment of the thermal state of the aquifer.

Future perspectives

Even more efficient than the exploitation of individual ATES systems would be the use of collaborative systems, in which wells are connected in a grid that allows exchange of thermal energy between users. This offers opportunities to optimize exploitation of the well field following the dynamic energy demand of the different users. Optimization of well locations and dynamic control for systems that belong to multiple independent users, however, does require development of management strategies, and also procedures on how to act in case of conflicts or when systems do not behave as expected. From a technical perspective such flexible use of the subsurface can be achieved, however, organizational aspects will become more complex. Possible governance tools to approach optimal and sustainable use of the subsurface for ATES are explored by Bloemendal et al. [49]. They consider the subsurface as a common resource pool in which self-organization or self-governance can be applied. They speculate that such an approach may more than double the amount of thermal storage in the subsurface, in comparison with the current practice. For an aquifer with no ambient flow they derive that well-to-well distances can theoretically be reduced to $1.4 R_{th}$ instead of $3 R_{th}$, which is used as a rule of thumb in current design. When wells are arranged in a square grid, this would allow developing 4.6 times more wells in a certain area. The results of the economic optimization presented in chapter 5 show that the amount of energy that can be supplied from an aquifer volume, expressed by the energy ratio, increases from 17% at the $3 R_{th}$ -norm to 95% at the economic maximum, which would imply an improvement by a factor 5.6. This is even slightly higher than the theoretical estimate based on Bloemendal et al. [49], because it optimizes positive interference by clustering wells with similar storage temperature. As mentioned before, this analysis assumes a fully deterministic approach and should therefore be considered as an upper maximum.

7.5 Combining ATES with biostimulation in contaminated aquifers

Research question: What are the anticipated effects and possibilities of combining ATES with biostimulation in a CAH contaminated aquifer?

Many urbanized centres deal with contaminated soil and groundwater. Therefore, an increasing number of ATES ambitions is confronted with the presence of contaminants. Hence, the well-designed combination of ATES with natural attenuation or biostimulation could be a promising integrated technique, both for remediation of contaminants as for development of ATES (Figure 7.3). Combining ATES with groundwater remediation has received growing interest [97, 98] which resulted in two on-going field pilots [99, 100]. Although enhanced reductive dechlorination (ERD) of CAH is a widely studied approach for in situ remediation with many successful field applications [94, 95, 247, 251, 290, 291], combination with ATES is not straightforward. The main differences are in the applied flow rates and volumes, which are much larger for ATES, induced temperature fluctuations, lifespan of the applications and possible unfavourable effects on the ATES system (i.e. well clogging). The numerical model presented in chapter 6 provides a comprehensive tool to assess the development of biochemical processes in a combined ERD-ATES concept. The reactive transport model was used to simulate the use of ATES as a continuous biostimulation tool for enhanced bioremediation of a hypothetical TCE contaminated aquifer. The model results suggest that complete dechlorination of TCE in the capture zone of an ATES well is possible following biostimulation by addition of electron donor. This is achieved by creating a zone around the wells where iron and sulphate reduction do not occur anymore and the electron donor is used for dechlorination. Although microbial processes are known to be temperature dependent, temperature changes induced by thermal storage did not significantly influence the overall dechlorination process.

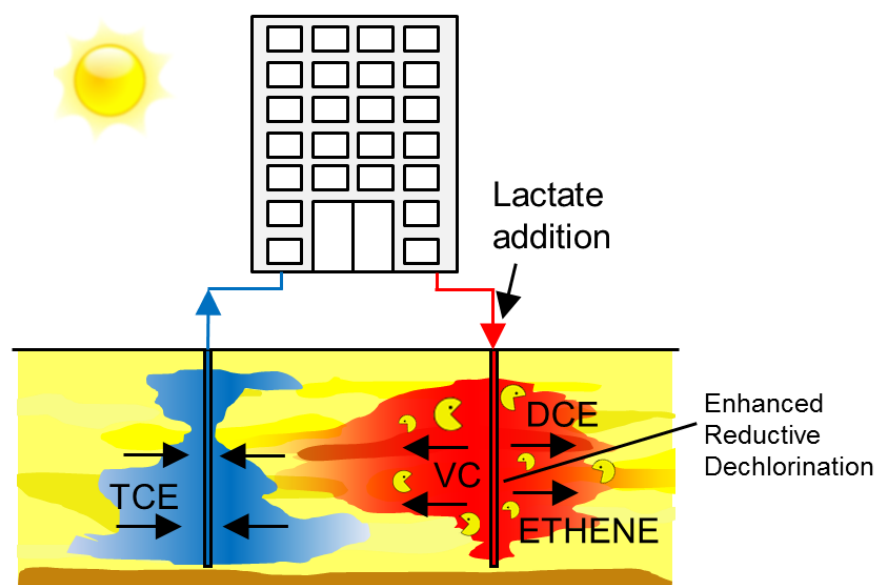


Figure 7.3 Combination concept of aquifer thermal energy storage with biostimulation

Knowledge gaps

Sophisticated modelling is a crucial step to explore the feasibility of the combined ATES and biostimulation concept. As shown by Chambon et al. [254] and Kouznetsova et al. [258] an increasing number of processes and interactions can be incorporated in numerical models. However, parameterization, especially for field applications, remains a challenge [254]. Reduction of iron oxides in our simulations (chapter 6) led to increasing pH values that are not reported for laboratory or field studies. While fermentation of electron donor is widely studied, there is a limited number of reports on iron reduction in reductive dechlorination studies [254]. Also, since well clogging due to microbial growth is a main concern for biostimulation using ATES, growth and mobility are important issues for further study. In the Netherlands only, there are already more than 10 000 sites contaminated with CAH [292] of which many in the urban environment. Therefore, the successful combination of ATES and biostimulation could potentially have a large impact on the remediation of these contaminated groundwater systems. Field studies are expected to improve the setting of boundary conditions for modelling and therefore model prediction which is needed to advance understanding of the combined ERD-ATES concept.

Bibliography

1. Dell, R.M. and D.A.J. Rand, *Energy storage — a key technology for global energy sustainability*. Journal of Power Sources, 2001. **100**(1–2): p. 2-17.
2. Asif, M. and T. Muneer, *Energy supply, its demand and security issues for developed and emerging economies*. Renewable and Sustainable Energy Reviews, 2007. **11**(7): p. 1388-1413.
3. Shafiee, S. and E. Topal, *When will fossil fuel reserves be diminished?* Energy Policy, 2009. **37**(1): p. 181-189.
4. Zecca, A. and L. Chiari, *Fossil-fuel constraints on global warming*. Energy Policy, 2010. **38**(1): p. 1-3.
5. Wuebbles, D.J. and A.K. Jain, *Concerns about climate change and the role of fossil fuel use*. Fuel Processing Technology, 2001. **71**(1–3): p. 99-119.
6. Holdren, J.P., K.R. Smith, T. Kjellstrom, D. Streets, X. Wang, and S. Fischer, *Energy, the environment and health*. New York: United Nations Development Programme, 2000.
7. Correlje, A. and C. Van der Linde, *Energy supply security and geopolitics: a European perspective*. Energy Policy, 2006. **34**(5): p. 532-543.
8. Dorian, J.P., H.T. Franssen, and D.R. Simbeck, *Global challenges in energy*. Energy Policy, 2006. **34**(15): p. 1984-1991.
9. Gao, Q., M. Li, M. Yu, J.D. Spitler, and Y. Yan, *Review of development from GSHP to UTES in China and other countries*. Renewable and Sustainable Energy Reviews, 2009. **13**(6): p. 1383-1394.
10. Paksoy, H.Ö., *Thermal energy storage for sustainable energy consumption*. 2007: Springer.
11. Vanhoudt, D., J. Desmedt, J. Van Bael, N. Robeyn, and H. Hoes, *An aquifer thermal storage system in a Belgian hospital: Long-term experimental evaluation of energy and cost savings*. Energy and Buildings, 2011. **43**: p. 3657-3665.
12. Hasnain, S., *Review on sustainable thermal energy storage technologies, Part I: heat storage materials and techniques*. Energy Conversion and Management, 1998. **39**(11): p. 1127-1138.
13. Dincer, I., *On thermal energy storage systems and applications in buildings*. Energy and Buildings, 2002. **34**(4): p. 377-388.
14. Omer, A.M., *Energy, environment and sustainable development*. Renewable and Sustainable Energy Reviews, 2008. **12**(9): p. 2265-2300.
15. De Rosa, M., V. Bianco, F. Scarpa, and L.A. Tagliafico, *Heating and cooling building energy demand evaluation; a simplified model and a modified degree days approach*. Applied Energy, 2014. **128**(0): p. 217-229.

16. Doughty, C., G. Hellström, C.F. Tsang, and J. Claesson, *A dimensionless parameter approach to the thermal behavior of an aquifer thermal energy storage system*. Water Resources Research, 1982. **18**(3): p. 571-587.
17. Kangas, M.T. and P.D. Lund, *Modeling and Simulation of Aquifer Storage Energy-Systems*. Solar Energy, 1994. **53**(3): p. 237-247.
18. Sauty, J.P., A.C. Gringarten, A. Menjoz, and P.A. Landel, *Sensible energy storage in aquifers: 1. Theoretical study*. Water Resources Research, 1982. **18**(2): p. 245-252.
19. Snijders, A.L. and M.M.v. Aarsen, *Big is beautiful? Application of large-scale energy storage in the Netherlands*, in *Futurestock, 9th International conference on thermal energy storage*. 2003, Institute of heat engineering, Warsaw University of Technology: Warsaw, Poland.
20. Verburg, R., H. Slenders, N. Hoekstra, E. van Nieuwker, R. Guijt, B. van der Mark, and J. Mimpfen, *Handleiding BOEG: bodemenergie en grondwaterverontreiniging*, NVOE, Editor. 2010: Den Bosch.
21. Bonte, M., P.J. Stuyfzand, A. Hulsmann, and P. Van Beelen, *Underground thermal energy storage: environmental risks and policy developments in the Netherlands and European Union*. Ecology and Society, 2011. **16**(1): p. 22.
22. Haehnlein, S., P. Bayer, and P. Blum, *International legal status of the use of shallow geothermal energy*. Renewable and Sustainable Energy Reviews, 2010. **14**(9): p. 2611-2625.
23. B. Sanner, F. Kabus, P. Seibt, and J. Bartels. *Underground thermal energy storage for the german parliament in Berlin, system concept and operational experience*. in *Proceedings world geothermal congress*. 2005. Antalya, Turkey: International geothermal association.
24. G. Schout, B. Drijver, M. Gutierrez-Neri, and R. Schotting, *Analysis of recovery efficiency in high-temperature aquifer thermal energy storage: a Rayleigh-based method*. Hydrogeology Journal, 2013.
25. F. Kabus, M. Wolfgramm, A. Seibt, U. Richlak, and H. Beuster. *Aquifer thermal energy storage in Neubrandenburg: monitoring throughout three years of regular operation*. in *EFFSTOCK Conference*. 2009. Stockholm, Sweden.
26. B. Drijver, M. van Aarssen, and B.d. Zwart. *High-temperature aquifer thermal energy storage (HT-ATES): sustainable and multi-usable*. in *Innostock*. 2012. Lleida, Spain: International Energy Agency.
27. Snijders, A. *Lessons from 100 ATES projects—the developments of aquifer storage in Netherlands*. in *Proceedings of TERRASTOCK*. 2000.
28. Thorne, D., C.D. Langevin, and M.C. Sukop, *Addition of simultaneous heat and solute transport and variable fluid viscosity to SEAWAT*. Computers & Geosciences, 2006. **32**(10): p. 1758-1768.
29. Visser, P.W., H. Kooi, and P.J. Stuyfzand, *The thermal impact of aquifer thermal energy storage (ATES) systems: a case study in the Netherlands, combining monitoring and modeling*. Hydrogeology Journal, 2015: p. 1-26.
30. Allen, D.M., *Modelling protocol for successful simulations of flow and heat transport in ATES systems*. Earth Sciences Program, 2002.
31. Bridger, D. and D. Allen, *Influence of geologic layering on heat transport and storage in an aquifer thermal energy storage system*. Hydrogeology Journal, 2014. **22**(1): p. 233-250.
32. Lo Russo, S., G. Taddia, and V. Verda, *Development of the thermally affected zone (TAZ) around a groundwater heat pump (GWHP) system: A sensitivity analysis*. Geothermics, 2012. **43**(0): p. 66-74.

33. Self, S.J., B.V. Reddy, and M.A. Rosen, *Geothermal heat pump systems: Status review and comparison with other heating options*. Applied Energy, 2013. **101**: p. 341-348.
34. Florides, G. and S. Kalogirou, *Ground heat exchangers—A review of systems, models and applications*. Renewable Energy, 2007. **32**(15): p. 2461-2478.
35. Barbier, E., *Geothermal energy technology and current status: an overview*. Renewable and Sustainable Energy Reviews, 2002. **6**(1): p. 3-65.
36. Yang, H., P. Cui, and Z. Fang, *Vertical-borehole ground-coupled heat pumps: a review of models and systems*. Applied Energy, 2010. **87**(1): p. 16-27.
37. Lund, J.W., D.H. Freeston, and T.L. Boyd, *Direct utilization of geothermal energy 2010 worldwide review*. Geothermics, 2011. **40**(3): p. 159-180.
38. Tsang, C.F., D. Hopkins, and G. Hellstrom, *Aquifer thermal energy storage - a survey*. 1980, Lawrence Berkeley Laboratory
39. Meurs, A.M., *Seasonal heat storage in the soil*. 1985, Technische Hogeschool Delft: Pijnacker.
40. Brons, H., *Biogeochemical aspects of aquifer thermal energy storage*. 1992, Landbouwniversiteit te Wageningen.
41. Paksoy, H., Z. Gürbüz, B. Turgut, D. Dikici, and H. Evliya, *Aquifer thermal storage (ATES) for air-conditioning of a supermarket in Turkey*. Renewable Energy, 2004. **29**(12): p. 1991-1996.
42. Paksoy, H., A. Snijders, and L. Stiles. *Aquifer Thermal Energy Cold Storage System at Richard Stockton College*. in *Effstock*. 2009. Stockholm.
43. Sanner, B., F. Kabus, P. Seibt, and J. Bartels. *Underground thermal energy storage for the German Parliament in Berlin, system concept and operational experiences*. in *Proceedings World Geothermal Congress*. 2005.
44. Andersson, O., J. Ekkestubbe, and A. Ekdahl, *UTES (Underground Thermal Energy Storage)—Applications and Market Development in Sweden*. J. Energ. Pow. Eng, 2013. **7**: p. 669.
45. CBS, *Hernieuwbare energie in Nederland 2012 (Renewable energy in the Netherlands 2012)*. 2013, Centraal bureau voor de statistiek: Den Haag.
46. Saner, D., R. Juraske, M. Kübert, P. Blum, S. Hellweg, and P. Bayer, *Is it only CO₂ that matters? A life cycle perspective on shallow geothermal systems*. Renewable and Sustainable Energy Reviews, 2010. **14**(7): p. 1798-1813.
47. Ferguson, G. and A.D. Woodbury, *Observed thermal pollution and post-development simulations of low-temperature geothermal systems in Winnipeg, Canada*. Hydrogeology Journal, 2006. **14**(7): p. 1206-1215.
48. Herbert, A., S. Arthur, and G. Chillingworth, *Thermal modelling of large scale exploitation of ground source energy in urban aquifers as a resource management tool*. Applied Energy, 2013. **109**: p. 94-103.
49. Bloemendal, M., T. Olsthoorn, and F. Boons, *How to achieve optimal and sustainable use of the subsurface for Aquifer Thermal Energy Storage*. Energy Policy, 2013.
50. Possemiers, M., M. Huysmans, and O. Batelaan, *Influence of Aquifer Thermal Energy Storage on groundwater quality: A review illustrated by seven case studies from Belgium*. Journal of Hydrology: Regional Studies, 2014. **2**(0): p. 20-34.
51. Snijders, A. and d.K. Wit. *Solar heating of a large office building using seasonal aquifer thermal energy storage*. in *First E.C. conference on solar heating*. 1984. Amsterdam, the Netherlands.
52. van der Bruggen, R.J.A. and A. Snijders. *Heating of an office building using solar energy in combination with a heatpump and seasonal heat storage*. in *Enerstock*. 1985. Toronto, Canada.

53. Snijders, A. and A.A.F. van Woerkom. *The feasibility of seasonal storage of excess heat for the district heating system at Almere*. in *Enerstock*. 1985. Toronto, Canada.
54. Stolker, L., T. Klip-Martin, H. Buitenhuis, M. Moorman, P. Smit, C. Zijdeveld, L. Verheijen, P. Glas, B. van de Griendt, W. van Vliet, and C. Moons, *Groenlicht voor Bodemenergie (Greenlight for Geothermal Energy)*. 2009, Taskforce WKO.
55. CBS, *Duurzame energie in Nederland 2003 (Sustainable energy in the Netherlands 2003)*. 2004, Centraal bureau voor de statistiek: Voorburg/Heerlen.
56. CBS, *Duurzame energie in Nederland 2004 (Sustainable energy in the Netherlands 2004)*. 2005, Centraal bureau voor de statistiek: Voorburg/Heerlen.
57. CBS, *Duurzame energie in Nederland 2005 (Sustainable energy in the Netherlands 2005)*. 2006, Centraal bureau voor de statistiek: Voorburg/Heerlen.
58. CBS, *Duurzame energie in Nederland 2006 (Sustainable energy in the Netherlands 2006)*. 2007, Centraal bureau voor de statistiek: Voorburg/Heerlen.
59. CBS, *Duurzame energie in Nederland 2007 (Sustainable energy in the Netherlands 2007)*. 2008, Centraal bureau voor de statistiek: Voorburg/Heerlen.
60. CBS, *Duurzame energie in Nederland 2008 (Sustainable energy in the Netherlands 2008)*. 2009, Centraal bureau voor de statistiek: Den Haag/Heerlen.
61. CBS, *Hernieuwbare energie in Nederland 2009 (Renewable energy in the Netherlands 2009)*. 2010, Centraal bureau voor de statistiek: Den Haag/Heerlen.
62. CBS, *Hernieuwbare energie in Nederland 2010 (Renewable energy in the Netherlands 2010)*. 2011, Centraal bureau voor de statistiek: Den Haag/Heerlen.
63. CBS, *Hernieuwbare energie in Nederland 2011 (Renewable energy in the Netherlands 2011)*. 2012, Centraal bureau voor de statistiek: Den Haag/Heerlen.
64. CBS, *Hernieuwbare energie in Nederland 2013 (Renewable energy in the Netherlands 2013)*. 2014, Centraal bureau voor de statistiek: Den Haag.
65. CBS, *Environmental accounts of the Netherlands 2012*. 2012, CBS statistics Netherlands: Den Haag.
66. Kim, J., Y. Lee, W.S. Yoon, J.S. Jeon, M.-H. Koo, and Y. Keehm, *Numerical modeling of aquifer thermal energy storage system*. *Energy*, 2010. **35**(12): p. 4955-4965.
67. Kowalczyk, W. and J. Havinga, *91 5th International Conference on Thermal Energy Storage*. 1991.
68. Lee, K.S., *A Review on Concepts, Applications, and Models of Aquifer Thermal Energy Storage Systems*. *Energies*, 2010. **3**(6): p. 1320-1334.
69. Lee, K.S. and S.J. Jeong, *Numerical modeling on the performance of aquifer thermal energy storage system under cyclic flow regime*. *International Journal of Green Energy*, 2008. **5**(1-2): p. 1-14.
70. Hähnlein, S., P. Bayer, G. Ferguson, and P. Blum, *Sustainability and policy for the thermal use of shallow geothermal energy*. *Energy Policy*, 2013. **59**: p. 914-925.
71. SKB, *Handreiking masterplannen bodemenergie*. 2011, SKB duurzame ontwikkeling ondergrond.
72. Verburg, R., A. Alphenaar, H. Slenders, and A. Vugt, *De ordening van bodemenergie in de ondergrond (The arrangement of geothermal energy in the subsurface)*. *Bodem*, 2012(1): p. 33-35.
73. Bradley, P.M., *Microbial degradation of chloroethenes in groundwater systems*. *Hydrogeology Journal*, 2000. **8**(1): p. 104-111.

74. Henry, S.M. and S.D. Warner, *Chlorinated solvent and DNAPL remediation: An overview of physical, chemical, and biological processes*, in *Chlorinated Solvent and Dnapl Remediation - Innovative Strategies for Subsurface Cleanup*. 2003, Washington: Amer Chemical Soc.
75. ITRC, *Overview of In Situ Bioremediation of Chlorinated Ethene DNAPL Source Zones*. 2005: Washington D.C.
76. Smidt, H. and W.M. de Vos, *Anaerobic microbial dehalogenation*. *Annu. Rev. Microbiol.*, 2004. **58**: p. 43-73.
77. WHO, *World Health Organization Guidelines for Drinking-Water Quality*. 2004: Geneva, Switzerland.
78. Stroo, H.F. and C.H. Ward, *In situ remediation of chlorinated solvent plumes*. Vol. 2. 2010: Springer.
79. Picone, S., *Transport and biodegradation of volatile organic compounds: influence on vapor intrusion into buildings*. 2012, Wageningen University: Wageningen.
80. Kurtz, J., E. Wolfe, A. Woodland, and S. Foster, *Evidence for Increasing Indoor Sources of 1, 2 - Dichloroethane Since 2004 at Two Colorado Residential Vapor Intrusion Sites*. *Groundwater Monitoring & Remediation*, 2010. **30**(3): p. 107-112.
81. Picone, S., J. Valstar, P. van Gaans, T. Grotenhuis, and H. Rijnaarts, *Sensitivity analysis on parameters and processes affecting vapor intrusion risk*. *Environmental Toxicology and Chemistry*, 2012. **31**(5): p. 1042-1052.
82. Zuurbier, K.G., N. Hartog, J. Valstar, V.E. Post, and B.M. van Breukelen, *The impact of low-temperature seasonal aquifer thermal energy storage (SATES) systems on chlorinated solvent contaminated groundwater: Modeling of spreading and degradation*. *Journal of contaminant hydrology*, 2013. **147**: p. 1-13.
83. Bonte, M., B.M. van Breukelen, and P.J. Stuyfzand, *Temperature-induced impacts on groundwater quality and arsenic mobility in anoxic aquifer sediments used for both drinking water and shallow geothermal energy production*. *Water Research*, 2013. **47**(14): p. 5088-5100.
84. Bonte, M., P.J. Stuyfzand, and B.M.v. Breukelen, *Reactive Transport Modeling of Thermal Column Experiments to Investigate the Impacts of Aquifer Thermal Energy Storage on Groundwater Quality*. *Environmental Science & Technology*, 2014. **48**(20): p. 12099-12107.
85. Gossett, M.M. *Bioremediation of chloroethenes in the third millennium: year-1 update*. in *Sixth international in-situ and on-site bioremediation symposium*. 2001. San Diego, CA.
86. Luciano, A., P. Viotti, and M.P. Papini, *Laboratory investigation of DNAPL migration in porous media*. *Journal of Hazardous Materials*, 2010. **176**(1): p. 1006-1017.
87. Aulenta, F., M. Majone, and V. Tandoi, *Enhanced anaerobic bioremediation of chlorinated solvents: environmental factors influencing microbial activity and their relevance under field conditions*. *Journal of Chemical Technology and Biotechnology*, 2006. **81**(9): p. 1463-1474.
88. Ballapragada, B.S., H.D. Stensel, J. Puhakka, and J.F. Ferguson, *Effect of hydrogen on reductive dechlorination of chlorinated ethenes*. *Environmental Science & Technology*, 1997. **31**(6): p. 1728-1734.
89. Bennett, P., D. Gandhi, S. Warner, and J. Bussey, *In situ reductive dechlorination of chlorinated ethenes in high nitrate groundwater*. *Journal of Hazardous Materials*, 2007. **149**(3): p. 568-573.
90. Boopathy, R., *Factors limiting bioremediation technologies*. *Bioresource Technology*, 2000. **74**(1): p. 63-67.
91. Fowler, T. and K. Reinauer, *Enhancing Reductive Dechlorination With Nutrient Addition*. *Remediation Journal*, 2013. **23**(1): p. 23-35.

92. McCarty, P.L., M.-Y. Chu, and P.K. Kitanidis, *Electron donor and pH relationships for biologically enhanced dissolution of chlorinated solvent DNAPL in groundwater*. European Journal of Soil Biology, 2007. **43**(5): p. 276-282.
93. Ni, Z., M. Smit, T. Grotenhuis, P. van Gaans, and H. Rijnaarts, *Effectiveness of stimulating PCE reductive dechlorination: A step-wise approach*. Journal of contaminant hydrology, 2014. **164**: p. 209-218.
94. Schaefer, C.E., D.R. Lippincott, and R.J. Steffan, *Field - Scale Evaluation of Bioaugmentation Dosage for Treating Chlorinated Ethenes*. Groundwater Monitoring & Remediation, 2010. **30**(3): p. 113-124.
95. Scheutz, C., N.d. Durant, P. Dennis, M.H. Hansen, T. Jørgensen, R. Jakobsen, E.e. Cox, and P.L. Bjerg, *Concurrent ethene generation and growth of Dehalococcoides containing vinyl chloride reductive dehalogenase genes during an enhanced reductive dechlorination field demonstration*. Environmental science & technology, 2008. **42**(24): p. 9302-9309.
96. Tiehm, A. and K.R. Schmidt, *Sequential anaerobic/aerobic biodegradation of chloroethenes— aspects of field application*. Current opinion in biotechnology, 2011. **22**(3): p. 415-421.
97. Bonte, M., W.F. Röling, E. Zaura, P.W. van der Wielen, P.J. Stuyfzand, and B.M. van Breukelen, *Impacts of shallow geothermal energy production on redox processes and microbial communities*. Environmental science & technology, 2013. **47**(24): p. 14476-14484.
98. Ni, Z., M. Smit, T. Grotenhuis, N. Hartog, and H. Rijnaarts, *Findings on Limiting Factors of Intrinsic Bioremediation of Chlorinated Ethenes Combined with Aquifer Thermal Energy Storage (ATES)*. Aquaconsol, Barcelona, 2013: p. 16-19.
99. Slenders, H.L., P. Dols, R. Verburg, and A.J. de Vries, *Sustainable remediation panel: Sustainable synergies for the subsurface: Combining groundwater energy with remediation*. Remediation Journal, 2010. **20**(2): p. 143-153.
100. Dinkla, I., S. Lieten, E. De Vries, N. Hartog, and N. Hoekstra, *Meer met bodemenergie: effecten op sanering ("More with subsurface energy: effect on remediation")*, M. Koenders, Editor. 2012.
101. De Vries, E. and N. Hoekstra, *Meer met bodemenergie: Mogelijkheden voor combinatie van KWO met bodemsanering*, MMB, Editor. 2012.
102. Sommer, W., B. Drijver, R. Verburg, H. Slenders, E. de Vries, I. Dinkla, I. Leusbrock, and T. Grotenhuis. *Combining shallow geothermal energy and groundwater remediation*. in *European geothermal congress*. 2013. Pisa, Italy: EGEC.
103. Boer, S.d., I. Dinkla, B. Drijver, N. Hartog, M. Koenders, and H. Mathijssen, *Meer met bodemenergie*, S.d.o. ondergrond, Editor. 2012: Pijnacker.
104. Lieten, S., E.d. Vries, E.v. Baaren, M. Bakr, G. Oude Essink, N. Hartog, W. Meindertsma, E.v. Nieuwkerk, N.v. Oostrom, M. Woning, B. Drijver, H. Krajenbrink, H. Mathijssen, and R. Wennekes, *Meer met bodemenergie - Literatuuronderzoek*, M. Koenders, Editor. 2012.
105. Bridger, D. and D. Allen, *Heat transport simulations in a heterogeneous aquifer used for aquifer thermal energy storage (ATES)*. Canadian geotechnical journal, 2010. **47**(1): p. 96-115.
106. Chevalier, S. and O. Banton, *Modelling of heat transfer with the random walk method. Part 1. Application to thermal energy storage in porous aquifers*. Journal of Hydrology, 1999. **222**(1): p. 129-139.
107. Ferguson, G., *Heterogeneity and thermal modeling of ground water*. Groundwater, 2007. **45**(4): p. 485-490.
108. Hidalgo, J.J., J. Carrera, and M. Dentz, *Steady state heat transport in 3D heterogeneous porous media*. Advances in water resources, 2009. **32**(8): p. 1206-1212.

109. Raymond, J., R. Therrien, L. Gosselin, and R. Lefebvre, *Numerical analysis of thermal response tests with a groundwater flow and heat transfer model*. Renewable Energy, 2011. **36**(1): p. 315-324.
110. Vandenbohede, A., T. Hermans, F. Nguyen, and L. Lebbe, *Shallow heat injection and storage experiment: heat transport simulation and sensitivity analysis*. Journal of Hydrology, 2011. **409**(1): p. 262-272.
111. Sanner, B., C. Karytsas, D. Mendrinou, and L. Rybach, *Current status of ground source heat pumps and underground thermal energy storage in Europe*. Geothermics, 2003. **32**(4): p. 579-588.
112. Van Dalfsen, W., *Geothermal investigation in shallow observation wells: the shallow subsurface temperature field in the Netherlands*. TNO, Utrecht, The Netherlands, 1981.
113. Harper, M., *Approximate geothermal gradients in the North Sea basin*. 1971.
114. Dickinson, J.S., N. Buik, M.C. Matthews, and A. Snijders, *Aquifer thermal energy storage: theoretical and operational analysis*. Geotechnique, 2009. **59**(3): p. 249-260.
115. Dickinson, J., N. Buik, M. Matthews, and A. Snijders, *Aquifer thermal energy storage: theoretical and operational analysis*. Geotechnique, 2009. **59**(3): p. 249-260.
116. Drijver, B., M. van Aarssen, and B. Zwart. *High-temperature aquifer thermal energy storage (HT-ATES): sustainable and multi-usable*. in *InnoStock*. 2012. Catalonia, Spain.
117. Bakr, M., N. van Oostrom, and W. Sommer, *Efficiency of and interference among multiple Aquifer Thermal Energy Storage systems; A Dutch case study*. Renewable Energy, 2013. **60**: p. 53-62.
118. Herbert, A., S. Arthur, and G. Chillingworth. *Large scale exploitation of ground source energy for heating and cooling: resource constraints and management options in urban aquifers*. in *InnoStock*. 2012. Catalonia, Spain.
119. Kangas, M. and P. Lund, *Modeling and simulation of aquifer storage energy systems*. Solar Energy, 1994. **53**(3): p. 237-247.
120. Sauty, J.P., A.C. Gringarten, A. Menjoz, and P.A. Landel, *Sensible Energy-Storage in Aquifers .1. Theoretical-Study*. Water Resources Research, 1982. **18**(2): p. 245-252.
121. Kim, J., Y. Lee, W.S. Yoon, J.S. Jeon, M.H. Koo, and Y. Keehm, *Numerical modeling of aquifer thermal energy storage system*. Energy, 2010. **35**(12): p. 4955-4965.
122. Kowalczyk, W. and J. Havinga. *A case study on the influence of the distance between wells on a doublet well aquifer thermal performance*. in *Thermastock 91*. 1991. Scheveningen, The Netherlands.
123. Sommer, W.T., J. Valstar, P.F.M.v. Gaans, J.T.C. Grotenhuis, and H.H.M. Rijnaarts, *The impact of aquifer heterogeneity on the performance of aquifer thermal energy storage*. Water Resources Research, 2013. **49**.
124. Berendsen, H.J.A., *De vorming van het land*. 2004: Uitgeverij Van Gorcum.
125. de Mulder, E.F., M.C. Geluk, I. Ritsema, W.E. Westerhoff, and T.E. Wong, *De ondergrond van Nederland*. 2003: Wolters-Noordhoff.
126. Vernes, R. and T.H. Van Doorn, *Van gidslaag naar hydrogeologische eenheid, toelichting op de totstandkoming van de dataset REGIS II [From Marker Layer to Hydrogeological Unit, Explanatory Notes to the making of the REGIS II dataset]*. TNO report NITG, 2005: p. 05-038.
127. Weerts, H.J.T., P. Cleveringa, J. Ebbing, F. De Lang, and W. Westerhoff, *De lithostratigrafische indeling van Nederland: formaties uit het Tertiair en Kwartair*. 2000: Nederlands Instituut voor Toegepaste Geowetenschappen TNO.

128. Starink, L. and M. Hehenkamp, *Koude-/ warmteopslag noordwesthoek Uithof Utrecht: effectenstudie grondwatersysteem*. 2001, If-Technology: Arnhem, the Netherlands.
129. Glorie, F.H. and F. den Hartog, *Report of well constructions*. 2001, De Ruiter Boringen en Bemalingen: Zwanenburg, the Netherlands.
130. Sommer, W.T., P.J. Doornenbal, B.C. Drijver, P.F.M. van Gaans, J.T.C. Grotenhuis, I. Leusbrock, and H.H.M. Rijnaarts, *Thermal performance and heat transport in aquifer thermal energy storage*. Hydrogeology Journal, 2013.
131. Koenders, M.J.B., Zwart, B. de, *Koude/warmteopslag in de praktijk: Meetgegevens van 67 projecten*. 2007.
132. Staatscourant. *Wijzigingsbesluit bodemenergiesystemen no. 4830, p 29*. 2011 October 2013]; Available from: <https://zoek.officielebekendmakingen.nl/stcrt-2011-4830.html>.
133. Vogt, T., P. Schneider, L. Hahn-Woernle, and O.A. Cirpka, *Estimation of seepage rates in a losing stream by means of fiber-optic high-resolution vertical temperature profiling*. Journal of Hydrology, 2010. **380**(1): p. 154-164.
134. Selker, J.S., L. Thevenaz, H. Huwald, A. Mallet, W. Luxemburg, N. Van De Giesen, M. Stejskal, J. Zeman, M. Westhoff, and M.B. Parlange, *Distributed fiber - optic temperature sensing for hydrologic systems*. Water Resources Research, 2006. **42**(12).
135. SIKB. 2010 December 2012]; Available from: www.sikb.nl.
136. Sensor.net. December 2012]; Available from: www.sensor.net.co.uk.
137. Buik, N., A. Willemsen, and C. Verbeek, *Effecten van thermische opslagsystemen*.
138. Kipp, K.L., *HST3D; a Computer Code for Simulation of Heat and Solute Transport in Three-dimensional Ground-water Flow Systems*. 1987.
139. Ward, D.J., C.T. Simmons, and P.J. dillon, *A theoretical analysis of mixed convection in aquifer storage and recovery: How important are density effects?* Journal of Hydrology, 2007(343): p. 169-186.
140. Buik, N. and A. Snijders. *Clogging of recharge wells in porous media*. in *InnoStock*. 2012. Catalonia, Spain.
141. Molz, F., A. Parr, and P. Andersen, *Thermal energy storage in a confined aquifer: Second cycle*. Water Resources Research, 1981. **17**(3): p. 641-645.
142. Sauty, J.P., A.C. Gringarten, H. Fabris, D. Thiery, A. Menjoz, and P.A. Landel, *Sensible Energy-Storage in Aquifers 2. Field Experiments and Comparison with Theoretical Results*. Water Resources Research, 1982. **18**(2): p. 253-265.
143. Molz, F., J. Melville, A. Parr, D. King, and M. Hopf, *Aquifer thermal energy storage: a well doublet experiment at increased temperatures*. Water Resources Research, 1983. **19**(1): p. 149-160.
144. Van De Giesen, N., S.C. Steele-Dunne, J. Jansen, O. Hoes, M.B. Hausner, S. Tyler, and J. Selker, *Double-ended calibration of fiber-optic Raman spectra distributed temperature sensing data*. Sensors, 2012. **12**(5): p. 5471-5485.
145. Hausner, M.B., F. Suárez, K.E. Glander, N.v.d. Giesen, J.S. Selker, and S.W. Tyler, *Calibrating single-ended fiber-optic Raman spectra distributed temperature sensing data*. Sensors, 2011. **11**(11): p. 10859-10879.
146. Bridger, D.W. and D.M. Allen, *Heat transport simulations in a heterogeneous aquifer used for aquifer thermal energy storage (ATES)*. Canadian Geotechnical Journal, 2010. **47**(1): p. 96-115.
147. NVOE, *Werkwijzen en richtlijnen ondergrondse energieopslag (Methods and guidelines underground energy storage)*. 2006, Nederlandse vereniging voor ondergrondse energieopslag (Dutch society for subsurface energy storage),.

148. Chevalier, S. and O. Banton, *Modelling of heat transfer with the random walk method. Part 1. Application to thermal energy storage in porous aquifers*. Journal of Hydrology, 1999. **222**(1-4): p. 129-139.
149. Doughty, C., G. Hellstrom, C.F. Tsang, and J. Claesson, *A Dimensionless Parameter Approach to the Thermal-Behavior of an Aquifer Thermal-Energy Storage-System*. Water Resources Research, 1982. **18**(3): p. 571-587.
150. Bakr, M., N.v. Oostrom, and W.T. Sommer, *Efficiency of and Interference among Multiple Aquifer Thermal Energy Storage Systems; a Dutch Case study*. Renewable Energy, 2013.
151. Molz, F.J., A.D. Parr, and P.F. Andersen, *Thermal-Energy Storage in a Confined Aquifer - 2nd Cycle*. Water Resources Research, 1981. **17**(3): p. 641-645.
152. Molz, F.J., J.G. Melville, A.D. Parr, D.A. King, and M.T. Hopf, *Aquifer Thermal-Energy Storage - a Well Doublet Experiment at Increased Temperatures*. Water Resources Research, 1983. **19**(1): p. 149-160.
153. Stolker, L., *Groenlicht voor Bodemenergie (Greenlight for geothermal energy)*. 2009, commissioned by the Ministry of housing, spatial planning and environment.
154. Haehnlein, S., P. Bayer, and P. Blum, *International legal status of the use of shallow geothermal energy*. Renewable and Sustainable Energy Reviews, 2010. **14**: p. 2611–2625.
155. Dagan, G. and S.P. Neuman, *Subsurface Flow and Transport: A Stochastic Approach*. illustrated, reprint ed. 2005: Cambridge University Press.
156. Gelhar, L.W., *Stochastic subsurface hydrology*. 1993: Prentice-Hall.
157. Hoeksema, R.J. and P.K. Kitanidis, *Analysis of the Spatial Structure of Properties of Selected Aquifers*. Water Resources Research, 1985. **21**(4): p. 563-572.
158. Sudicky, E.A., *A Natural Gradient Experiment on Solute Transport in a Sand Aquifer - Spatial Variability of Hydraulic Conductivity and Its Role in the Dispersion Process*. Water Resources Research, 1986. **22**(13): p. 2069-2082.
159. Vereecken, H., U. Doring, H. Hardelauf, U. Jaekel, U. Hashagen, O. Neuendorf, H. Schwarze, and R. Seidemann, *Analysis of solute transport in a heterogeneous aquifer: the Krauthausen field experiment*. Journal of Contaminant Hydrology, 2000. **45**(3-4): p. 329-358.
160. Rehfeldt, K.R., J.M. Boggs, and L.W. Gelhar, *Field Study of Dispersion in a Heterogeneous Aquifer 3. Geostatistical Analysis of Hydraulic Conductivity*. Water Resources Research, 1992. **28**(12): p. 3309-3324.
161. Ferguson, G., *Heterogeneity and thermal modeling of ground water*. Ground Water, 2007. **45**(4): p. 485-490.
162. Caljé, R.J., *Future use of aquifer thermal energy storage below the historic centre of Amsterdam*. 2010, Waternet: Amsterdam.
163. Woodbury, A.D. and E.A. Sudicky, *The Geostatistical Characteristics of the Borden Aquifer*. Water Resources Research, 1991. **27**(4): p. 533-546.
164. Kennedy, P.L. and A.D. Woodbury, *Geostatistics and Bayesian updating for transmissivity estimation in a multiaquifer system in Manitoba, Canada*. Ground Water, 2002. **40**(3): p. 273-283.
165. Allen, D.M. and D.W. Bridger. *ATES Systems in Heterogeneous Aquifers: A Modelling Case Study*. in *Futurestock*. 2003. Warsaw, Poland: 9th International Conference on Thermal Energy Storage.
166. Freeze, R.A., *Stochastic-Conceptual Analysis of One-Dimensional Groundwater Flow in Nonuniform Homogeneous Media*. Water Resources Research, 1975. **11**(5): p. 725-741.

167. Deutsch, C.V., *GSLIB: Geostatistical Software Library and User's Guide*. 1997, New York, United States: Oxford University Press.
168. Helsel and Hirsch, *Statistical methods in water resources*. Studies in Environmental Science 49. 1992, Amsterdam: Elsevier.
169. Harbaugh, A.W., *Modflow-2000, the U.S. Geological Survey modular ground-water model : user guide to modularization concepts and the ground-water flow process*. US Geological Survey open-file report. 2000, Reston, VA, Denver, CO: U.S. Geological Survey, Branch of Information Services [distributor]. vii, 121 p.
170. Zheng, C. and P.P. Wang, *MT3DMS: A Modular Three-Dimensional Multispecies Transport Model for Simulation of Advection, Dispersion, and Chemical Reactions of Contaminants in Groundwater Systems; Documentation and User's Guide*. 1999: Tuscaloosa, Alabama.
171. Hecht-Mendez, J., N. Molina-Giraldo, P. Blum, and P. Bayer, *Evaluating MT3DMS for heat transport simulation of closed geothermal systems*. Ground Water, 2010. **48**(5): p. 741-56.
172. Paksoy, H.O., Z. Gurbuz, B. Turgut, D. Dikici, and H. Evliya, *Aquifer thermal storage (ATES) for air-conditioning of a supermarket in Turkey*. Renewable Energy, 2004. **29**(12): p. 1991-1996.
173. Zuurbier, K.G., N. Hartog, J. Valstar, V.E. Post, and B.M. van Breukelen, *The impact of low-temperature seasonal aquifer thermal energy storage (SATES) systems on chlorinated solvent contaminated groundwater: Modeling of spreading and degradation*. Journal of Contaminant Hydrology, 2013(147).
174. Halford, K.J., R.T. Hanson, Santa Clara Valley Water District (Calif.), and Geological Survey (U.S.), *User guide for the drawdown-limited, multi-node well (MNW) package for the U.S. Geological Survey's modular three-dimensional finite-difference ground-water flow model, versions MODFLOW-96 and MODFLOW-2000*. Open-file report. 2002, Sacramento, Calif.: U.S. Dept. of the Interior, U.S. Geological Survey. v, 33 p.
175. Zheng, C., *MT3DMS v5.3 a modular three-dimensional multispecies transport model for simulation of advection, dispersion and chemical reactions of contaminants in groundwater systems: Supplemental User's Guide*, in Department of Geological Sciences. 2010, The University of Alabama: Tuscaloosa, Alabama, USA.
176. Fossoul, F., P. Orban, and A. Dassargues, *Numerical Simulation of Heat Transfer Associated with Low Enthalpy Geothermal Pumping in an Alluvial Aquifer*. Geologica Belgica, 2011. **14**(1-2): p. 45-54.
177. Lide, D.R., *CRC Handbook of Chemistry and Physics*. 74th edition ed, ed. D.R. Lide. 1993, Florida, US: CRC Press, inc.
178. Helsel, D.R. and R.M. Hirsch, *Statistical methods in water resources*. Vol. 49. 1992: Elsevier.
179. Attinger, S., I. Neuweiler, and W. Kinzelbach, *Macrodispersion in a radially diverging flow field with finite Peclet numbers 2. Homogenization theory approach*. Water Resources Research, 2001. **37**(3): p. 495-505.
180. Hsu, K.C., *Analytical expressions for macrodispersion coefficients in three-dimensional randomly heterogeneous porous media*. Journal of the Chinese Institute of Engineers, 2003. **26**(3): p. 375-380.
181. Chang, C.M. and H.D. Yeh, *Stochastic analysis of field-scale heat advection in heterogeneous aquifers*. Hydrology and Earth System Sciences, 2012. **16**(3): p. 641-648.
182. Vandenbohede, A., A. Louwyck, and L. Lebbe, *Conservative Solute Versus Heat Transport in Porous Media During Push-pull Tests*. Transport in Porous Media, 2009. **76**(2): p. 265-287.
183. Fitts, C.R., *Groundwater science*. 2002, Amsterdam ; Boston: Academic Press. xi, 450 p.

184. Li, Y.H. and S. Gregory, *Diffusion of Ions in Sea-Water and in Deep-Sea Sediments*. *Geochimica Et Cosmochimica Acta*, 1974. **38**(5): p. 703-714.
185. Sommer, W., J. Valstar, P. Gaans, T. Grotenhuis, and H. Rijnaarts, *The impact of aquifer heterogeneity on the performance of Aquifer Thermal Energy Storage*. *Water Resources Research*, 2013. **49**(12): p. 8128-8138.
186. Attinger, S., I. Neuweiler, and W. Kinzelbach, *Macrodispersion in a radially diverging flow field with finite Peclet Numbers: 2. Homogenization theory approach*. *Water Resources Research*, 2001. **37**(3): p. 495-505.
187. Technology, I., *Underground thermal energy storage: state-of-the art in 1994*. 1995, IF Technology: Arnhem.
188. Sanner, B., *High temperature underground thermal energy storage state-of-the-art and prospects; a review within energy conservation through energy storage (ECES)*. 1998, International Energy Agency IEA.
189. Dickinson, J.S., N. Buik, M.C. Matthews, and A. Snijders, *Geotechnique*. 2009. **59**(3): p. 249-260.
190. Snijders, A.L. *Lessons from 100 ATEs projects - The developments of aquifer storage in the Netherlands*. in *Terrastrack*. 2000. Stuttgart, Germany.
191. Kangas, M.T. and P.D. Lund, *Modeling and simulation of aquifer storage energysystems*. *Solar Energy*, 1994. **53**(3): p. 237-247.
192. Dagan, G., *The significance of heterogeneity of evolving scales to transport in porous formations*. *Water Resources Research*, 1994. **30**(12): p. 3327-3336.
193. Anderson, M.P., *Heat as a ground water tracer*. *Ground Water*, 2005. **43**(6): p. 951-68.
194. Bear, J., *Dynamics of Fluids in Porous Media*. 1972, New York: Dover.
195. Molson, J.W., E.O. Frind, and C.D. Palmer, *Thermal energy storage in an unconfined aquifer 2. Model development, validation and application*. *Water Resources Research*, 1992. **28**(10): p. 2857-2867.
196. De Marsily, G., *Quantitative Hydrogeology: Groundwater Hydrology for Engineers*. 1986, New York: Academic Press.
197. Molz, F.J., A.D. Parr, P.F. Anderson, V.D. Lucido, and J.C. Warman, *Thermal energy storage in a confined aquifer: experimental results*. *Water Resources Research*, 1979. **15**(6): p. 1509-1514.
198. Shen, P.Y., H.N. Pollack, S. Huang, and K. Wang, *Effects of subsurface heterogeneity on the inference of climate change from borehole temperature data: model studies and field examples from Canada*. *Journal of Geophysical Research-Solid Earth*, 1995. **100**(B4): p. 6383-6396.
199. Cox, M.H., G.W. Su, and J. Constantz, *Heat, chloride, and conductance as ground water tracers near streams*. *Ground Water*, 2007. **42**(2): p. 187-195.
200. Ghergut, I., M. Sauter, H. Behrens, T. Licha, C.I. McDermott, and M. Herfort. *Tracer tests evaluating hydraulic stimulation at deep geothermal reservoirs in Germany*. in *Thirty-second workshop on geothermal reservoir engineering 2007*. Stanford, California: Stanford University.
201. Hall, S. and H.J.R. Raymond. *Geohydrologic characterization for aquifer thermal energy storage*. in *The 1992 intersociety energy conversion engineer conference*. 1992. San Diego, California.
202. Li, T., C. Leven, P. Dietrich, P. Grathwohl, and P. Blum. *Evaluation of a thermal tracer test in a porous aquifer*. in *EGU General Assembly*. 2009. Vienna, Austria: Geophysical Research Abstracts.
203. Lowry, C.S., J.F. Walker, R.J. Hunt, and M.P. Anderson, *Identifying spatial variability of groundwater discharge in a wetland stream using a distributed temperature sensor*. *Water Resources Research*, 2007. **43**(10).

204. Van Oostrom, N.G.C. and M. Bakr, *Meer Met Bodemenergie rapport 7-Interferentie, Effecten van bodemenergiesystemen op hun omgeving - modellering grootschalige inpassing in stedelijke gebieden*. 2012, Deltares: Delft. p. 1-76.
205. Roelofsen, F., *Grondwatereffecten aan de oppervlakte (gebracht); Onderzoek naar effecten van stopzetting grondwateronttrekking; DSM Delft*. 2008, Deltares: Delft.
206. Sommer, W.T., J. Valstar, P.F.M.v. Gaans, J.T.C. Grotenhuis, and H.H.M. Rijnaarts, *Large-scale application of ATES (submitted)*. Applied Energy, 2013.
207. B. Sanner, C. Karytsas, D. Mendrinou, and L. Rybach, *Current status of ground source heat pumps and underground thermal energy storage in Europe*. Geothermics, 2003. **32**: p. 579-588.
208. Novo, A.V., J.R. Bayon, D. Castro-Fresno, and J. Rodriguez-Hernandez, *Review of seasonal heat storage in large basins: Water tanks and gravel-water pits*. Applied Energy, 2010. **87**(2): p. 390-397.
209. Hamada, Y., K. Marutani, M. Nakamura, S. Nagasaka, K. Ochifuji, S. Fuchigami, and S. Yokoyama, *Study on underground thermal characteristics by using digital national land information, and its application for energy utilization*. Applied Energy, 2002. **72**(3-4): p. 659-675.
210. Cabeza, L.F., V. Martin, and J. Yan, *Advances in energy storage research and development: The 12th International Conference on Energy Storage Innostock 2012*. Applied Energy, 2013. **109**(0): p. 291-292.
211. IF Technology, *Masterplan bodemenergie Stationskwartier (Masterplan geothermal energy Stationskwartier)*. 2011, If Technology.
212. Zwanenburg, H., *Province of North-Holland, The Netherlands*. personal communication, 2013.
213. Vernes, R.W. and T.H.M. van Doorn, *Van gidslaag naar hydrogeologische eenheid, toelichting op de totstandkoming van de dataset REGIS II (From marker layer to hydrogeological unit, explanatory notes to the making of the REGIS II dataset)*. 2005, TNO: Utrecht, The Netherlands.
214. Zhang, C., *MT3DMS v5.3 Supplemental User's Guide*. 2010, Department of Geological Sciences, The University of Alabama: Washington, DC 20314.
215. Langevin, C.D., A.M. Dausman, and M.C. Sukop, *Solute and Heat Transport Model of the Henry and Hilleke Laboratory Experiment*. Ground Water, 2010. **48**: p. 757-770.
216. Ingebritsen, S.E. and S. W.E., *Groundwater in Geologic Processes*. 1998, Cambridge, UK: Cambridge University Press.
217. Kranz, S. and S. Frick, *Efficient cooling energy supply with aquifer thermal energy storages*. Applied Energy, 2013. **109**(0): p. 321-327.
218. Oasen, *Voorkomen en verwijderen van putverstopping door deeltjes op de boorgatwand (Prevention and removal of well clogging by particles on the borehole wall)*. 2006: Kiwa N.V. Nieuwegein.
219. Koenders, M.J.B. and B.d. Zwart, *Koude/warmteopslag in de praktijk (Geothermal storage in practice)*. 2007, IF Technology: Arnhem.
220. engineeringtoolbox. 2013 [cited 2013 20 December 2013]; Available from: http://www.engineeringtoolbox.com/heat-pump-efficiency-ratings-d_1117.html.
221. Omer, A.M., *Ground-source heat pumps systems and applications*. Renewable and Sustainable Energy Reviews, 2008. **12**(2): p. 344-371.
222. Sarbu, I. and C. Sebarchievici, *General review of ground-source heat pump systems for heating and cooling of buildings*. Energy and Buildings, 2013.
223. National Association of Home Builders, *Study of life expectancy of home components*. 2007: Washington, DC.

224. Pirouti, M., A. Bagdanavicius, J. Ekanayake, J. Wu, and N. Jenkins, *Energy consumption and economic analysis of a district heating network*. Energy, 2013. **57**: p. 149-159.
225. Eijgenraam, C.J.J., C.C. Koopmans, P.J.G. Tang, and A.C.P. Verster, *Evaluatie van grote infrastructuurprojecten (Evaluation of big infrastructure projects)*. 2000, Ministry of transport, public works and water management.
226. Saltelli, A., M. Ratto, T. Andres, F. Campolongo, J. Cariboni, D. Gatelli, M. Saisana, and S. Tarantola, *Global sensitivity analysis*. 2008, West Sussex, England: John Wiley & Sons Ltd.
227. Sobol, I.M., V.I. Turchaninov, and Y.L. Levitan, *LPTAU51; Quasirandom Sequence Generators*. 1992, B.V. Shukman Keldysh Institute of Applied Mathematics Russian Academy of Sciences: Moscow.
228. Jenkins, D., Y. Liu, and A.D. Peacock, *Climatic and internal factors affecting future UK office heating and cooling energy consumptions*. Energy and Buildings, 2008. **40**(5): p. 874-881.
229. Papadopoulos, A.M., S. Oxizidis, and G. Papandritsas, *Energy, economic and environmental performance of heating systems in Greek buildings*. Energy and Buildings, 2008. **40**(3): p. 224-230.
230. Sarak, H. and A. Satman, *The degree-day method to estimate the residential heating natural gas consumption in Turkey: a case study*. Energy, 2003. **28**(9): p. 929-939.
231. Ghaebi, H. and M.N. Bahadori, *Performance analysis and parametric study of thermal energy storage in an aquifer coupled with a heat pump and solar collectors, for a residential complex in Tehran, Iran*. Applied Thermal Engineering, 2014. **62**(1): p. 156-170.
232. Segers, R., *Rendementen en CO₂-emissie van elektriciteitproductie in Nederland, update 2011 [Efficiency and CO₂-emission of electricity production in the Netherlands, update 2011]*. 2013, Centraal Bureau voor de Statistiek: Den Haag/Heerlen.
233. EN 15603:2008, *Energy performance of buildings - overall energy use and definition of energy ratings*. 2008.
234. CBS. CBS. 2007 [cited 2013 20 December 2013]; Available from: <http://www.cbs.nl/en-GB/menu/themas/industrie-energie/publicaties/artikelen/archief/2007/2007-2187-wm.htm?Languageswitch=on>.
235. Bergh, K.v.d., E. Delarue, and W. D'haeseleer, *Impact of renewables deployment on the CO₂ price and the CO₂ emissions in the European electricity sector*. Energy Policy, 2013. **63**: p. 1021-1031.
236. Sandwell, D.T., *Biharmonic spline interpolation of GEOS-3 and SEASAT altimeter data*. Geophysical Research Letters, 1987. **2**: p. 139-142.
237. Korolija, I., *Heating, ventilating and air-conditioning system energy demand coupling with building loads for office buildings*. 2011, De Montfort University: Leicester.
238. Kolokotroni, M., X. Ren, M. Davies, and A. Mavrogianni, *London's urban heat island: Impact on current and future energy consumption in office buildings*. Energy and Buildings, 2012. **47**: p. 302-311.
239. Lee, K.S., *Aquifer Thermal Energy Storage*, in *Underground Thermal Energy Storage*. 2013, Springer. p. 59-93.
240. Sommer, W., J. Valstar, I. Leusbrock, T. Grotenhuis, and H. Rijnaarts, *Optimization and spatial pattern of large-scale aquifer thermal energy storage*. Applied Energy, 2015. **137**: p. 322-337.
241. Snijders, A., *Aquifer thermal energy storage in the Netherlands status beginning of 2005*. IFTech International BV, Arnhem, 2005.

242. van Wezel, A.P., R.O. Franken, E. Drissen, K.C. Versluijs, and R. Van den Berg, *Societal cost - benefit analysis for soil remediation in the Netherlands*. Integrated environmental assessment and management, 2008. **4**(1): p. 61-74.
243. Bedient, P.B., H.S. Rifai, and C.J. Newell, *Ground water contamination: transport and remediation*. 1994: Prentice-Hall International, Inc.
244. Linn, W., L. Appel, G. Davis, R. DeZeeuw, C. Dukes, P. Eriksen, J. Farrell, D. Fitton, J. Gilbert, J. Haas, L. Henning, R. Jurgens, B. Pyles, R. Schmidt, J. So, A. Spencer, D. Trippler, and P. Wilson, *Conducting Contamination Assessment Work at Dry Cleaning Sites*. 2004.
245. Wiedemeier, T.H., *Natural attenuation of fuels and chlorinated solvents in the subsurface*. 1999: John Wiley & Sons.
246. Nipshagen, A. and T. Praamstra, *VOCL - volatile hydrogen chlorides (VOCl) in the soil*. 2010.
247. Grindstaff, M., *Bioremediation of chlorinated solvent contaminated groundwater*. 1998: US Environmental Protection Agency, Office of Solid Waste and Emergency Response, Technology Innovation Office.
248. McCarty, P.L., *Groundwater contamination by chlorinated solvents: History, remediation technologies and strategies*, in *In Situ Remediation of Chlorinated Solvent Plumes*. 2010, Springer. p. 1-28.
249. Newell, C.J., L.P. Hopkins, and P.B. Bedient, *A Hydrogeologic Database for Ground - Water Modeling*. Groundwater, 1990. **28**(5): p. 703-714.
250. Teutsch, G., P. Gratwohl, and T. Schiedik, *Literaturstudie zum natürlichen Rückhalt / Abbau von Schadstoffen im Grundwasser*. 1997: Baden-Württemberg.
251. Bradley, P.M., *History and ecology of chloroethene biodegradation: a review*. Bioremediation Journal, 2003. **7**(2): p. 81-109.
252. Mulligan, C.N. and R.N. Yong, *Natural attenuation of contaminated soils*. Environment international, 2004. **30**(4): p. 587-601.
253. Scow, K.M. and K.A. Hicks, *Natural attenuation and enhanced bioremediation of organic contaminants in groundwater*. Current Opinion in Biotechnology, 2005. **16**(3): p. 246-253.
254. Chambon, J.C., P.L. Bjerg, C. Scheutz, J. Bælum, R. Jakobsen, and P.J. Binning, *Review of reactive kinetic models describing reductive dechlorination of chlorinated ethenes in soil and groundwater*. Biotechnology and bioengineering, 2013. **110**(1): p. 1-23.
255. Holliger, C., G. Wohlfarth, and G. Diekert, *Reductive dechlorination in the energy metabolism of anaerobic bacteria*. FEMS Microbiology Reviews, 1998. **22**(5): p. 383-398.
256. Lovley, D.R., *Cleaning up with genomics: applying molecular biology to bioremediation*. Nature Reviews Microbiology, 2003. **1**(1): p. 35-44.
257. Hartog, N. *Anticipated temperature effects on biogeochemical reaction rates in seasonal aquifer thermal energy storage (ATES) systems: an evaluation using the Arrhenius equation*. in *Nationaal Congres Bodemenergie*. 2011. Utrecht, Netherlands.
258. Kouznetsova, I., X. Mao, C. Robinson, D.A. Barry, J.I. Gerhard, and P.L. McCarty, *Biological reduction of chlorinated solvents: Batch-scale geochemical modeling*. Advances in Water Resources, 2010. **33**(9): p. 969-986.
259. Malaguerra, F., J.C. Chambon, P.L. Bjerg, C. Scheutz, and P.J. Binning, *Development and sensitivity analysis of a fully kinetic model of sequential reductive dechlorination in groundwater*. Environmental science & technology, 2011. **45**(19): p. 8395-8402.

260. Parkhurst, D.L. and C. Appelo, *User's guide to PHREEQC (Version 2): A computer program for speciation, batch-reaction, one-dimensional transport, and inverse geochemical calculations*. 1999.
261. Valstar, J. and D. Maljers, *Geohydrological modelling - predictions for an area-oriented approach for groundwater contamination in the city of Utrecht*. 2013, EU project CityChlor, <http://www.citychlor.eu/>.
262. Clement, T.P., C.D. Johnson, Y. Sun, G.M. Klecka, and C. Bartlett, *Natural attenuation of chlorinated ethene compounds: model development and field-scale application at the Dover site*. *Journal of Contaminant Hydrology*, 2000. **42**(2): p. 113-140.
263. Farrell, J. and A. Rose, *Temperature effects on microorganisms*. *Annual Reviews in Microbiology*, 1967. **21**(1): p. 101-120.
264. Price, P.B. and T. Sowers, *Temperature dependence of metabolic rates for microbial growth, maintenance, and survival*. *Proceedings of the National Academy of Sciences of the United States of America*, 2004. **101**(13): p. 4631-4636.
265. Zoetemeyer, R., P. Arnoldy, A. Cohen, and C. Boelhouwer, *Influence of temperature on the anaerobic acidification of glucose in a mixed culture forming part of a two-stage digestion process*. *Water Research*, 1982. **16**(3): p. 313-321.
266. Friis, A.K., A.C. Heimann, R. Jakobsen, H.-J. Albrechtsen, E. Cox, and P.L. Bjerg, *Temperature dependence of anaerobic TCE-dechlorination in a highly enriched Dehalococcoides containing culture*. *Water research*, 2007. **41**(2): p. 355-364.
267. Schaefer, C.E., C.W. Condee, S. Vainberg, and R.J. Steffan, *Bioaugmentation for chlorinated ethenes using Dehalococcoides sp.: Comparison between batch and column experiments*. *Chemosphere*, 2009. **75**(2): p. 141-148.
268. Amos, B.K., E.J. Suchomel, K.D. Pennell, and F.E. Löffler, *Spatial and temporal distributions of Geobacter lovleyi and Dehalococcoides spp. during bioenhanced PCE-NAPL dissolution*. *Environmental science & technology*, 2009. **43**(6): p. 1977-1985.
269. Mendoza-Sanchez, I., R.L. Autenrieth, T.J. McDonald, and J.A. Cunningham, *Effect of pore velocity on biodegradation of cis-dichloroethene (DCE) in column experiments*. *Biodegradation*, 2010. **21**(3): p. 365-377.
270. Holm, P.E., P.H. Nielsen, H.-J. Albrechtsen, and T.H. Christensen, *Importance of unattached bacteria and bacteria attached to sediment in determining potentials for degradation of xenobiotic organic contaminants in an aerobic aquifer*. *Applied and Environmental Microbiology*, 1992. **58**(9): p. 3020-3026.
271. Lehman, R.M., F.S. Colwell, and G.A. Bala, *Attached and unattached microbial communities in a simulated basalt aquifer under fracture-and porous-flow conditions*. *Applied and environmental microbiology*, 2001. **67**(6): p. 2799-2809.
272. Furrer, G., U. von Gunten, and J. Zobrist, *Steady-state modelling of biogeochemical processes in columns with aquifer material 1. Speciation and mass balances*. *Chemical Geology*, 1996. **133**(1): p. 15-28.
273. Deng, Y., *Effect of pH on the reductive dissolution rates of iron (III) hydroxide by ascorbate*. *Langmuir*, 1997. **13**(6): p. 1835-1839.
274. Bonneville, S., P. Van Cappellen, and T. Behrends, *Microbial reduction of iron (III) oxyhydroxides: effects of mineral solubility and availability*. *Chemical Geology*, 2004. **212**(3): p. 255-268.

275. Wu, L., B.L. Beard, E.E. Roden, and C.M. Johnson, *Influence of pH and dissolved Si on Fe isotope fractionation during dissimilatory microbial reduction of hematite*. *Geochimica et Cosmochimica Acta*, 2009. **73**(19): p. 5584-5599.
276. Appelo, C.A.J. and D. Postma, *Geochemistry, groundwater and pollution*. 2005: CRC Press.
277. Robinson, C. and D. Barry, *Design tool for estimation of buffer requirement for enhanced reductive dechlorination of chlorinated solvents in groundwater*. *Environmental Modelling & Software*, 2009. **24**(11): p. 1332-1338.
278. Brovelli, A., D.A. Barry, C. Robinson, and J.I. Gerhard, *Analysis of acidity production during enhanced reductive dechlorination using a simplified reactive transport model*. *Advances in Water Resources*, 2012. **43**: p. 14-27.
279. Robinson, C., D. Barry, P.L. McCarty, J.I. Gerhard, and I. Kouznetsova, *pH control for enhanced reductive bioremediation of chlorinated solvent source zones*. *Science of the total environment*, 2009. **407**(16): p. 4560-4573.
280. Griffioen, J., *Kation-uitwisselingspatronen bij zoet/zout grondwaterverplaatsingen (translation: Cation-exchange patterns with fresh/salt groundwater movement)*. *Stromingen*, 2003. **9**(4).
281. Aulenta, F., A. Pera, S. Rossetti, M. Petrangeli Papini, and M. Majone, *Relevance of side reactions in anaerobic reductive dechlorination microcosms amended with different electron donors*. *Water research*, 2007. **41**(1): p. 27-38.
282. Lendvay, J., F.E. Löffler, M. Dollhopf, M. Aiello, G. Daniels, B. Fathepure, M. Gebhard, R. Heine, R. Helton, and J. Shi, *Bioreactive barriers: a comparison of bioaugmentation and biostimulation for chlorinated solvent remediation*. *Environmental Science & Technology*, 2003. **37**(7): p. 1422-1431.
283. Distefano, T.D., J. Gossett, and S. Zinder, *Hydrogen as an electron donor for dechlorination of tetrachloroethene by an anaerobic mixed culture*. *Applied and Environmental Microbiology*, 1992. **58**(11): p. 3622-3629.
284. Mazur, C.S. and W.J. Jones, *Hydrogen concentrations in sulfate-reducing estuarine sediments during PCE dehalogenation*. *Environmental science & technology*, 2001. **35**(24): p. 4783-4788.
285. Vainberg, S., C.W. Condee, and R.J. Steffan, *Large-scale production of bacterial consortia for remediation of chlorinated solvent-contaminated groundwater*. *Journal of industrial microbiology & biotechnology*, 2009. **36**(9): p. 1189-1197.
286. Widdowson, M.A., *Modeling natural attenuation of chlorinated ethenes under spatially varying redox conditions*. *Biodegradation*, 2004. **15**(6): p. 435-451.
287. Bonte, M., *Impacts of Shallow Geothermal Energy on Groundwater Quality: A Hydrochemical and geomicrobial study of the effects of ground source heat pumps and aquifer thermal energy storage*. 2013.
288. Bonte, M., P. Stuyfzand, G. Van den Berg, and W. Hijnen, *Effects of aquifer thermal energy storage on groundwater quality and the consequences for drinking water production: a case study from the Netherlands*. *Water Science & Technology*, 2011. **63**(9): p. 1922-1931.
289. Caljé, R.J., *Future use of Aquifer Thermal Energy Storage below the historic centre of Amsterdam*. 2011, Master thesis, Delft University of Technology.
290. Aulenta, F., A. Canosa, M. Leccese, M. Petrangeli Papini, M. Majone, and P. Viotti, *Field study of in situ anaerobic bioremediation of a chlorinated solvent source zone*. *Industrial & Engineering Chemistry Research*, 2007. **46**(21): p. 6812-6819.
291. Morrill, P., B. Sleep, D. Seepersad, M. McMaster, E. Hood, C. LeBron, D. Major, E. Edwards, and B. Sherwood Lollar, *Variations in expression of carbon isotope fractionation of chlorinated*

- ethenes during biologically enhanced PCE dissolution close to a source zone. Journal of contaminant hydrology*, 2009. **110**(1): p. 60-71.
292. Nipshagen, A. and T. Praamstra, *VOCL: Vluchtige chloorkoolwaterstoffen (VOCL) in de bodem*. 2010, Stichting kennisontwikkeling Kennisoverdracht Bodem: Gouda, the Netherlands.

Summary

Aquifer thermal energy storage (ATES) is applied world-wide to provide heating and cooling to buildings. Application of ATES, instead of traditional heating and cooling installations, reduces primary energy consumption and related CO₂ emissions. Intensified use of the subsurface for thermal applications requires more accurate methods to measure and predict the development of thermal plumes in the subsurface and address issues related to subsurface urban planning and wide spread presence of contaminants in urban groundwater systems. This thesis approaches these challenges from multiple perspectives. From a physical point of view, subsurface heat transport in ATES and the associated influence on storage performance for thermal energy was assessed. From an economic and environmental benefits perspective, planning of large-scale application of ATES and optimal use of aquifer volume were studied. Finally opportunities have been explored related to combining ATES with soil and groundwater remediation.

Chapter 2: Thermal performance and heat transport in aquifer thermal energy storage

In this chapter, an assessment was made of (1) the thermal storage performance, and (2) the heat transport around the wells of an existing ATES system. Reconstruction of flow rates and injection and extraction temperatures from hourly logs of operational data between 2005 and 2012 show that on average 82% of the stored cold is recovered and 68% of the stored heat. Detailed monitoring of subsurface temperature development was achieved by a unique application of Distributed Temperature Sensing (DTS) using glass fibre optical cables that were installed around the wells of the system. The measurements reveal unequal distribution of flow rate over different parts of the well screen and preferential flow due to aquifer heterogeneity. Higher than average flow rates in discrete parts of the well screen increase the radius of thermal influence at these depths. This may influence optimal well-to-well distances in areas with a high density of ATES systems. Comparison with a numerical model shows that even with preferential flow the thermal impact of the system is smaller than permitted because the system operates at approximately 54% of the permitted flow rate.

Chapter 3: The impact of aquifer heterogeneity on the performance of aquifer thermal energy storage

As shown in chapter 2, heterogeneity in hydraulic conductivity may affect heat transport in ATES. This in turn has an impact on the amount of thermal energy that is recovered and the thermal balance of the system. In this chapter, the influence of heterogeneity on the performance of a doublet well system was quantified using stochastic heat transport modelling. Sensitivity analyses were conducted to assess the influence of heterogeneity under different design condition (well-to-well distance, orientation of the doublet with respect to regional groundwater flow) and hydrogeological conditions (groundwater velocity). The results show that on average, thermal recovery decreases with increasing heterogeneity. Furthermore, heterogeneity at the scale of a doublet ATES system introduces an uncertainty in the amount of expected thermal interference between the warm and cold storage. This results in an uncertainty in thermal recovery that also increases with heterogeneity and decreases with increasing distance between ATES wells. To account for heterogeneity whilst using homogeneous models, an attempt was made to express the effect of heterogeneity by an apparent macrodispersivity. As expected, the apparent macrodispersivity increases with increasing heterogeneity. However, the appropriate range of dispersivities not only depends on the statistical characteristics of the heterogeneous aquifer, but also on groundwater velocity and well-to-well distance, thus limiting the practical applicability of the macrodispersivity approach.

Chapter 4: Efficiency of and interference among multiple aquifer thermal energy storage systems; a Dutch case study

Efficiency and interference among existing ATES systems installed in the city of The Hague, the Netherlands were analysed. In this city, a total of 19 ATES systems are installed within an area of about 3.8 km² with a total of 76 operating wells. The analysis focused on the development of a coupled groundwater flow and heat transfer model. Efficiency of individual systems, individual wells, and interference among wells within and between systems were analysed. The analysis shows that efficiency tends, in general, to increase over time and stabilize at an asymptotic value after approximately 5 years. Efficiency of the ATES systems ranges between 40% and 89%. It was found that asymptotic energy efficiency (represented by model results after 10 years of operation) is mainly sensitive to the stored volume and increases from 50% for a well with a low flow rate (9 100 m³/year) to 90% for wells with larger flow rate (250 000 m³/year). Performance of the ATES systems in the study area varies among systems due to either negative impact (least favourite) or positive impact (favourite) of interference among wells of the same system or wells of other systems. Several factors influence the impact of thermal interference on the efficiency of an ATES system including the spatial distributions of wells, their pumping and injection rates,

and hydraulic and thermal characteristics of the hosting aquifers. In the study area, the interference phenomenon affects efficiency, in general, positively where it increases the efficiency of individually operating wells by a maximum of 10%. However, the phenomenon also affects efficiency of some wells negatively where it reduces the efficiency of individually operating wells also by a maximum of 10%. On average, systems in the study area are positively affected by interferences among each other with an overall average of 2.5% for all wells. This can be attributed equally to interference between wells within a system as interference with wells of other systems.

Chapter 5: Optimization and spatial pattern of large-scale aquifer thermal energy storage

The energy that can be supplied by large-scale application of ATES is limited by thermal interference between the warm and cold storage. In this chapter, the potential thermal performance of large-scale application of ATES was determined using a simplified hydrogeological model. Different zonation patterns were compared and the influence of well-to-well distances on thermal interference was determined. Also, a method is provided to determine the amount of thermal interference that is acceptable from an economical and environmental perspective. To this end, a set of dimensionless parameters was introduced that characterize the thermal performance of large-scale ATES. The method was demonstrated using the hydrogeological conditions of Amsterdam, the Netherlands, which is a city with a high concentration of ATES systems. Results for this case study show that it is cost-effective to allow a limited amount of thermal interference, such that 30–40% more energy can be provided in a given area compared to the case in which all negative thermal interference is avoided. Sensitivity analysis indicates that optimal well distance is moderately insensitive to changes in hydrogeological and economic conditions. Maximum economic benefit compared to conventional heating and cooling systems on the other hand is sensitive, especially to changes in the gas price and storage temperatures.

Chapter 6: Reactive transport modelling of TCE bioremediation combined with aquifer thermal energy storage

Because many urbanized areas deal with contaminated soil and groundwater, ambitions to increase the number of ATES systems in order to achieve sustainable energy targets are confronted with the presence of groundwater contaminants. At this moment, ATES systems are rarely placed in contaminated groundwater systems, although there may be new opportunities to combine ATES with groundwater remediation. Hence, the well-designed combination of ATES with natural attenuation or biostimulation could be a promising integrated technique, both for remediation of contaminants as for development of ATES. In this chapter, a reactive transport

model was developed to simulate the use of ATES as a continuous biostimulation tool for enhanced reductive dechlorination (ERD) of a hypothetical TCE contaminated aquifer. In several scenarios, the influence of design conditions, i.e. storage temperatures and electron donor dose, were studied for their effect on bioremediation. Furthermore the effects of spreading of biodegradation potential upon assumptions regarding biomass mobility in the affected area were simulated. Model results show reduction of iron and sulphate in the groundwater injected by the ATES system upon biostimulation by lactate addition, followed by complete reductive dechlorination. Progress of dechlorination is dictated by lactate dose and amounts of electron acceptors. Although microbial processes are known to be temperature dependent, temperature changes induced by thermal storage did not significantly influence the overall dechlorination rate. Simulations also reveal that further study is required on (1) reduction of iron oxide, related to increasing pH of the infiltrated groundwater, and (2) growth and mobility of bacteria related to well clogging, which is a main concern for biostimulation using ATES.

Chapter 7: Opportunities and challenges for implementation of ATES in urban areas

In this final chapter, the research questions are addressed and implications for design of ATES systems and planning and management of large-scale application are discussed.

Samenvatting

Opslag van thermische energie in de bodem, ook wel bekend als warmte koude opslag (WKO), wordt wereldwijd toegepast om gebouwen te koelen en te verwarmen. Toepassing van WKO in plaats van traditionele verwarmings- en koelingsinstallaties, kan het gebruik van primaire energie en de daaraan gerelateerde CO₂ uitstoot verminderen. Daarnaast kan WKO een besparing opleveren op kosten voor verwarming en koeling. Op sommige locaties wordt inmiddels zo intensief gebruik gemaakt van WKO dat nauwkeuriger methoden nodig zijn om de verspreiding van thermische energie in de bodem te kunnen meten en te voorspellen. Doordat ruimte in de ondergrond voor bodemenergie beperkt is, ontstaan nieuwe vragen omtrent planning van systemen en optimaal gebruik van de bodem. Daarnaast bestaat er onzekerheid over de invloed van bodemenergiesystemen op bodem en grondwatervervuiling. In dit proefschrift worden deze zaken vanuit verschillend perspectief benaderd. Allereerst is warmtetransport in de bodem bestudeerd. Dit is van belang, omdat het gedrag van warmte rondom de bronnen van een WKO systeem onder meer bepaalt hoeveel van de opgeslagen energie teruggewonnen kan worden. Vervolgens is vanuit een economisch en milieutechnisch perspectief onderzocht hoe optimaal gebruik kan worden gemaakt van het beschikbare volume aan watervoerend pakket bij grootschalige toepassing van WKO. Tot slot wordt de mogelijkheid verkend om WKO te combineren met bodem en grondwater sanering.

Hoofdstuk 2: Opslag rendement en warmtetransport bij warmte koude opslag

In dit hoofdstuk zijn (1) het opslag rendement voor thermische energie, en (2) warmtetransport rond de bronnen van een bestaand systeem onderzocht. Uit operationele data die elk uur gelogd worden in het gebouw beheer systeem, zijn de bron debieten en injectie en extractie temperaturen bepaald tussen 2005 en 2012. Analyse van deze gegevens laat zien dat in deze periode gemiddeld 82% van de opgeslagen koude en 68% van de opgeslagen warmte is teruggewonnen. Daarnaast is de verspreiding van warmte en koude in de bodem gevolgd door temperatuur monitoring met behulp van Distributed Temperature Sensing (DTS) in glasvezelkabels. Temperatuurmonitoring met glasvezelkabels is een bestaande technologie, maar

in deze studie wel voor het eerst toegepast op bodemenergiesystemen. De glasvezelkabels zijn op verschillende afstanden van de WKO bronnen in de bodem gebracht tot een diepte van 50 meter in speciaal voor dit doel geboorde boorgaten. Gedurende een periode van bijna 1.5 jaar zijn met tussenposen van maximaal 1 uur temperatuur profielen verzameld over de gehele lengte van de kabel. Daarmee biedt dit een dataset van ongekend detail in ruimte en tijd. De metingen onthullen dat niet alle delen van het bronfilter evenveel bijdragen aan het totale debiet en het optreden van voorkeursstroming door heterogeniteit in het watervoerend pakket. Een hoger dan gemiddeld debiet in specifieke delen van het bronfilter vergroot het thermisch beïnvloed gebied op deze diepten. Dit kan de optimale afstand tussen de bronnen beïnvloeden in gebieden waar veel WKO systemen worden gerealiseerd. Vergelijking van de metingen met de resultaten van een warmtetransport model laten zien dat, ondanks het optreden van voorkeursstroming, de thermische invloed van het systeem kleiner is dan ingeschat in de milieueffectrapportage doordat maar circa 54% van het vergunde debiet wordt gebruikt.

Hoofdstuk 3: De invloed van heterogeniteit op het opslagrendement van warmte koude opslag

In hoofdstuk 2 is aangetoond dat heterogeniteit van een watervoerend pakket invloed kan hebben op de verspreiding van thermische energie rond de bronnen van een WKO systeem. Dit kan invloed hebben op de mate waarin opgeslagen energie teruggewonnen kan worden en op de thermische balans van het systeem. In dit hoofdstuk is de invloed van heterogeniteit op het opslagrendement van een doublet WKO systeem onderzocht door middel van warmtetransport modellering. Een gevoeligheidsanalyse is uitgevoerd om de invloed van heterogeniteit te onderzoeken onder verschillende ontwerp condities (afstand tussen de bronnen, oriëntatie van het doublet ten opzicht van regionale grondwaterstroming) en hydrogeologische condities (grootte van de regionale grondwaterstroming). Resultaten van de modellering laten zien dat het opslagrendement afneemt met toenemende heterogeniteit. Daarnaast resulteert heterogeniteit op de schaal van het doublet systeem in een onzekerheid in de verwachte thermische interferentie tussen de bronnen. Dit uit zich in een onzekerheid in het opslagrendement die ook toeneemt bij toenemende heterogeniteit en afneemt met toenemende afstand tussen de bronnen. Heterogeniteit kan expliciet meegenomen worden in warmtetransport modellering, maar hierdoor worden modellen wel complexer en trager. Bovendien is de heterogeniteit in de praktijk vaak niet goed gekarakteriseerd. In dit geval kan de onzekerheid ten gevolge van heterogeniteit worden meegenomen door meerdere realisaties te simuleren waardoor modellen nog complexer worden. Daarom is getracht het effect van heterogeniteit uit te drukken in een effectieve macro-dispersiviteit. Zoals verwacht mag worden, neemt de effectieve macro-dispersiviteit toe bij toenemende heterogeniteit. De bandbreedte in waarden voor de effectieve macro-dispersiviteit

blijkt echter niet alleen afhankelijk van de statistische eigenschappen van het heterogene watervoerend pakket, maar ook van de regionale grondwater stroomsnelheid en de afstand tussen de bronnen. Hierdoor is de praktische toepasbaarheid van deze aanpak nog beperkt.

Hoofdstuk 4: Opslagrendement en interferentie tussen meerdere WKO systemen; een Nederlandse casus

In dit hoofdstuk is een analyse gemaakt van het opslagrendement en interferentie tussen WKO systemen in Den Haag. In het onderzoeksgebied zijn maar liefst 19 WKO systemen, met in totaal 76 bronnen, gerealiseerd in een gebied van maar 3.8 km². Het hoofdstuk beschrijft de ontwikkeling van een grondwaterstroming en warmtetransport model. Met dit model zijn het opslagrendement van de individuele systemen en bronnen bepaald en de mate van interferentie tussen bronnen van hetzelfde systeem en met bronnen van naburige WKO systemen. De modelresultaten laten zien dat het opslagrendement van de individuele systemen varieert tussen de 40% en 89%. Over het algemeen neemt het opslagrendement toe na ingebruikname van het systeem, totdat deze stabiliseert na ongeveer 5 jaar. Het uiteindelijke opslagrendement lijkt voornamelijk af te hangen van het volume grondwater dat wordt verpompt en neemt toe van 50% (bij een grondwatervolume van 9 100 m³/jaar) tot 90% (bij een grondwatervolume van 250 000 m³/jaar). Het opslagrendement van de systemen wordt zowel positief als negatief beïnvloedt door de aanwezigheid van andere bodemenergiesystemen. De mate van interferentie wordt met name bepaald door de ruimtelijke ligging van de bronnen, hun debiet en de hydraulische en thermische eigenschappen van het watervoerend pakket. Over het algemeen worden systemen in het studiegebied positief beïnvloedt door thermische interferentie zodat hun opslagrendement toeneemt met 2.5%. Dit komt in ongeveer gelijke mate door de aanwezigheid van andere bronnen van hetzelfde systeem als bronnen van andere systemen. De maximale invloed op het opslagrendement is 10%, zowel in positieve als negatieve richting.

Hoofdstuk 5: Planning en optimalisatie van grootschalige toepassing van WKO

De totale hoeveelheid energie die geleverd kan worden door grootschalige toepassing van WKO is gelimiteerd door interferentie tussen de warme en koude bronnen. In dit hoofdstuk wordt met een versimpeld hydrogeologisch model de maximale energie bepaald die geleverd kan worden door grootschalige toepassing van WKO. Verschillende manieren om koude en warme bronnen te rangschikken worden vergeleken, en voor elk bronnenpatroon wordt de invloed van afstand tussen de bronnen bepaald. Vervolgens wordt bepaald welke mate van thermische interferentie acceptabel is vanuit een economisch en milieutechnisch perspectief. Een set van dimensieloze getallen wordt geïntroduceerd waarmee het thermisch gedrag van grootschalige toepassing van WKO kan worden beschreven. Om het gebruik van de methode te demonstreren is deze

toegepast op de hydrogeologische condities van Amsterdam. Resultaten voor deze casus laten zien dat het kosteneffectief is om een bepaalde mate van thermische interferentie toe te staan waardoor 30 tot 40% meer energie kan worden geleverd dan wanneer alle interferentie zou worden vermeden. Een gevoeligheidsanalyse laat zien dat de optimale afstand tussen bronnen maar in beperkte mate gevoelig is voor veranderingen in hydrogeologische of economische condities. Het maximaal economische voordeel dat wordt behaald door toepassen van WKO in plaats van conventionele verwarmings- en koelingsystemen, daarentegen, is sterk afhankelijk van de prijs van gas en de opslagtemperaturen die worden toegepast.

Hoofdstuk 6: Modellerings van WKO gecombineerd met gestimuleerde biologische afbraak van een TCE verontreiniging

Veel binnenstedelijke gebieden hebben te maken met bodem en grondwaterverontreinigingen. Omdat WKO vooral wordt toegepast in het stedelijk gebied, wordt in de planning en aanleg fase een groeiend aantal systemen geconfronteerd met de aanwezigheid van verontreiniging. Op dit moment worden WKO systemen maar zelden in een verontreinigd watervoerend pakket gerealiseerd vanwege onzekerheid over de effecten van het WKO systeem op de verspreiding en het gedrag van deze verontreiniging. Er zijn echter ook mogelijkheden om WKO te combineren met bodemsanering zodat de voordelen van WKO benut worden en tegelijkertijd de verontreiniging wordt aangepakt. Daarom is de combinatie van WKO met bodemsanering een veelbelovende technologie. In dit hoofdstuk wordt een reactief transport model beschreven waarmee het gebruik van WKO voor gestimuleerde biologisch afbraak van een hypothetische TCE verontreiniging kan worden gesimuleerd. In een aantal scenario's wordt de invloed van ontwerp factoren (opslag temperaturen en elektron donor dosis) op het verloop van de biologische afbraak verkend. Daarnaast worden aannames betreffende de mobiliteit van biomassa onderzocht. Modelresultaten laten zien dat na het toedienen van lactaat als elektron donor, eerst ijzer en sulfaat reductie optreedt. Pas daarna komt de elektron donor beschikbaar voor dechlorering, waarbij TCE via DCE en VC volledig afbreekt naar Ethene. Het verloop van de dechlorering is voornamelijk afhankelijk van de lactaat dosis en de aanwezigheid van electron acceptors. Hoewel het bekend is dat microbacteriële processen temperatuurafhankelijk zijn, bleek het verhogen van opslag temperaturen van 15 naar 25 °C geen significant effect te hebben op de dechlorering. De simulaties laten ook zien dat met name de rol van ijzerreductie in relatie tot een stijging van de pH en de groei en mobiliteit van biomassa in verband met putverstopping aanvullend onderzoek vereisen.

Hoofdstuk 7: Kansen en uitdagingen voor toepassing van WKO in stedelijk gebied

In dit laatste hoofdstuk worden de onderzoeksvragen die in de inleiding geïntroduceerd zijn behandeld. Daarnaast worden de onderzoeksresultaten in breder perspectief besproken en worden implicaties bediscussieerd voor het ontwerp van WKO systemen, planning en management van grootschalige systemen en kansen en uitdagingen voor toepassing van WKO in stedelijk gebied.

List of publications

Sommer, W.T., Drijver, B.C., Verburg, R., Slenders, H., de Vries, E., Dinkla, I., Leusbrock, I. and Grotenhuis, J.T.C. (2013). *Combining shallow geothermal energy and groundwater remediation*. In Proceedings of the European Geothermal Congress 2013, 03-07 June 2013, Pisa, Italy.

Sommer, W.T., Valstar, J., van Gaans, P.F.M., Grotenhuis, J.T.C., and Rijnaarts, H.H.M. (2013). *The impact of aquifer heterogeneity on the performance of aquifer thermal energy storage*. Water Resources Research 49(12), 8128-8138.

Bakr, M., van Oostrom, N., and Sommer, W.T. (2013). *Efficiency of and interference among multiple aquifer thermal energy storage systems; A Dutch case study*. Renewable Energy 60, 53-62.

Sommer, W.T., Doornenbal, P.J., Drijver, B.C., van Gaans, P.F.M., Leusbrock, I., Grotenhuis, J.T.C. and Rijnaarts, H.H.M. (2014). *Thermal performance and heat transport in aquifer thermal energy storage*. Hydrogeology Journal, 22(1), 263-279.

Sommer, W.T., Valstar, J., Leusbrock, I., Grotenhuis, J.T.C. and Rijnaarts, H.H.M. (2015). *Optimization and spatial pattern of large-scale aquifer thermal energy storage*. Applied energy, 137, 322-337.

Zeghici, R., Oude Essink, G., Hartog, N. and Sommer, W.T. (2015). *Integrated assessment of variable density-viscosity groundwater flow for a high temperature mono-well aquifer thermal energy storage (HT-ATES) system in a geothermal reservoir*. Geothermics, 55, 58-68.

Acknowledgements

First of all I would like to express my gratitude to my promotor Huub Rijnaarts, who offered me the opportunity to pursue this PhD project and gave me the trust and freedom to choose my own approach and direction in this research. Also I would like to thank my daily supervisors for their time and efforts to keep me on track. Johan Valstar, whom I didn't have to explain anything, Pauline van Gaans, for her solid reasoning, Tim Grotenhuis, who can compactly formulate the practical impact of a scientific result, and Ingo Leusbrock, for always making an effort to review my manuscripts.

The majority of the findings in this thesis originate from calculations and theoretical analysis that were done at Deltares in Utrecht. I would like to express my sincere gratitude to my colleagues there, who made working so enjoyable. In particular I would like to thank Bob, Frans, Gerrit, Marta and Vince for nice discussions and pleasant coffee breaks. Special thanks also to Pieter P., with whom, as a fellow PhD candidate, I could share the blessings and burdens of pursuing a PhD. Also I enjoyed very much the excursions with Pieter D., testing and installing new monitoring installations using Distributed Temperature Sensing. Tinkering with ice buckets, isolation materials and temperature sensors learned me a great deal about the challenges of good data calibration. This was also very useful for the data handling and interpretation that I did later on. Also I thank the master students Veronica, Barbora, Clothilde and Nivedita for their interest and hard work. It was a pleasure to be your supervisor.

Regular trips to Wageningen University provided the opportunity to broaden my perspective due to the wide variety of research that is done at the department of environmental technology. Working there was nice due to a relaxed atmosphere and many pleasant colleagues. In particular I would like to mention cooperation with Zhuobiao. We started around the same time within the same project, however with a very different approach. I am glad that we managed to combine our work in a joined paper (chapter 6 in this thesis), where his knowledge on microbiology and degradation processes was very helpful.

I am also very grateful to Benno Drijver. His extensive knowledge on thermal energy storage systems was very helpful in many stages of this research. Also he enabled me to spend some time at IF Technology where I could develop a feeling for the state-of-practice in aquifer thermal energy storage.

Although it was a pleasure to work on this topic, it was also very nice to have friends who show you there is more to life than scripts and data. Many thanks therefore to Quinten, Paul, Bas (2x), Ronald, Razvan, Annemiek, Wouter, Eef, Steven, Lennert, Rutger, Hans, Wenjing and Tessa, for dinners, entertainment, recreation and travels. Special thanks also to Hans van Helden for the beautiful cover.

Finally I thank my family for supporting me. My parents, where I happily hit the blisters on my hands while chopping down a tree and countless other therapeutical activities. Dien, whose memorable boiled beef provided me with many tasteful moments and saved me a lot of hours in the kitchen. Lies, Marco and the little monkeys for playful times and epic campfires.

Curriculum Vitae

Wijbrand Sommer (27 November 1983, Leiden) grew up in the city Gorinchem. After completing his secondary school (Gymnasium Camphusianum) he moved to Utrecht to study Physics and Astronomy at Utrecht University. In 2005 he finished his Bachelor with a study on reconstruction of historical surface temperatures at Hoftedahlsfonna from a temperature profile along a vertical ice core. In 2008 he graduated at the same University for a master on Geophysics with a focus on hydrogeology. During this master he spent 3 months at Witteveen+Bos to supervise the installation of an aquifer thermal energy storage system and study the influence of design conditions on the thermal storage performance of those systems. For his master research he travelled to Kazan, Russia, to study density dependent transversal dispersion. Between 2008 and 2010 he worked on a variety of subsurface related projects as part of a traineeship at the Dutch organisation for applied scientific research TNO. There, he focussed mainly on geomechanics related to gas and salt mining, geophysical prospecting and risk assessment related to planned CO₂ storage activities. After finalizing this traineeship he started a PhD project at Wageningen University and Deltares, entitled “*Assessing environmental impacts and benefits of regional implementation of combined groundwater-energy technologies*” that led to this thesis.



*Netherlands Research School for the
Socio-Economic and Natural Sciences of the Environment*

D I P L O M A

For specialised PhD training

The Netherlands Research School for the
Socio-Economic and Natural Sciences of the Environment
(SENSE) declares that

Wijbrand Teunis Sommer

born on 27 November 1983 in Leiden, The Netherlands

has successfully fulfilled all requirements of the
Educational Programme of SENSE.

Wageningen, 4 June 2015

the Chairman of the SENSE board

Prof. dr. Huub Rijnaarts

the SENSE Director of Education

Dr. Ad van Dommelen

The SENSE Research School has been accredited by the Royal Netherlands Academy of Arts and Sciences (KNAW)



K O N I N K L I J K E N E D E R L A N D S E
A K A D E M I E V A N W E T E N S C H A P P E N



The SENSE Research School declares that **Mr Wijbrand Sommer** has successfully fulfilled all requirements of the Educational PhD Programme of SENSE with a work load of 44.3 EC, including the following activities:

SENSE PhD Courses

- o Environmental Research in Context (2011)
- o Research in Context Activity: 'Developing and inviting expert and stakeholder feedback to new Wikipedia entry on: Aquifer Thermal Energy Storage' (2014)

Other PhD and Advanced MSc Courses

- o Introduction to PhreeqC, Freie Universitat Berlin (2011)
- o Matlab introductory course, Wageningen University (2011)
- o Voice matters- Voice and Presentation Skills Training, Wageningen University (2013)
- o International course on ground source heat pumps, University of Pisa (2013)

Management and Didactic Skills Training

- o Supervision of four MSc thesis students (2011-2014)
- o Teaching assistant 'Inleiding omgevingswetenschappen' (2011-2013)

Selection of Oral Presentations

- o *The effect of soil heterogeneity on thermal interference between ATEs wells.* 17th Bodem Breed Symposium, 29-30 November 2011, Lunteren, The Netherlands
- o *Aquifer thermal energy storage: soil heterogeneity and thermal interference.* European Geosciences Union (EGU), 22-27 April 2012, Vienna, Austria
- o *Efficiency and interference among multiple Aquifer Thermal Energy Storage (ATES) systems.* AquaConSoil 2013 — 12th International UFZ-Deltares Conference on Groundwater-Soil-Systems and Water Resource Management, 16-19 April 2013, Barcelona, Spain
- o *Thermal performance of Aquifer Thermal Energy Storage and subsurface heat transport.* European geothermal PhD days, 5-7 May 2013, Szeged, Hungary
- o *Combining shallow geothermal energy and groundwater remediation.* European Geothermal Congress (EGC2013), 3-7 June 2013, Pisa, Italy
- o *Optimization and spatial pattern of large-scale aquifer thermal energy storage.* European geothermal PhD days, 31 March- 2 April 2014, Darmstadt, Germany

SENSE Coordinator PhD Education



Dr. ing. Monique Gulickx

This research was carried out within the framework of the project Meer Met Bodemenergie (“More with geothermal energy”). We thank the participating institutions for their contribution: Deltares, Essent, WMD, and IF-Technology.

Printed by: Gildeprint - The Netherlands

Cover design: kleurholland.nl

